



UNIVERSITY OF NAIROBI

**Evaluation of volcanic ash along Maai Mahiu-Narok road and its effect on road stability
after long rains**

AMOLLO KENNETH OTIENO

F16/39624/2011

A project submitted as a partial fulfillment

Of the requirement for the award of the degree of

BACHELOR OF SCIENCE IN CIVIL ENGINEERING

2016

Abstract

Volcanic soils are widely distributed group of soils, which cover significant parts of the world's surface including areas occupied by urban settlements, structures and infrastructure, and may create geo-engineering problems. These soils exhibit a distinctive behavior that is a consequence of their formation history, mineralogy and structure. Some part of the subsoil of a large area along Maai Mahiu - Narok Road in Kenya mainly consists of volcanoclastic deposits. This paper presents the results of the part of a research programme aiming at geotechnically characterizing the uppermost layer of this volcanoclastic sequence, particularly focusing on its collapse potential, shear behavior and the influence of microstructure on these behaviours. In addition, its main features were investigated and the stability of sub-vertical cuts in this soil was also assessed. The experimental investigation mainly consisted of index and classification tests, consolidation and direct shear box tests to assess the collapse potential and shear behaviour of the soil, respectively. Matric suction of the samples was also determined for preliminary evaluation of the influence of suction on collapse and shear behaviors of the soil. In addition, thin-section studies, X-ray diffraction (XRD) and scanning electron microscopy (SEM) analysis were also conducted to determine mineralogical and microstructural features and to evaluate their influences on the mechanical behavior of the volcanic soil.

In order to conclusively research on this phenomenon, the following areas were highlighted as the key areas of interest;

- a) Geology of the area;
- b) Hydrology of the area, extending to the surrounding hills;
- c) Geotechnical engineering of the underlying soils, to be aided by deep exploration works;
- d) Engineering solution to preservation of the road in geologically active areas.

To meet the primary objectives, the research work comprised of four key components:

- a) Geophysical Analysis (2D ERT and MASW)
- b) Geological Analysis (Geological Structural Analysis of the area e.g. Faults)
- c) Geotechnical Analysis (Drilling and Laboratory testing)
- d) Hydrology of the area

Dedication

I would like to dedicate this project to my dad, Eng. L.A. Ajwallah.

Acknowledgement

I would like to acknowledge and thank The Almighty God for the gift of life, good health and for the wisdom and understanding He has imparted on me especially during this five year period of undertaking my undergraduate studies.

I would like to acknowledge and appreciate the efforts made by my parents, who have been there for me financially and for their guidance during this research period and throughout the entire 5 years of my studies.

My appreciation goes to the University of Nairobi, College of Architecture and Engineering, School of Engineering, Department of Civil and Construction Engineering for giving me the opportunity to partake my undergraduate studies at such a prestigious institution of higher learning and excellence.

My sincere gratitude goes to Dr. Eng. S.N. Osano, my project supervisor, for the whole project process. His guidance, assistance, constructive criticism and advice have been very valuable in my start and completion of this project.

The department of Civil and Construction Engineering soils laboratory was of great assistance in providing administrative and technical support in particular; the Chief Technologist, Mr. J.B. Ogallo, the laboratory team, Mr. Oyier A Elly, Mr. Martin Mburu, Mrs. Eunice and Mr. Mathew among others.

To Dr. A. Waswa of the Department of Geology, University of Nairobi and Mr. John Bosco, the Geophysical expert at Treavic Geosystems & Engineering; the least I could say is thank you for your contribution towards this research paper.

Lastly my sincere gratitude goes to my fellow classmates for the knowledge and advice they have been able to share with me throughout my time as an undergraduate student at the university.

God bless you all.

To God be the glory.

DECLARATION

I hereby declare that this project report entitled:

**Evaluation of volcanic ash along Maai Mahiu-Narok road and its effect on road stability
after long rains**

is written by me and is my own effort and that no part has been plagiarized without citations.

SIGNED:

DATE:

AMOLLO O. KENNETH

2016.

CERTIFICATION

I have read this report and approve it for examination

SIGNED:

DATE:

DR.ENG. S.N. OSANO

2016.

Table of Contents

Abstract.....	ii
Dedication.....	iii
Acknowledgement	iv
Chapter One Introduction	1
1.1 General.....	1
1.2 Problem statement.....	1
1.3 Historical cases	7
1.4 Scope and Objectives	9
Chapter two Literature review	11
2.1 Introduction.....	11
2.2 Parent Materials	11
2.3 Distribution	12
2.4. Classification.....	12
2.5 Soil Liquefaction.....	14
2.6 Fault lines and Seismic Activities	15
2.7 Geology of the region.....	17
Chapter three Methodology	21
3.1 Electrical Resistivity Method.....	21
3.2 Multi-Channel Analysis of Surface Wave (MASW) Method	22
3.3 Fixed Receiver Spread Configuration (FRSC)	27
3.4 Geological Study.....	27
3.5 Field sampling procedure	29
3.6 The proposed work-plan	31
3.7 Statistical analysis.....	33
3.8 Expected results	34
Chapter four: Results and Analysis.....	35
4.1 Bulk density	35
4.2 Atterberg limits	37
4.3 Particle size	37
4.4 Specific gravity	41
4.5 Proctor compaction	44

4.6	California Bearing Ratio	47
4.7	Shear strength.....	48
4.8	Consolidation	50
4.9	Geology of the region.....	51
4.10	Climate and vegetation.....	58
4.11	Hydrological analysis.....	59
4.12	Physiography and drainage	61
4.13	Electrical resistivity tomography survey (ERT)	63
4.14	Multi-Channel Analysis of Surface Waves (MASW).....	67
Chapter five: Discussion		81
5.1	Soil Structure	81
5.2	Soil Liquefaction.....	82
5.3	Fault lines and Seismic Activities	82
5.4	Sink holes.....	82
5.4	Field Observations	84
Chapter six: Conclusion		84
Chapter seven: Recommendations		84
References		86
Appendix		88

Table of Tables

Table 1: <i>1D MASW Data Acquisition Parameters</i>	24
Table 2: <i>2D MASW Data Acquisition Parameters</i>	26
Table 3: <i>Bulk density of the sample</i>	36
Table 4: <i>Particle size analysis for Cu and Cc</i>	41
Table 5: <i>Specific gravity ranges for different soils</i>	42
Table 6: <i>Specific gravity values for samples</i>	43
Table 7: <i>Proctor Compaction test results</i>	45
Table 8: <i>CBR Range for soils with different strength properties</i>	47
Table 9: <i>Test results for CBR</i>	48
Table 10: <i>Typical factor of safety values for geotechnical works</i>	49
Table 11: <i>Bearing capacity of samples</i>	50
Table 12: <i>Consolidation test results</i>	50
Table 13: <i>Spatial Variability of Average Annual Surface Water Availability</i>	60
Table 14: <i>List of Equations used to calculate Elastic/Dynamic Parameters</i>	78
Table 15: <i>Ranges of the calculated elastic parameters of the lithological units within the project site</i>	78
Table 16: <i>List of Equations used to calculate Engineering Parameters</i>	79
Table 17: <i>Ranges of engineering parameter results for the subsurface layers</i>	80
Table 18: <i>Summary of Ranges of the calculated engineering parameters of the bedrock layers</i>	80

Table of Figures

Figure 1: <i>Maai Mahiu-Narok Road</i>	1
Figure 2: <i>(a) Cracks along the road and (b) Repair works at the damaged section which started on May 19, 2012 causing a heavy traffic snarl-up</i>	2
Figure 3: <i>Pictures taken on 10th October, 2015 showing the current status of the fissures that formed on 19th May 2012</i>	3
Figure 4: <i>A section of recurrent pavement failure</i>	3
Figure 5: <i>RHS of the fissure on Maai Mahiu road</i>	4
Figure 6: <i>Other developing fissure on Maai Mahiu-Narok road</i>	4
Figure 7: <i>The Maai Mahiu-Naivasha C88 Road fissure</i>	5
Figure 8: <i>The mysterious crack measures 100m wide and 3km long. (Courtesy; pan P, 2011)</i>	8
Figure 9: <i>General soil classification map of Kenya</i>	13
Figure 10: <i>Types of Fault Movement</i>	17
Figure 11: <i>Vesicular basalts within the project area</i>	20
Figure 12: <i>Wenner Method Test circuit arrangement</i>	21
Figure 13: <i>Electrical Resistivity Imaging model. Source: Fieldwork by Johnbosco</i>	22
Figure 14: <i>1D MASW survey spread configuration</i>	23
Figure 15: <i>Example of 1D MASW output</i>	25
Figure 16: <i>Example of 2DMASW Final Output</i>	26
Figure 17: <i>2D MASW Cross-sectional Models for previous project carried out by Johnbosco</i>	27
Figure 18: <i>A) Fresh developing crack on the road pavement; B) Fissure developed during the period when the road was cut off; and C) Wide fissure formed northwest of the research project area.</i>	28
Figure 19: <i>Schedule of works</i>	33
Figure 20: <i>(a) Sampling for bulk density investigation; (b) wrapping of the samples in polythene bags to avoid moisture loss</i>	35
Figure 21: <i>Bulk density histogram</i>	36
Figure 22: <i>Plastic limit by casagrande method</i>	37
Figure 23: <i>Wet sieving and hydrometer analysis</i>	38
Figure 24: <i>Particle size curve for trial pit 1</i>	38
Figure 25: <i>Particle size curve for trial pit 2</i>	39
Figure 26: <i>Particle size curve for trial pit 3</i>	39
Figure 27: <i>Particle size curve for trial pit 4</i>	40
Figure 28: <i>Specific gravity at the laboratory</i>	42
Figure 29: <i>Line graph comparing specific gravity of samples tested</i>	43
Figure 30: <i>Compaction test</i>	44
Figure 31: <i>Compaction graph TP1</i>	45
Figure 32: <i>Compaction graph TP2</i>	46
Figure 33: <i>Compaction graph TP3</i>	46
Figure 34: <i>Compaction graph TP4</i>	47
Figure 35: <i>CBR values analysis</i>	48
Figure 36: <i>(a) Shear box test being conducted; (b) Oven drying of the samples after being tested</i>	49

Figure 37: Settlement analysis of the samples	51
Figure 38: Source: Mines and Geological Department, Government of Kenya	52
Figure 39: Source-Geological map of Kenya: Ministry of Energy and Regional Development of Kenya.	53
Figure 40: Source: Mines and Geological Department, Government of Kenya	54
Figure 41: Source: Mines and Geological Department, Government of Kenya	55
Figure 42: (a) Pumice observation on the southern part of the project area (b) Volcanic ash and black sand (GPS reading 37M0216126, 9904912).....	56
Figure 43: (a) Stratified pyroclastic materials on the western part of the site (b) Stratified pyroclastic materials with lapilli at the base on the western part of the site	56
Figure 44: Stratigraphy of the volcanic ash is well displayed on river bank cut (River Kedong).....	57
Figure 45: Lapilli samples floating on water.....	58
Figure 46: Map of rivers within area of study.....	59
Figure 47: Section of the road that was washed away.....	60
Figure 48: Part of the Dry Water Bed of river Tongi Tongi	61
Figure 49: A) Flooded road at the Longonot town center, B) A section of the Maai Mahiu-Naivasha highway.....	62
Figure 50: A section of Registry Index Map for Kijabe/Kijabe Block 1 (Sheet 4).....	63
Figure 51: Gravelly to loamy fine sand formation.....	64
Figure 52: Modeled resistivity section along the Electrical Resistivity Tomography (ERT) Profile 1	65
Figure 53: Modeled resistivity section along the Electrical Resistivity Tomography (ERT) Profile 2	65
Figure 54: Modeled resistivity section along the Electrical Resistivity Tomography (ERT) Profile 3	66
Figure 55: Seismic lines and site Classification zones	69
Figure 56: a) Dispersion Curve, b) 1D shear wave velocity and c) 2D shear wave velocity model	70
Figure 57: a) Dispersion Curve, b) 1D shear wave velocity and c) 2D shear wave velocity model	71
Figure 58: a) Dispersion Curve, b) 1D shear wave velocity and c) 2D shear wave velocity model for spread 3	73
Figure 59: a) Dispersion Curve, b) 1D shear wave velocity and c) 2D shear wave velocity model for spread 1	74
Figure 60: a) Dispersion Curve, b) 1D shear wave velocity and c) 2D shear wave velocity model for spread 2	75
Figure 61: a) Dispersion Curve, b) 1D shear wave velocity and c) 2D shear wave velocity model for spread 3	77
Figure 62: Road surface remained intact.	81
Figure 63: Development of sink holes as a result of subterranean erosion.	83
Figure 64: No horizontal or vertical displacements occurred.	83

Table of Appendices

Appendix I: Bulk Density	88
Appendix II: Specific Gravity	90
Appendix III: Particle size distribution	91
Appendix IV: Sieve and Hydrometer Analysis	92
Appendix V: Proctor Compaction	104
Appendix VI: California Bearing Ratio	110
Appendix VII: Consolidation	114
Appendix VIII: Direct Shear Box	122
Appendix IX: Atterberg Limits	126
Appendix X: Electrical Resistivity Tomography	130
Appendix XI: MASW Dispersion curves	133
Appendix XII: Geophone coordinates	141
Appendix XIII: Field photos	148

Acronyms

XRD	X-Ray Diffraction
SEM	Scanning Electron Microscopy
ERT	Electrical Resistivity Tomography
MASW	Multi-channel Analysis of Surface Wave
MTRD	Materials Testing and Roads Department
KRB	Kenya Roads Board
KENHA	Kenya National Highways Authority
HGV	Heavy Goods Vehicle
RQD	Road Quality Designation
OMC	Optimum Moisture Content
MDD	Maximum Dry Density
BS	British Standards
ASTM	American Society for Testing Materials
AASHTO	American Association of State Highway and Transportation Officials
WRB	World Reference Base
K	Potassium
RHS	Right Hand Side

Chapter One Introduction

1.1 General

Kenya has a very wide range of soils that resulted from the variation in geology of the parent material, in relief and climate. Soil resources vary from sandy to clayey, shallow to very deep and low to high fertility. However, most of them have serious limitations such as salinity, acidity, fertility and drainage problems. The major soils used in agriculture are ferralsols, vertisols, Acrisols, Lixisols, Luvisols and Nitisols (Gachene & Kimaru, 2003).

1.2 Problem statement

1.2.1 Introduction

The Maai Mahiu - Narok highway in Kenya (Fig. 1) was closed on May 19, 2012 by the Kenya National Highway Authority after cracks emerged on the surface of the road. The width of the cracks when measured varied from 25.0 mm to 2.0 m (Fig. 2a). This came just days after huge gullies erupted in the surrounding region swallowing a house, trees and farmland. The gullies extended progressively and approached the main highway. Temporary repair works commenced immediately (Fig. 2b) to seal the cracks from May 19 to May 23 after which traffic flow was resumed.

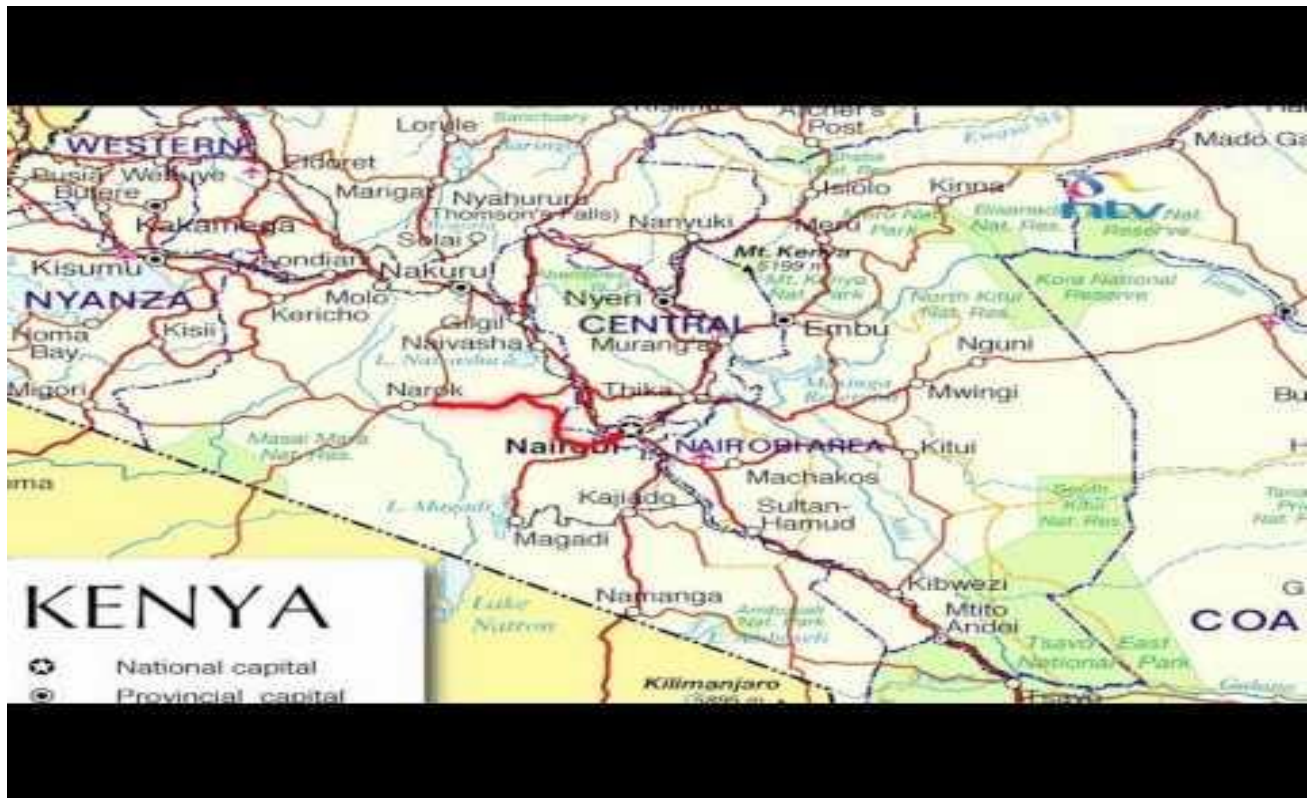


Figure 1: Maai Mahiu-Narok Road



(a)



(b)

Figure 2: (a) Cracks along the road and (b) Repair works at the damaged section which started on May 19, 2012 causing a heavy traffic snarl-up

1.2.2 Reconnaissance Survey Works

The researcher was tasked with the responsibility of conducting a rigorous evaluation on the causes of these fissures. The research was to provide a geotechnical, hydrological and geological input into the investigations and to process results in order to prepare a technical report of the research findings to mitigate such catastrophic occurrences from future re-occurrence.

As reported by Kirui in The Star Daily, Chairman of Narok Central Business Association said that traders had lost over KSh.150 million since the road was closed. Business people had incurred losses amounting to over KSh100 million while livestock traders who ferried their stock to Nairobi had run into losses of over KSh50 million because they had been forced to take longer routes. A visit was made to MTRD (Materials Testing and Roads Department) and KRB (Kenya Roads Board) offices in order to get a preview of what was to be expected on site visit.

After consultations with the officers from these departments; Mr. George O. Ogutu (MTRD) and Eng. Koskei (KRB), including looking into the minutes of an initial briefing that took place on 17th June 2015 at KRB offices, a site visit of the area was made and it was observed that the fissures still existed (Fig. 3a and b), with overgrown vegetation covering some of the cracks. Despite the repair work done, it was observed that the cracks have started developing again, which is an indication that the problem is eminent and not yet resolved.



(a)



(b)

Figure 3: Pictures taken on 10th October, 2015 showing the current status of the fissures that formed on 19th May 2012

The site visit interviews with the locals, the area Chief and visual inspection resulted in the following observations;

- a) At Km 1+900 from Maai Mahiu shopping center, a recurrent road failure occurring on a 5m wide spot had emerged (Fig. 4). On further inspection, it was noted that it could be a localized failure of pavement due to weak construction materials or poor subgrade. The pavement was also vibrating when trafficked by HGV ($\geq 30T$ trucks). The section of the road was currently being repaired by West Minister contractors who were working on site.



(a)



(b)

Figure 4: A section of recurrent pavement failure

- b) On the RHS there was no indication of fissures but the local Chief reported that this particular side is a flood plain (Fig. 5) with extensive silt deposits. A box culvert was placed approximately 50m from where the fissures occurred to help drain storm water.



Figure 5: RHS of the fissure on Maai Mahiu road

- c) At Km 9+400, occurrence of similar nature was observed (Fig. 6). On inspection it was concluded that there was manifestation of developing fissures from offsets where river flows. A cross culvert has been constructed at this locations.



Figure 6: Other developing fissure on Maai Mahiu-Narok road

- d) At a completely different location, at Km 5+500 from Maai Mahiu shopping centre 200m off the Maai Mahiu – Naivasha road, a similar manifestation of fissures was observed. The fissure here is as wide as observed on the Maai Mahiu – Narok B3 road but is far from the road (Fig. 7). The Chief explained that there was a water pan on a borrow pit previously excavated for rehabilitation of the road. The fissure drained all the water and cutting an access road. The exact timing of occurrence was not given but comparing the shape and status of the vegetation it was likely around the same time.



Figure 7: The Maai Mahiu-Naivasha C88 Road fissure

1.2.3 Past Researches

Laboratory simulation of field stress-strain conditions under a pavement and the evaluation of the Modulus / Time relationship for murrum, red soil and black cotton soils were conducted by Gichaga, (1971). Tests were carried out in a triaxial apparatus under static loading conditions on a closed drainage system. He concludes that traffic loads exhibit dynamic effects on subsoils due to their short duration and the development of distortional deformations due to the creep phenomenon of soils is a function of time.

Gichaga (1971) results indicate that with poor drainage conditions and with increased degree of saturation, the shear strength of soils decrease under a pavement structure. These findings are in agreement with work done by Onyancha *et al* (2009) who concluded that differential movement of foundations is largely caused by differences in moisture content as the soil strength weakens.

Shallow investigations of the fissures were conducted by Otieno Otieno Denis, as a Final year Project, supervised by Dr. S.N. Osano of Department of Civil Engineering, University of Nairobi. Their findings were that the fault line activity indicated that the failure was as a result of the subterranean erosion along the existing fault line which occurred due to heavy flooding. The overlying unconsolidated volcanoclastic sediments became oversaturated with water. The water reduced the shear strength of the sediments and also introduced extra loading through saturation leading to subterranean erosion along the fault line. The unconsolidated sediments then collapsed into the subsurface water channels which closely followed the fault zones, leading to formation of “sinkholes”.

Kenneth B. A. and Greg Usher (2011) studies the potential of Longonot area for a potential development of a geothermal system, located in the Kenya Rift Valley NW of Nairobi and 10 km East of the Olkaria Domes geothermal field. Mt Longonot, a trachytic stratovolcano SE of Lake Naivasha, is in an area of active west-to-east extension (the Rift Valley) as well as an area of crustal uplift and thinning (the Kenya Dome). Results obtained during a comprehensive geological, geochemical and geophysical field program in 2010 were being used to develop a conceptual model of this high-temperature system. The findings indicate that this area, which is also adjacent to where the fissures occurred, has extensive weak volcanic soils and flowing underground water system that results in liquefaction of the underlying soils strata. The formation of the fissures could have been as a result of this complex readjustment of the soil strata as a result of the volcanic activities taking place.

1.3 Historical cases

Cracks and fissures are mostly caused by earthquakes, heavy rain, mudslides, and tectonic plates moving. The following are some of the cracks recorded in history;

(a) Arizona, USA - September 11, 1927

An earth fissure or crack in the ground, believed to be of unusual origin occurred on September 11, 1927 at a point 3 miles South East of Picacho, Arizona, USA, after a severe rain and wind storm of the afternoon and night before (Leornard, 1929).

(b) Iceland - October 1, 2001

Icelanders are accustomed to their land being stretched, split, and torn by violent earthquakes and haphazardly rebuilt by exploding volcanoes. But everyone was surprised when a large lake began to disappear into a long fissure created by a previous summer's earthquakes (Bijal, 2001).

(c) Ethiopia - September 2009

A crack in the Earth's crust – which could be the forerunner to a new ocean – ripped open in just days. The opening was located in the far region of Ethiopia. It began to open up in September 2005, when a volcano at the northern end of the rift, called Dabbahu, erupted (MacGregor C., 2009).

(d) Queen Creek, Arizona, USA - February 14, 2010

This well-known "Y-crack" earth fissure near Queen Creek, south of Phoenix, occurred following heavy rainstorms. The hole opened around four residential water valves. It was approximately 20 feet deep.

(e) Birch Creek, Alaska, USA - June 10, 2010

One day the land was flat and filled with trees shooting straight into the air. Twenty-four hours later there was a 600-ft-long crack and 4-ft deep twisting its way through the woods - and those vertical trees were then pointed 30 degrees left and right where the earth had mounded 15 feet high.

(f) Menominee, Michigan, USA – October 8, 2010

A large crack suddenly appeared after what seemed like an earthquake in Menominee Township of Michigan, USA. This crack was over 600 ft long and 5 ft deep.

(g) Chucuito, Southern Peru - February 25, 2011

The sudden appearance early in the morning of an enormous crack, measuring 100 m wide and 3 km long caused confusion among residents of the Huacullani District in the Chucuito Province, Southern Peru (Fig. 8).



Figure 8: *The mysterious crack measures 100m wide and 3km long. (Courtesy; pan P, 2011)*

(h) Nantou, Taiwan - March 15, 2011

A large crack measuring 20 m long appeared on the ground at a local elementary school in Lushan of Nantou County.

1.4 Scope and Objectives

The primary objective of this research is to investigate the state and properties of underlying volcanic soil along Maai Mahiu - Narok Road in Kenya during the long rain season of February to May 2012 and its effect on road stability.

Following the reconnaissance survey works, it is observed that the fissure occurrence is largely a geological and a geotechnical engineering problem. The general behavior is that the problem affects a bigger area and not a localized phenomenon.

In order to conclusively research this phenomenon, the following areas are highlighted as the key areas of interest to this project;

- a. Geology of the area;
- b. Hydrology of the area, extending to the surrounding hills;
- c. Geotechnical engineering of the underlying soils, to be aided by deep exploration works;
- d. Engineering solution to preservation of the road in geologically active areas.

To meet the primary objectives, the research work will be comprised of four key components:

- i. Geophysical Analysis (2D ERT and MASW)
- ii. Geological Analysis (Geological Structural Analysis of the area e.g. Faults)
- iii. Geotechnical Analysis (Drilling and Laboratory testing)
- iv. Hydrology of the area,

A detailed description is as follows;

a) Geophysical Analysis (2D ERT and MASW)

Seismic surveys (MASW) and Topographic surveys

Multi-Channel Analysis of Surface Wave (MASW) method is a non-invasive method recently developed to estimate in shear wave velocity profile from surface wave energy. This research shall discuss the MASW technique for measuring shear wave velocities and for the delineation of possible liquefaction potential in 2D within the project problem area.

Deep seismic survey will deliver an overall picture of the stratigraphy and tectonic situation of the target area. Topographic survey work will result in the 3D modeling of the site surface.

2D Electrical Resistivity Tomography (ERT)

The Resistivity Survey shall be used to investigate the hydrogeological conditions of the underlying soil mass, possible presence of quick sands, moist silt mass and possible presence of

fault gouges within the study area. The interpretation of the ERT surveys will provide the ground model allowing selection of locations with anomalies that will require borings for sampling.

b) Physical Geological Survey

Geological mapping shall be focused on the tectonics and faults within the research area. This component of the research project was included after intuitively realized that the cracks on the road pavement are aligned in the same orientation as fault trend during the reconnaissance study.

c) Boring campaigns

The interpretation of the seismic surveys and ERT will provide the ground model allowing selection of locations for borings. 4No. boreholes at a grid of 500m x 500m will be explored. The depth of exploration will be confirmed on site but will not be lower than 10m for each borehole. The information obtained from the high quality deep borings will allow an understanding of the stratigraphic, tectonic and geotechnical conditions in the area.

d) Hydrology

A scientific study of the movement, distribution, and quality of water on the site and the surrounding environment, including the hydrologic cycle, water resources and environmental watershed will result in 3D modeling of the events before, during and after the fissure occurrence.

Laboratory testing

The laboratory testing will include pilot and production testing. The objective of the pilot testing will be to clarify procedures to be applied during production testing. The objective of the production testing will be to establish soil properties as measured in the laboratory as small scale testing with the identified procedures. A considerable number of laboratory tests such as different kinds of oedometer tests, triaxial tests and direct simple shear tests will be performed for the different soil units.

These geological, hydrological and geotechnical investigations will answer the following questions:

- (a) Why did the fissures occur?
- (b) Will the process of fissure formation occur again?
- (c) Are there measures to be taken to mitigate against the formation of the fissures?

Chapter two Literature review

2.1 Introduction

Many volcanic soils have excellent physical properties that make them highly desirable for a wide range of uses. Chemically, they suffer from high phosphate retention, and they may be limiting in K and some micronutrients.

Volcanic soils cover 1% of the Earth's surface yet support 10% of the world's population, including some of the highest human population densities. This is usually attributed to their high natural fertility. However, this is true only in part. Clearly such soils represent the surface areas of our planet that are being replenished with new minerals escaping from the interior of the Earth. However, some deep magmatic processes do lead to an imbalance of elements in volcanic soil parent materials which can impact on the health of plants and animals growing in or on them. In contrast, all other soils express various stages of the degradation (weathering) of these minerals (Takahashi & Shoji, 2002).

2.2 Parent Materials

This grouping of soils is found only on volcanic parent materials. Few other soils are restricted to a single type of material except organic soils derived from peat, and rendzinas from limestone. Only under strong tropical weathering will lavas weather to finer grained volcanic soils, so it is usually parent materials of a volcanoclastic origin which result in the high-producing volcanic soils of the world. Volcanoclastics are usually grouped into two main divisions of pyroclastic (explosive) and epiclastic (erosional) origin. Pyroclastics include the deposits of incandescent, high velocity gas charged clouds with entrained rocks and sand; close to source ballistics that include molten volcanic bombs or vesiculated scoria (or cinders); and aerially ejected particles that travel high into the atmosphere (tephra) before falling back to earth, usually cold. Tephra particles range from ash (<2 mm), to lapilli (2-64 mm), to blocks (solid) and bombs (molten) (>64 mm). Epiclastics include all the forms of volcanoclastic remobilization on the landscape post-deposition and include deposits from volcanic debris avalanches; volcanic mudflows, debris flows and hyper-concentrated streamflows (lahars); alluvium on the flanks of a volcano; and volcanic loess (deposited by the wind in more arid and high altitude environments). Out of soils directly formed from lava, it is basaltic lavas that form the most extensive volcanic soil parent materials because of this lava's low viscosity and ability to flow large distances on low gradients (Ping, 2000).

Irrespective of the chemical composition of the volcanics, all will contain varying proportions of volcanic glass which provides the initial distinctive weathering products of this soil grouping. Two other variables are the initial grain size and the vesicularity of the parent materials. For example, a dense, high silica rhyolite will weather considerably more slowly than a less dense and highly vesicular pumice of identical composition. This is mainly related to the

much greater surface area available in the pumice to weather and break down to primary weathering products.

Volcanic soils are usually the dominant soil in young volcanic landscapes (but may be in association with lesser areas of other soils such as organic soils). Coarser textured soils tend to occur on the flanks of most stratovolcanoes, shield volcanoes and tuff cones, as well as in proximity to calderas, where they are usually pumice dominant.

2.3 Distribution

Volcanic soils cover more than 124 million hectares of the Earth's surface. The major areas of volcanic soils rim the Pacific where oceanic plate subduction produces extensive rhyolitic and andesitic volcanism. Major areas of volcanic soils occur in Chile, Peru, Ecuador, Colombia, Central America, the United States, Kamchatka, Japan, the Philippines, Indonesia, New Zealand, and the independent island states of the South-West Pacific. Basaltic volcanism dominates in the islands of the Pacific, Indian and Atlantic oceans where new lithosphere is being added to existing plates, such as in Iceland or where hot mantle plumes pierce through the lithosphere, as in Hawaii.

The second major area of volcanic soils extends along the East African Rift Valley where the Nubian and Somalian plates diverge, and through the Mediterranean region where the Nubian and European plates converge. The third significant region is in the equatorial Atlantic, principally comprising the Canary Islands and the Azores, plus the many islands of the West Indies, where volcanic soils are a major natural resource to the economies of many small island states (Gachene & Kimaru, 2003).

2.4. Classification

An in-depth study and classification of volcanic soils received major attention in the second half of the 20th century. The aim was to quantitatively define what is meant by a volcanic soil, in particular in countries of the circum-Pacific margin. In Japan, these soils carried an unusually dark black topsoil (epipedon) assigned by the name "ando" or dark soil. Apparently, these black surface layers are not so much a result of the volcanic origin but of a property inherited from the original vegetation.

When the FAO/UNESCO (1974) Soil Map of the World was compiled, there was international agreement that volcanic soils be designated in their own order of Andosols. Key criteria included a low bulk density ($<0.85 \text{ g/cm}^3$ in the $< 2 \text{ mm}$ fraction at $- 33 \text{ kPa}$ water retention); an exchange complex dominated by amorphous material; and/or $\geq 60\%$ vitric volcanic ash, cinders or other vitric pyroclastic material in the profile. Four suborders were recognized, three of them being based on the nature of the organic horizon at the surface; they were

distinguished into Mollic, Humic and Ochris Andosols. The fourth suborder identified the glassy or pumiceous Vitric Andosols (Soil Taxonomy, 1999).

The soils around the study area have been studied to have low bulk densities (MTRD, Issa Ismael *et al*).

The low bulk density will be helpful in determining the vertical variation of the density and confirm and possible liquefaction levels.

The general soil classification map of Kenya is shown in Fig. 9.

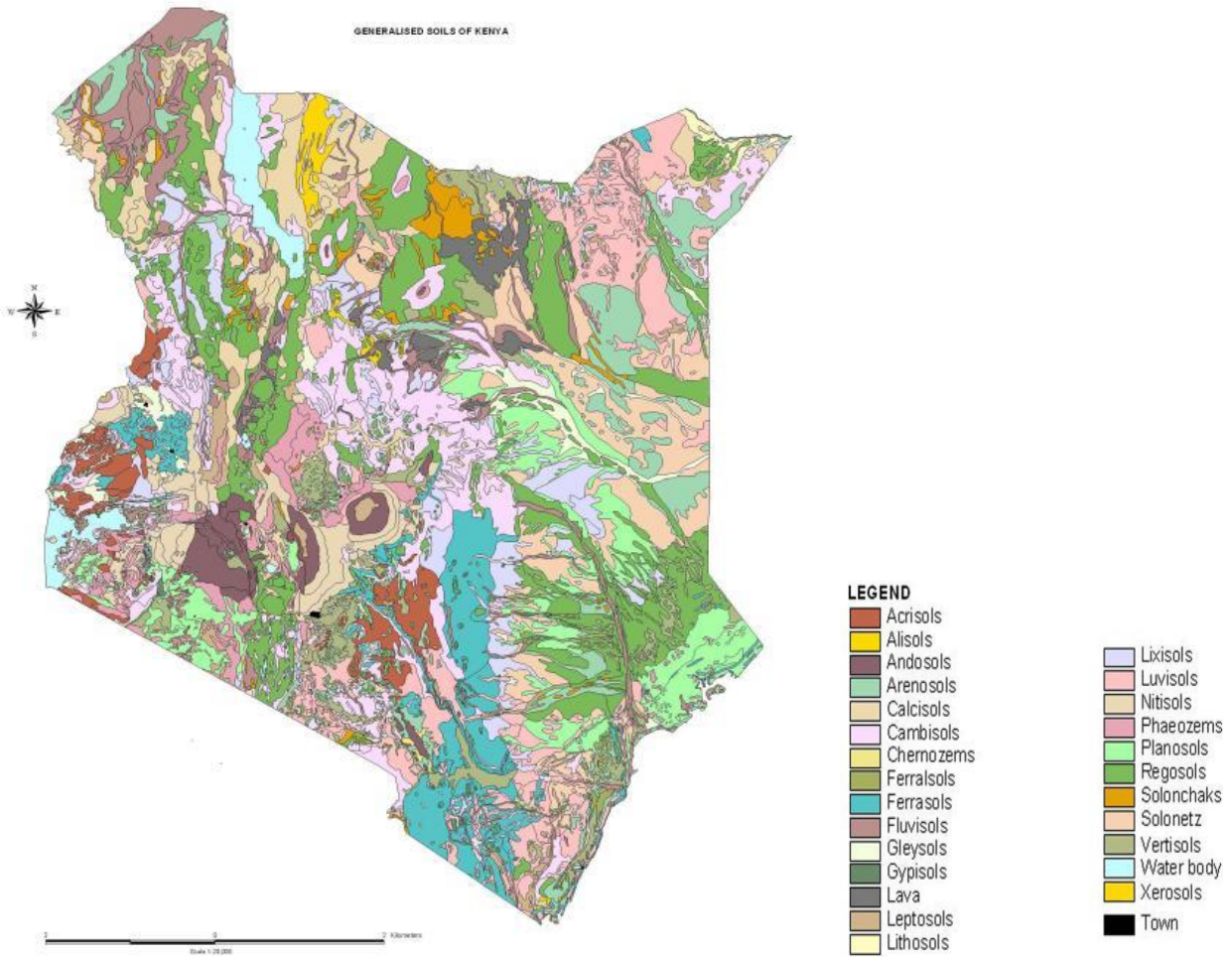


Figure 9: General soil classification map of Kenya

2.5 Soil Liquefaction

According to Salcon (1997), soil liquefaction is a phenomenon whereby a saturated or partially saturated soil substantially loses strength and stiffness response to an applied stress, usually earthquake shaking or other sudden change in stress condition, causing it to behave like a liquid. Liquefaction occurs when the pressure of the water in the pores is great enough to carry the entire load; it will have the effect of holding the particles apart and of producing a condition that attempts to flow out from the soil to zones of low pressure usually upward towards the ground surface. However, if the loading is rapidly applied and large enough, or is repeated many times such that it does not flow out in time before the next cycle of load is applied, the water pressures may build to an extent where they exceed the contact stresses between the grains of soil that keep them in contact with each other.

These contacts between grains are the means by which the weight from buildings and overlying soil layers are transferred from the ground surface to layers of soil or rock at greater depths. This loss of soil structure causes it to lose all of its strength that enables it to transfer shear stress and it may be observed to flow like a liquid hence liquefaction (Toumie et al, 2003). Davis et al (2003) notes that, when undertaking the construction of roads, engineers need to understand the effects of liquefaction on the failure of roads.

The destruction of the road section along Maai Mahiu-Narok road could have been as a result of soil liquefaction where effective stress of soil is reduced to zero with a complete loss of shear strength. Additionally, cyclic loading due to shaking that exerts repeated change in soil stress condition causes soil saturation. The soil is in a loose state and generates significant pore water pressure on a change in load and is most likely to liquefy (Hoyle & Woods, 1997). This is because a loose soil has the tendency to compress when sheared, generating large excess pore water pressure as load is transferred from the soil skeleton to adjacent pore water during undrained loading.

Strain-softened soils, such as loose sands, can be triggered to collapse, either monotonically or cyclically, if the static shear stress is greater than the ultimate or steady-state shear strength of the soil (Toll & Ong, 2003). In this case flow liquefaction occurs, where the soil deforms at a low constant residual shear stress. If the soil strain-hardens, such as moderately dense to dense sand, flow liquefaction will generally not occur.

The resistance of less cohesive soils to liquefaction will depend on the density of the soil, confining stresses, soil structure which includes fabric, age and cementation. It also includes the magnitude with which shear stress reversal occurs. Pressure occurs when heavy vehicles commonly pass along the road repeatedly. Pressure is generated with continued shaking of the road causing the liquefied sand and excess water to force its way to the ground surface from several meters below the ground hence forming small volcanic craters (Salcon, 1997). It is evident that upward flow of water initiates liquefaction in overlying non-liquefied sandy deposits due to buoyancy. According to Kohler & Koenders (2003), land instability causes cracking due

to the movement of the ground towards unsupported margins of roads. It is evident that the effect of soil liquefaction on roads can be extremely damaging. Roads constructed on less cohesive soils that liquefy usually experience a sudden loss of support causing large cracks or fissures in the ground, and cause significant damage to bridges and roads among other services installed in the affected ground.

This results in drastic and irregular settlement of the road causing structural damage including cracking of foundations and damage to the building structure itself. It may also leave the road unserviceable afterwards, even without structural damage.

Where a thin crust of non-liquefied soil exists between building foundation and liquefied soil, a punching shear type foundation failure may occur (Jenkins & Hanes, 1998). The upward pressure applied by the movement of liquefied soil through the crust layer can crack weak foundation slabs and enter road structures through service ducts, and may allow water to damage the road contents. It is advisable for road engineers to determine the slope of the ground on where to construct roads. This reduces the chances of sliding on a liquefied soil layer hence causing large cracks or fissures in the ground, and cause significant damage to bridges and roads among other services installed in the affected ground.

2.6 Fault lines and Seismic Activities

According to Civjan et al (2000), roads serve as critical lifelines in the delivery of basic daily needs. Therefore, it is important to ensure that they function even in the face of adverse weather and natural hazards. Natural disasters such as earthquakes, hurricanes, and floods can be costly natural disasters that lead to failure of roads. An earthquake is a sudden ground motion or trembling caused by an abrupt release of accumulated strains acting on the tectonic plates that comprise the Earth's crust. Earthquakes often trigger other devastating events such as landslides, fires and lateral spreads such as displacements of sloping ground, primarily due to soil liquefaction. In addition to destroying buildings, earthquakes can damage bridges, tunnels, pavements, and other components of highway infrastructure. Roussell et al (2000) argue that, relatively speaking, the probability of large, destructive earthquakes is much lower than hurricanes and floods. Nevertheless, an earthquake can, without warning, ravage an enormous area in less than 2 minutes through ground shaking; surface fault rupture which is displacement due to the movement of tectonic plates, and ground failures such as landslides, liquefaction, and lateral spreads (Dan, 2002).

However, faults related to past tectonics may be reactivated by present-day tectonics in seismically active areas and can also be activated by anthropogenic (man-made) activities such as impoundment of a reservoir by a dam or injection of fluids such as waste liquids deep into the subsurface (Jefferies, 2006). The maximum size of an earthquake on an anthropogenically reactivated fault is a subject of some controversy. Not all faults along which relative movement

is occurring are a source of earthquakes. Some faults may be on surfaces along which relative movement is occurring at a slow, relatively continuous rate, with an insufficient stress drop to cause an earthquake. Such movement is called fault creep (Emerson, 2002).

Fault creep may occur along a shallow fault, where the low overburden stress on the fault results in a relatively low threshold stress for initiating displacement along the fault. Alternatively, a creeping fault may be at depth in soft and/or ductile materials that deform plastically. Also, there may be a lack of frictional resistance or asperities (non-uniformities) along the fault plane, allowing steady creep and the associated release of the strain energy along the fault. Fault creep may also prevail where phenomena such as magma intrusion or growing salt domes activate small shallow faults in soft sediments (Bardet, 1996).

Faults generated by extraction of fluids such as oil or water which causes ground settlement and thus activates faults near the surface may also result in fault creep. Faults activated by other non-tectonic mechanisms like faults generated by gravity slides that take place in thick, unconsolidated sediments, could also produce fault creep. Active faults that extend into crystalline bedrock are generally capable of building up the strain energy needed to produce, upon rupture, earthquakes strong enough to affect transportation facilities. Fault ruptures may propagate from the crystalline bedrock to the ground surface and produce ground rupture. Fault ruptures which propagate to the surface in a relatively narrow zone of deformation that can be traced back to the causative fault in crystalline rock are sometimes referred to as primary fault ruptures (Civjan et al, 2000). They may also propagate to the surface in diffuse, distributed zones of deformation which cannot be traced directly back to the basement rock. In this case, the surface deformation may be referred to as secondary fault rupture.

There are different types of faults that may be broadly classified according to their mode, or style of relative movement or displacement as discussed below.

2.6.1 Strike Slip Faults

These are faults along which relative movement is essentially horizontal. Here, the opposite sides of the fault slide past each other laterally. Strike slip faults are often essentially linear or planar features. Strike slip faults that are not fairly linear may produce complex surface features. Strike slip faults may sometimes be aligned in en-echelon fashion wherein individual sub-parallel segments are aligned along a linear trend. En-echelon strike slip faulting is sometimes accompanied by step over zones where fault displacement is transferred from adjacent strike slip faults. Ground rupture patterns within these zones may be particularly complex.

2.6.2 Dip Slip Faults

These are faults in which the deformation is perpendicular to the fault plane may occur due to either normal (extensional) or reverse (compressional) motion. Reverse faults are also referred to as thrust faults. Dip slip faults may produce multiple fractures within rather wide and irregular fault zones.

2.6.3 Other Special Cases

These are faults that show both strike slip and dip slip displacement and may be referred to as oblique slip faults.

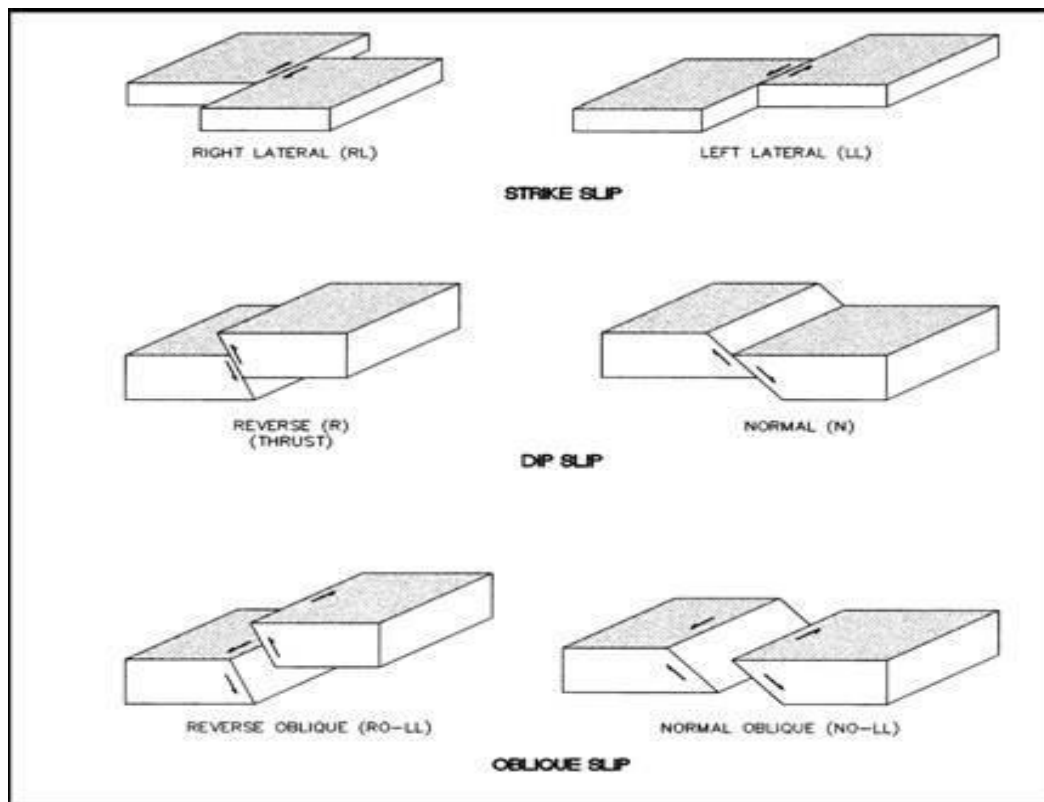


Figure 10: *Types of Fault Movement*

Source: (Reitherman & Robert, 2012)

2.7 Geology of the region

The bulk of the area falls in the Rift Valley Province of Kenya. This report describes an area of approximately 3,175 km² lying between longitudes 36°00'E and 36°30' E, and latitudes 0°0' S and 1°30' S in the Great Rift Valley. The area is surrounded by Suswa Mountain, a volcano of Quaternary age which is composed of phonolites and pyroclastics and mount Longonot of a similar volcanic origin. The remainder of the area is composed of basalts, alkali trachytes and pyroclastics of Upper Tertiary and Quaternary age. Locally, sediments are also present.

The research entailed mapping of the suswa area, along maai mahiu-Narok road toward mount Longonot. This involved a reconnaissance study with a series of field work following a photogeological exercise. The rapid fieldwork, the lack of age dates and problems of correlating lithologically-similar volcanic units in such a complex and strongly faulted area have unfortunately meant that there are several stratigraphic anomalies present in the report. However,

such anomalies have been reconciled by subsequent work, footnotes and appropriate references have been provided.

Maps for Preliminary Plot maps on the scale of 1:50,000 cover of the area were used in this survey. These are the GSGS 4786 Second Edition Sheets 147/I-IV. These maps were based on air photographs taken by the RAF between 1948 and 1952. A newer set of RAF photographs (on contract to the Survey of Kenya) were taken between 1960 and 1961 and were used routinely during this survey with their principle points marked on the map. None of the GSGS sheets at the scale of 1:50,000 were contoured, but the 1:250,000 Y503-Narok sheet has form lines for the whole area, and those produced on the map with this report are a combination of those form lines and spot heights taken during the survey with an aneroid barometer, and should be regarded as approximate only. Geological information was plotted in the field, directly onto the air photographs and was later transferred to the 1:50,000 maps.

2.7.1 Geological setting

The geological history of Maai Mahiu/Longonot area has been dominated by volcanic activity whereby a thick succession of alkaline lavas associated tuffs began accumulating in Mid-Miocene time and continued into Upper Pleistocene.

Practically the entire area is covered by these volcanic rocks derived from the Longonot Mountain and estimated to accumulate in huge volume and covering the entire project area. The main geologic formations in project area include trachytes, basalts, pumice, volcanic ash, lapilli and tuffs.

2.7.2 Regional Geological Formations

Longonot area is found in the Rift valley. The Rift Valley floor is filled by sediments and rocks of the Tertiary-Quaternary volcanic suite. Different episodes of volcanicity were always accompanied by faulting and fracturing.

The Maai Mahiu area, like any other area in the Rift Valley is filled by volcanic material and sediments of various ages and different origin. The Maai Mahiu Basin is covered by Pleistocene Volcanics overlain by younger Pleistocene and Holocene sediments, laid down during moist periods (pluvials) when a lake of varying size, covered much of the Rift floor between the present day Maai Mahiu and Narok. Lacustrine sediments are found on the surface of the entire Maai Mahiu Basin area except where erosion had removed them and also occur below and between the older volcanics. They are described in boreholes as being principally obsidic and trachytic, but more likely to be waterlain ash and other pyroclastic material intercalated within these formations, (Thompson 1958).

Geological formations at the site have been identified as the Olkaria Comendites with intercalated pyroclastics and sediments at depth; pantellerite laval flows, Akira pumice and lacustrine sediments.

2.7.3 The Stratigraphy of the region

a) Olkaria Comendites

Olkaria Comendites are sodic rhyolites (fine-grained to glassy acid volcanic rocks) erupted from vents within the Complex. They comprise individual domes formed of lava flows and/or welded pyroclastic rocks, or as thick lava flows of limited lateral extent.

b) Pantellerite Lava Flows

They occur as dark-coloured fine-grained or glassy to coarse-grained lavas. Obsidian and pumice are also abundant in the rocks of this area. These contain intercalated beds comprising of clayey and sandy material with a mixture of pyroclasts (scoriae, pumice and tuffs) which represent buried OLSs.

c) Akira Pumice

These consist of trachyte, syenite and agglomerate. In the trachyte and syenite lithics phenocryst contents and the coarseness of the groundmass vary considerably. The phenocryst includes anorthoclase, augite, sodalite, magnetite and rare subhedral fayalite and the groundmass is composed of glass, anorthoclase, sodic plagioclase, subpoikilitic aegerine-augite, magnetite and apatite.

d) Lacustrine sediments

Although a variety of sedimentary beds exist in the Naivasha area, the body of sediment that is relevant to the project area is that of the Gamblian Pluvial. These beds were laid down in a large lake that reached elevations of about 2000 m amsl some 70,000 years ago.

2.7.4 Geological Resources Available on the investigated

The study area is covered by very fine brownish soil derived from the underlying trachytes and basalts of Upper Pleistocene age. These are underlain by pyroclastics and sediments of Middle Pleistocene and lacustrine deposits which are of Quaternary age. To the south of the investigated area, the Quaternary pyroclastics and lacustrine deposits are exposed. Much of the pumice in the area is probably of normal rhyolitic composition, and it is known that some of the most recent phases of volcanicity have been characterized by pumice ejection. The pumiceous rhyolites are spongy, highly porous whitish to dirty grey rocks, usually able to float on water for a limited period.



Figure 11: *Vesicular basalts within the project area*

Chapter three Methodology

3.1 Electrical Resistivity Method

One of the hypotheses put forward for this research to the cause of the distress on the road pavement is the possible liquefaction of the saturated sandy volcanic soil especially during rainy seasons.

Currently, electrical resistivity imaging methods are mostly used in geohazard and environmental investigations to help characterize the liquefaction potential region. In many geological situations, 2D imaging surveys can give useful results that are complementary to the information obtained by other geophysical methods. The Schlumberger array is very sensitive to horizontal changes in resistivity, so it can be addressed to map vertical structures such as cavities, and buried objects. On the other hand, Wenner array can give useful information on vertical discontinuities, so the integration of the two methods (Wenner-Schlumberger) can be very important to understand the subsurface structure (McNeill, 1994; Jordant and Costantini, 1995; Loke, 1999). These two resistivity methods were used in the present research work. The objective of electrical sounding was to deduce the variation of electrical resistivity with depth below a given point on the surface, and to correlate it with geological knowledge in order to infer the subsurface structure in the greater detail. The horizontal resistivity profiling technique was used for the detection of lateral variation in a certain subsurface layer. Generally, the Wenner and Schlumberger arrays provided good vertical resolution for horizontal structures (Barker, 1981; Dahlin and Zhou, 2004). The technique involved measurements at a grid of observation points using an electrode array deployed at a fixed spacing.

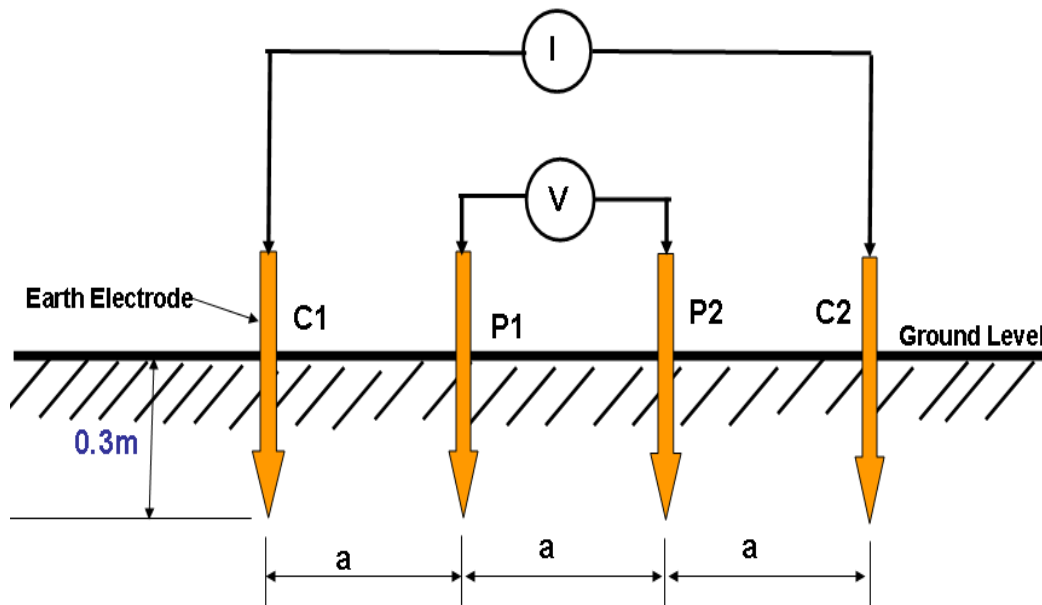


Figure 12: Wenner Method Test circuit arrangement

The 2-D electrical imaging/tomography surveys was carried out using a large number of electrodes, connected to a multi-core cable. A laptop microcomputer together with an electronic switching unit was used to automatically select the relevant four electrodes for each measurement. A constant spacing of 3m between adjacent electrodes was used. The multi-core cable was attached to an electronic switching unit which was connected to a laptop computer. The sequence of measurements to take, the type of array to use and other survey parameters (such the current to use) was entered into a text file which could be read by a computer program in a laptop computer. Different resistivity meters use different formats for the control file. After reading the control file, the computer program then automatically selected the appropriate electrodes for each measurement.

In a typical survey, most of the fieldwork is in laying out the cable and electrodes. After that, the measurements were taken automatically and stored in the computer. Most of the survey time was spent waiting for the resistivity meter to complete the sets of measurements. The analysis of the resistivity was done by RES2DINV software. The presence of low resistivity zones were construed to represent wet clay and wet sands which could be related to possible liquefaction material as a result of shaking of the ground from the traffic vehicles (Fig. 13 showing resistivity pseudosection for the past work done by Johnbosco). From the resistivity survey the hydrogeological status of the underlying soil mass sediments was studied. The study of liquefaction involved characterization of saturation levels that resulted in flow of the solid fractions in lightweight materials. From the resistivity results, the drilling program helped in detecting the potential depth targets for undisturbed sampling.

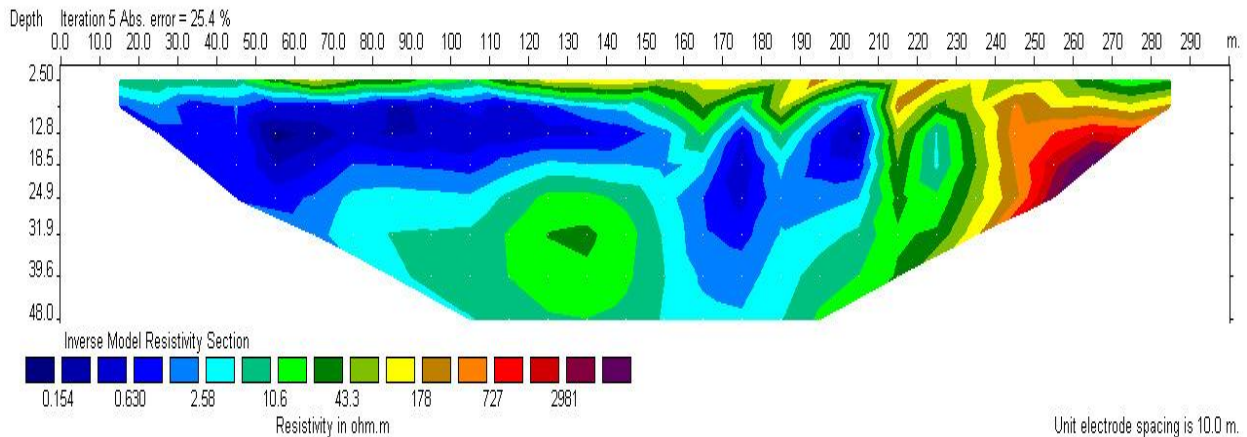


Figure 13: *Electrical Resistivity Imaging model. Source: Fieldwork by Johnbosco*

3.2 Multi-Channel Analysis of Surface Wave (MASW) Method

The MASW test is non-invasive, expedient, and cost effective. It was used to produce a single 1-D VS profile as well as 2-D VS profile that covered a wide range of area. Liquefaction potential analysis based on MASW imaging is effective for estimating the extent of potential liquefaction hazard, so as to justify further detailed investigation or plan ground improvement.

Shear wave velocity tests measured the small-strain shear modulus (stiffness) of the soil, and thus they represented an engineering property measurement rather than an index test.

During the fieldwork data acquisition, two methods were employed:

- 1D MASW Data Acquisition
- 2D MASW Data Acquisition

For data acquisition, 24 geophones were distributed in a line at spacing of 3 metres so as to achieve a depth of at least 30 metres below the ground level. A sledge Hammer of 20lbs was used to generate energy for the active 1D MASW data acquisition. For 1D MASW surveying, a linear spread configuration was used (Fig. 14 below). The geophones were configured in a straight line on the ground and interconnected with a spread cable (black line). The distance between the first and last active geophone was the *spread length* or *total offset* and the distance between the shot location and the nearest active geophone was the *near offset*. The resultant Vs curve was the average over the spread and accordingly was located at the centre of the spread.

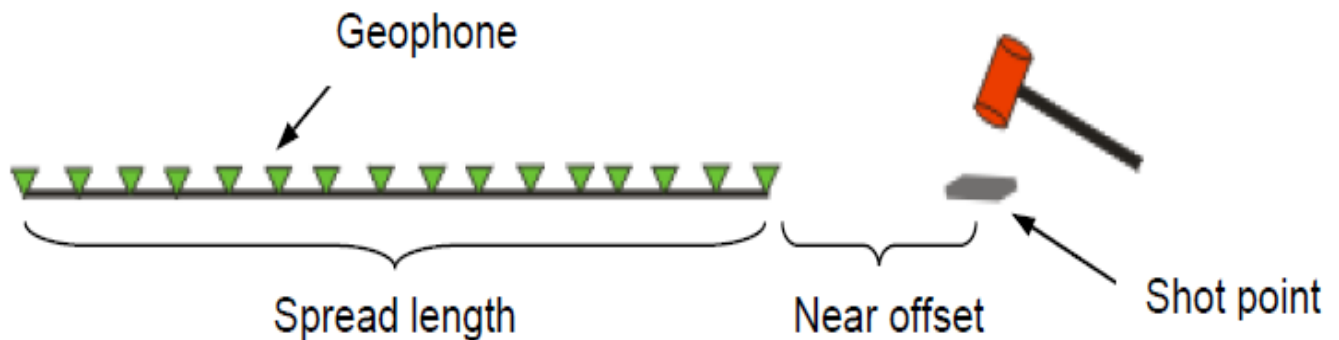


Figure 14: 1D MASW survey spread configuration

For an active source survey with a sledgehammer, a geophone interval of 3 meters was suggested. Using a 24-channel seismograph, it gave a spread length of 69 meters. Applying the one-half-wavelength (or spread length) rule of thumb, the depth of sampling was about 30 meters. Depending on the site materials and conditions, source energy from the Sledge Hammer of 20lbs (9.5kg) was used to propagate enough energy to all the channels. At least 2 shots per spread was used to acquire data, the near off shots (both forward and reverse shots) were 10 to 20% of spread length. To increase the quality of the data acquired, at least 5 stacking were done to improve data quality. Table 1 shows the acquisition parameters applied in this research work and Fig. 15 is the output.

Table 1: 1D MASW Data Acquisition Parameters

PARAMETER	SETTING
Spread configuration	Linear
Spread length	About equal to two times depth of interest (at least 20 m). The spread length was 46 m
Geophone interval	2 m
Total number of Geophones	24
Geophone type	4.5 Hz vertical geophones
Shot locations	Minimum of one shot, located in-line and off-end (either end) of spread; reverse shots suggested
Shot near offset	About 10 to 20% of spread length; an additional shot located at about 40% of spread length was suggested.
Source equipment	Sledgehammer (most common), 20 lbs (9 kg) and striker plate
Trigger	Hammer switch taped to sledgehammer handle and connected to seismograph trigger port
Sample interval	0.5 milliseconds (ms)
Record length	1 to 2 seconds (s), long enough to enclose the surface wave train.
Stacking	At least 5 times so as to improve data quality, shots were made at quiet times to allow full data acquisition.

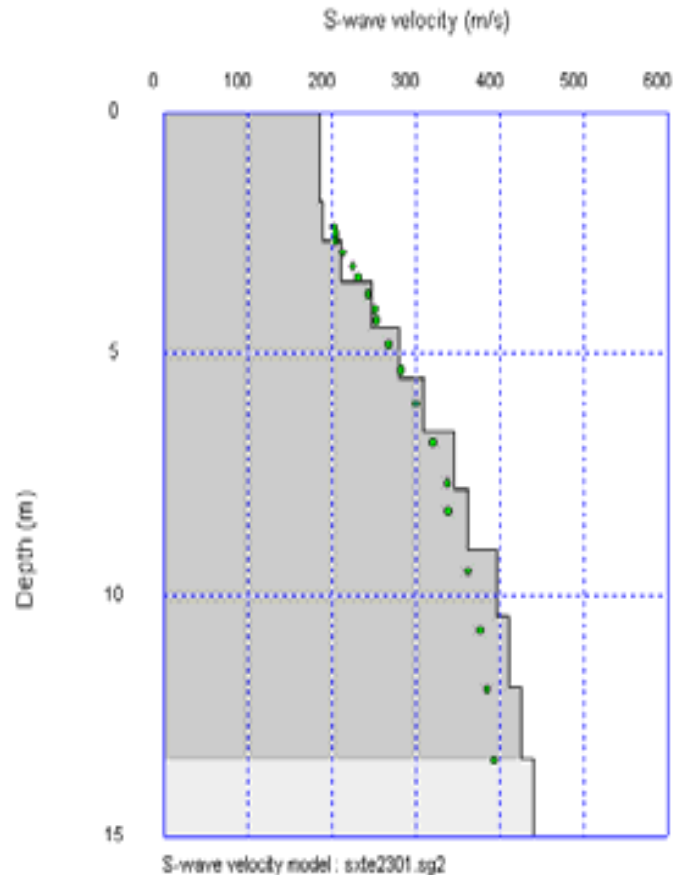


Figure 15: *Example of 1D MASW output*

As with 1D MASW surveying described above, 2D MASW surveys was used with an active source with a linear spread of geophones. Instead of one shot however as with the case of 1D, numerous shots were taken at incrementing locations, and the geophone spread was not fixed depending on the total survey line length. (Remember here that 1D and 2D refer to the type of results, that is, Vs curve or cross-section, respectively, not to the spread configuration.) Acquisition of numerous shot records allowed SeisImager/SW software to calculate a Vs cross-section. One method of data acquisition was applied depending on the length of the survey line and this included:

- Fixed Receiver Spread Configuration (FRSC)
- Continuous Fixed Receiver Spread Configuration (CFRSC)

The data acquisition parameters were the same as the 1D MASW described above. Table 2 is the data acquisition parameters and Fig. 16 the output.

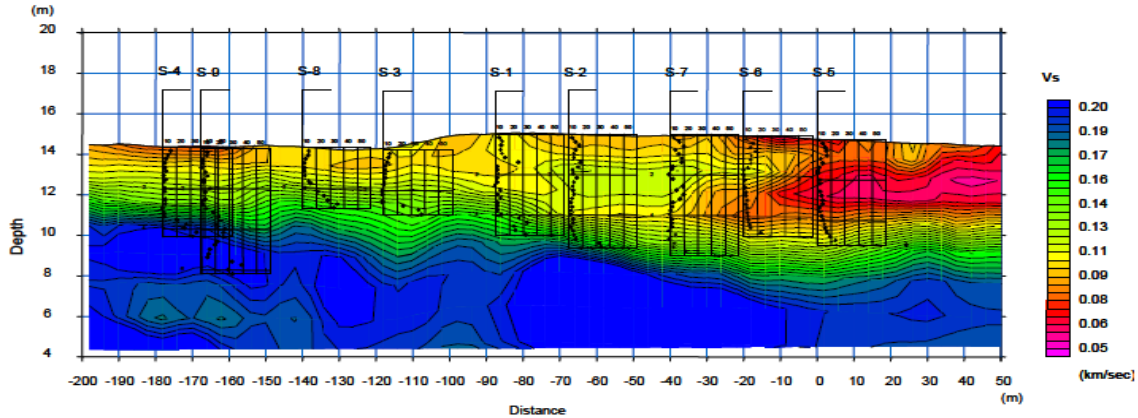


Figure 16: Example of 2DMASW Final Output

Table 2: 2D MASW Data Acquisition Parameters

PARAMETER	SETTING
Spread configuration	Linear
Spread length	About equal to two times depth of interest (at least 20 m). Spread length was 46 m
Geophone interval	2 m
Total number of geophones	24
Geophone type	4.5 Hz vertical geophones
Shot locations	Minimum of one shot, located in-line and off-end (either end) of spread; reversed shots suggested
Shot near offset	About 10 to 20% of spread length
Source equipment	Sledgehammer (most common), 20 lbs (9 kg) and striker plate
Trigger	Hammer switch taped to sledgehammer handle and connected to seismograph trigger port
Sample interval	0.5 milliseconds (ms)
Record length	1 to 2 seconds (s), long enough to enclose the surface wave train.
Stacking	At least 5 times so as to improve data quality, shots were made at quiet times to allow full data acquisition.

3.3 Fixed Receiver Spread Configuration (FRSC)

The simplest configuration for 2D MASW surveys to be applied on short survey length shall be *fixed receiver spread*. The geophones were set up in a line at fixed locations and the shots were moved through the spread. The first shot was located off-end at a near offset of one-half the geophone interval. The shot was then advanced at an increment equal to the geophone interval so subsequent shots were located midway between geophones. As the *Shot number* increased, the shot location advanced by one interval across the *Survey distance*. In all the seismic lines, the acquisition of seismic data comprised of 26 shot locations selected both at the end of the profile and between two geophones. i.e. at -2m, 1m, 3m, 5m, 7m, 9m, 11m, 13m, 15m, 17m, 19 m, 21m, 23 m, 25 m, 27m, 29 m, 31m, 33m, 35m, 37m,, 39 m, 41m, 43m, 45m, 47m, 53m. The geographical locations (x,y,z) of all the geophones were obtained using a hand held GPS following the predefined traverse. The last shot was located off the opposite end by the same near offset of one-half the geophone interval. The *Spread length (a)* equaled the survey line length over which there are active geophones. The survey depth was approximately $a/4$ to $a/2$.

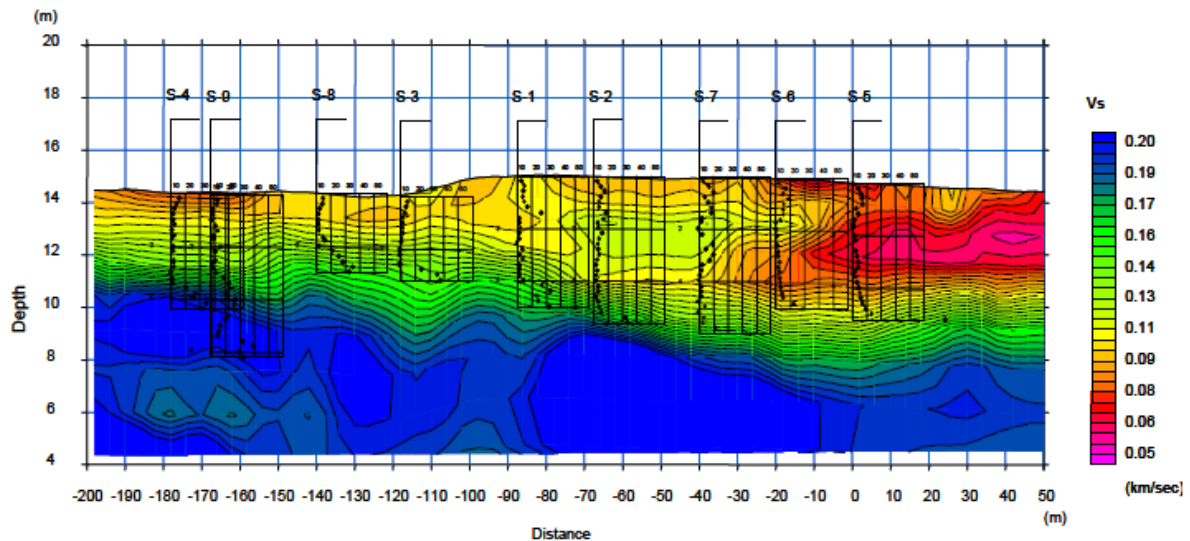


Figure 17: 2D MASW Cross-sectional Models for previous project carried out by Johnbosco

3.4 Geological Study

During the field reconnaissance site visit, it was observed that the distressed pavement developed cracks (fissures) whose alignment/orientation was in perfect match with the orientation of the regional fault line within the area. Therefore, one of the hypotheses postulated is that the problem in consideration could be related to geo-tectonics (buried Fault gouge material) within the area. All the gulleys/fissures developed in the area (Fig. 18) were undoubtedly within the buried fault zones. Therefore, geological consideration for this research was important to supplement the other component. It was realized that most of the sinkhole occurrence in the area were in the same alignment as the regional fault line orientation.

Detailed fault survey was conducted with the research project area using resistivity and past geological literature available.



Figure 18: A) Fresh developing crack on the road pavement; B) Fissure developed during the period when the road was cut off; and C) Wide fissure formed northwest of the research project area.

Geological field appraisal in the proposed sites involved the process of selecting an area of interest and identifying all the geological aspects of the areas with the purpose of preparing a detailed geological evaluation of research area. A geological map was thus expected to show the various geological structures, geological formations, geomorphology etc. and all these features may have been superimposed over the base map. The geological structural analysis aided in evaluating the current condition of fractures such as fissures, crevices, faults and cavities and future impact, which could contribute or initiate future road pavement distress. Also included in the research paper is seismic study of the area. The analysis of the geological structures helped in comprehending of possible future failure of the road pavement.

3.5 Field sampling procedure

A rigorous site exploration exercise was conducted to investigate the volcanic soil conditions along the Maai-Mahiu – Narok Road.

Accurately, the topography of the site was prepared to determine nature of the geological deposits underlying and to determine their engineering properties during the testing of the recovered samples. All available information with regard to the site and its geological environments involved search through records, maps (topography and geological), and any other information relevant to geology, history and present condition of the area. At this stage, a preliminary analysis of the geology by preparing sections was done. A visit to the site was made to confirm observations and predictions made (Dumbleton & West, 1971).

Both laboratory and field tests were conducted. Here trenches were excavated to gain access to deeper areas.

Sampling was carried out either in pits accessible from ground level. A number of sites were reviewed along the road for data collection on this ‘fissure prone areas’. Sites were chosen to range over the localized geological scene (Rowe, 1968).

For cohesive soils such as clays at shallow depths or in test pits, a steel tube, 4 in. in diameter and 12 in. long with one end turned down to a knife-edge and this edge burnished in 0.001 in. to give clearance to the sample, was used. This procedure is described in Rowe (1968).

For fairly cohesive soils containing large grains and occurring at surface or in pits, an irregular sample was secured and carefully coated with a known volume and weight of paraffin.

For cohesionless soils e.g. sand, a small steel or brass cylinder of known volume and with burnished edge was used.

Filed sampling procedures, tests conducted to the samples and how results were obtained are outlined below:

- 1) Core drill boring was utilized to obtain rock sample. Auger borings was used to secure samples at any depth. Core drilling was carried out to obtain sub-surface information from all materials recovered.

Core drilling adapted the following procedure:

- a. Core Drilling was performed by use of hydraulic driven rotary machines, at the locations, in the directions and up to the depth as specified or directed from information collected during geophysical investigations.
- b. The work aimed at an optimum of 100% core recovery in both rock and unconsolidated deposits.

- c. The recovered core samples were placed in core run order in core boxes, protected from further moisture loss by polythene sheeting and was transported with due care to the laboratory for testing. Each core box had five grooves; each groove with adequate dimensions for containing one meter of core section. Accordingly, every core box contained core samples of 5 m section. The core samples were placed in order, in the same length of grooves of the core box as the length which had been drilled. Marks were put regularly to the grooves to indicate depths of sampling. Every core box had been marked with the pit number and depth of the section of which the core samples was collected.
 - d. All core boxes were, before the core boxes are stacked, photographed from the zenith in color so that details marked on the inside of the box are visible. All photographs were taken with the cores shaded from direct sunlight and using flash. The cores were arranged to reveal the most interesting characteristics such as seams, strata change etc.
 - e. All core boxes were stored in designated safe place with no sample distortion. The full core boxes were stored in a secure weather proof shed and stacked in such a way as to permit ready identification and removal of selected boxes.
- 2) Laboratory tests of soil and rock core samples was performed to obtain the index and engineering properties of the recovered materials applying BS and ASTM standards as required. Samples were sent to the laboratory to examine the physical and mechanical characteristics relevant in civil engineering and other auxiliary works as feasible as possible. Laboratory testing included but not limited to the list below:
- Moistures Content - **BS 1377 Part 2:1990**
 - Atterberg Limits (Cone Penetrometer)- **BS 1377 Part 2:1990**
 - Plasticity Limit and Plasticity Index- **BS 1377 Part 2:1990**
 - Linear Shrinkage- **BS 1377 Part 2:1990**
 - Shear box test-Undrained Shear Strength- **BS 1377 Part 7:1990**
 - direct shear tests- **BS 1377 Part 2:1990**
 - Particle size analysis (sieve and hydrometer)- **BS 1377 Part 2:1990**
 - Compaction –Modified Method- **BS 1377 Part 4:1990**
 - Compaction –Standard (light Weight) Method- **BS 1377 Part 4:1990**
 - specific gravity- **BS 1377 Part 2:1990**
 - unit weight/Particle density/Bulk Density- **BS 1377 Part 2:1990**

Laboratory testing of the sample from several sample pits at the site was tested during the fieldworks at University of Nairobi Laboratory and during the detailed geotechnical investigations (core boring). The tests are described above.

- 3) A results and analysis report was prepared containing all collected and analyzed data with conclusions and recommendations of the findings.

The report included but not limited to the following items:

- Description of site materials with comparison to regional topography;
- Results of laboratory tests with technical interpretation and comments;
- Photographs of core samples;

The timelines for implementation of field work, laboratory testing, analysis and final reporting was as presented in an activity plan matrix after determination of the scope of work.

In soft clays that are sensitive to ‘disturbance’, piston-sampling techniques in association with large diameter samples will be used. Details are given in Rowe (1968).

In-situ testing was carried out. Vane shear apparatus were used for the in-place strength determination of soft and sensitive clays (Skempton, 1985). Dynamic testing methods were used for assessment of sands and gravels (Fletcher, 1965).

In clays and soft rocks, the laboratory shear box apparatus were used (Bishop, 1966). Strengths and formation measurements in the laboratory were carried out on undisturbed U_{100} samples where feasible.

3.6 The proposed work-plan

The proposed work-plan consisted of four phases that were designed to achieve the objectives within the scope previously outlined. The work was planned by phase as is presented below.

Phase 1:

Literature review,

A literature review was to collect known information on tectonic movement, soil stabilization and volcanic soil formation will be carried out.

Topographic Survey and setting out

Topographic Survey and Seismic survey work was then rolled-out at the site on an area measuring 500m x 500m. Setting out for Trial Pits was carried out immediately and the exact locations and quantity was decided on site. The setting out activities for this phase was carried out as laid below;

- a) Assembling the apparatus
- b) Careful selection of pure soil
- c) Mapping of soil

In selection of the pure soil, work done by Visweswaraiya, Sahu and Gichaga on Geotechnical Properties of Nairobi soils was useful.

Phase 2: Testing

The seismic survey work resulted in exact location and depth of trial pits. Sinking would also proceed. After all the necessary data has been collected, Phase 3 would then follow.

Phase 3: Analysis and deductions

A thorough analysis of the results would then commence and deductions established.

Phase 4: Recommendation and report development

Based on the results from Phase 1 through 3, conclusions and recommendations were developed. Recommendations addressed additional requirements in terms of further research necessary to be undertaken to cover for all volcanic soils in the country. The whole report was critically developed.

Phase 5: Presentation and printing of final report

The final report composed of all the phases from one to four compiled together. This entailed power point creation for presentation purposes and printing and submission of a hard copy for evaluation.

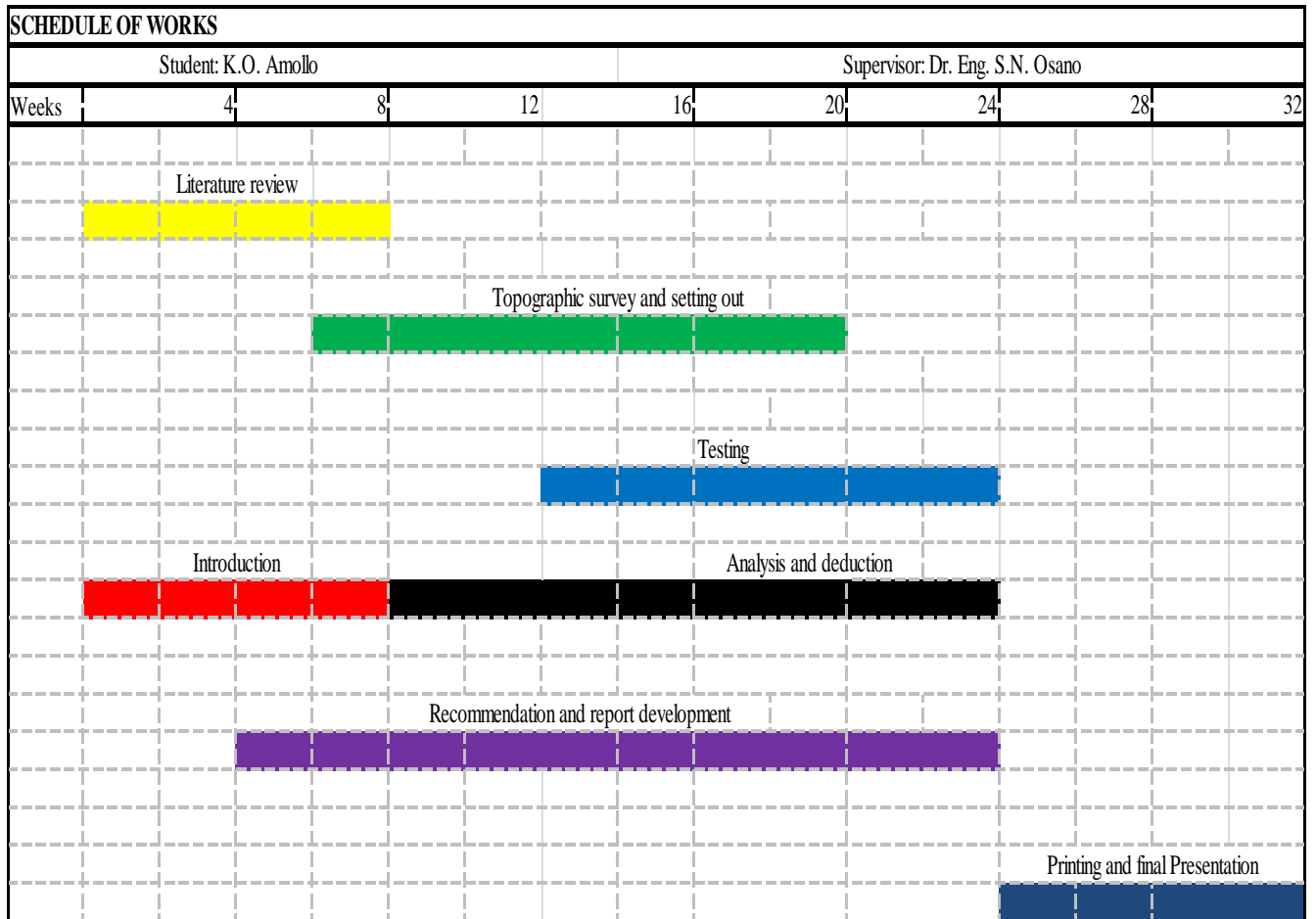


Figure 19: *Schedule of works*

3.7 Statistical analysis

Cluster sampling was the predominant form of sampling.

Data was arranged into classes and their frequency table. From here, several statistical tools were employed to represent data. They include;

- Histogram
- Frequency polygon
- Cumulative frequency polygon
- Pie-chart
- Lorenz curve

Then measures of central tendency was deduced which included the arithmetic mean, population mean sample, median, mode, weighted mean etc.

3.8 Expected results

It was expected that at the end of the investigations, the following questions and problems would be addressed;

- (a) Why did the fissures occur?
- (b) Will the process of fissure formation occur again?
- (c) Are there measures to be taken to mitigate against the formation of the fissures?
- (d) Input in the Design Manual for improved approach to the design criteria for purposes of design taking account of drainage and geologically active areas;
- (e) Input to maintenance in collapsing lined drains in the area.

Deep seismic surveys would deliver an overall picture of the stratigraphy and tectonic situation of the area. The information obtained from the high quality deep borings would allow an understanding of the stratigraphic, tectonic and geotechnical conditions in the area.

Laboratory testing established soil properties as measured in the laboratory as small scale testing with the identified procedures.

Therefore, it could be said that this research improved an understanding of ground movements facing this country and measures to be taken to mitigate against future catastrophic occurrences.

Chapter four: Results and Analysis

Data analysis is the process of packaging the collected information, evaluating it, putting it in order and structuring its main component in a way that findings can be easily interpreted (Mugenda and Mugenda, 2003). After testing the soil samples, the researcher did a thorough analysis of the collected information. The researcher used both quantitative and qualitative data analysis methods. The data was first edited to check for clarity, consistency and completion of information.

4.1 Bulk density

Sampling of the undisturbed soil sample was done in the field to ascertain the bulk density of the soil. The sampling was done at an interval of 0.5m depth up to a depth of 1.5m. The samples were then taken to the laboratory for test and results computed. The sampling process is as described in fig. 20 (a) below and samples were wrapped in polythene bags to avoid loss of moisture as described in figure 20 (b).



(a)

(b)

Figure 20: (a) Sampling for bulk density investigation; (b) wrapping of the samples in polythene bags to avoid moisture loss

Bulk density of Andisols tends to be relatively low, and this is one of the defining characteristics of these soils according to Soil Taxonomy and the WRB. Of the four test pits analyzed in the region, the average bulk density is 1.0533 g cm⁻³ (fig. 21).

Table 3: Bulk density of the sample

Depth/Test pit	TP1	TP2	TP3	TP4
0.5m	1.176	0.945	0.782	0.981
1m	1.177	0.997	1.239	0.939
1.5m	1.447	0.934	1.031	0.992

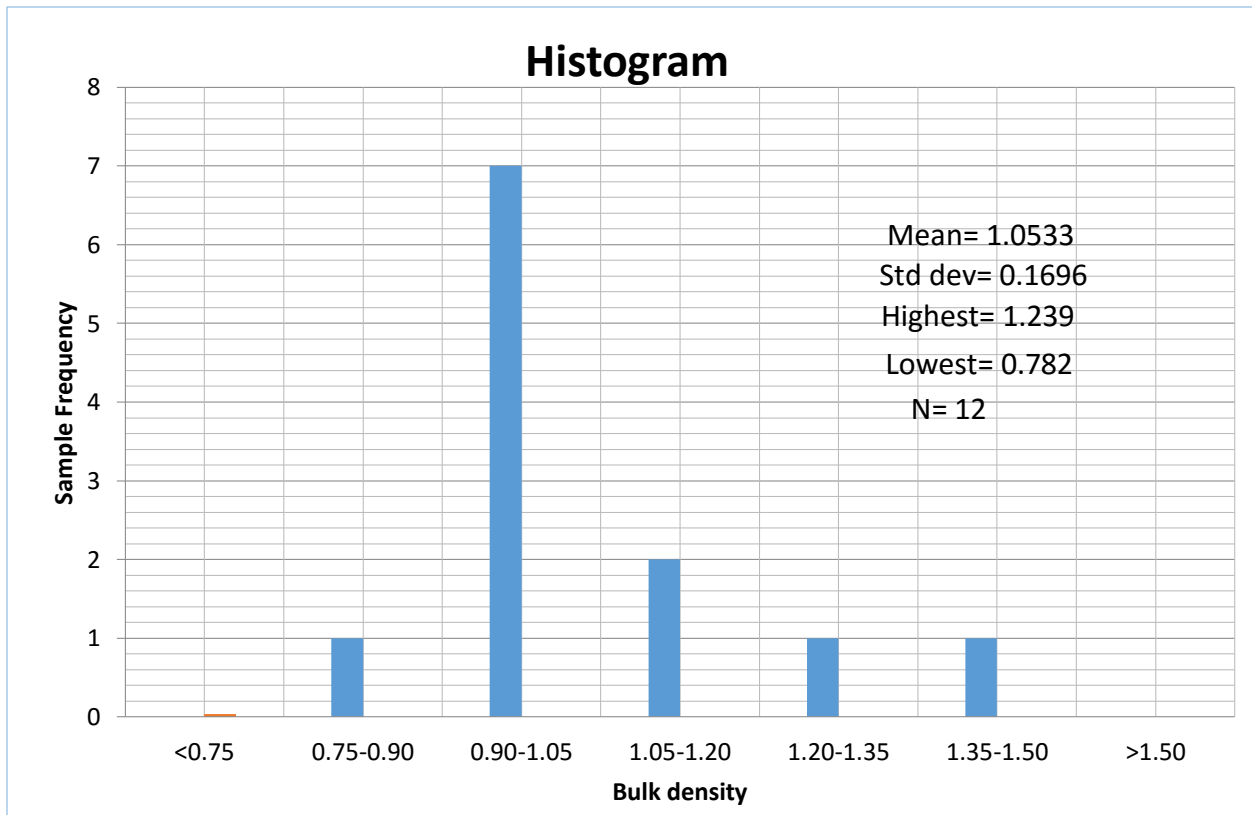


Figure 21: Bulk density histogram

However, ~95 percent of the horizons have bulk densities of >0.90 g cm⁻³, suggesting that mixing and/or compaction, both of which would tend to increase bulk density, have occurred since deposition. Because bulk density is inversely related to porosity, an ash cap with a bulk density of 0.90 g cm⁻³ may have ~40 percent more porosity than a typical mineral soil with a bulk density of 1.3 g cm⁻³.

4.2 Atterberg limits

The samples were taken to the laboratory and atterberg classification test conducted according to BS 1377 Part 2:1990. The other test done to ascertain the plasticity of the soil included Liquid limit, Plastic limit and shrinkage limit of the soil (fig.22)



Figure 22: *Plastic limit by casagrande method*

The result of the plasticity investigation denoted that the volcanic ash is non-plastic and highly silt in nature (Appendix IX).

4.3 Particle size

Wet sieving was done to the samples and what passed through sieve 200 was oven dried and hydrometer analysis conducted on it; as shown in fig. 23. The results for each sample are in appendix IV. The sieve analysis curves were constructed for every test pit to analyze the particle size distribution.



(a)Wet sieving



(b) Hydrometer analysis

Figure 23: Wet sieving and hydrometer analysis

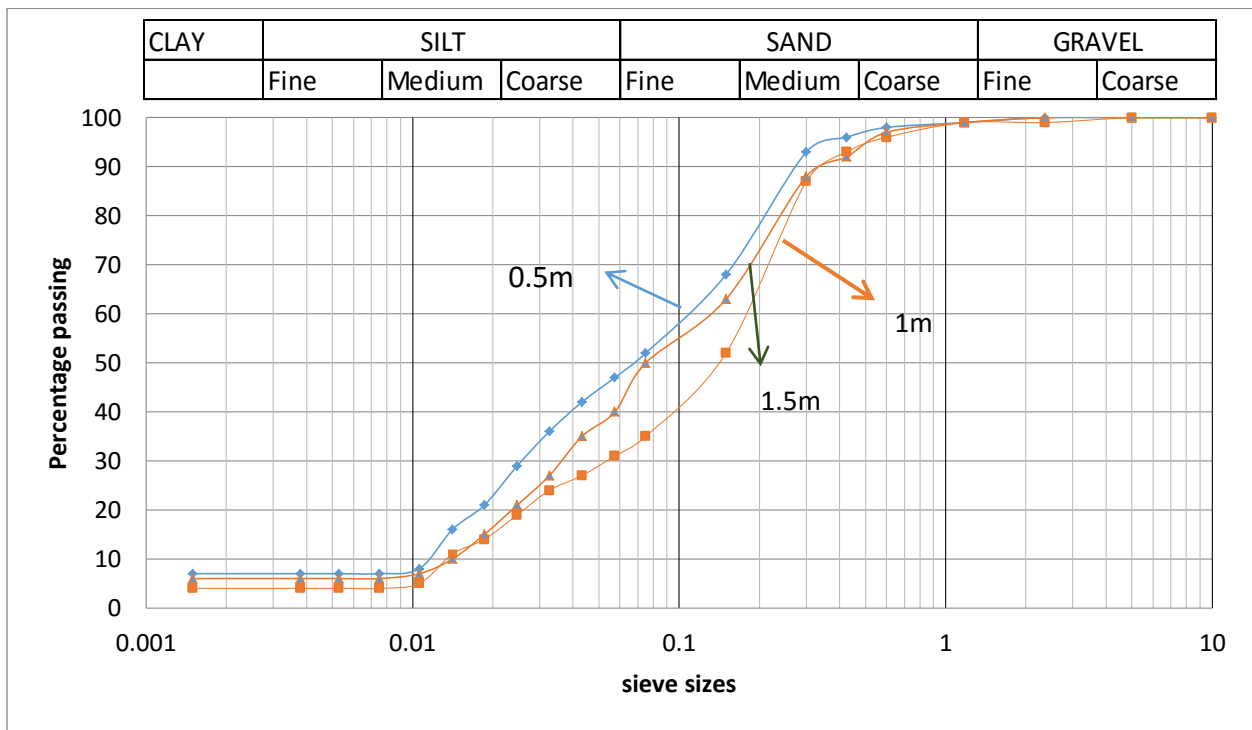


Figure 24: Particle size curve for trial pit 1

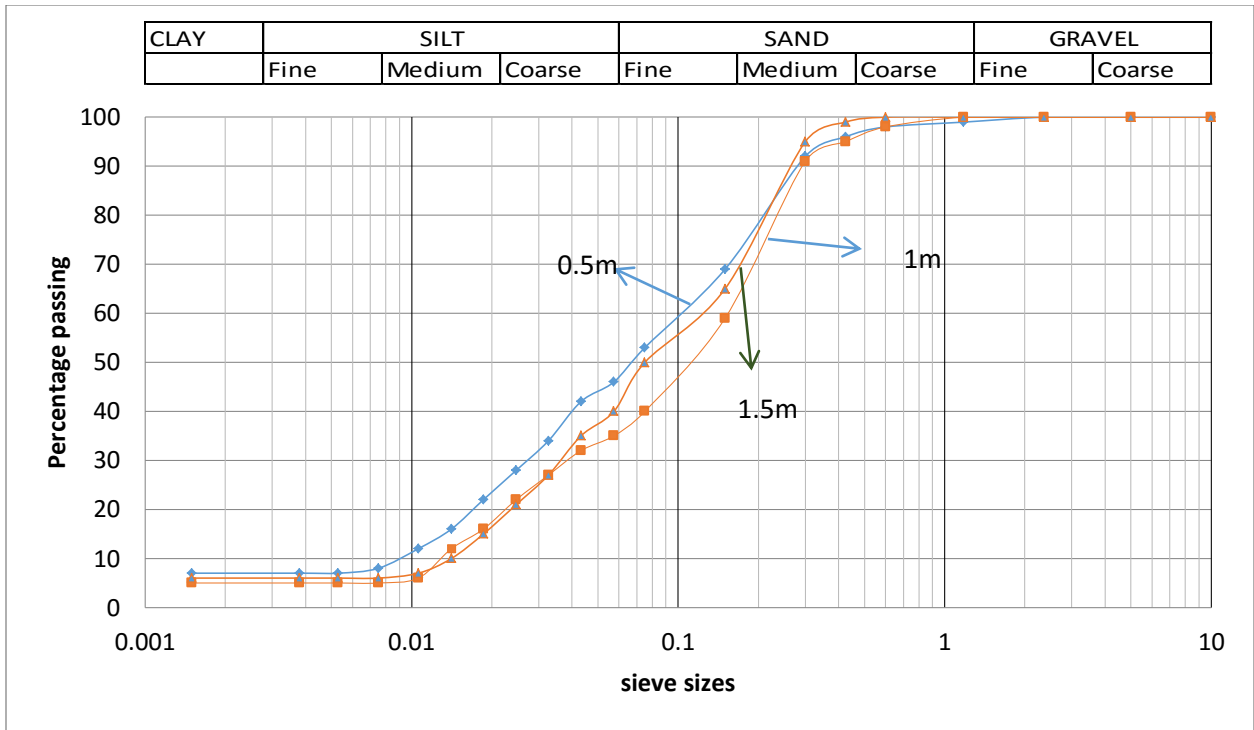


Figure 25: Particle size curve for trial pit 2

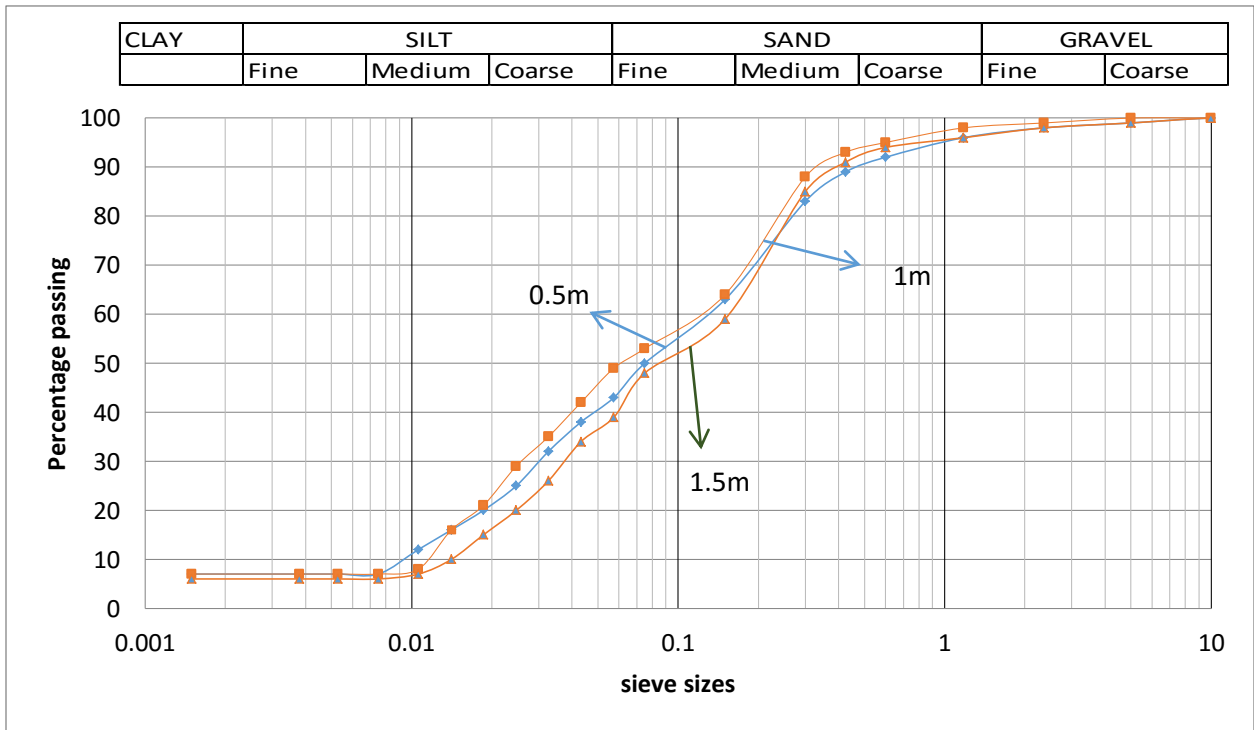


Figure 26: Particle size curve for trial pit 3

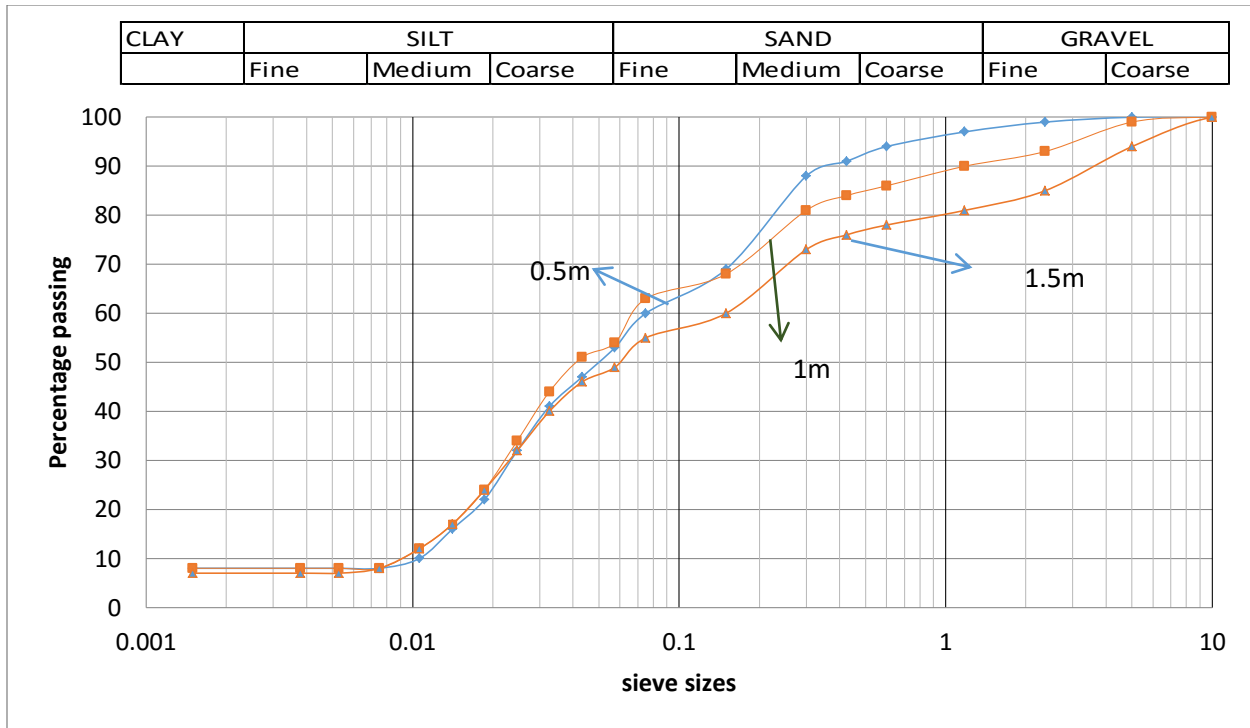


Figure 27: Particle size curve for trial pit 4

Particle size analysis

The soils are generally heterogeneous with fine silt and silty sandy particles (silt 70%, sand 25%, organics/others 5%).

The sieve analyses for the twelve soil samples indicate percentage passing Sieve No. 200(0.075mm), grain size for fine sand is only approximately 50% for the all samples. This means that all the samples are fine grained (FINES) and classification can effectively only be done using hydrometer analysis. The envelope of the grading analysis was provided.

Particle size gradation

The results of particle size analysis from soil sample from several test pits from the Maai Mahiu-Narok site are presented in the grain size distribution. The distinction between poorly graded and uniformly graded soils according to USBR is made between the coefficient of uniformity, C_u and the coefficient of curvatures, C_c .

$$\text{Where } C_u = \frac{D_{60}}{D_{10}} \text{ and } C_c = \frac{D_{30}^2}{D_{30}D_{10}}$$

Where D_{60} , D_{30} and D_{10} are particle sizes diameters corresponding to 60%, 30% and 10% finer on the particle grain size cumulative distribution curve, respectively. Well (broadly)

graded soils are defined by the following C_u and C_c parameters, $C_u > 4$, $1 < C_c < 3$ while for poorly (uniformly) graded soils $C_u < 4$ and/or $1 < C_c$ or $C_c > 3$ (C_c is not in the range of 1 and 3).

Table 4: Particle size analysis for C_u and C_c

Soil parameters		D60	D30	D10	C_u	C_c
TP1	0.5m	0.12	0.025	0.012	10	2.083333
	1m	0.18	0.055	0.014	12.85714	3.928571
	1.5m	0.15	0.035	0.015	10	2.333333
TP2	0.5m	0.1	0.028	0.009	11.11111	3.111111
	1m	0.16	0.038	0.014	11.42857	2.714286
	1.5m	0.14	0.037	0.015	9.333333	2.466667
TP3	0.5m	0.14	0.03	0.0095	14.73684	3.157895
	1m	0.13	0.025	0.013	10	1.923077
	1.5m	0.17	0.038	0.015	11.33333	2.533333
TP4	0.5m	0.075	0.024	0.011	6.818182	2.181818
	1m	0.065	0.023	0.009	7.222222	2.555556
	1.5m	0.15	0.024	0.009	16.66667	2.666667
summation		1.58	0.382	0.1455		
Average		0.131667	0.031833	0.012125	10.85911	2.62543

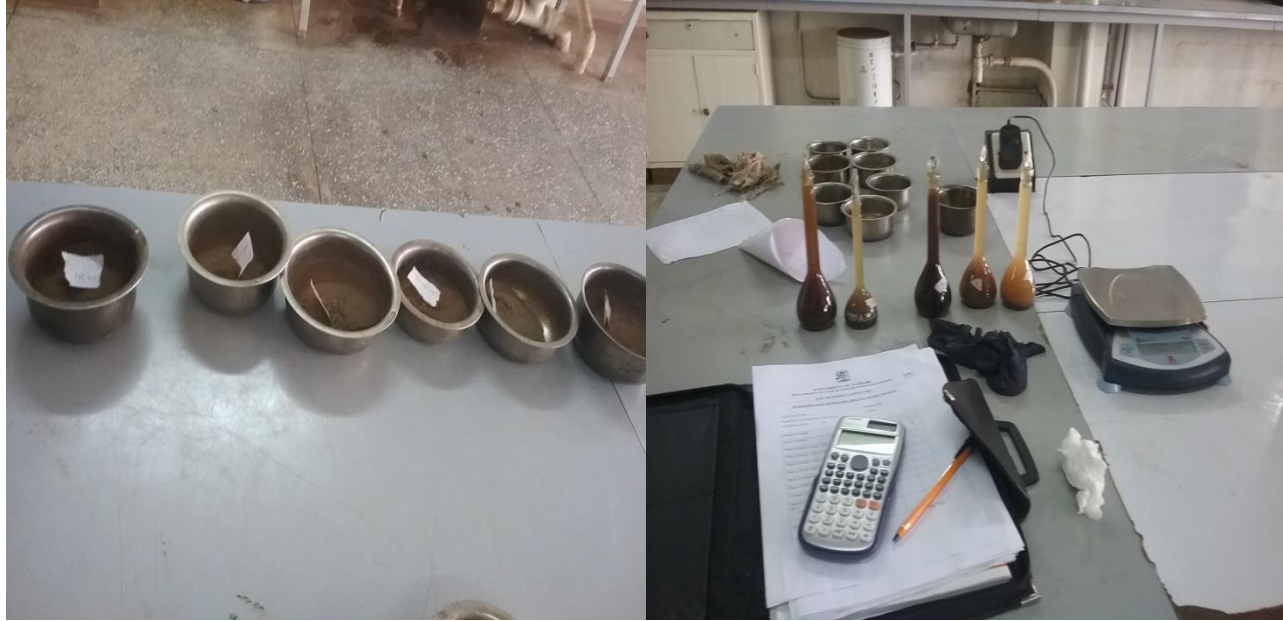
From the soil particle size test results; $D_{60} = 0.131667$, $D_{30} = 0.031833$ and $D_{10} = 0.012125$ (Average figures)

$$C_u = \frac{D_{60}}{D_{10}} = 10.85911$$

$$C_c = \frac{D_{30}^2}{D_{60}D_{10}} = 2.62543, \text{ the soils can be classified as well graded soils}$$

4.4 Specific gravity

Three samples from each of the four trial pits were investigated to determine individual specific gravity in the laboratory according to BS 1377 Part 2:1990. The set-up is as described in figure 28 below.



(a) Sampling

(b) Specific gravity test

Figure 28: *Specific gravity at the laboratory*

This value indicates how much heavier/lighter a material is than water. In soils, SG refers to the mass of solid matter of a given soil sample as compared to an equal volume of water. The value of specific gravity is necessary to compute the soils void ratio and for determining the grain size distribution in hydrometer analysis.

Table 5: *Specific gravity ranges for different soils*

General Ranges of SG For Soils	
Sand	2.63-2.67
Silt	2.65-2.7
Clay and silty clay	2.67-2.9
Organic soils	<2.0

The test results from the trial pits indicate a range between 2.114-2.419 denoting a rather light soil within the given depth of 0.5m to 1.5m, as described in table 6 and analyzed in the diagram 27.

Table 6: Specific gravity values for samples

TEST PIT	DEPTH	SPECIFIC GRAVITY	AVERAGE
TP1	0.5M	2.419	2.375333
	1M	2.419	
	1.5M	2.288	
TP2	0.5M	2.323	2.302667
	1M	2.308	
	1.5M	2.277	
TP3	0.5M	2.188	2.228
	1M	2.188	
	1.5M	2.308	
TP4	0.5M	2.114	2.170333
	1M	2.143	
	1.5M	2.254	

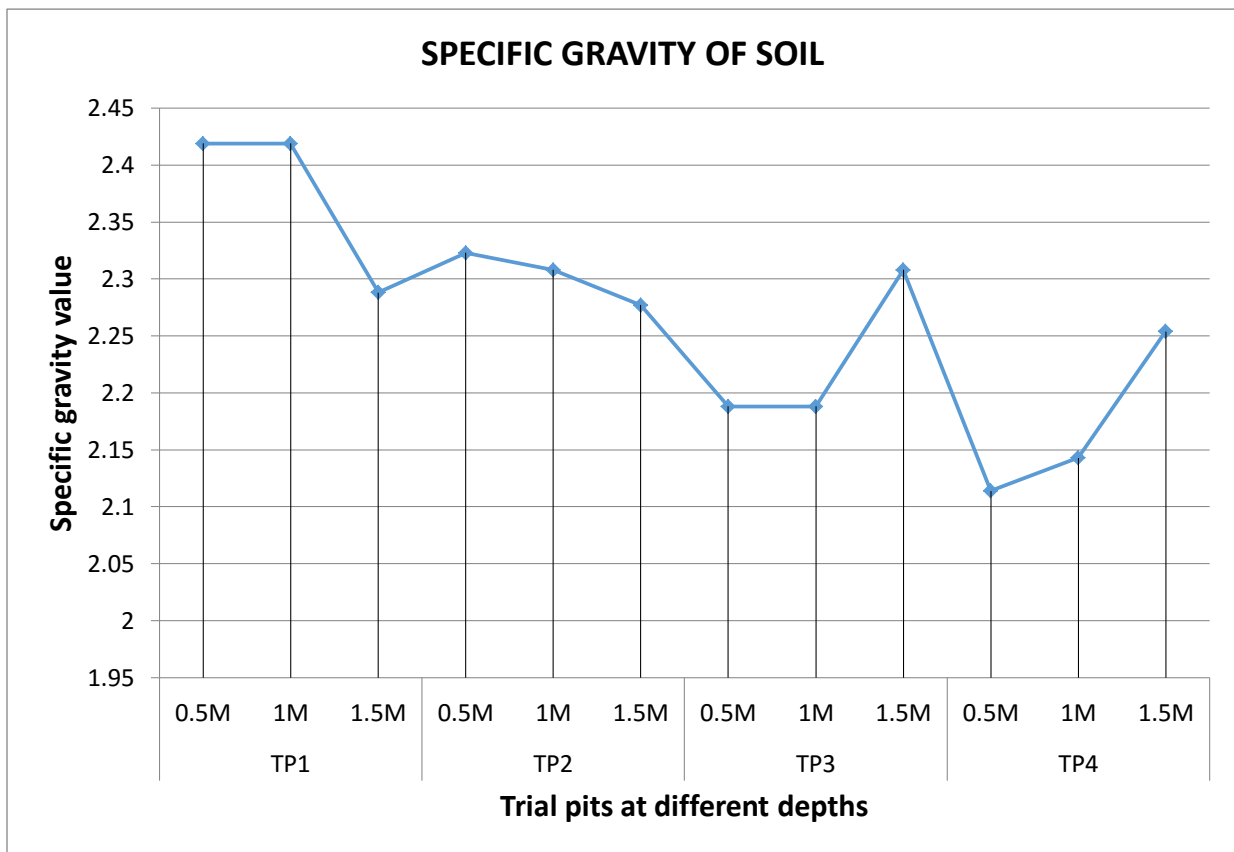


Figure 29: Line graph comparing specific gravity of samples tested

4.5 Proctor compaction

In geotechnical engineering, soil compaction is the process in which a stress applied to a soil causes densification as air is displaced from the pores between the soil grains. When stress is applied that causes densification due to water (or other liquid) being displaced from between the soil grains then consolidation, not compaction, has occurred. Normally, compaction is the result of heavy machinery compressing the soil, but it can also occur due to the passage of locomotive or animal feet.

Compaction test was done in order to determine the maximum dry density and the optimum moisture content of the soil sample (fig.30).



Figure 30: *Compaction test*

The Proctor compaction test is a laboratory method of experimentally determining the optimal moisture content at which a given soil type will become most dense and achieve its maximum dry density. The results were tabulated as below:

Table 7: Proctor Compaction test results

Test Pits	Depth	NMC	OMC	MDD
TP1	0.5M	4.06	24.9	1443.3
	1M	4.1	20.6	1416.9
	1.5M	4.3	23.7	1420
TP2	0.5M	4.64	24.1	1402.2
	1M	4.82	23.3	1441.9
	1.5M	6.43	25.6	1435.7
TP3	0.5M	7.77	20.6	1487.2
	1M	8.56	25.4	1433.3
	1.5M	8.7	24.5	1417.4
TP4	0.5M	5.04	24.8	1435.4
	1M	16.2	30.3	1351.4
	1.5M	17.37	32.4	1309.4
AVERAGE		7.665833	25.01667	1416.175

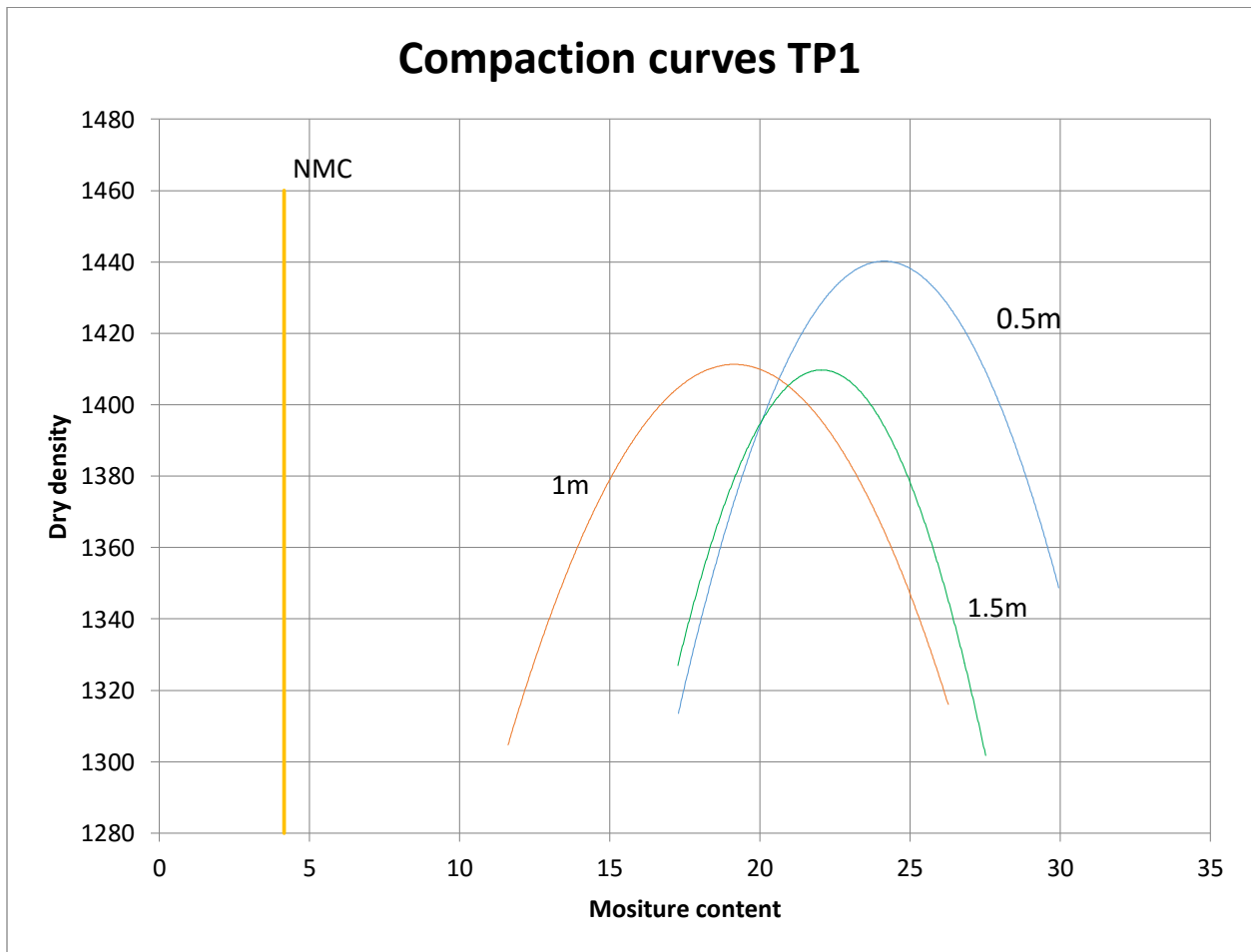


Figure 31: Compaction graph TP1

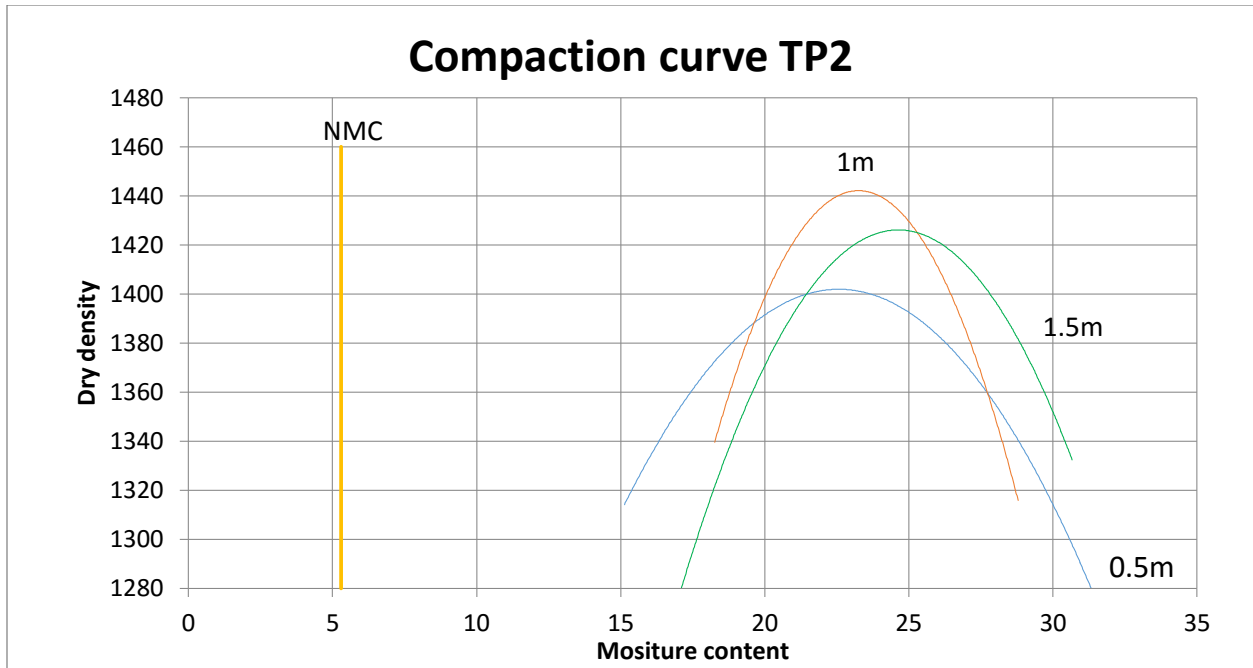


Figure 32: *Compaction graph TP2*

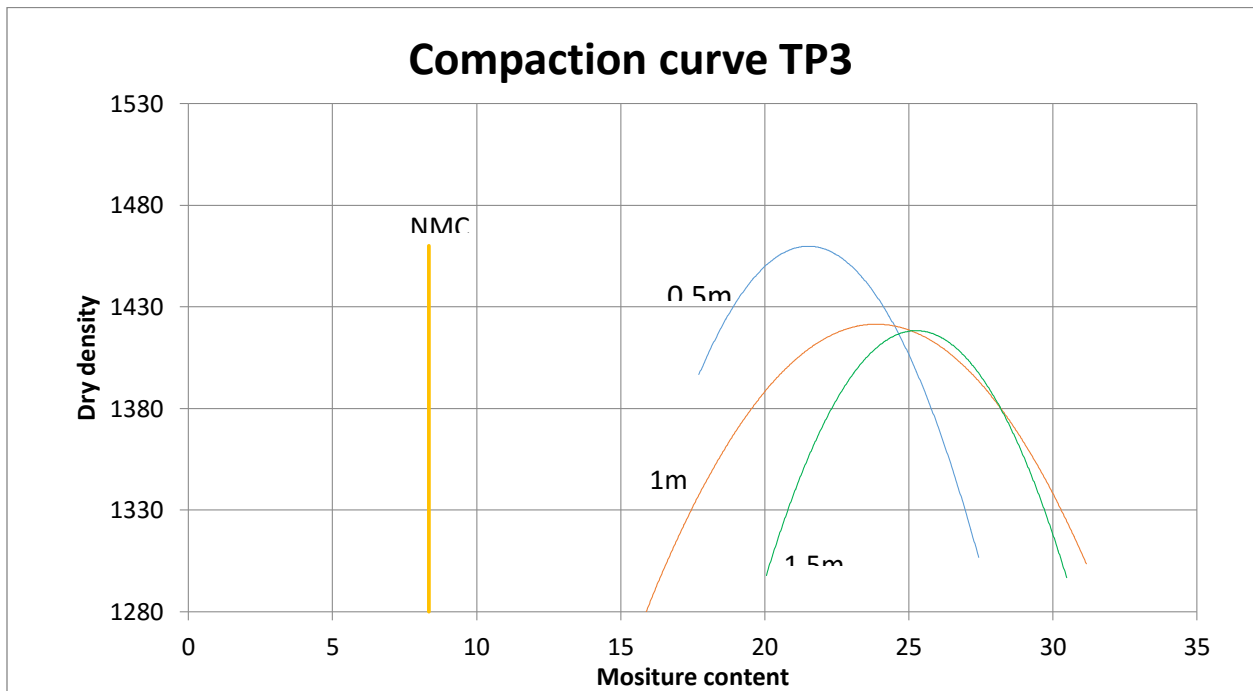


Figure 33: *Compaction graph TP3*

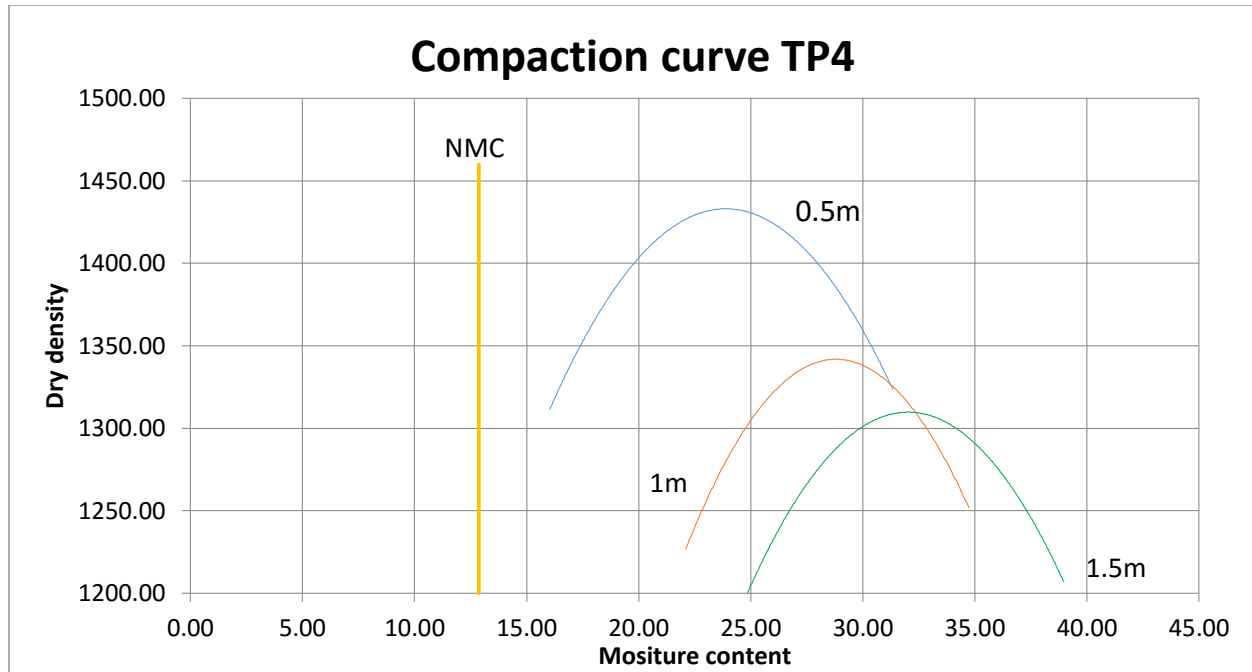


Figure 34: *Compaction graph TP4*

4.6 California Bearing Ratio

For a rational approach to pavement design, the most important characteristic of the subgrade is its elastic modulus. However, the measurement of this modulus requires fairly complicated and time consuming tests. However, it has been proved that there is a good correlation between the California bearing ratio and the elastic modulus of Kenyan soils. CBR is the quantitative means of estimating the subgrade bearing strength.

Soils are classified into 6 bearing strength classes, as described in Materials Branch Report Number 345 as shown:

Table 8: *CBR Range for soils with different strength properties*

Soil class	CBR Range	Median	Description
S1	2-5	3.5	Poor quality soils- excavated and replaced.
S2	5-10	7.5	Low bearing strength properties
S3	7-13	10	Low bearing strength properties
S4	10-18	14	Low bearing strength properties
S5	15-30	22.5	Gravelly material or unsoaked soil
S6	30		Comply with plasticity requirements for natural material for sub-base

From the trial pits test results of CBR, it depicts a series of poor soils with low bearing strength properties as shown in the table below.

Table 9: Test results for CBR

Test Pit	Depth	CBR (%)	Soil class
TP1	1.5M	4	S1 (poor quality soils)
TP2	1.5M	21	S5 (unsoaked and scattered soil)
TP3	1.5M	11	S5 (unsoaked and scattered soil)
TP4	1.5M	4	S1 (poor quality soils)

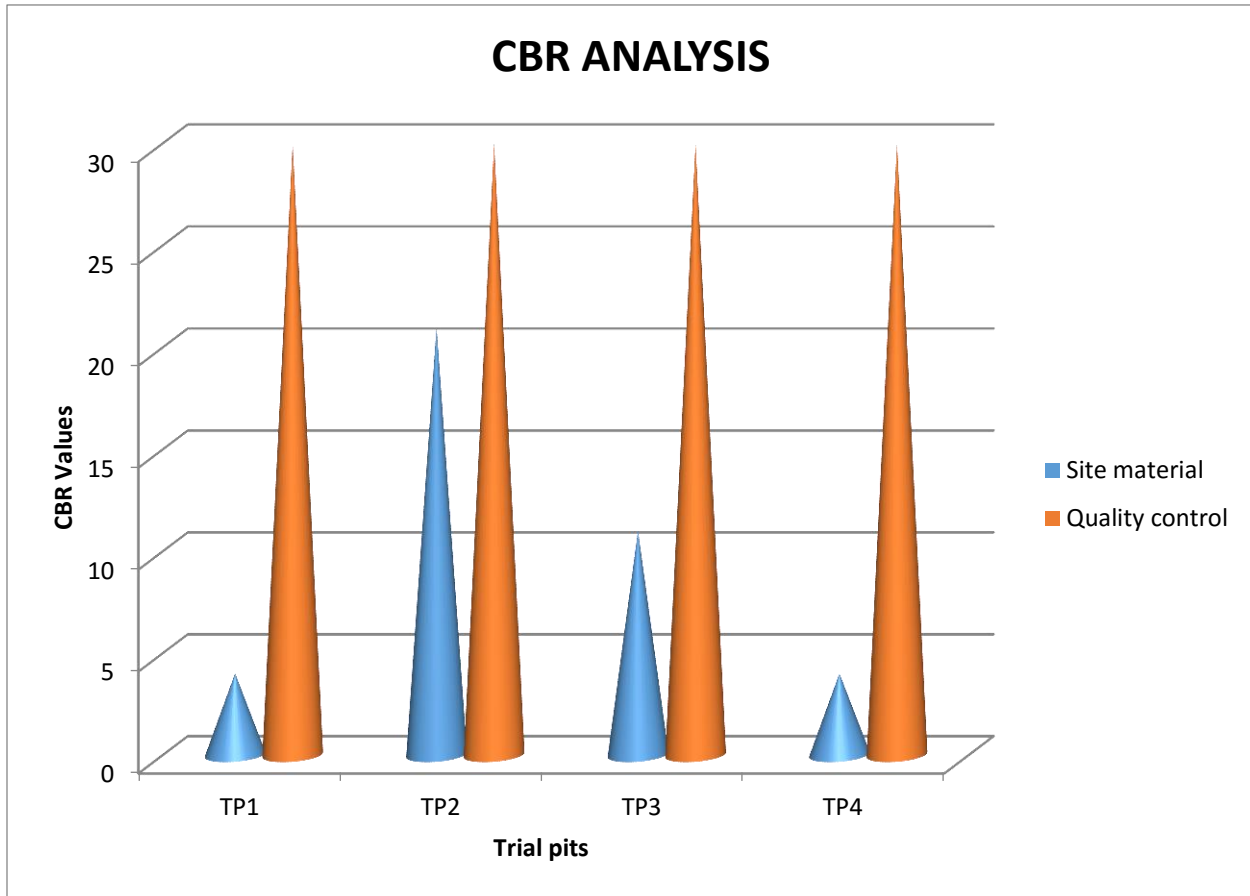


Figure 35: CBR values analysis

4.7 Shear strength

The actual pressure on the soil due to the weight of the structure is called the total foundation pressure q . The net foundation pressure q_{net} is the increase in the pressure at the foundation level. This is the total foundation pressure less the effective weight of the soil permanently removed during excavation.

The safe net bearing pressure (q_{safe}) is the net bearing pressure factored by an appropriate factor of safety.

$$q_{safe} = q_{net} / FOS$$

It is usual to use conservative factors of safety usually between 3 and 5. Due to uncertainties in

- ✓ The determination of the strength parameters
- ✓ Determination of the of the service load

Table 10: Typical factor of safety values for geotechnical works

Failure mode	Type of works	FOS
Shear	Earthworks	1.2-1.6
Shear	Retaining walls	1.5-2.0
Shear	Sheet piles	1.2-1.5
Seepage	Uplift	1.5-2.5
Shear	Bearing Capacity	3-5



(a)



(b)

Figure 36: (a) Shear box test being conducted; (b) Oven drying of the samples after being tested

From the different trial pits, the calculated safe bearing capacity values from the shear box analysis are as given in the table 11. An in-depth analysis of the Q_{safe} values indicate that the soils have very low strength properties and are therefore very inappropriate for conducting any construction purpose without improvements or cut and spoil method.

Table 11: Bearing capacity of samples

Test Pit	Depth	C	ϕ	Q safe (KN/m ³)
TP1	1.5M	0.02	27	130.46
TP2	1.5M	0.03	26	77.1
TP3	1.5M	0.04	26	85.08
TP4	1.5M	0.03	27	89.44

4.8 Consolidation

This test is performed to determine the magnitude and rate of volume decrease that a laterally confined soil undergoes when subjected to different vertical pressures. From the measured data, the consolidation curve (pressure-void ratio relationship) can be plotted. This data is useful in determining the compression index, the recompression index and the pre-consolidation pressure (or maximum past pressure) of the soil. In addition, the data obtained can also be used to determine the coefficient of consolidation and the coefficient of secondary compression of the soil.

From the oedometer tests carried out of the soil samples for the test pits, the following were taken as representative of the site material. This result depicts very high settlement properties denoting that the soil settles so much over the years due to high void ratios as shown in fig.37.

Table 12: Consolidation test results

Test Pit	$m_v = (dH/H1) * 1/dp * 10^{-4}$	$cc = (e^1 - e^0) / \log_{10}(\sigma^1 - \sigma^0) * 10^{-2}$	Settlement * 10 ⁰
	(m ² /KN)	mm ² /s	Mm/year
TP1	0.3	0.435	6.5217391
TP2	0.3	0.435	6.5217391
TP3	0.9	1.304	19.565217
TP4	0.7	0.87	13.043478

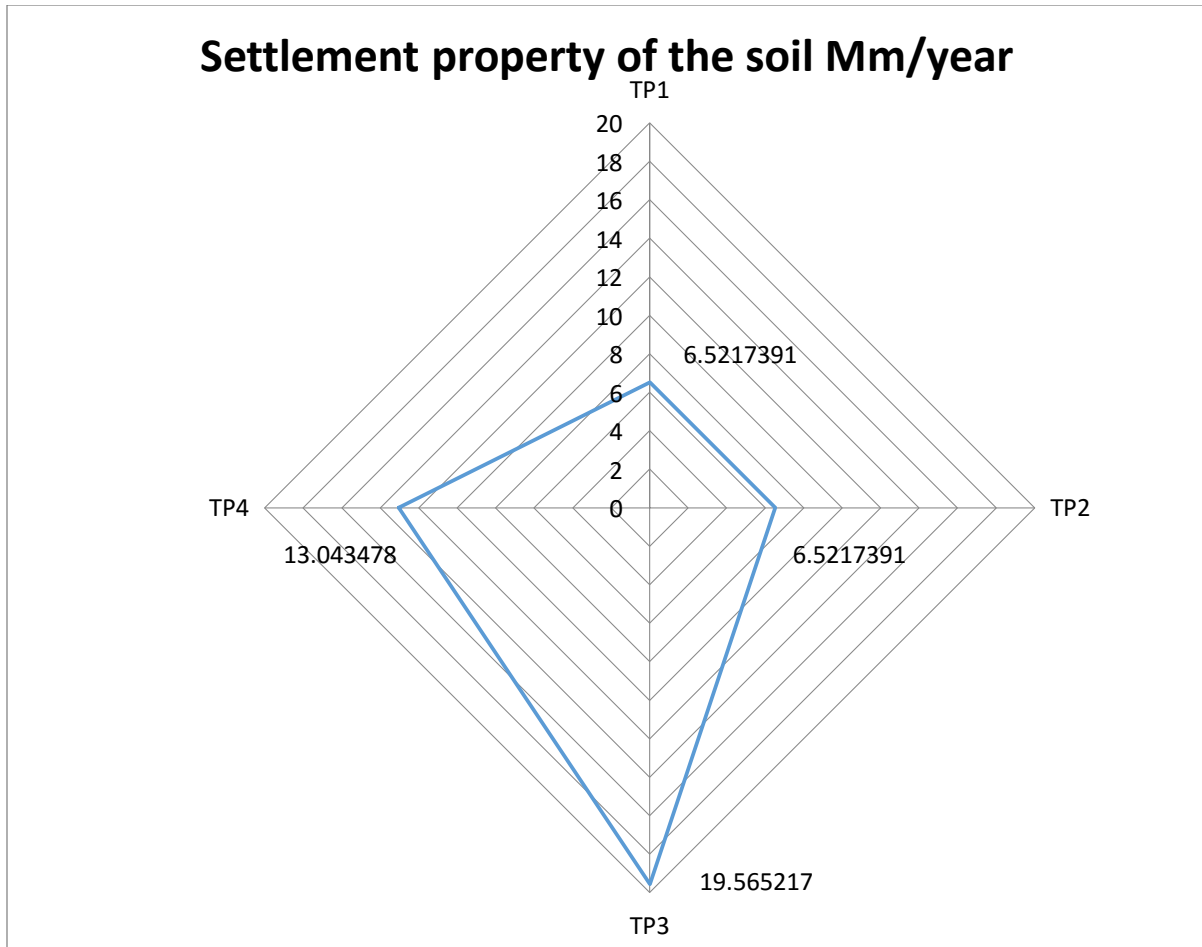


Figure 37: Settlement analysis of the samples

4.9 Geology of the region

4.9.1 Geological Structures

The main structural features in Maai Mahiu/Narok region are described using the maps of Rift valley province (fig.39), Suswa (fig. 40) and Naivasha (fig. 38 and 41) region. Within the investigated area there are fault lines oriented in a north- south direction. Small fractures and joints could also be observed on the basaltic outcrops. Structural features such as faults in the rocks often optimize storage, transmissivity and recharge, particularly when they occur adjacent to, or within, drainage systems. In the present study area, faults run through the valley in a more or less N-S direction, in keeping with the rift faulting.

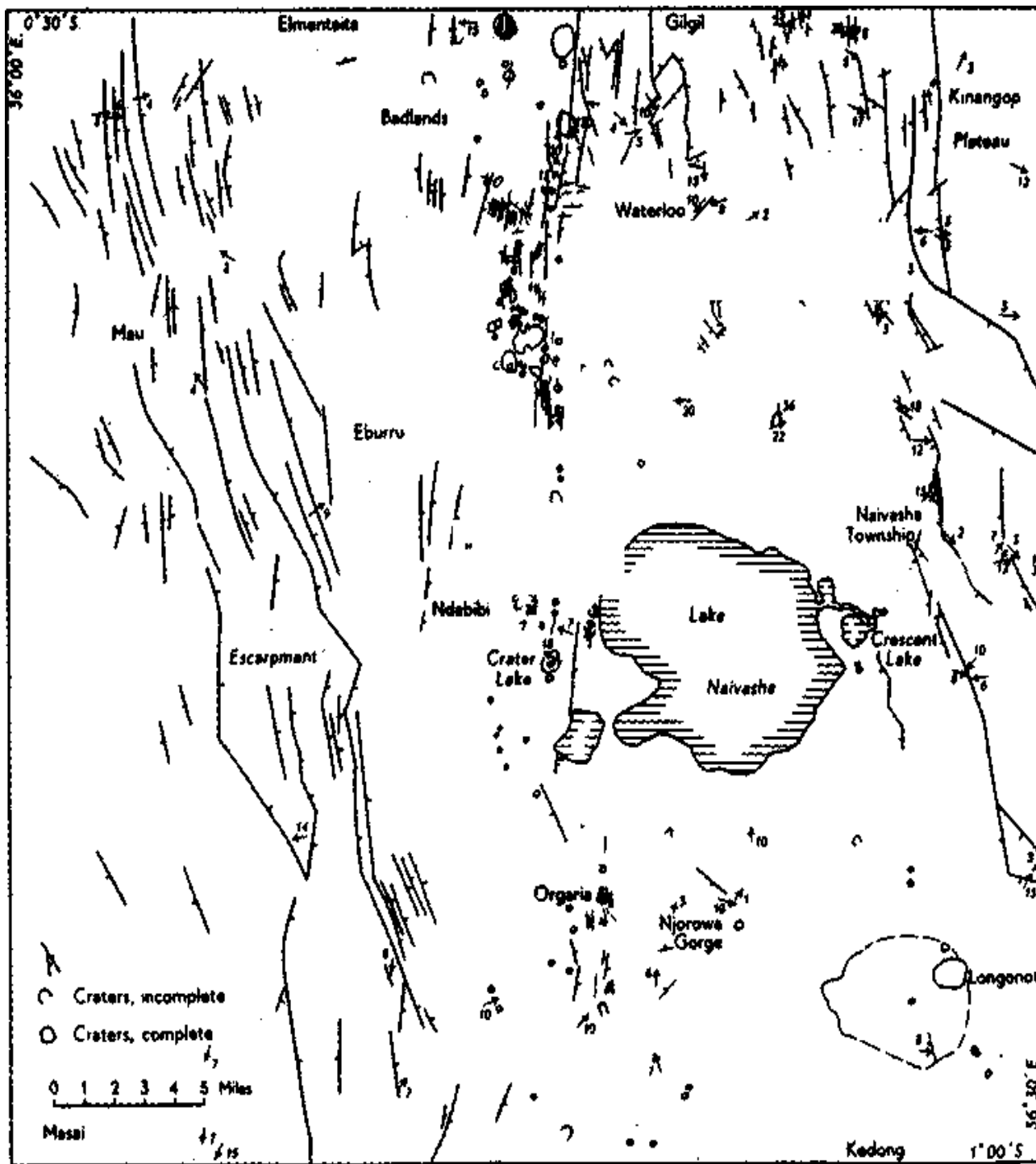
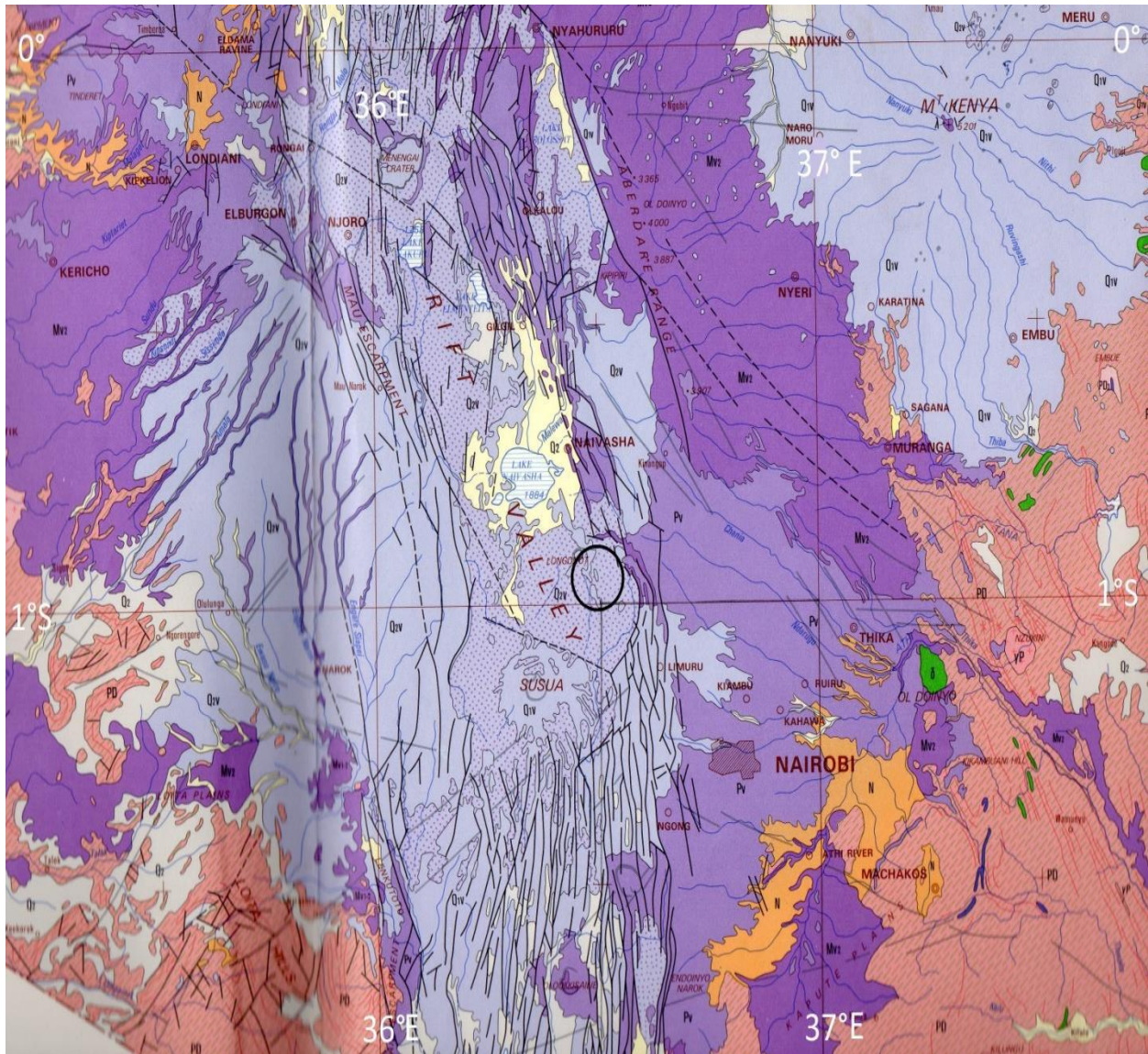


Figure 38: Source: Mines and Geological Department, Government of Kenya

Structural Map of the Naivasha Area



Key:

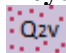
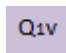


-  Q2v - Holocene. Basalt flows, pyroclastics, volcanic soils.
-  Q1v - Pleistocene. Trachytes, basalts and pyroclastics
-  - Fault Lines.
-  - Area of study.

Figure 39: Source-Geological map of Kenya: Ministry of Energy and Regional Development of Kenya.

GEOLOGICAL MAP OF THE SUSWA AREA.

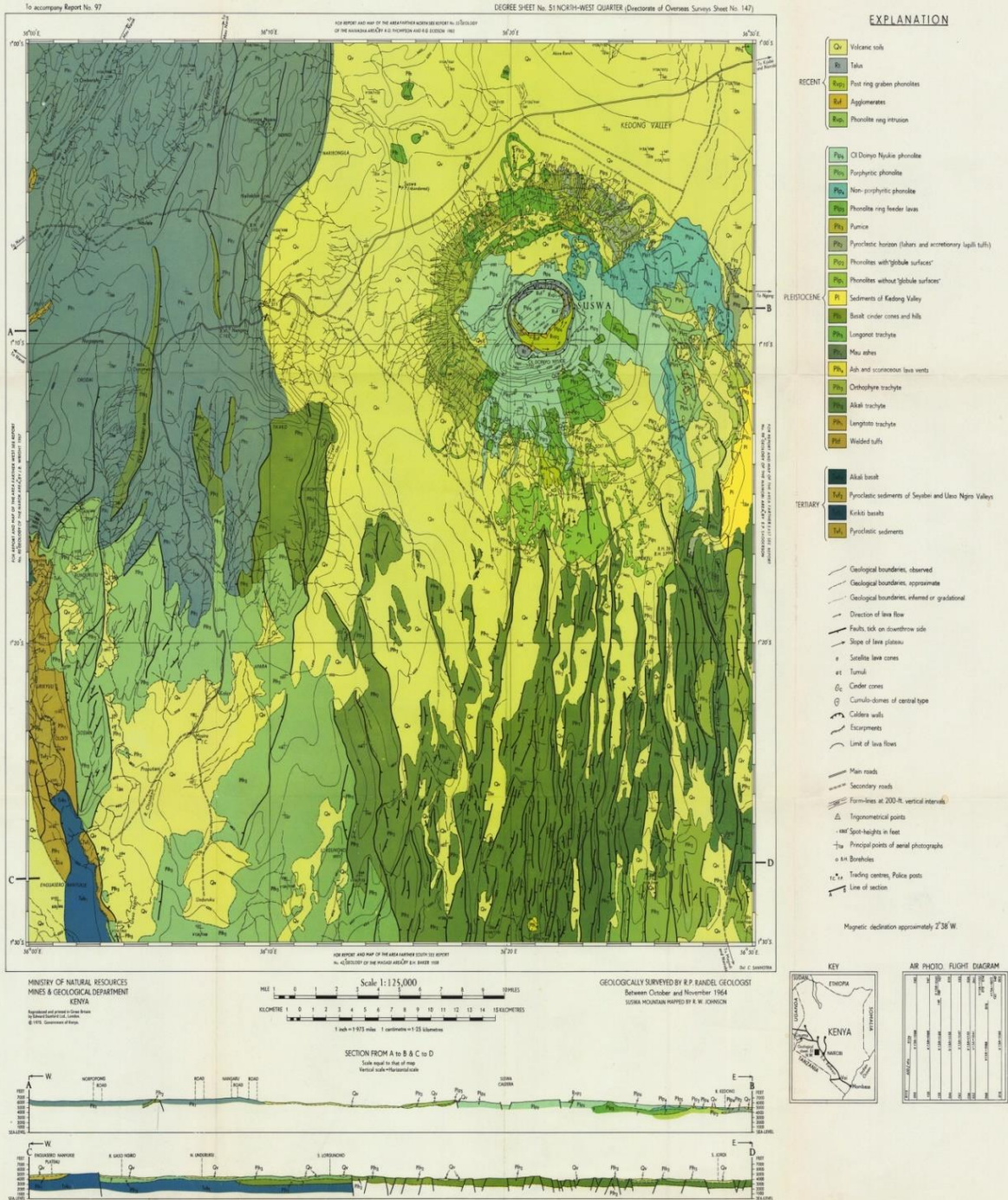


Figure 40: Source: Mines and Geological Department, Government of Kenya

Geological map of Suswa area

GEOLOGICAL MAP OF THE NAIVASHA AREA

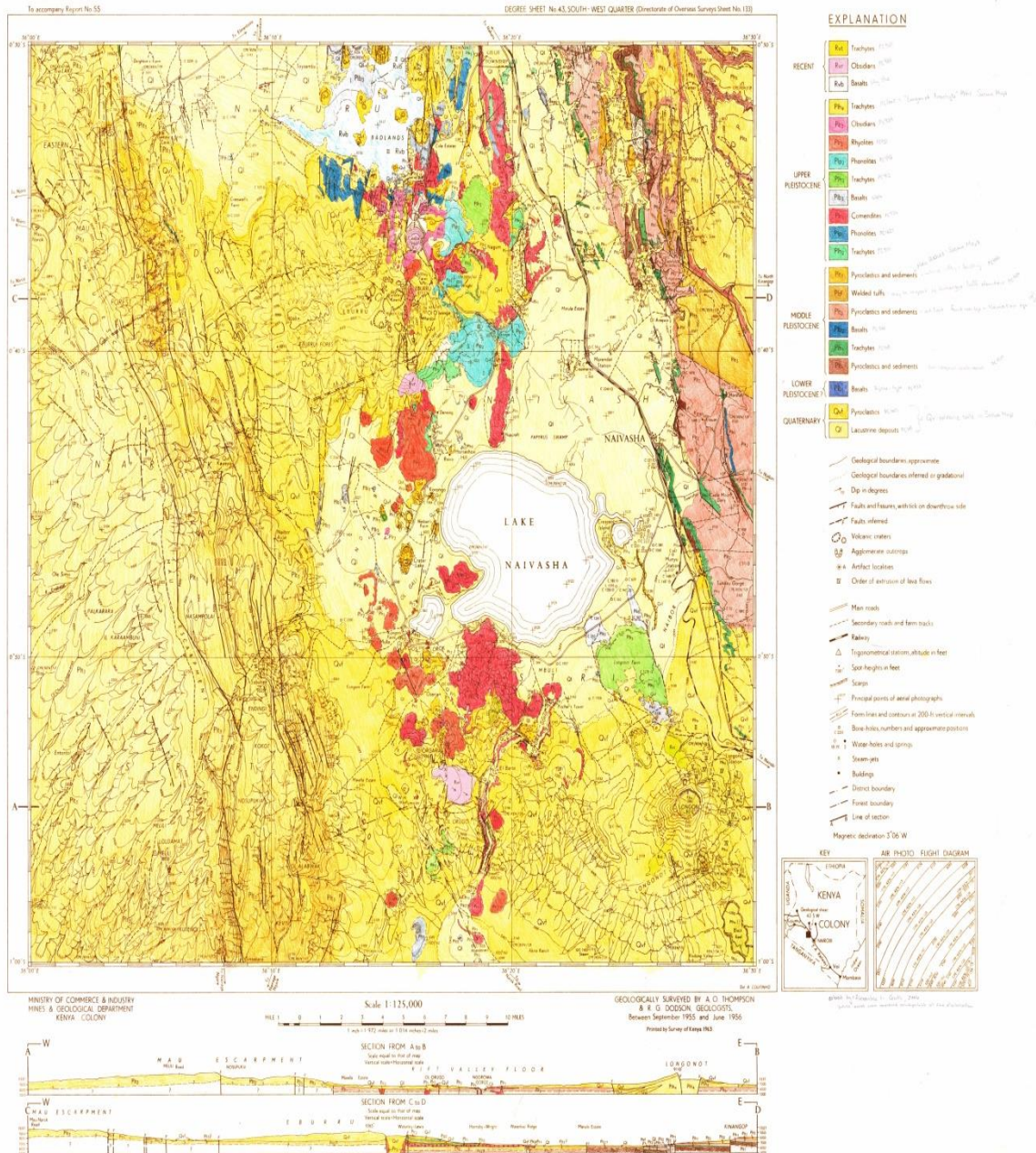


Figure 41: Source: Mines and Geological Department, Government of Kenya

Geological map of Naivasha area

4.9.6 Geological Observations

The project area is occupied by an alternation of lapili and ash/ black sand. This means that the ejection of lava from Mt. Longonot took place at different episode with difference in temperature/ pressure and chemical composition. This type of volcano is referred to as a strato volcano.



(a)

(b)

Figure 42: (a) Pumice observation on the southern part of the project area (b) Volcanic ash and black sand (GPS reading 37M0216126, 9904912)



(a)

(b)

Figure 43: (a) Stratified pyroclastic materials on the western part of the site (b) Stratified pyroclastic materials with lapili at the base on the western part of the site

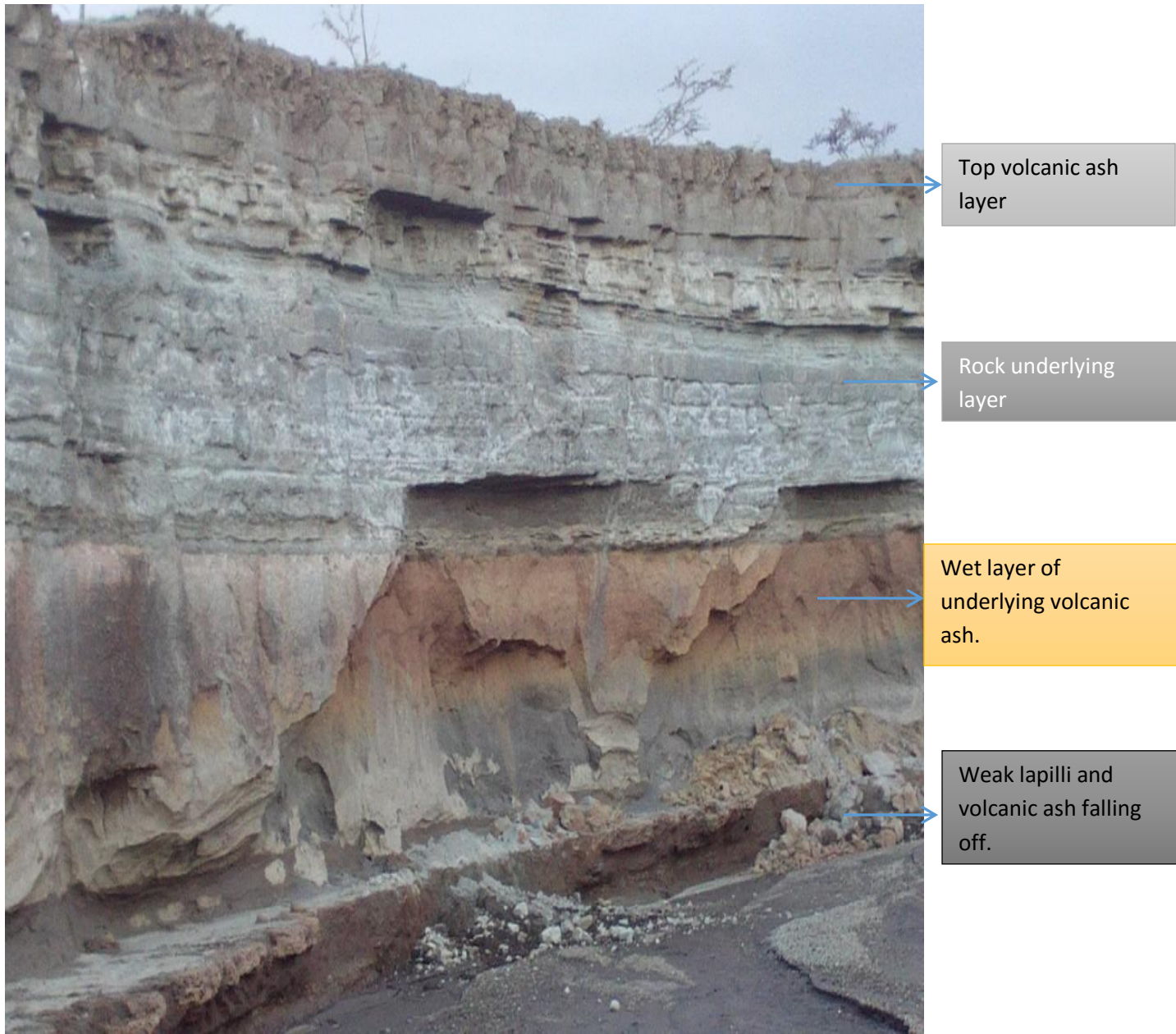


Figure 44: *Stratigraphy of the volcanic ash is well displayed on river bank cut (River Kedong)*

4.9.7 Results for rock density determination

Lapilli samples were seen to float on water meaning that the specific gravity of lapilli and pumice is less than that of water. This kind of material can easily be eroded by heavy downpour causing mass movement of material over the surface of the earth.

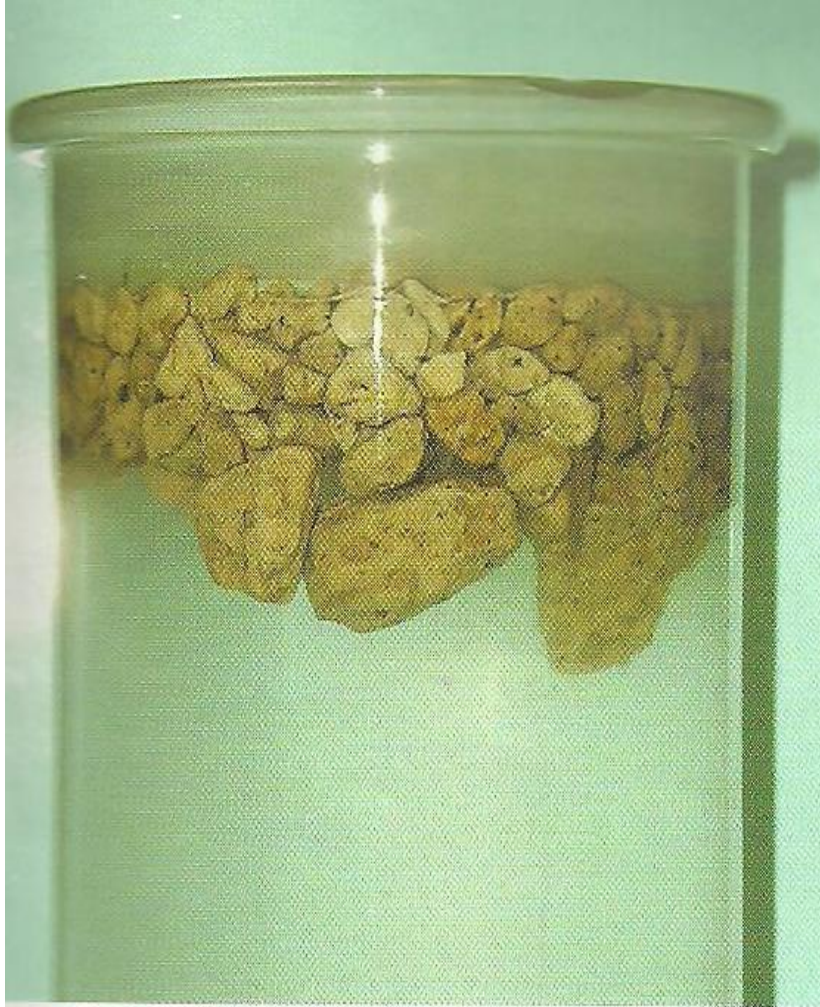


Figure 45: *Lapilli samples floating on water*

4.10 Climate and vegetation

The climate is generally dry and hot. The low rainfall, which occurs over most of the area, combined with the lavas which form the bedrock, produce a semi-arid landscape. Rainfall in the study area is however concentrated in to two rainy seasons of; March - May and October – November. Mean annual temperature is 16 - 18 °C. Mean maximum temperature is 22 - 24 °C and mean minimum temperature is 10 to 12 °C which is described as cool temperate climate. The average annual potential evaporation is between 1650 and 2300 mm. The vegetation is generally composed of stunted thorn bushes (including the whistling thorn, *Acacia drepanolobium*) and patches of grass, but river and stream beds are often marked by lines of trees and seasonal rivers such as the Ewaso Ngiro, the Seyabei and the Kedong have thicker vegetation along their banks. The drainage from fault blocks and from Suswa does not extend for any great distance but rapidly infiltrates the thick cover of soil and alluvium.

4.11 Hydrological analysis

Maai Mahiu is georeferences at $0^{\circ} 59' 28.19''$ S, $36^{\circ} 15.18''$ E it lies on the floor of the great Rift Valley and surrounded by Mt. Longonot towards the North which is at the height of 7972 ft above sea level on the South West lies the Mt Suswa whereas on the East is Kijabe Hill. The plain is traversed by deep galleys due to erosion by flash floods.

Besides the low rainfall, Maai- Mahiu Division has very few surface water bodies; the most notable one being a dam at Maai Mahiu Township. The division lacks sufficient water schemes with those existing being run by individuals or self-help groups. The bore holes that have been drilled by individuals have yielded salty or hot water while others have not yielded any water.

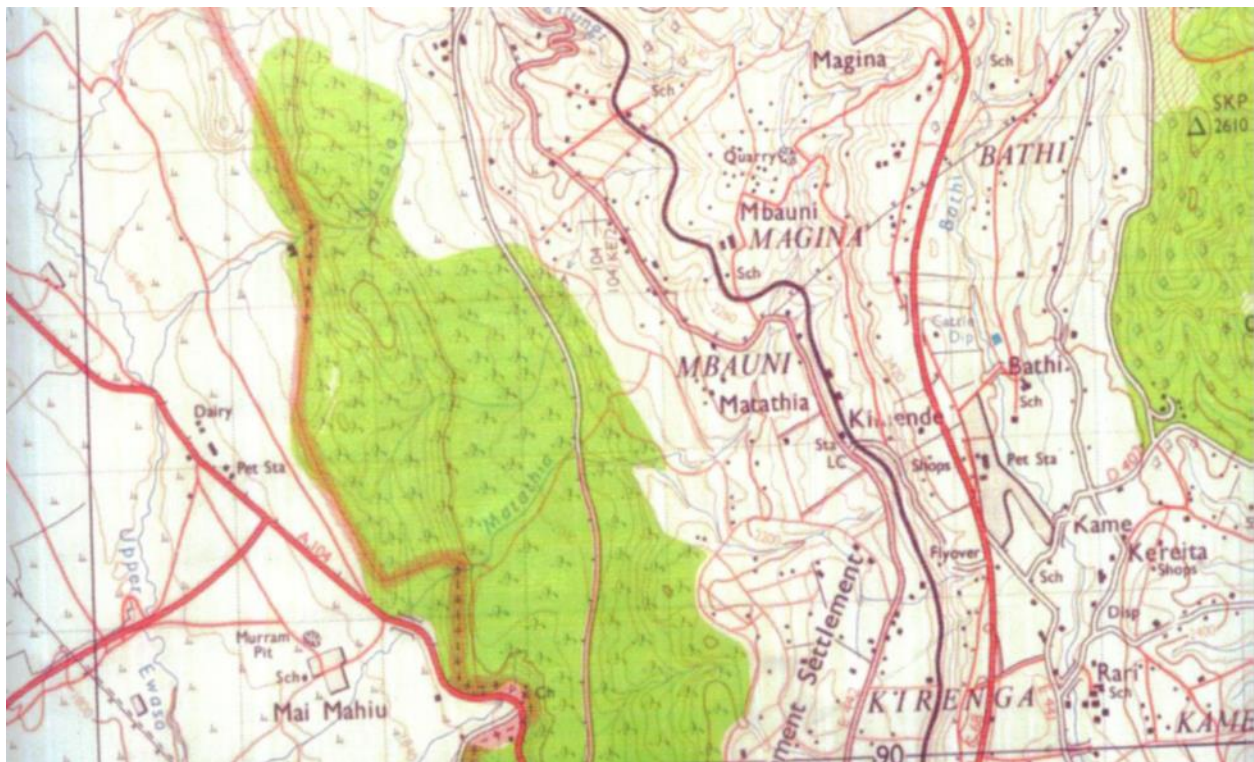


Figure 46: Map of rivers within area of study

From the findings of the research, the respondent's view of Maai Mahiu was that the area experiences very low annual rainfall. The fact is that Maai Mahiu lies on an Arid and Semi-Arid Land. According to Hutchison (1977) in the tropics Arid Lands receive an annual rainfall between 25 and 250mm of rainfall. This was noted by the presence of many respondents who rated general aridity as affecting water scarcity to a great extent. A good number of respondents were also convinced that there were presence of few lakes and rivers in the Division. The Division has no existing lake or large water mass. A low ground water supply is used by majority of the respondents as a means of acquiring water in Maai Mahiu. During the dry seasons most of

the water was lost from the soils through percolation and rapid evaporation as the temperature within this period would rise to very high degrees. These high temperatures lead to rapid depletion of water from the unconfined shallow aquifers during the dry seasons.

Table 13: *Spatial Variability of Average Annual Surface Water Availability*

Drainage area	Volume in million cubic meters per year	Percentage of water abstracted
Lake Victoria	11,672	2.2
Rift valley	2,784	1.7
Athi River	1,152	11.6
Tana River	3,744	15.9
Ewaso Ng'iro	339	12.4
National	20,291	5.3

Source: United Nations Water Report (2006)

It is observed that all the perennial rivers that existed in the area in the past few decades had dried and in their place were gulleys and dry river beds. With the climate variations, a section of the Maai Mahiu – Narok Road got washed away by the recent floods in the district. On a visit to the scene where the Maai Mahiu – Narok had shown cracks forcing the closure of the road on the 17th of May, 2012, it is noted that the area lied on an extinct river. Due to the heavy downpour the water had found its way to the river bed and this led to the washing away of the section of the road. As shown in the image below, figure 47, the section of the road lied directly on an extinct waterway.



Figure 47: *Section of the road that was washed away*



Figure 48: *Part of the Dry Water Bed of river Tongi Tongi*

The Google map image (Figure 47) above, clearly shows the dried up river bed and the point it intersects with the road. For the planners and contractors of the road, this intersection should have been designated as a bridge and this goes to show the importance of looking at the past so as to clearly see the future. This is an essential aspect of planning.

4.12 Physiography and drainage

Though commonly referred to as a plateau, the investigated area is really a step on the side of the Rift Valley. The site lies at an altitude of about 1937 m, on a gently undulating terrain with occasional deep incisions of river terraces. The site is covered by light coloured soils developed on volcanic ashes, weathering and erosion processes of pyroclastics and sediments. The higher grounds on the steep hill and its slopes are covered by boulders of welded pyroclastics and comendite clasts. An eruption fissure oriented in N-S direction is inferred from the geological map. The fissure is not very clear on the surface though its presence could have been obscured by the thick pyroclastic and lacustrine sedimentary formations.

The pictures below indicate two scenarios on the situation in Maai Mahiu during the long rains. In the first picture, an entire internal road has been turned into a waterway due to the lack of a proper road and drainage system which can be attributed to poor planning. The second shows a section of the Longonot Township, along the Nairobi-Maai Mahiu-Naivasha Road during the same period. This is a clear indication of plenty of water going down the drain.



(A)

(B)

Figure 49: A) *Flooded road at the Longonot town center, B) A section of the Maai Mahiu-Naivasha highway*

Whilst climate change and increased intensity of rainfall may be blamed for the recent rampant flooding, the fundamental problem is that water courses are being blocked as a result of human activities such as building houses across water ways, the lack of adequate and the right drainage infrastructure and the siltation of the only dam in the division.

Figure 50 below is a Registry Index map, Kijabe/Kijabe Block Sheet 4, showing the uncoordinated subdivisions in one of the settlements in Kijabe Location in which Maai Mahiu Township falls. As clearly indicated the parcel number 3723 is a designated Dam. Nevertheless, as the findings indicated that this land has been encroached. The dam does not have an intake or a spill way since the land suitable for these facilities have been encroached and the land

subdivided and the parcels developed. It is observed that an abattoir lies about 400 meters upstream and discharged its liquid wastes into the dam.

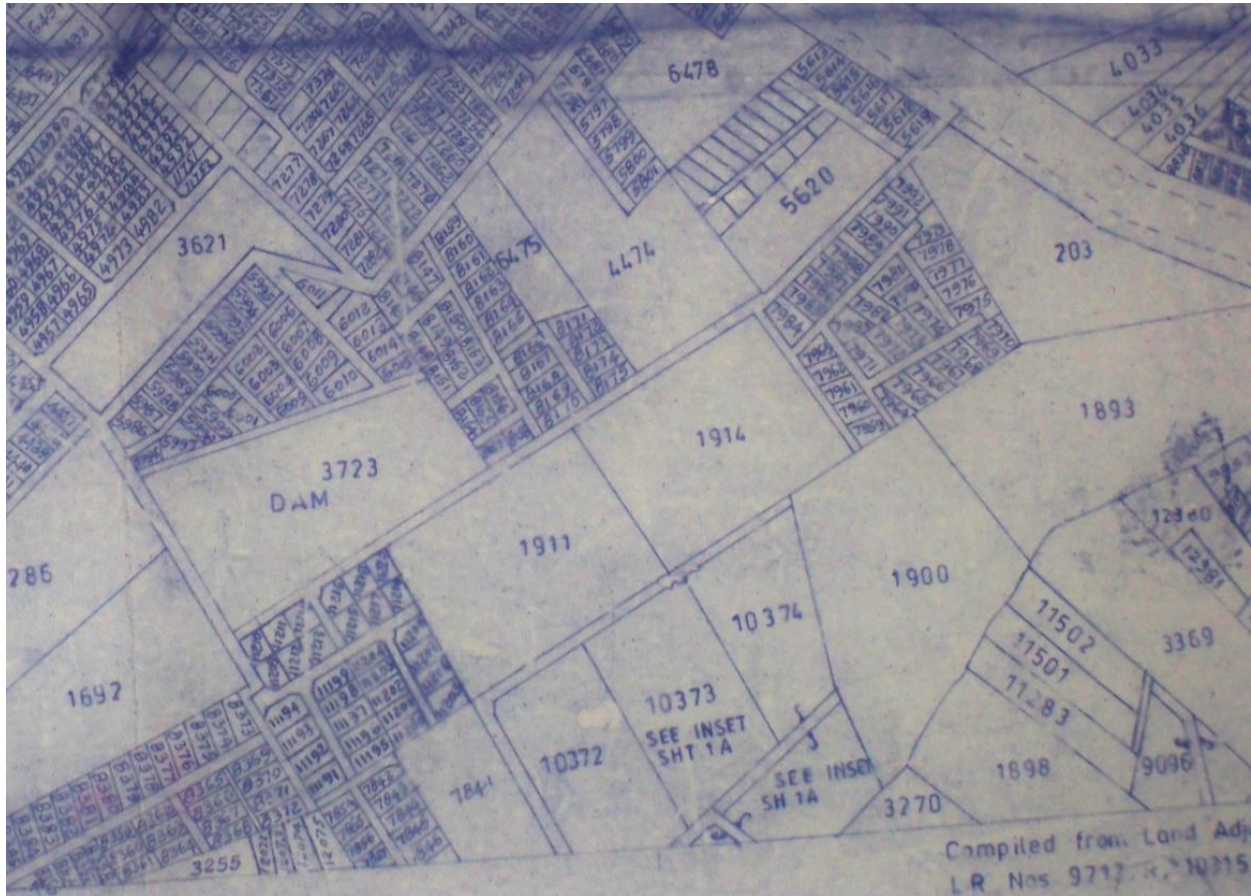


Figure 50: A section of Registry Index Map for Kijabe/Kijabe Block 1 (Sheet 4)

Source: Provincial Survey Office (2012)

4.13 Electrical resistivity tomography survey (ERT)

The electrical resistivity method is used to study the distribution of electrical properties in the subsurface by injecting electrical current and measuring the induced potential difference at various locations along the ground surface. These variations in electrical resistivity are used to map out vertical and horizontal discontinuities within the area of interest.

In this study electrical resistivity tomography data were acquired along three profiles. Profile 1 and 2 stretch over a distance of 300 metres each while profile 3 stretches over a distance of 200 metres. Profile one was performed along nearly south– north transect, profile 2 was oriented in

northwest-southeast direction while profile 3 was in west-east direction. All the ERT measured were acquired with an electrode spacing of 5 metres.

4.13.1 Electrical Resistivity tomography profile 1 (S-N)

The tomogram for the profile 1 conducted on the proposed site is presented in Figure 52. The profile runs nearly South-North direction and divides the proposed site into two equal regions. The electrodes were spaced a distance of 5 metres, which probed the earth's subsurface to a depth of 37.3 m below the ground surface. The ERT profile stretched over a distance of about 320 metres.

The tomogram shows an overall wide range in resistivity values of the formations probed that ranges from 1 Ωm to over 726 Ωm . Resistivity distribution in (Fig. 52) indicates the unsaturated near surface soil represented by high resistivity (339-726 Ωm), almost along the entire profile line. Local high resistivity in the near surface material is due to or can be attributed to the presence of gravelly to loamy fine sand which are very dusty. The thickness of this top layer varies between 0.5–5 m along the entire profile line. There are some local high resistivity zones (>726 Ωm) near the surface between horizontal distance 25 m and 205 m, indicating localized lateral resistivity inhomogeneities in the near surface material (dark purple), which are due to the presence of medium size dry boulders of pumiceous tuffs; such features are observed at this site.



Figure 51: *Gravelly to loamy fine sand formation*

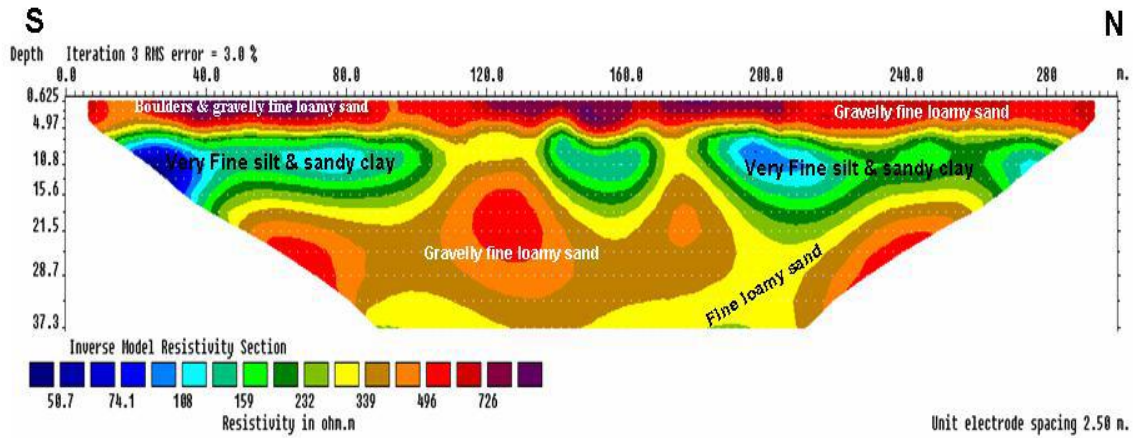


Figure 52: Modeled resistivity section along the Electrical Resistivity Tomography (ERT) Profile 1

Notably, just below the top layer along the entire profile line there is distinct decrease in resistivity values with resistivity ranging from 50 to 232 Ω m. This characterized the presence of finer materials (silt and clay which is a product of volcanic ash) with variable but low moisture content. Below this layer is another formation with equivalent physical characteristics as the first layer (top layer).

4.13.2 Electrical Resistivity tomography profile 2 (N40°W-S40°E)

The tomogram for the profile 3 is presented in Figure 53. The total length of the profile is 300 metres and oriented in a N40°W-S40°E and electrode spacing along the profile was also 5 metres, which still probed to a depth of 37.3 metres below the ground surface.

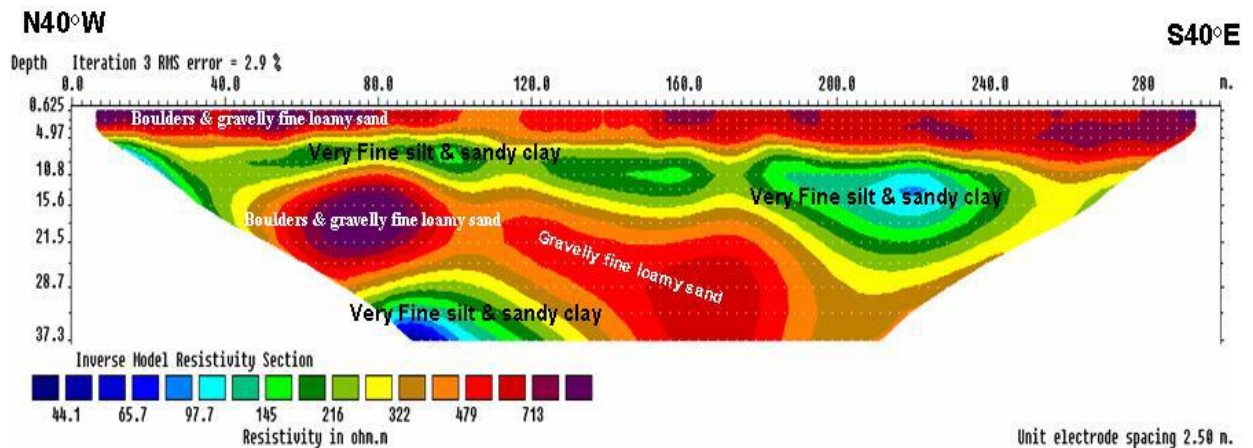


Figure 53: Modeled resistivity section along the Electrical Resistivity Tomography (ERT) Profile 2

This geo-electric model has similar physical characteristics as the profile 1 described above. The first layer shows high resistivity values representing near surface gravelly to loamy fine sands. Below it indicates another layer sandwiched between two similar formations with reduced resistivity values ranging from 44-216 ohm metre. This layer runs along the entire profile line and represents a finer material whose formation can be attributed to a matrix of compact fine silts and clay. The same layer appears to the northwest of the profile at a depth below 28.7 metres between horizontal distance of 70 metres and 135 metres.

4.13.3 Electrical Resistivity tomography profile 3 (W-E)

The tomogram for the profile 3 is presented in Figure 54. The total length of the profile is 300 metres and oriented in a W- E and electrode spacing along the profile was also 5 metres, which still probed to a depth of 37.3 metres below the ground surface. The resistivity distribution for this model is more or less similar to the two models described above with resistivity ranging from 54 Ω m to 792 Ω m.

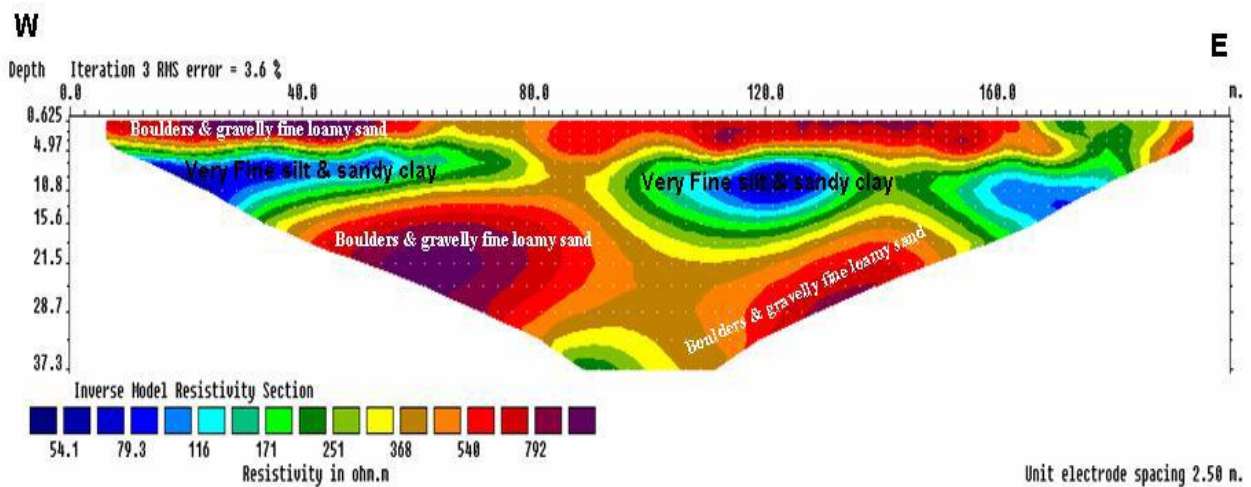


Figure 54: Modeled resistivity section along the Electrical Resistivity Tomography (ERT) Profile 3

Resistivity distribution in Fig. 54 designates the dry near surface soil represented by high resistivity (368-792 Ω m) which can be interpreted as gravelly to fine loamy sand as depicted in the other two models above. Underlying this top layer is another low resistivity zone with resistivity values ranging from 54-251 Ω m, this layer can be interpreted as very fine formation of silt and clay with low content of moisture. There are localized zones of high resistivity (purple colour) below the low resistivity formation whose physical characteristics are comparable to the first layer. However, all the tomograms show that the lithological formations in the area have high resistivity values ranging from 44 Ω .m – 792 Ω .m. This is not ideal for grounding and therefore it calls for careful designing and selection of earth resistance electrode that will be

suitable for earthing system. There is also a need to look for an artificial soil with good resistivity (low resistivity values) to be used within the road construction.

4.14 Multi-Channel Analysis of Surface Waves (MASW)

4.14.1 Analysis of the Data

MASW survey was done on two profiles within the site whereby each profile has got three seismic spreads. Acquired MASW data were processed and interpreted using SeisImager/SW software to determine shear-wave velocity (Vs). This software has three more modules i.e. Pickwin, WaveEq and GeoPlot for the analysis of surface wave data. The first step in the analysis is making the file list in which all waveform files and source receiver configuration are mentioned and then cross correlation CMP gather is calculated. Dispersion curves were calculated by converting the data into frequency domain through Fourier transformation of the data and then checked. Generation of a dispersion curve is one of the most critical steps for generating an accurate shear wave velocity profile. Dispersion curves are generally displayed as phase velocity versus frequency. This relation can be established by calculating the phase velocity from the linear slope of each component of the swept frequency record. The 1D shear wave velocity profiles are calculated using non-linear least square method using the dispersion data.

The 1D shear wave velocity profiles are calculated using the dispersion curves obtained from waveform data by non-linear least square method. Then, by placing each 1D Vs profile at a surface corresponding to the middle of the survey line, a 2D Vs map is constructed in GeoPlot software. That is, multiple Vs profiles obtained are then used for a 2D interpolation to create the final map. The kriging method is used for this interpolation. This is a geostatistical interpolation method that considers both the distance and the degree of variation between known data points when estimating unknown areas. Kriging method is particularly appropriate where best estimates are required, data quality is good, and error estimates are essential.

4.14.2 Seismic site characterization using Vs30

The shear wave velocity averaged over the top 30m of soil is referred as Vs30 and is computed by dividing 30 m with the travel time from the surface to 30 m as given by the following Equation:

$$V_{s30} = \frac{30}{\sum_{i=1,N} \frac{h_i}{V_i}}$$

Where, h_i and V_{si} denote the thickness and shear wave velocity of the N layers existing in the top 30 meters. V_{s30} can also be automatically generated by the SeisImager/SW. Modern seismic codes like NEHRP, UBC97, IBC2000 and Eurocode8 use V_{s30} for doing the site characterization. The site classes estimated from shallow shear wave velocity models are also important in deriving strong motion prediction equations and in applications of building codes to specific sites.

Profile 1

Profile 1 is comprised of three seismic spreads and in each spread both 1D and 2D seismic survey were conducted. The V_{s30} for all the test sites are calculated using the above equation. For spread 1 the values of V_{s30} are ranging from 262 to 397 m/s. Spread 2 the values range from 297 to 389 m/s and for spread 3 the values vary between 520 and 598 m/s.

Profile 2

Profile 1 is comprised of three seismic spreads and in each spread both 1D and 2D seismic survey were conducted. The V_{s30} for all the test sites are calculated using the above equation. For spread 1 the values of V_{s30} are ranging from 169 to 350 m/s. Spread 2 the values range from 216 to 354 m/s and for spread 3 the values vary between 480 and 615 m/s.

It has been observed that shear-wave velocities measured using MASW within the project site correlate well with geological settings. It is evident from the site study that the soil is stiff from the surface to 8 m depth ($V_s \sim 180\text{--}360$ m/s), followed by partially weathered and marginally fractured rocks to a varying depth of 18 m (velocity ranging from 360 to 500 m/s). In most of the study areas of Maai Mahiu V_{s30} falls in the range 250–350 m/s, except the southern part of the site which has velocity of 360–530 m/s. Based on V_{s30} of the soils, a major portion of the study area is predominantly classified as D-type (180–360 m/s) in accordance with the 1997 NEHRP provision. Sites located in the southern part of the area have V_{s30} values larger than 360 m/s, thereby qualifying the soils as NEHRP class C-type (360–760 m/s).

Data was analyzed using SeisImager/SW software and two dimensional shear wave velocity models at every 5m depth from ground surface was developed. Also, the average shear wave velocity up to 30m (V_{s30}) was measured which is used for site characterization. Based on the V_{s30} value, Maai Mahiu Quantum site has been divided into two seismic zones i.e., zone A ($V_{s30} > 350$ m/s) which has been classified as class C and zone B ($250 \leq V_{s30} \leq 350$) as class D (see Figure 55 below).

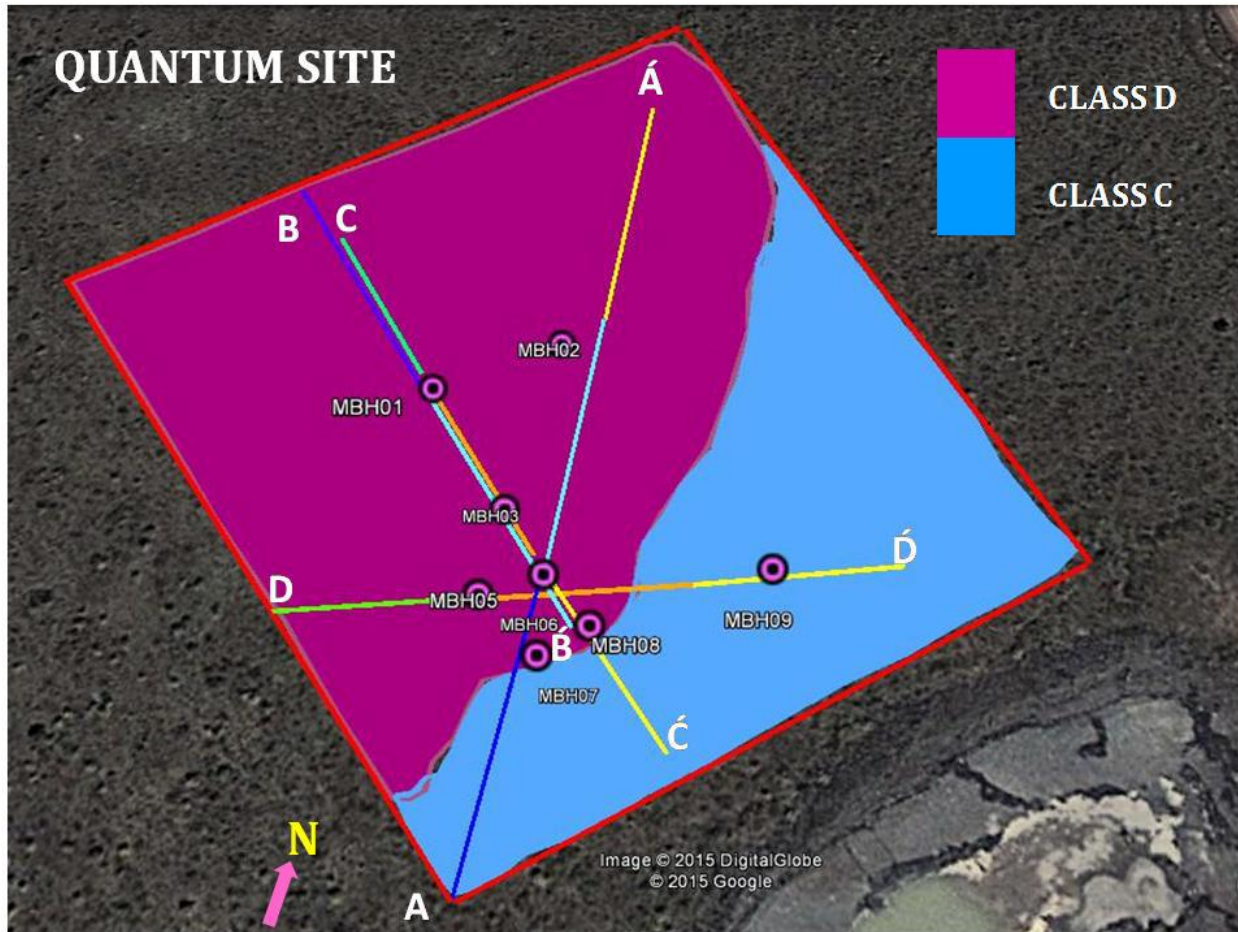
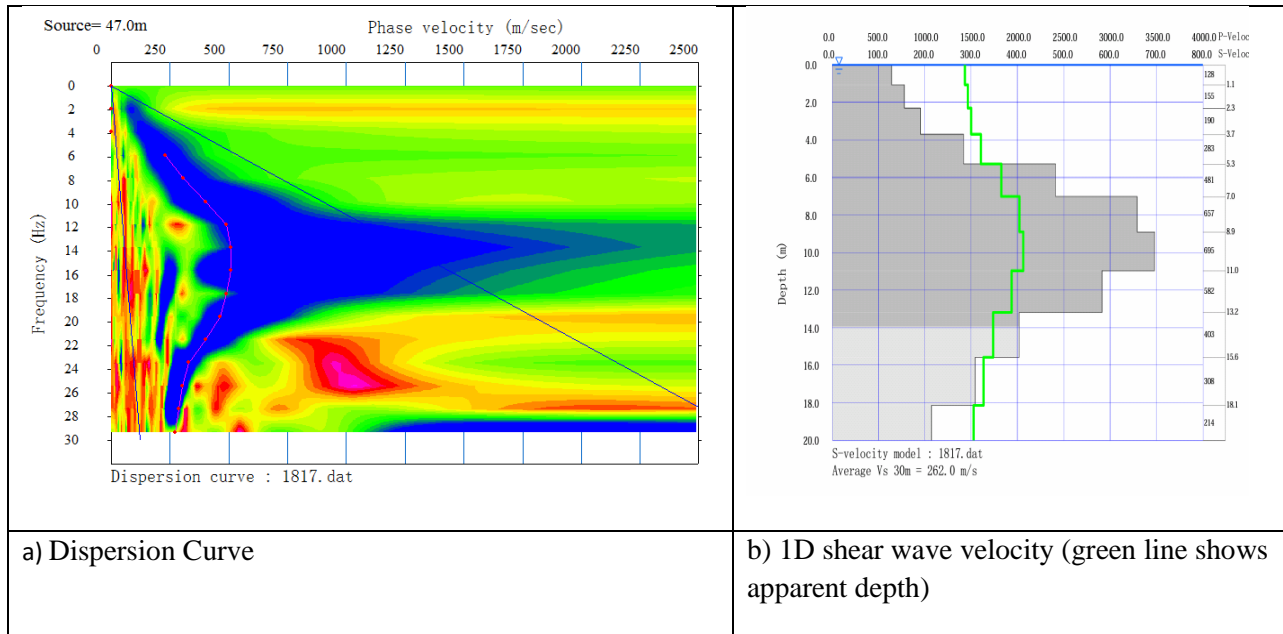


Figure 55: Seismic lines and site Classification zones

4.14.3 Data Interpretation of Active MASW

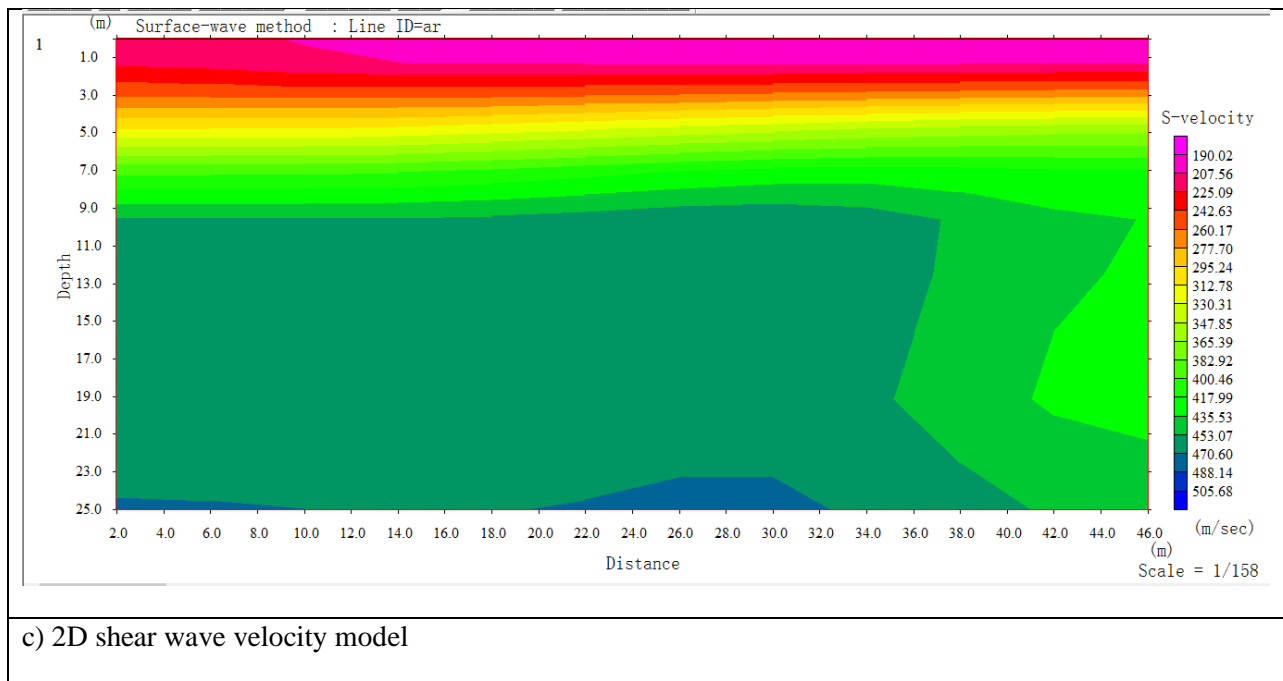
(a) Profile 1 (Spread 1)

Profile 1 is designated by line CC' in Figure 55 above and is comprised of three spreads, each represented by different colour (See Fig. 55) with the general orientation of the profile is in NW-SE direction. The results of MASW data (Fig. 56) indicated that the site has three layers. The upper layer (pink to red colour) has V_S ranges from 190 m/sec to 277 m/sec (overburden material) attaining maximum depth thickness of 3 m and is interpreted as gravelly silty sand with admixture of lake sediments. The middle layer (designated by light green colour) with V_S ranging between 277 m/sec to 470 m/sec is interpreted to be composed of fractured and weathered pumitic trachyte. This layer extends to a depth greater than 30 m between 40 m mark and beyond 46 m mark. The lower layer (dark green colour) which is the basement trachyte rock with V_S ranging between 470 m/sec to over 505.68 m/sec is composed of fractured basement trachyte rock. Below a depth of 25 m an intrusion of basaltic rock is captured.



a) Dispersion Curve

b) 1D shear wave velocity (green line shows apparent depth)



c) 2D shear wave velocity model

Figure 56: a) Dispersion Curve, b) 1D shear wave velocity and c) 2D shear wave velocity model

(b) Profile 1 (Spread 2)

The results of MASW data (Fig.57) indicated that the site has three layers with reduced rock strength as compared to the first spread. The upper layer has VS ranges from 155.74 m/sec to 182.16 m/sec (overburden material). The middle layer VS ranged between 182.16 m/sec to 327.51 m/sec (highly fractured and weathered trachyte). The third layer had VS ranges between

327.51 m/sec to over 393.57 m/sec (partially fractured and marginally weathered basement rock composed of trachyte).

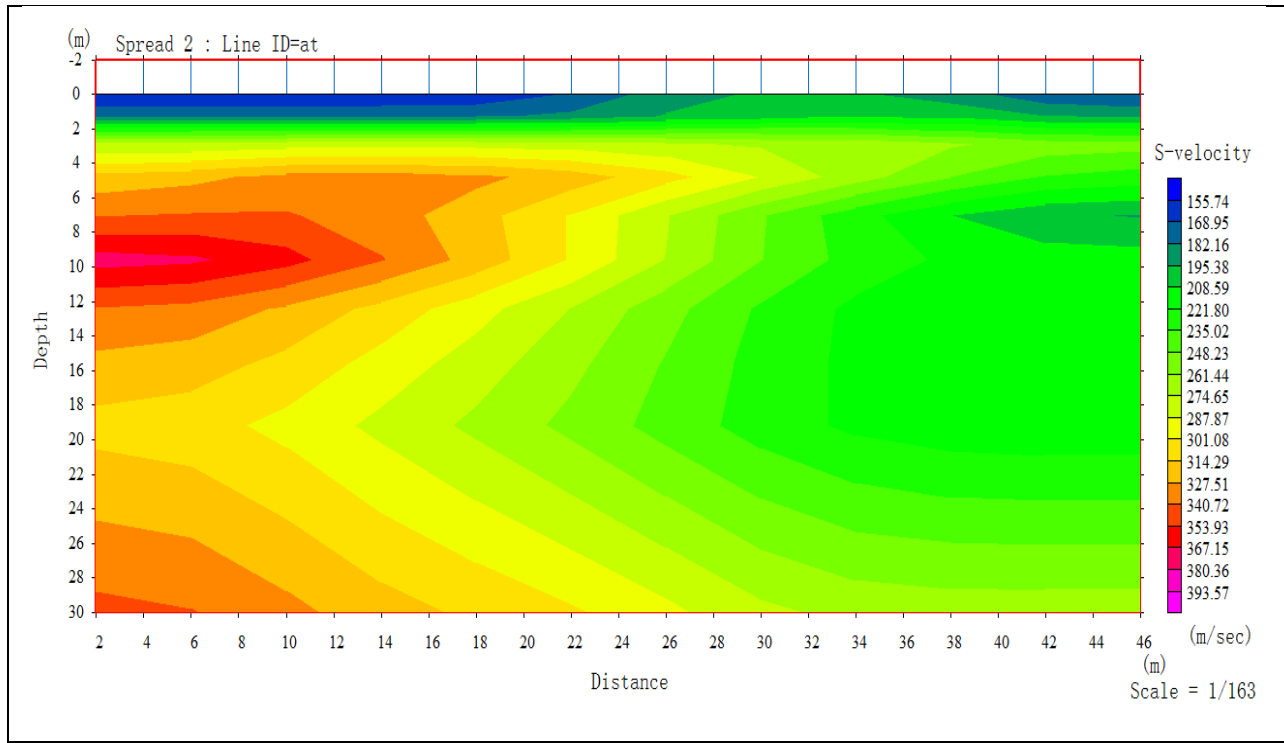
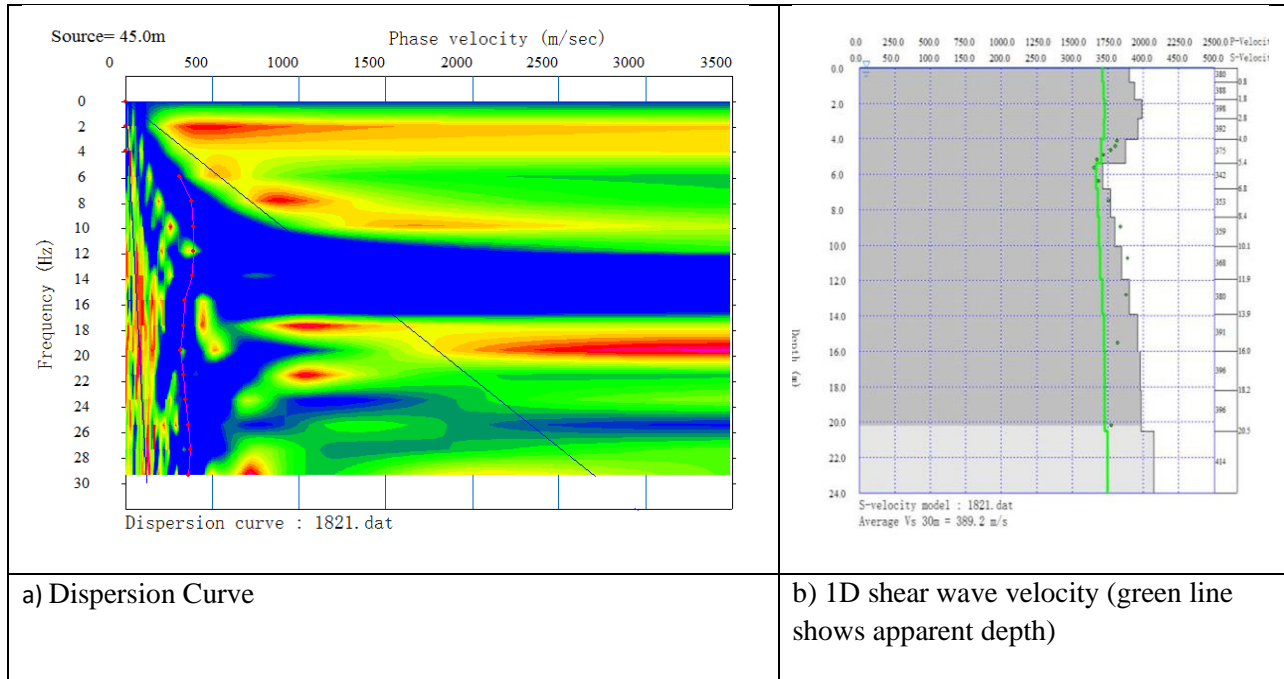
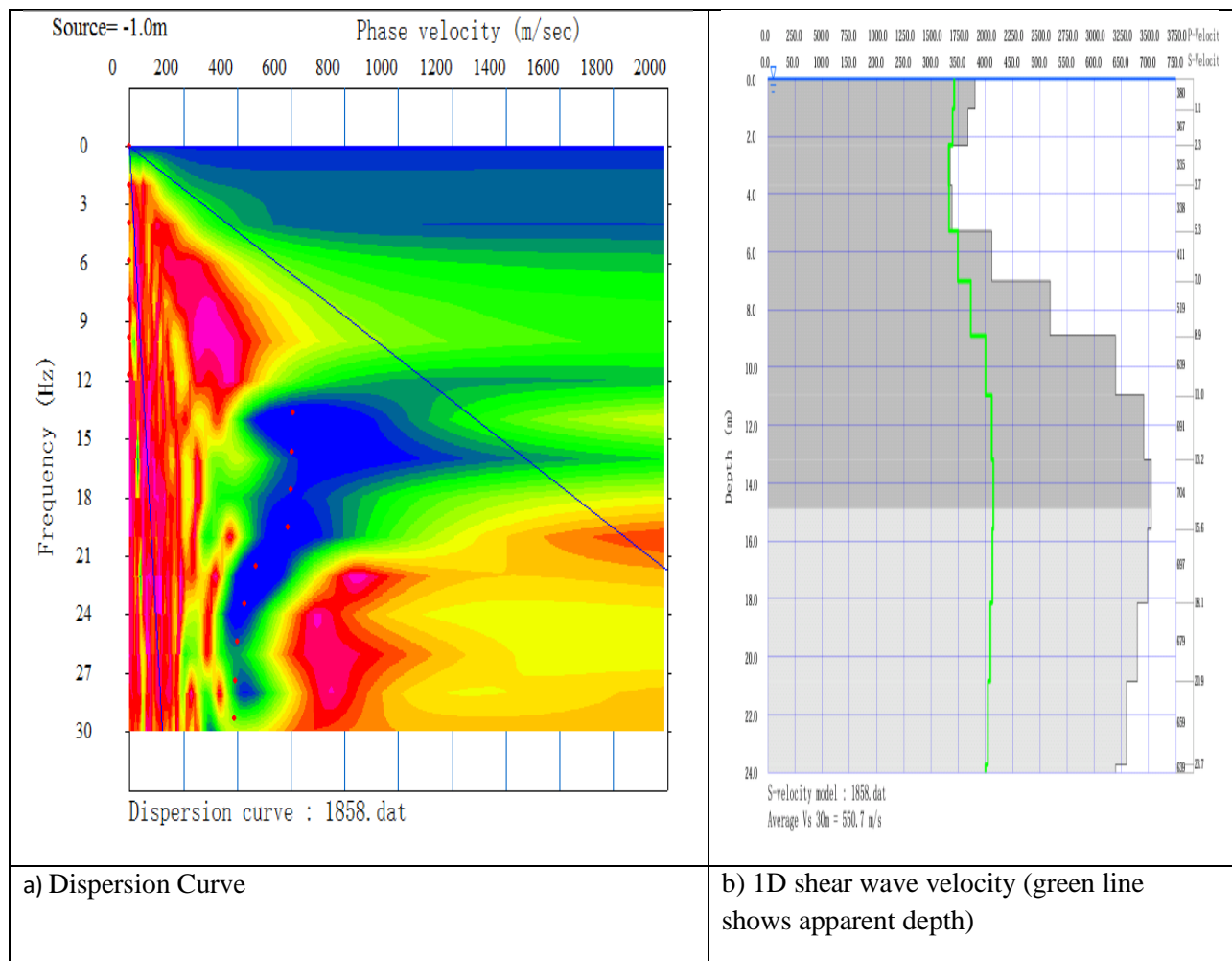


Figure 57: a) Dispersion Curve, b) 1D shear wave velocity and c) 2D shear wave velocity model

(c) Profile 1 (Spread 3)

The results of MASW data (Fig.58) indicated that the site has four layers. The upper layer has VS ranges from 195.96 m/sec to 297.41m/sec (overburden material). The middle layer VS ranged between 297.41 m/sec to 551.02 m/sec (fractured and weathered trachyte). The third layer had Vs ranges between 505.68 m/s to 601.74m/sec (competent rock) and finally the lower layer had VS ranges between 601.74 m/sec to over 652.46 m/sec (fractured and weathered trachyte). The volcanic flow/intrusion (possibly basalt) is captured between a depth of 12 m and 17 below the ground level and is interpreted as a lens of sill structure. The rock sill is overlain by pumitic rock and underlain by trachyte between the horizontal distance 0 m mark and 28 m mark before widening out to form dyke whose depth root goes beyond 30 m below the ground level. Both sill and dyke is characterized by high velocity values.



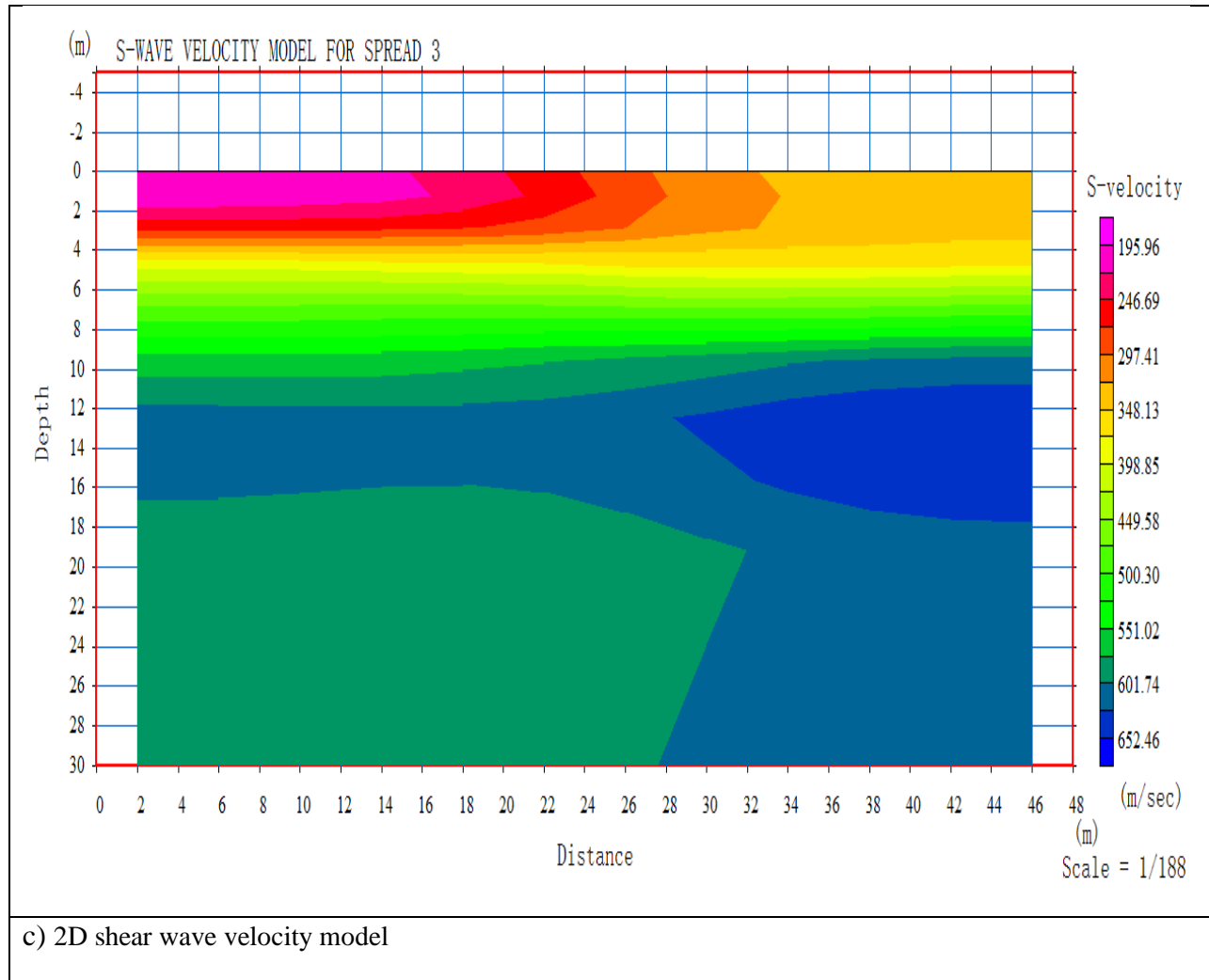
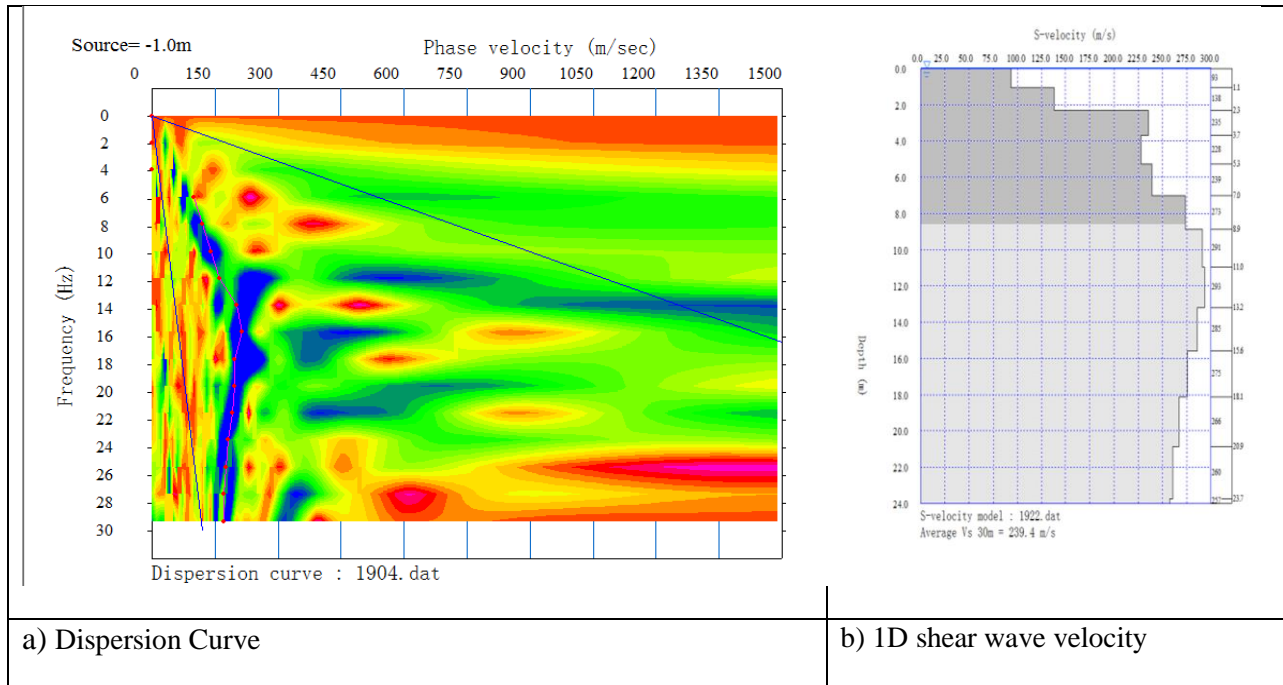


Figure 58: a) Dispersion Curve, b) 1D shear wave velocity and c) 2D shear wave velocity model for spread 3

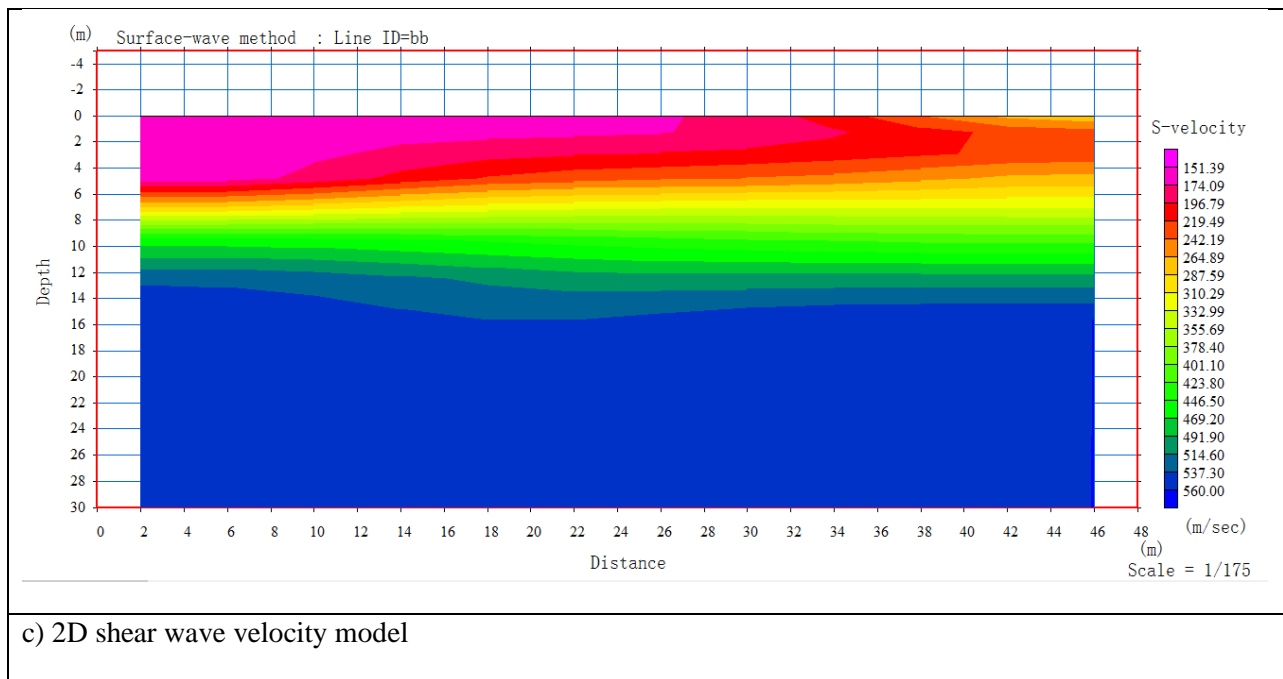
Profile 2 (Spread 1)

Profile 2 is designated by line DD' in Figure 55 above and is comprised of three spreads, each represented by different colours (See Fig. 55) with the general orientation of the profile is nearly W-E direction. The results of MASW data (Fig.59) indicate that the site has three layers. The upper layer had VS ranges from 151.39 m/sec to 219.49m/sec (overburden material) and is interpreted as gravelly silty sand composed lake sediments. The middle layer VS ranged between 219.49 m/sec to 491.90 m/sec and is interpreted as fractured and weathered trachyte. The third layer forms the basement rock and has Vs ranges between 491.90 m/s to 560 m/sec fractured rock and is interpreted as composed of moderately hard and soft basaltic rock.



a) Dispersion Curve

b) 1D shear wave velocity



c) 2D shear wave velocity model

Figure 59: a) Dispersion Curve, b) 1D shear wave velocity and c) 2D shear wave velocity model for spread 1

Profile 2 (Spread 2)

The results of MASW data (Fig. 60) indicated that the site has two layers. The upper layer has VS ranges from 142.96 m/sec to 185.53m/sec (overburden material) and is interpreted as gravelly silty sand composed lake sediments with conglomerate of decomposed pumitic

trachytes. The second layer which is the basal layer has VS ranges between 185.53 m/sec to 270.68 m/sec and is interpreted as fractured and weathered trachyte. The fractured and weathered rock is outcropping on the surface between 18 m mark and 36 m mark. The depth ranging between 8 m and 18 m is characterized by highly weathered and fractured rock (decomposed). Beyond 18 m below the ground level is composed of marginally weathered and partially fractured trachyte (rock).

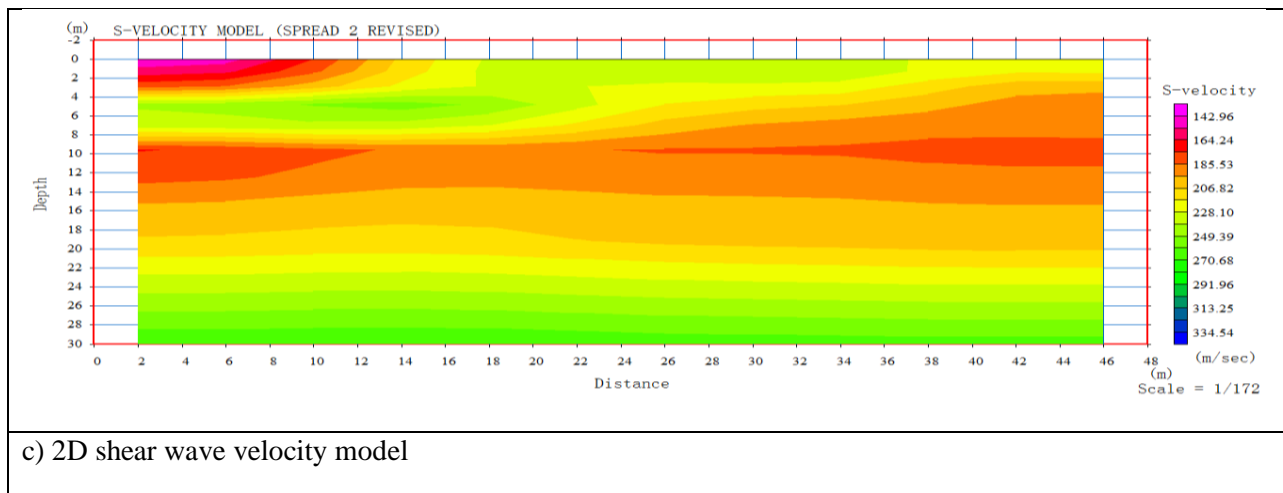
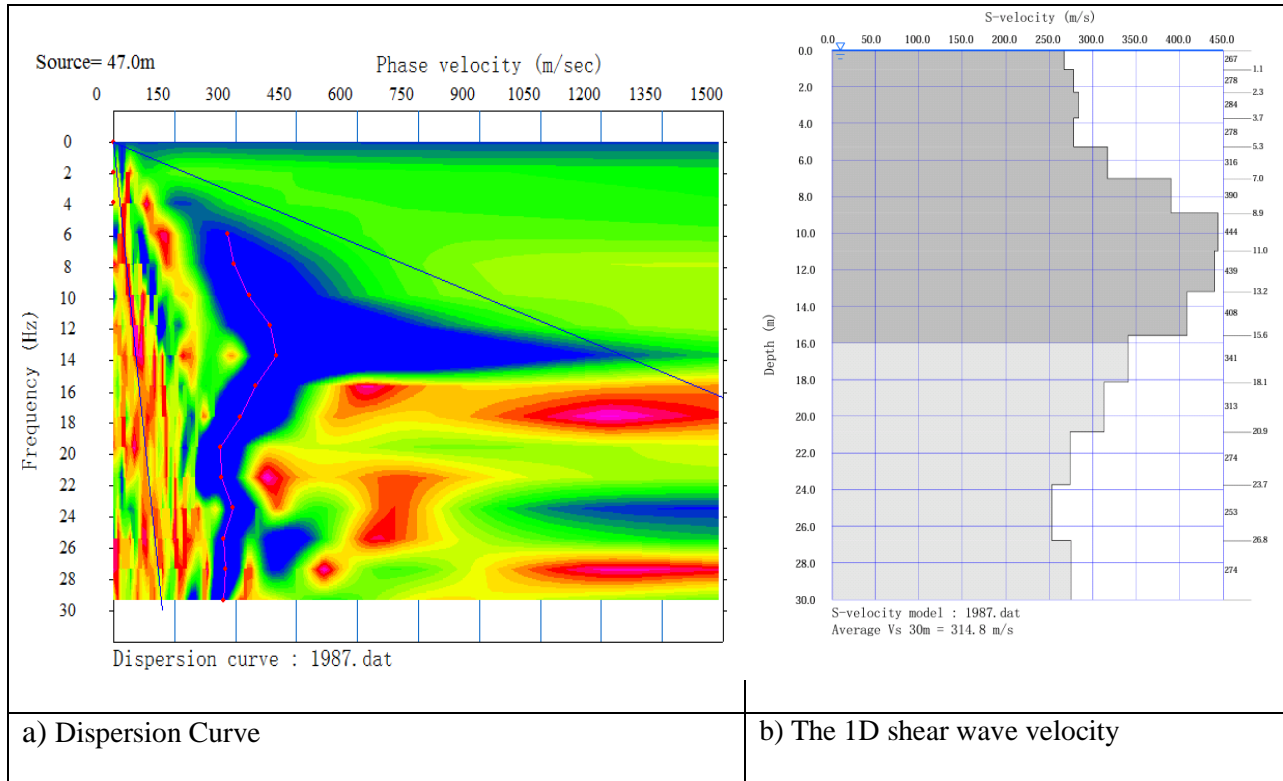
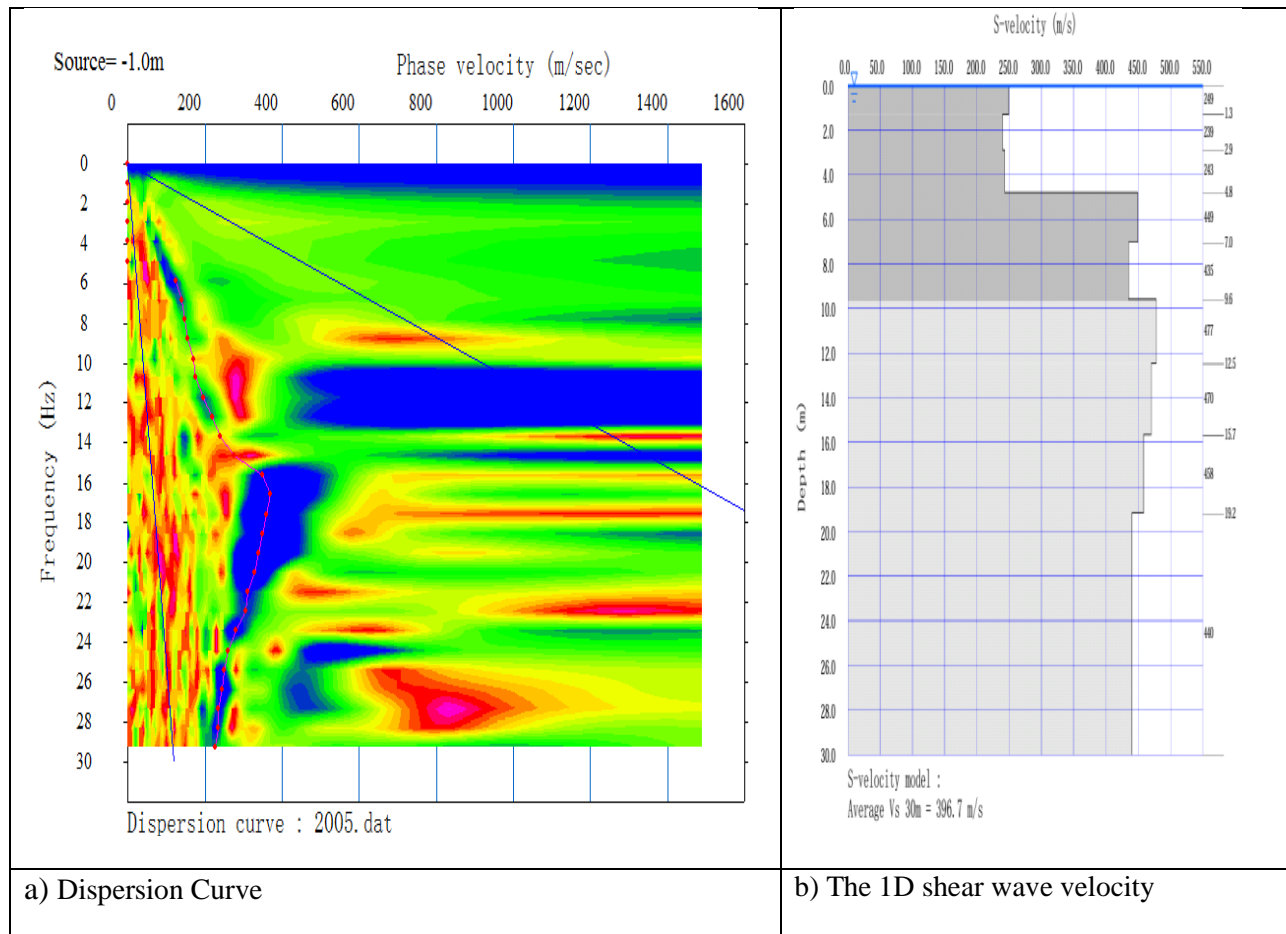


Figure 60: a) Dispersion Curve, b) 1D shear wave velocity and c) 2D shear wave velocity model for spread 2

(d) Profile 2 (Spread 3)

The results of MASW data (Fig. 61) indicated that the site has four layers. The upper layer had VS ranges from 93.68 m/sec to 179.84m/sec (overburden material) represented by pink to red colours which is only captured to the east of the profile. The middle layer (designated by blue colour) has VS ranges between 438.34 m/sec to 481.42 m/sec (fresh and competent rock). The third layer had which is the basal layer has Vs ranges between 179.84 m/s to 438.34 m/sec (marginally fractured trachyte). The volcanic flow/intrusion (possibly basalt) is captured between a depth of 7 m and 16 m below the ground level and is interpreted as a lense of sill volcanic structure composed of volcanic rocks (basalt). The sill structure is overlain by pumitic trachytic rocks and underlain by trachyte for the entire length of the seismic spread. The sill structure is characterized by high velocity values.



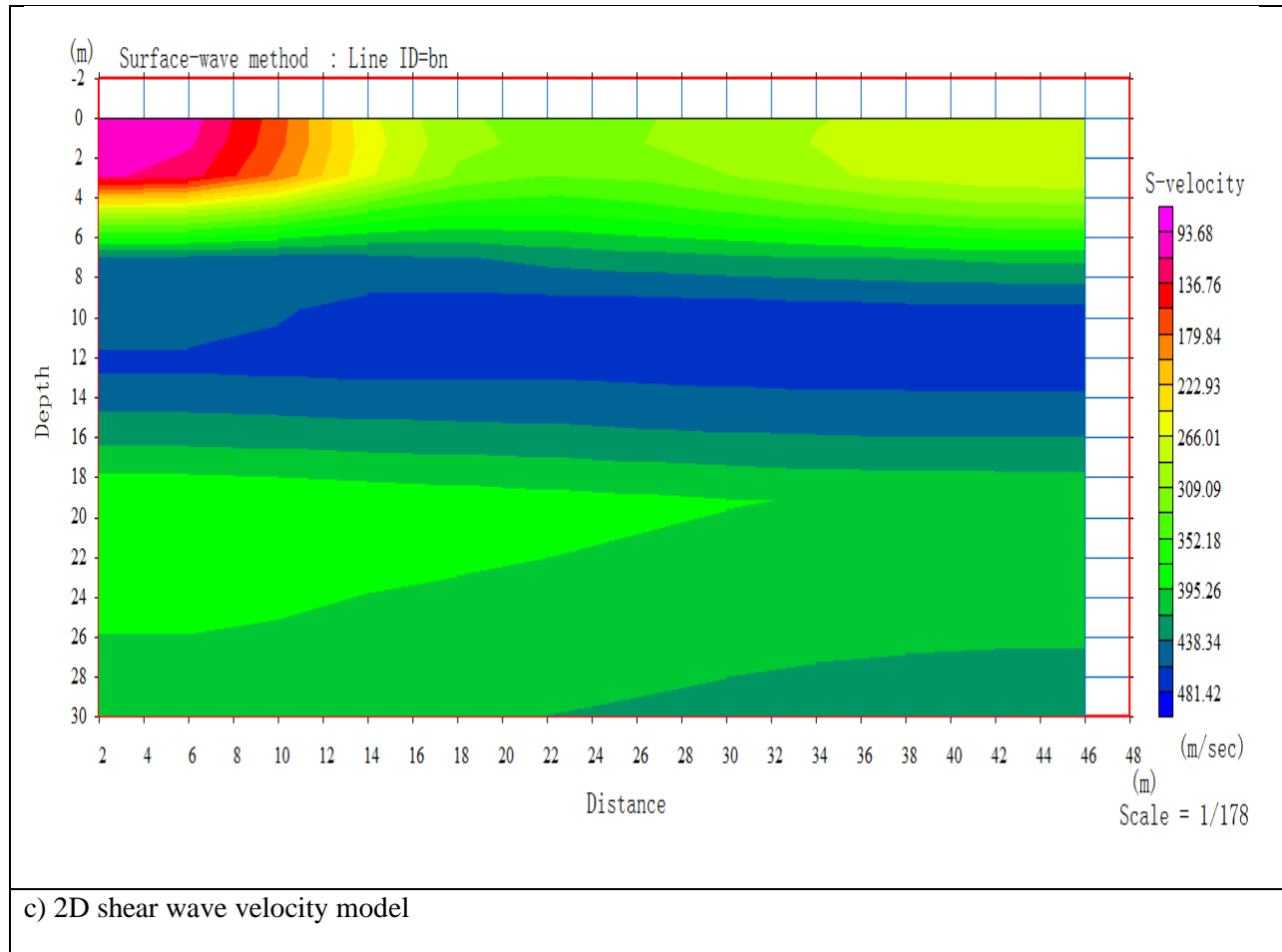


Figure 61: a) Dispersion Curve, b) 1D shear wave velocity and c) 2D shear wave velocity model for spread 3

4.14.4 Site Engineering Parameters

To calculate engineering parameters which are given in Table (9), the values of P-wave velocity and S-wave velocity, In Situ field Density (ρ), Poisson's Ratio (σ), Young's Modulus (E), and the Shear Modulus (μ) were required. To calculate elastic modulus we used the equation given in Table (6). The P-waves were obtained from the acquired seismic refraction while S-waves obtained from MASW. The density values for different layers were obtained from MASW in the field. It is important to note that the density of material can also be derived from laboratory tests (rocks) and field density test (soils) by using Sand cone experiment. The field density derived from MASW analysis of 1st layer ranges from 1.72 to 1.79 gm/cc, 2nd layer ranges between 1.85 to 1.908 gm/cc while ranges from 1.89 to 1.981gm/cc for 3rd layer, which is characterized by relatively high rock density. Table 7 contains elastic/dynamic parameters of lithology across the right the project area.

Table 14: List of Equations used to calculate Elastic/Dynamic Parameters

Elastic parameters	Used equation
Poisson's Ratio	$\sigma = \frac{1}{2} \left[1 - \frac{1}{\left(\frac{v_s}{v_p}\right)^2 - 1} \right]$
Young's Modulus	$E = \rho \left[\frac{3V_p^2 - 4V_s^2}{\left(\frac{v_s}{v_p}\right)^2 - 1} \right]$
Shear Modulus	$\mu = \left[\frac{E}{2(1 + \sigma)} \right]$

Table 15: Ranges of the calculated elastic parameters of the lithological units within the project site

Layer	V_p (ms^{-1})	V_s (ms^{-1})	Density (ρ)-gm/cc	Poisson's Ratio (σ)	Young's Modulus (E) - Mpa	Shear Modulus (μ) - Mpa
PROFILE 1						
Spread 1						
1	468	234	1.72	0.33	262.8	98.8
2	1,056	615	1.908	0.24	1,782	718.8
3	3,200	1,872	1.981	0.23	16,551	6,728.1
Spread 2						
1	473	240	1.79	0.34	276.3	103.1
2	1,252	687	1.85	0.25	2,076.4	798.6
3	2,637	1,439	1.89	0.28	10,019	3,913.7

The elastic moduli results for the subsurface layers can be summarized as follows:

a) Poisson's Ratio (σ)

Layer 1 across the site is typified by σ ranging from 0.30 to 0.34 and is characterized by relative high Poisson's Ratio, which indicates incompetent soil/rock. Layer 2 has poisson's values ranging from 0.24 to 0.3, which indicates fairly to moderate competent rock. Layer 3 has values ranging from 0.247 to 0.244. The 3rd layer is characterized by relatively low Poisson's Ratio, which indicates relatively competent rock materials.

b) Young's Modulus (E)

Layer 1 is epitomized by E ranging between 262 to 276 Mpa. Layer 2 has values varying between 1782 to 2076 Mpa. Lastly, layer 3 has E values ranging between 10,019 to 16561Mpa. The 3rd layer is characterized by relatively high values of Young's modulus.

c) Shear Modulus (μ) or Rigidity

Layer 1 has shear modulus values ranging from 98.8 to 103.1Mpa. Layer 2 has values varying between 718.8 Mpa and 798.6 Mpa. Finally, layer 3 has values ranging between 3913.7 to 6728.1Mpa. The 3rd layer is characterized by relatively high rigidity or shear modulus (μ) values.

Table 16: List of Equations used to calculate Engineering Parameters

Engineering Parameter	Used Formula
Stress Ratio	$S_i = 1 - 2 \left(\frac{V_s}{V_p} \right)^2$
Index Material	$V = \frac{3 - (V_p / V_s)^2}{(V_p / V_s)^2 - 1}$
Concentration Index	$C_i = \left[3 - 4 \left(\frac{V_s^2}{V_p^2} \right) \right] / \left[1 - 2 \left(\frac{V_s^2}{V_p^2} \right) \right]$
Density Gradient	$D_i = \left[\left(\frac{3}{V_p^2} \right) - \left(\frac{4\mu}{E} - 1 \right) \right] = \left[\left(\frac{3}{V_p^2} \right) - \left(\frac{1-\delta}{1+\delta} \right) \right]$

Table 17: Ranges of engineering parameter results for the subsurface layers

Layer	V_p (ms^{-1})	V_s (ms^{-1})	Stress Ratio (Si)	Index Material (v)	Concentration Index (Ci)	Density Gradient (Di)
PROFILE 1						
Spread 1						
1	468	234	0.50	-0.33	4.0	-0.50
2	1,056	615	0.32	0.026	5.11	-0.61
3	3,200	1,872	0.31	0.041	5.17	-0.63
Spread 2						
1	473	240	0.49	-0.31	4.02	-0.49
2	1,252	657	0.45	-0.24	4.23	-0.54
3	2,637	1,439	0.40	-0.15	4.47	-0.56

The engineering parameter results for the subsurface layers can be summarized as follows:

- 1) The first Layer is characterized by low Concentration Index (Ci) and high Stress Ratio (Si) which reflects weak incompetent soil (rock).
- 2) The second layer was characterized by relative low Concentration Index (Ci) and less Stress Ratio (Si) which reflected fairly competent soil.
- 3) The third layer was characterized by relative high Concentration Index (Ci) and low Stress Ratio (Si).which reflected Moderate competent soil.
- 4) The material Index (v) values for the 1st layer reflected incompetent to slightly competent soil , 2nd layer reflected fairly to moderate competent soil while for the 3rd layer reflects moderate competent to competent soil (rock).
- 5) The calculated Density Gradient (Di) for the 1st layer is characterized by relative high Density Gradient where 3rd layer reveals values characterized by relative low Density Gradient. The calculated engineering parameters for the whole region (project area) are given in Table (9) below.

Table 18: Summary of Ranges of the calculated engineering parameters of the bedrock layers

V_p m/s	V_s m/s	ρ gm/cc	σ	Ci	Si	V	Di	E (Mpa)	μ (Mpa)
LAYER 1									
468	234	1.72	0.33	4.0	0.50	-0.33	-0.50	262.8	98.8
473	240	1.79	0.34	4.02	0.49	-0.31	-0.49	276.3	103.1
LAYER 2									
1,056	615	1.908	0.24	5.11	0.32	0.026	-0.61	1,782	718.8
1,252	657	1.85	0.25	4.23	0.45	-0.24	-0.54	2,076.4	798.6
LAYER 3									
3,200	1,872	1.981	0.23	5.17	0.31	0.041	-0.63	16,551	6,728.1
2,637	1,439	1.89	0.28	4.47	0.40	-0.15	-0.56	10,019	3,913.7

Chapter five: Discussion

5.1 Soil Structure

Soil structure influences the failure of roads as a result of cracks occurring on the ground. The occurrence of cracks on roads depends on the strength of soil and its characteristics (Casagrande, 2006). During the rainy season, when most of the subsidence occurred, the overlying unconsolidated volcanoclastic sediments became oversaturated with water. The water reduced the shear strength of the sediments and also introduced extra loading through saturation leading to subterranean erosion. There are weaker soils where physical removal of sediment due to water run-off occurred leading to failure. Flooding of soils also caused grounds to swell leading to formation of cracks on the surface of the road.

From the results obtained from the research, it was evident that the failure was not only caused by the nature of the soil structure, but a combination of different aspects of geology, hydrology and geotechnical problem. The parameters obtained from the laboratory tests were not within the acceptable safe margins, depicting a very poor soil structure within the study area. The results indicate that the volcanic ash cannot be stabilized; leaving the option of cut and spoil, then bringing new material for road construction. Therefore, it should be noted that the road construction was done by soil brought from the nearby quarry. Figure 62 shows that there was no problem with the construction since the road at some points remained intact despite failure of the embankment.



Figure 62: *Road surface remained intact.*

5.2 Soil Liquefaction

Liquefaction occurs as a result of the vibrations from either earthquake or vehicle movements. The vibrations cause the individual grains in the soil to move around and re-adjust their positions. This ultimately results in a reduction in porosity and increase in pore water pressure, the soil finally loses its bearing capacity due to a drop in the shear strength, thus causing the subsidence. In this research, it was found out that failure at this location only occurs during the heavy rains thus ruling out the possibility of abnormal seismic activity; furthermore, there was no any earthquake or tremor signal detected by a system set up at Mt Kilimambogo by the department of Geology (University of Nairobi) which is capable of detecting any earthquake or tremor from all over the world (E. Dindi).

Even though the possibility of failure being caused by liquefaction cannot be completely ruled out, thus subject to further research, it's clear that in this case; the saturation leading to subterranean erosion along fault lines could have caused the failure.

5.3 Fault lines and Seismic Activities

The type of fault at the study region is a normal fault, it is estimated that millions of years from now the plate will dislodge (split into two) due to the presence of tensional forces (Chorowicz, Jean, 2005). The failure was caused by minor faults within the fault region in the north-south direction (E.Dindi).

In the process of road construction, it should be noted that in an attempt to make the foundation stronger and better, piling is impossible since the underlying surface is not stable. Care should also be taken to avoid construction along areas prone to faulting. High settlement levels also make the region not convenient for any form of construction to take place.

5.4 Sink holes

Subsidence in the area occurs in the form of sudden sinking or gradual downward settling of the earth surface with little or no horizontal motion (Abuuru, 1990). The subsidence episodes which have left a trail of sinkholes result from the collapsed infilling sediments after subterranean denudation along the north–south running fault zones. There is high surface-to-subsurface transition of flow in the study area due to prevalence of highly porous unconsolidated volcanoclastic sediments and numerous fissures along the surface run-off flow courses all the way from Mt Longonot and the surrounding escarpment to the study area.

As a result, subsurface streams with turbulent flow are formed within the fissure. The turbulent flow causes progressive erosion within the fissures leaving large subsurface activities which occur as long horizontal continuous channels. These subsurface channels finally develop to catastrophic dimensions and lose their stability. Some of the subsidence events are accelerated

by vibrations caused by heavy vehicle or blasting events in the surrounding quarries. The loss of stability results in underground collapse which reaches the surface of the earth where deep sinkholes are formed (Diagram 63). The dimensions and alignment of the sinkholes are controlled by the fault zones which form the main channels. Observation of the root systems of maize plantation in the collapsed zones indicates that no horizontal or vertical displacements occurred across the fissure zones (Fig. 64). The root systems of the maize plants were found to be exposed as the unconsolidated sediments sank into the cavity.

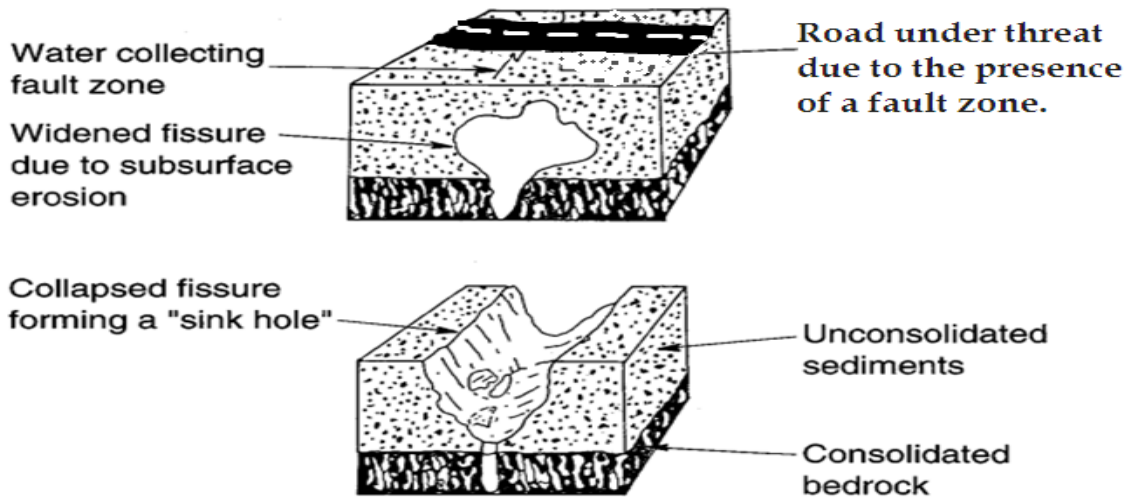


Figure 63: *Development of sink holes as a result of subterranean erosion.*



Figure 64: *No horizontal or vertical displacements occurred.*

5.4 Field Observations

The drainage was found not sufficient to drain the heavy surface run off from the Longonot Mountain and the surrounding escarpments. The road section at the study area was in a fill region, elevating the road surface thus creating a water collection point at the side of the road.

- The available culverts were heavily clogged by erosion materials.
- Failure did not only occurred at the road surface but extended to some further location along a linear north-south trending direction.
- There was a bumpy movement of vehicles at the repaired surface.

Chapter six: Conclusion

The fault line activity findings clearly indicate that the failure was as a result of the subterranean erosion along the existing fault line which occurred due to heavy flooding. The combination of geological, geotechnical and hydrological analysis indicate that the failure occurred particularly in a N-S direction, which is indication of fault line, moreover, it was after the long rains.

The overlying unconsolidated volcanoclastic sediments became oversaturated with water. The water reduced the shear strength of the sediments and also introduced extra loading through saturation leading to subterranean erosion along the fault line. The unconsolidated sediments then collapsed into the subsurface water channels which closely followed the fault zones, leading to formation of “sinkholes”.

Chapter seven: Recommendations

Subsurface denudation along the fault zones can be controlled by channeling the surface water run-off and surface drainage to suitable areas where water does not directly enter into the subsurface water system within the fault zones. This method will especially reduce the impact of flood water during the rainy season on the development of subsurface channels. This should enhance construction of proper drainage systems and reservoirs to avoid heavy surface flow of rain water.

In order to minimize accidents which occur as a result of sudden collapse of roads, warning signs should be erected at weak zones and faults. Intensive research should be conducted within this region to ascertain the fault prone zones and road sections re-aligned in order to avoid frequent collapse.

Within the region that is less prone to crack and fissure formation, rigid concrete pavement should be highly considered. In the rigid pavement structure, the concrete slab is the main load

carrying element, acting as a beam. Since concrete slab has a high modulus of elasticity, small depressions in the subgrade are easily bridged over but when these depressions are too large, the concrete slabs may crack.

Serious investigations of subsurface water channels should be carried out for the entire Maai Mahiu-Narok Road and risk maps produced so that the road users, the road engineers and other interested parties can be warned of the impending dangers. This would contribute to advanced mitigation measures being taken. In future, geological and geotechnical investigations should be carried out before the construction of new roads, the investigations should identify the exact locations of weak zones. Once this is achieved, the relevant parties can be informed and the necessary measure taken. Further detailed research should be done on the affected area to help in getting permanent solution to the problem. These should include the necessary road design for the fault prone areas.

Lastly, further intensive research should be conducted within the Maai Mahiu-Narok area in order to clearly determine the geological and geophysical properties of the region. This will provide guidance to future designs within highly tectonic areas by application of the findings within the road design manuals.

References

- Bijal P.T, 2001 'Iceland Lake Disappearing Into New Crack', National Geographic Channel, October 1, 2001.
- Bishop, A.W., (1966), "The strength of soils as engineering material", *Géotechnique*, Vol. 16, No. 2, pp 89 – 130.
- De Beer, E.E., (1963), "The scale effect in the transposition of the results of deep-sounding tests on the ultimate bearing capacity of piles and caisson foundations", *Géotechnique*. Vol.13 No. 1, pp 39 – 75.
- Dumbleton, N.L.J., and West, G., (1971), "Preliminary sources of information for site investigation in Britain", RRL Report No. LR 403, Transport and Road Research Lab., Berks, Crowthorne.
- Fletcher, G., (1965), "The standard penetration test: its use and abuses", *Proceedings, American Society of Civil Engineers*, Vol. 91, No. SM 4, pp 67 – 76.
- Gachene, C.K.K. and Kimaru, G. (2003). 'Soil Fertility and Land Productivity - A guide for extension workers in the eastern Africa region. Technical Handbook No.30. Regional Land Management Unit (RELMA)/ Swedish International Development Cooperation Agency (Sida). ISBN: 9966-896-66-X.
- Gichaga FJ (1971), 'A study of deflection characteristics and elastic response of flexible pavements in Kenya', MSc Thesis, University of Nairobi.
- MacGregor C., 2009, 'Giant crack in Africa formed in just days', *NewScientist.com*
- Dr. Aaron K. Waswa, Ph.D. 'Geotechnical investigation of Longonot gate project area'
- Ministry of Agriculture and Forestry (1964). *Volcanic Ash Soils in Japan*. Japanese Government, Tokyo.
- Onyancha C., Mathu E., Mwea S., and Ngecu W. (2009), 'Defects in structures in Nairobi city: causes and mitigative strategies', *International Journal for Disaster Management & Risk Reduction*. Vol. 2 Issue 1, Page 12 – 20.
- Pan P, 2011, 'Large crack opens in the earth in southern Peru', *livingnperu.com*.
- Ping, C-L. (2000). *Volcanic Soils*. In: Sigurdsson, H., ed.: *Encyclopedia of Volcanoes*. Academic Press, San Diego. pp. 1259-1270.
- Rowe, P. W., (1968), "Failure of foundations and slopes on layered deposits in relation to site investigation practice", *Proceedings, Institution of Civil Engineers, London, Paper 7075 S. Supplementary Volume*, pp 73 – 131.

- Rowe, P.W., (1972), “Géotechnique”, V.22 No. 2, pp 195 – 300.
- Skempton, A.W. (1985). “Residual strength of clays in landslides, folded strata and the laboratory”, *Géotechnique* 35, 3-8.
- Soil Taxonomy, 1999, ‘A Basic System of Soil Classification for. Making and Interpreting Soil Surveys. Second Edition, United States Department of Agriculture.
- Takahashi, T. and Shoji, S. (2002). ‘Distribution and Classification of Volcanic Ash Soils’. *Global Environmental Research* 6 : 83-97.
- Kenneth B. A. and Greg Ussher (2011), Sinclair Knight Merz, PO Box 9806 Newmarket, Auckland, New Zealand
- Driscollf.G. 1986. *Groundwater and Wells*, 2nd Ed. Johnson Division.
- Thomson A. O. and Dodson R.G. 1958. *Geology of the Naivasha Area*, Ministry of Environment and Natural Resources, Mines and Geology Department, Report no. 55, Nairobi
- Ground water survey (Kenya) Ltd, 1989. Borehole site investigations, Mott Farm; Naivasha, Nakuru District. Report no. 89/22, Nairobi
- Clarkem C. G., Woodhall D.G., Allen D. and Darling G. (1990) – *Geological, Volcanological and Hydrogeological Controls on the occurrence of Geothermal Activity in the surrounding Lake Naivasha, Kenya*, Ministry of Energy.
- Sombroek W. G, Braun H.M.H and Vanderpouw B.J.A (1982) – *Exploratory Soil Map and Agro-climatic Zone Map of Kenya*, 1980, Kenya Soil Survey.

Appendix

Appendix I: Bulk Density

BULK DENSITY					
SAMPLE SOURCE:	Maai Mahiu-Narok road				
Depth (m)	0.5M, 1.5M, 1M	Test pit ID:	TP1	Sample Type	UNDISTURBED SAMPLE
Test date:	10-Nov-15	Sample Description:	Volcanic Ash Soil		
Specification	According to BS 1377:1990			Location:	Lat -0.719044 Long 36.434251
Sample Depth		0.5M		1M	1.5M
Mass of core cutter + Wet soil(g)		2910		2670	2220
Mass of core cutter(g)		1020		945	1015
Mass of wet soil(g)		1890		1725	1205
Volume of core cutter(cm ³)		1532		1398	785
Bulk density (g/cm ³)		1.234		1.234	1.534
Container No.		53		134	146
Mass of wet soil + Container(g)		225		252.7	282
Mass of dry soil + Container(g)		219		246.1	272.4
Mass of Container(g)		97		109	112.8
Loss in Moisture (g)		6		6.6	9.6
Mass of Dry soil		122		137.1	159.6
Moisture Content (%)		4.9		4.8	6.0
Dry density(g/cm ³)		1.176		1.177	1.447
Project Student	K.O. Amollo		Verified :	Mr. J.B. Ogallo	
Date	11-Oct-15		Lab-in charge/Senior technologist		

BULK DENSITY					
SAMPLE SOURCE:	Maai Mahiu-Narok road				
Depth (m)	0.5M, 1M, 1.5M	Test pit ID:	TP2	Sample Type	UNDISTURBED SAMPLE
Test date:	10-Nov-15	Sample Description:	Volcanic Ash Soil		
Specification	According to BS 1377:1990			Location:	Lat -0.719044 Long 36.434251
Sample Depth		0.5M		1M	1.5M
Mass of core cutter + Wet soil(g)		2685		3665	2060
Mass of core cutter(g)		1280		2395	1175
Mass of wet soil(g)		1405		1270	885
Volume of core cutter(cm ³)		1405		1203	884
Bulk density (g/cm ³)		1.000		1.056	1.001
Container No.		145		222	110
Mass of wet soil + Container(g)		270		195	308.4
Mass of dry soil + Container(g)		261.3		188.8	295.5
Mass of Container(g)		112		83.7	115.6
Loss in Moisture (g)		8.7		6.2	12.9
Mass of Dry soil		149.3		105.1	179.9
Moisture Content (%)		5.8		5.9	7.2
Dry density(g/cm ³)		0.945		0.997	0.934
Project Student	K.O. Amollo		Verified :	Mr. J.B. Ogallo	
Date	11-Oct-15		Lab-in charge/Senior technologist		

BULK DENSITY

SAMPLE SOURCE:	Maai Mahiu-Narok road						
Depth (m)	0.5M, 1M, 1.5M	Test pit ID:	TP3	Sample Type	UNDISTURBED SAMPLE		
Test date:	10-Nov-15	Sample Description:		Volcanic Ash Soil			
Specification	According to BS 1377:1990			Location:	Lat -0.719044 Long 36.434251		
Sample Depth		0.5M	1M	1.5M			
Mass of core cutter + Wet soil(g)		5210	1530	2385			
Mass of core cutter(g)		3185	895	915			
Mass of wet soil(g)		2025	635	1470			
Volume of core cutter(cm ³)		2336	458	1246			
Bulk density (g/cm ³)		0.867	1.387	1.179			
Container No.		77	62	63			
Mass of wet soil + Container(g)		258.8	219	176.7			
Mass of dry soil + Container(g)		246.4	206.3	166.8			
Mass of Container(g)		132	100	98			
Loss in Moisture (g)		12.4	12.7	9.9			
Mass of Dry soil		114.4	106.3	68.8			
Moisture Content (%)		10.8	11.9	14.4			
Dry density(g/cm³)		0.782	1.239	1.031			
Project Student	K.O. Amollo		Verified :	Mr. J.B. Ogallo			
Date	11-Oct-15		Lab-in charge/Senior technologist				

BULK DENSITY

SAMPLE SOURCE:	Maai Mahiu-Narok road						
Depth (m)	0.5M, 1M, 1.5M	Test pit ID:	TP4	Sample Type	UNDISTURBED SAMPLE		
Test date:	10-Nov-15	Sample Description:		Volcanic Ash Soil			
Specification	According to BS 1377:1990			Location:	Lat -0.719044 Long 36.434251		
Sample Depth		0.5M	1M	1.5M			
Mass of core cutter + Wet soil(g)		3960	1700	1950			
Mass of core cutter(g)		1985	565	925			
Mass of wet soil(g)		1975	1135	1025			
Volume of core cutter(cm ³)		1818	1022	862			
Bulk density (g/cm ³)		1.087	1.111	1.189			
Container No.		197	133	185			
Mass of wet soil + Container(g)		240	179.1	190.5			
Mass of dry soil + Container(g)		224.7	169.3	172.9			
Mass of Container(g)		82.6	115.9	84			
Loss in Moisture (g)		15.3	9.8	17.6			
Mass of Dry soil		142.1	53.4	88.9			
Moisture Content (%)		10.8	18.4	19.8			
Dry density(g/cm³)		0.981	0.939	0.992			
Project Student	K.O. Amollo		Verified :	Mr. J.B. Ogallo			
Date	11-Oct-15		Lab-in charge/Senior technologist				

Appendix II: Specific Gravity

SPECIFIC GRAVITY						
project	Properties of volcanic ash soil					
Test date:	22-Oct-15		Sample Description:	Volcanic ash soil		
Specification	According to BS 1377:1990 Part				Location:	Maai Mahui-Narok road
Sample Number	TP1 0.5M	TP1 1M	TP1 1.5M	TP2 0.5M	TP2 1M	TP2 1.5M
Bottle Number	6	5	1	1	3	2
Mass of empty bottle (W_1)	36.9	35.9	61.5	61.5	65.5	59.7
Mass of bottle + Soil (W_2)	51.9	50.9	76.6	76.6	80.5	74.5
Mass of bottle + Soil+ Water (W_3)	97.5	96.5	183.4	183.5	188.8	172.6
Mass of bottle full of Water (W_4)	88.7	87.7	174.9	174.9	180.3	164.3
Mass of Water used ($W_3 - W_2$)	45.6	45.6	106.8	106.9	108.3	98.1
Mass of soil used ($W_2 - W_1$)	15	15	15.1	15.1	15	14.8
Volume of Soil ($(W_4 - W_1) - (W_3 - W_2)$)	6.2	6.2	6.6	6.5	6.5	6.5
Specific Gravity of Soil						
$G_s = \frac{(W_2 - W_1)}{(W_4 - W_1) - (W_3 - W_2)}$	2.419	2.419	2.288	2.323	2.308	2.277
Average G_s	2.375529488			2.302564103		
Project Student	K. O. Amollo		Verified :	Dr. S.N. Osano		
Date	22/10/2015			Project Supervisor		

SPECIFIC GRAVITY						
project	Properties of volcanic ash soil					
Test date:	22-Oct-15		Sample Description:	Volcanic ash soil		
Specification	According to BS 1377:1990 Part				Location:	Maai Mahui-Narok road
Sample Number	TP3 0.5M	TP3 1M	TP3 1.5M	TP4 0.5M	TP4 1M	TP4 1.5M
Bottle Number	7	4	3	2	5	4
Mass of empty bottle (W_1)	63.6	64.6	65.5	59.7	35.9	64.6
Mass of bottle + Soil (W_2)	78.7	79.7	80.5	74.5	50.9	79.7
Mass of bottle + Soil+ Water (W_3)	184.7	185.7	188.8	172.1	95.7	185.9
Mass of bottle full of Water (W_4)	176.5	177.5	180.3	164.3	87.7	177.5
Mass of Water used ($W_3 - W_2$)	106	106	108.3	97.6	44.8	106.2
Mass of soil used ($W_2 - W_1$)	15.1	15.1	15	14.8	15	15.1
Volume of Soil ($(W_4 - W_1) - (W_3 - W_2)$)	6.9	6.9	6.5	7	7	6.7
Specific Gravity of Soil						
$G_s = \frac{(W_2 - W_1)}{(W_4 - W_1) - (W_3 - W_2)}$	2.188	2.188	2.308	2.114	2.143	2.254
Average G_s	2.228167967			2.1702914		
Project Student	K. O. Amollo		Verified :	Dr. S.N. Osano		
Date	22/10/2015			Project Supervisor		

Appendix III: Particle size distribution

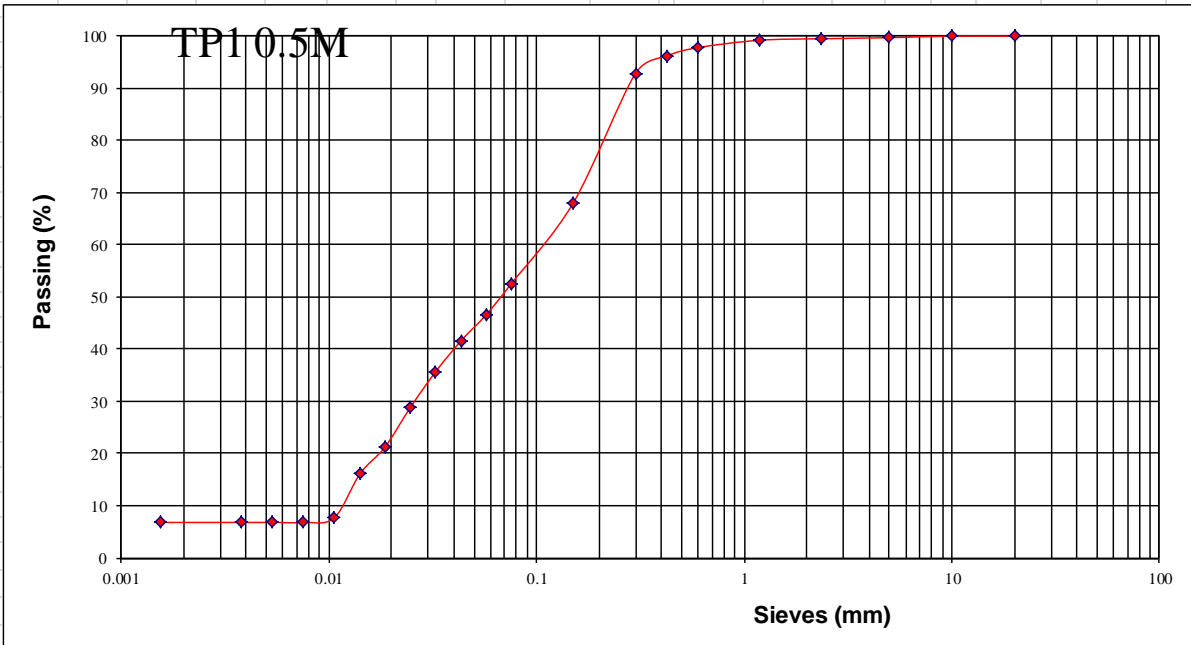
sieve sizes	TP1			TP2			TP1			TP1		
	0.5M	1M	1.5M	0.5M	1M	1.5M	0.5M	1M	1.5M	0.5M	1M	1.5M
20	100	100	100	100	100	100	100	100	100	100	100	100
10	100	100	100	100	100	100	100	100	100	100	100	100
5	100	100	100	100	100	100	99	100	99	100	99	94
2.36	100	99	100	100	100	100	98	99	98	99	93	85
1.18	99	99	99	99	100	100	96	98	96	97	90	81
0.6	98	96	97	98	98	100	92	95	94	94	86	78
0.425	96	93	92	96	95	99	89	93	91	91	84	76
0.3	93	87	88	92	91	95	83	88	85	88	81	73
0.15	68	52	63	69	59	65	63	64	59	69	68	60
0.075	52	35	50	53	40	50	50	53	48	60	63	55
0.0574	47	31	40	46	35	40	43	49	39	53	54	49
0.0432	42	27	35	42	32	35	38	42	34	47	51	46
0.0326	36	24	27	34	27	27	32	35	26	41	44	40
0.0247	29	19	21	28	22	21	25	29	20	32	34	32
0.0186	21	14	15	22	16	15	20	21	15	22	24	24
0.0141	16	11	10	16	12	10	16	16	10	16	17	17
0.0106	8	5	7	12	6	7	12	8	7	10	12	12
0.0075	7	4	6	8	5	6	7	7	6	8	8	8
0.0053	7	4	6	7	5	6	7	7	6	8	8	7
0.0038	7	4	6	7	5	6	7	7	6	8	8	7
0.0015	7	4	6	7	5	6	7	7	6	8	8	7

Appendix IV: Sieve and Hydrometer Analysis

SIEVE ANALYSIS

SITE	Maai Mahiu-Narok road							
Depth (m)	TP1	S/No	0.5M					
Test date:	22-Oct-15							
Specification	According to BS 1377:1990							
Pan mass (gm)	0							
Initial dry sample mass + pan (gm)								
Initial dry sample mass (gm)	100	Fine mass	52.4					
Washed dry sample mass + pan (gm)		Fine percent	52.4					
Washed dry sample mass (gm)	47.6	Acceptance Criteria						
Wet & Dry Sieve Analysis to BS 1377								
Sieve size (mm)	Retained mass (gm)	% Retained (%)	Cumulative passed percentage (%)					
20	0	0.0	100.0					
10	0	0.0	100.0					
5	0.3	0.3	99.7					
2.36	0.2	0.2	99.5					
1.18	0.3	0.3	99.2					
0.6	1.4	1.4	97.8					
0.425	1.6	1.6	96.2					
0.3	3.3	3.3	92.9					
0.15	24.9	24.9	68.0					
0.075	15.6	15.6	52.4					
<0.075	52.4	52.4						
TOTAL	100							
Hydrometer Analysis to BS 1377								
Date	Time In min	Temp ° C.	Rh1	Rh	HR	D(mm)	K(%)	K(corrected)
10AM	0.5	20	28	28.5	9	0.0574	89	47
	1	20	25	25.5	10.2	0.0432	79	42
	2	20	21.5	22	11.6	0.0326	68	36
	4	20	17.5	18	13.3	0.0247	55	29
	8	20	13	13.5	15.1	0.0186	41	21
	15	20	10	10.5	16.3	0.0141	31	16
	30	20	5	5.5	18.3	0.0106	15	8
	60	20	4.5	5	18.5	0.0075	13	7
	120	20	4.5	5	18.5	0.0053	13	7
	240	20	4.5	5	18.5	0.0038	13	7
1440	20	4.5	5	18.5	0.0015	13	7	

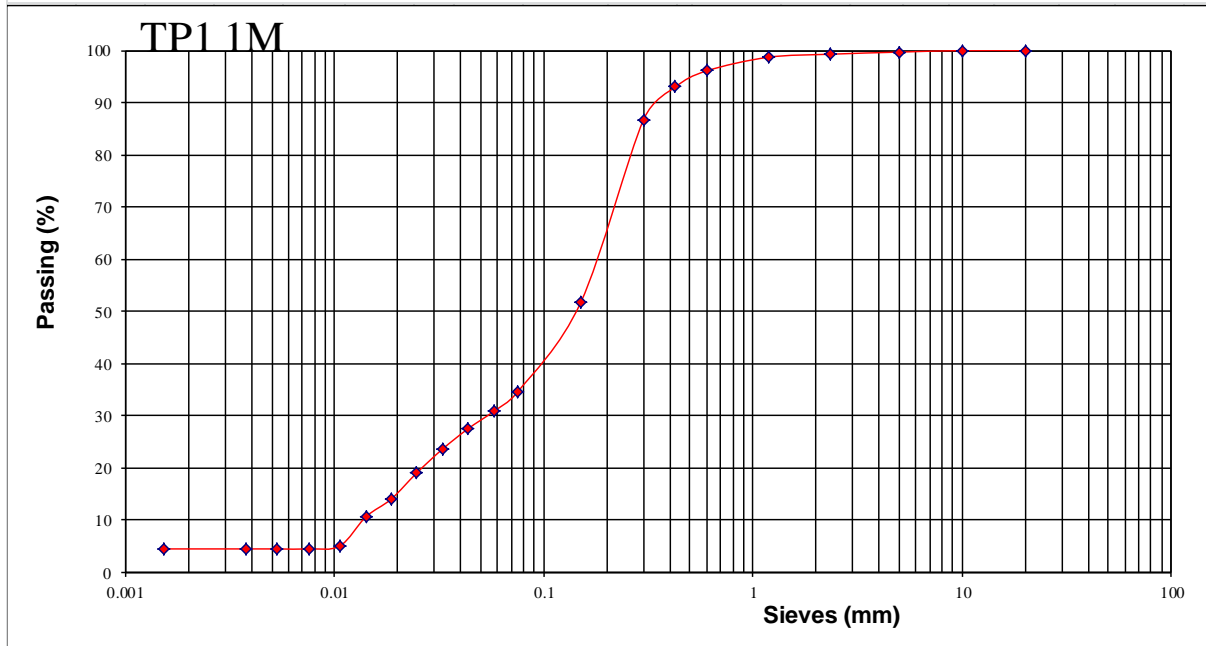
GRADING CURVE - HYDROMETER ANALYSIS



SIEVE ANALYSIS

SITE	Maai Mahiu-Narok road							
Depth (m)	TP1	S/No	1M					
Test date:	22-Oct-15							
Specification	According to BS 1377:1990							
Pan mass (gm)	0							
Initial dry sample mass + pan (gm)								
Initial dry sample mass (gm)	100	Fine mass	34.6					
Washed dry sample mass + pan (gm)		Fine percent	34.6					
Washed dry sample mass (gm)	65.4	Acceptance Criteria						
Wet & Dry Sieve Analysis to BS 1377								
Sieve size (mm)	Retained mass (gm)	% Retained (%)	Cumulative passed percentage (%)					
20	0	0.0	100.0					
10	0	0.0	100.0					
5	0.3	0.3	99.7					
2.36	0.4	0.4	99.3					
1.18	0.6	0.6	98.7					
0.6	2.6	2.6	96.1					
0.425	3.1	3.1	93.0					
0.3	6.2	6.2	86.8					
0.15	35.1	35.1	51.7					
0.075	17.1	17.1	34.6					
<0.075	34.6	34.6						
TOTAL	100							
Hydrometer Analysis to BS 1377								
Date	Time In min	Temp ° C	Rh1	Rh	HR	D(mm)	K(%)	K(corrected)
10AM	0.5	20	28	28.5	9	0.0574	89	31
	1	20	25	25.5	10.2	0.0432	79	27
	2	20	21.5	22	11.6	0.0326	68	24
	4	20	17.5	18	13.3	0.0247	55	19
	8	20	13	13.5	15.1	0.0186	41	14
	15	20	10	10.5	16.3	0.0141	31	11
	30	20	5	5.5	18.3	0.0106	15	5
	60	20	4.5	5	18.5	0.0075	13	4
	120	20	4.5	5	18.5	0.0053	13	4
	240	20	4.5	5	18.5	0.0038	13	4
	1440	20	4.5	5	18.5	0.0015	13	4

GRADING CURVE - HYDROMETER ANALYSIS



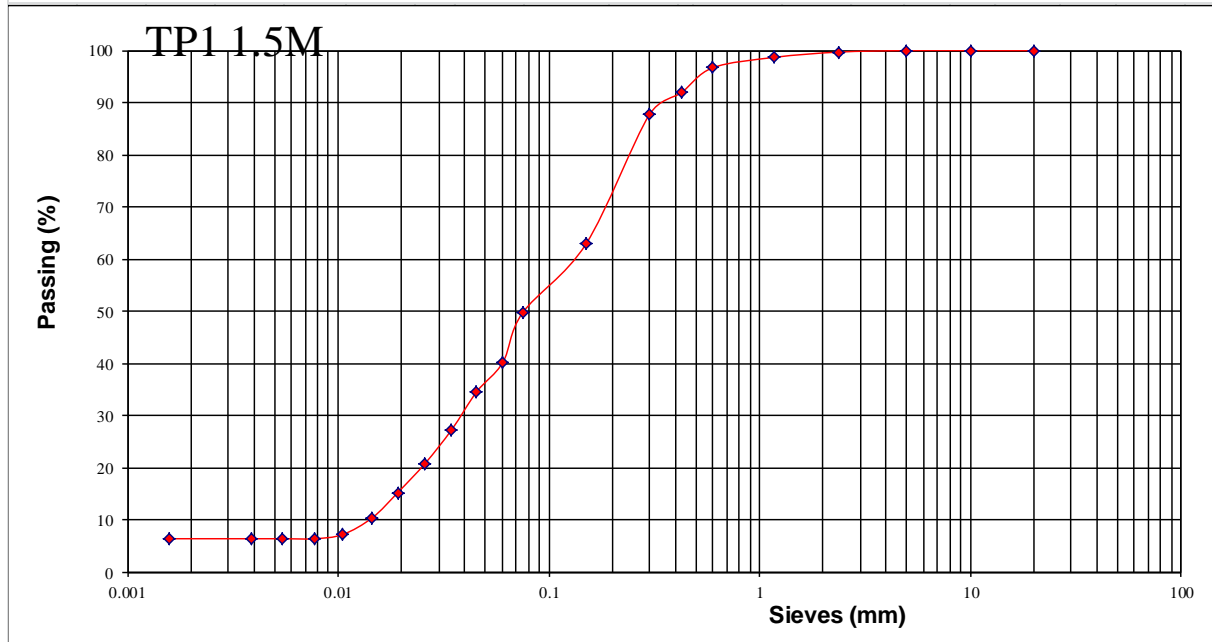
SIEVE ANALYSIS

SITE	Maai Mahiu-Narok road		
Depth (m)	TP1	S/No	1.5M
Test date:	22-Oct-15		
Specification	According to BS 1377:1990		

Pan mass	(gm)	0		
Initial dry sample mass + pan	(gm)			
Initial dry sample mass	(gm)	100	Fine mass	49.7
Washed dry sample mass + pan	(gm)		Fine percent	49.7
Washed dry sample mass	(gm)	50.3	Acceptance Criteria	

Wet & Dry Sieve Analysis to BS 1377				Hydrometer Analysis to BS 1377								
Sieve size (mm)	Retained mass (gm)	% Retained (%)	Cumulative passed percentage (%)	Date	Time In min	Temp ° C	Rh1	Rh	HR	D(mm)	K(%)	K(corrected)
				20	0	0.0	100.0	10AM	0.5	20	25.5	26
10	0	0.0	100.0		1	20	22	22.5	11.3	0.0455	70	35
5	0	0.0	100.0		2	20	17.5	18	13.1	0.0347	55	27
2.36	0.3	0.3	99.7		4	20	13.5	14	14.7	0.026	42	21
1.18	1	1.0	98.7		8	20	10	10.5	16.1	0.0192	31	15
0.6	2	2.0	96.7		15	20	7	7.5	17.3	0.0145	21	10
0.425	4.8	4.8	91.9		30	20	5	5.5	18.1	0.0105	15	7
0.3	4.2	4.2	87.7		60	20	4.5	5	19.4	0.0077	13	6
0.15	24.8	24.8	62.9		120	20	4.5	5	19.4	0.0054	13	6
0.075	13.2	13.2	49.7		240	20	4.5	5	19.4	0.0038	13	6
<0.075	49.7	49.7			1440	20	4.5	5	19.4	0.0016	13	6
TOTAL	100											

GRADING CURVE - HYDROMETER ANALYSIS



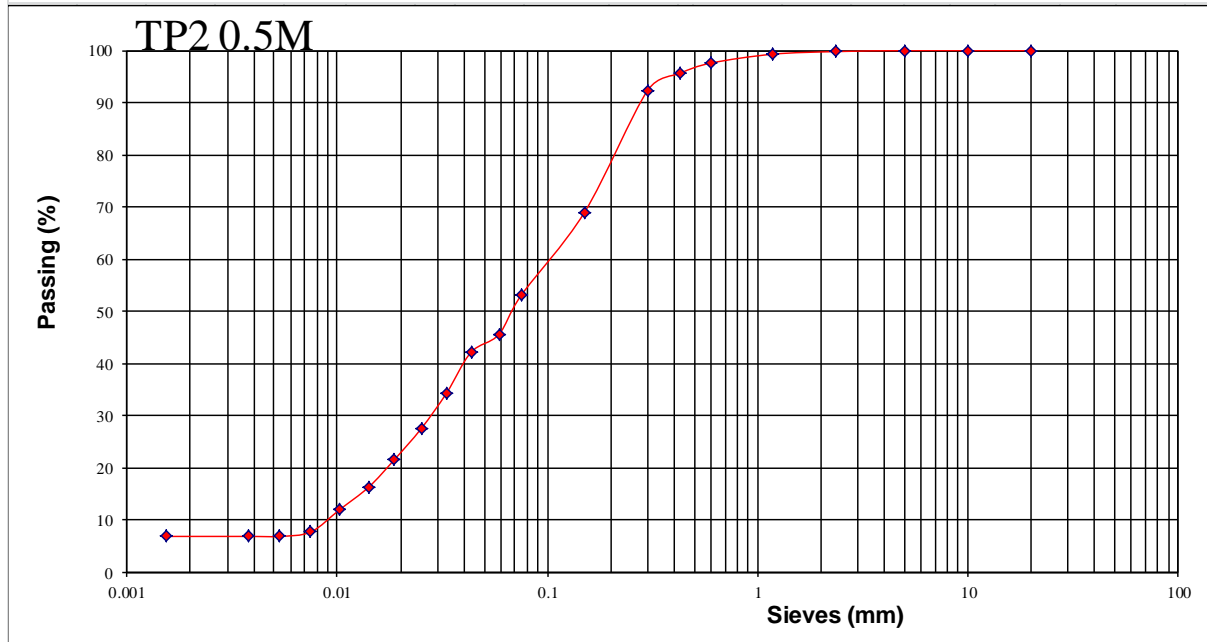
SIEVE ANALYSIS

SITE	Maai Mahiu-Narok road		
Depth (m)	TP2	S/No	0.5M
Test date:	22-Oct-15		
Specification	According to BS 1377:1990		

Pan mass	(gm)	0		
Initial dry sample mass + pan	(gm)			
Initial dry sample mass	(gm)	100	Fine mass	53.1
Washed dry sample mass + pan	(gm)		Fine percent	53.1
Washed dry sample mass	(gm)	46.9	Acceptance Criteria	

Wet & Dry Sieve Analysis to BS 1377				Hydrometer Analysis to BS 1377								
Sieve size (mm)	Retained mass (gm)	% Retained (%)	Cumulative passed percentage (%)	Date	Time In min	Temp ° C	Rh1	Rh	HR	D(mm)	K(%)	K(corrected)
				20	0	0.0	100.0	10AM	0.5	20	27	27.5
10	0	0.0	100.0		1	20	25	25.5	10.2	0.0432	79	42
5	0	0.0	100.0		2	20	20.5	21	12	0.0332	65	34
2.36	0.2	0.2	99.8		4	20	16.5	17	13.7	0.0251	52	28
1.18	0.5	0.5	99.3		8	20	13	13.5	15.1	0.0186	41	22
0.6	1.7	1.7	97.6		15	20	10	10.5	16.3	0.0141	31	16
0.425	2	2.0	95.6		30	20	7.5	8	17.3	0.0103	23	12
0.3	3.2	3.2	92.4		60	20	5	5.5	18.3	0.0075	15	8
0.15	23.4	23.4	69.0		120	20	4.5	5	18.5	0.0053	13	7
0.075	15.9	15.9	53.1		240	20	4.5	5	18.5	0.0038	13	7
<0.075	53.1	53.1			1440	20	4.5	5	18.5	0.0015	13	7
TOTAL	100											

GRADING CURVE - HYDROMETER ANALYSIS



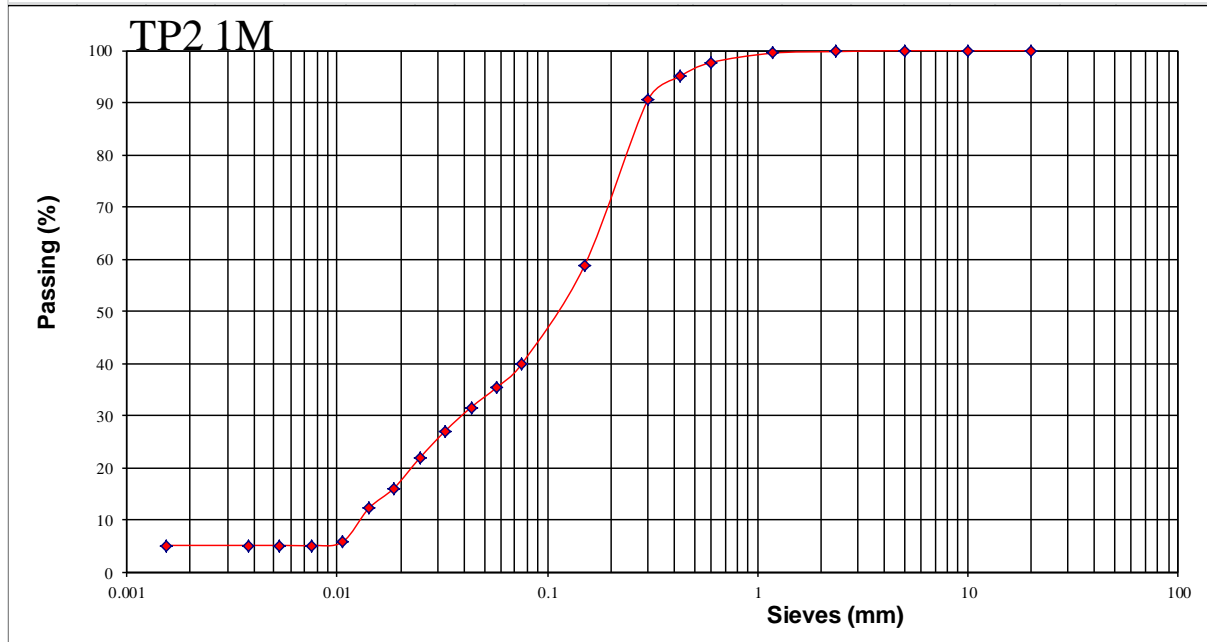
SIEVE ANALYSIS

SITE	Maai Mahiu-Narok road		
Depth (m)	TP2	S/No	1M
Test date:	22-Oct-15		
Specification	According to BS 1377:1990		

Pan mass	(gm)	0		
Initial dry sample mass + pan	(gm)			
Initial dry sample mass	(gm)	100	Fine mass	39.8
Washed dry sample mass + pan	(gm)		Fine percent	39.8
Washed dry sample mass	(gm)	60.2	Acceptance Criteria	

Wet & Dry Sieve Analysis to BS 1377				Hydrometer Analysis to BS 1377									
Sieve size (mm)	Retained mass (gm)	% Retained (%)	Cumulative passed percentage (%)	Date	Time In min	Temp ° C	Rh1	Rh	HR	D(mm)	K(%)	K(corrected)	
20	0	0.0	100.0	10AM	0.5	20	28	28.5	9	0.0574	89	35	
10	0	0.0	100.0		1	20	25	25.5	10.2	0.0432	79	32	
5	0	0.0	100.0		2	20	21.5	22	11.6	0.0326	68	27	
2.36	0.2	0.2	99.8		4	20	17.5	18	13.3	0.0247	55	22	
1.18	0.3	0.3	99.5		8	20	13	13.5	15.1	0.0186	41	16	
0.6	1.8	1.8	97.7		15	20	10	10.5	16.3	0.0141	31	12	
0.425	2.7	2.7	95.0		30	20	5	5.5	18.3	0.0106	15	6	
0.3	4.5	4.5	90.5		60	20	4.5	5	18.5	0.0075	13	5	
0.15	31.7	31.7	58.8		120	20	4.5	5	18.5	0.0053	13	5	
0.075	19	19.0	39.8		240	20	4.5	5	18.5	0.0038	13	5	
<0.075	39.8	39.8			1440	20	4.5	5	18.5	0.0015	13	5	
TOTAL	100												

GRADING CURVE - HYDROMETER ANALYSIS



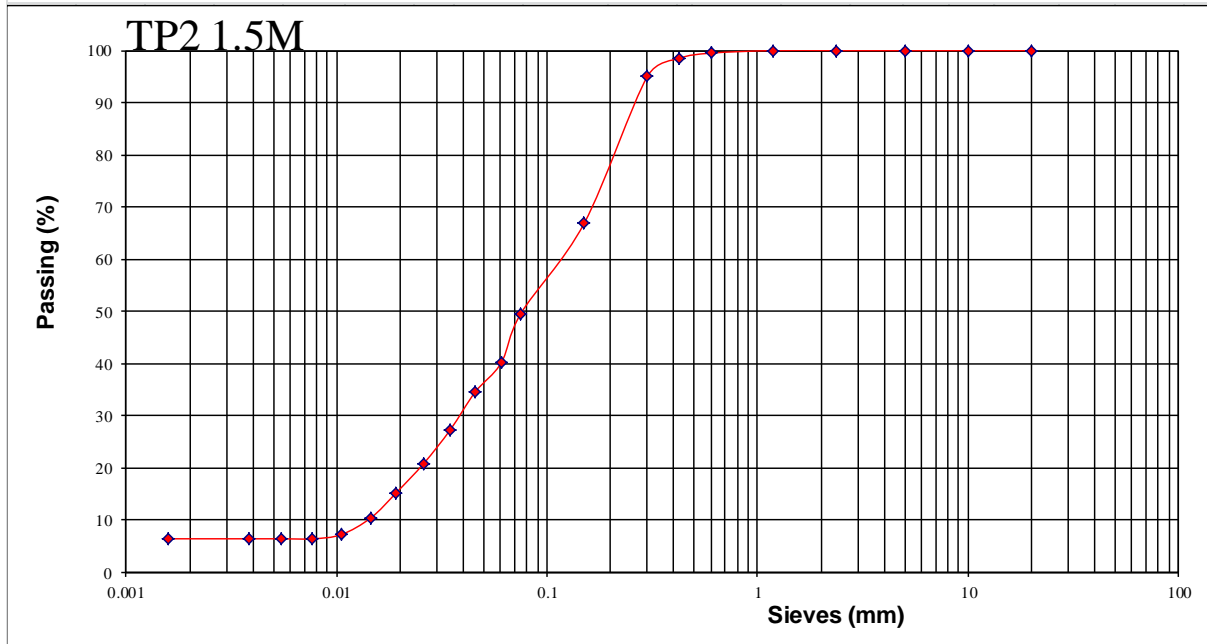
SIEVE ANALYSIS

SITE	Maai Mahiu-Narok road		
Depth (m)	TP2	S/No	1.5M
Test date:	22-Oct-15		
Specification	According to BS 1377:1990		

Pan mass	(gm)	0		
Initial dry sample mass + pan	(gm)			
Initial dry sample mass	(gm)	100	Fine mass	49.6
Washed dry sample mass + pan	(gm)		Fine percent	49.6
Washed dry sample mass	(gm)	50.4	Acceptance Criteria	

Wet & Dry Sieve Analysis to BS 1377				Hydrometer Analysis to BS 1377								
Sieve size (mm)	Retained mass (gm)	% Retained (%)	Cumulative passed percentage (%)	Date	Time In min	Temp ° C	Rh1	Rh	HR	D(mm)	K(%)	K(corrected)
				20	0	0.0	100.0	10AM	0.5	20	25.5	26
10	0	0.0	100.0		1	20	22	22.5	11.3	0.0455	70	35
5	0	0.0	100.0		2	20	17.5	18	13.1	0.0347	55	27
2.36	0	0.0	100.0		4	20	13.5	14	14.7	0.026	42	21
1.18	0	0.0	100.0		8	20	10	10.5	16.1	0.0192	31	15
0.6	0.5	0.5	99.5		15	20	7	7.5	17.3	0.0145	21	10
0.425	1	1.0	98.5		30	20	5	5.5	18.1	0.0105	15	7
0.3	3.4	3.4	95.1		60	20	4.5	5	19.4	0.0077	13	6
0.15	28.2	28.2	66.9		120	20	4.5	5	19.4	0.0054	13	6
0.075	17.3	17.3	49.6		240	20	4.5	5	19.4	0.0038	13	6
<0.075	49.6	49.6			1440	20	4.5	5	19.4	0.0016	13	6
TOTAL	100											

GRADING CURVE - HYDROMETER ANALYSIS



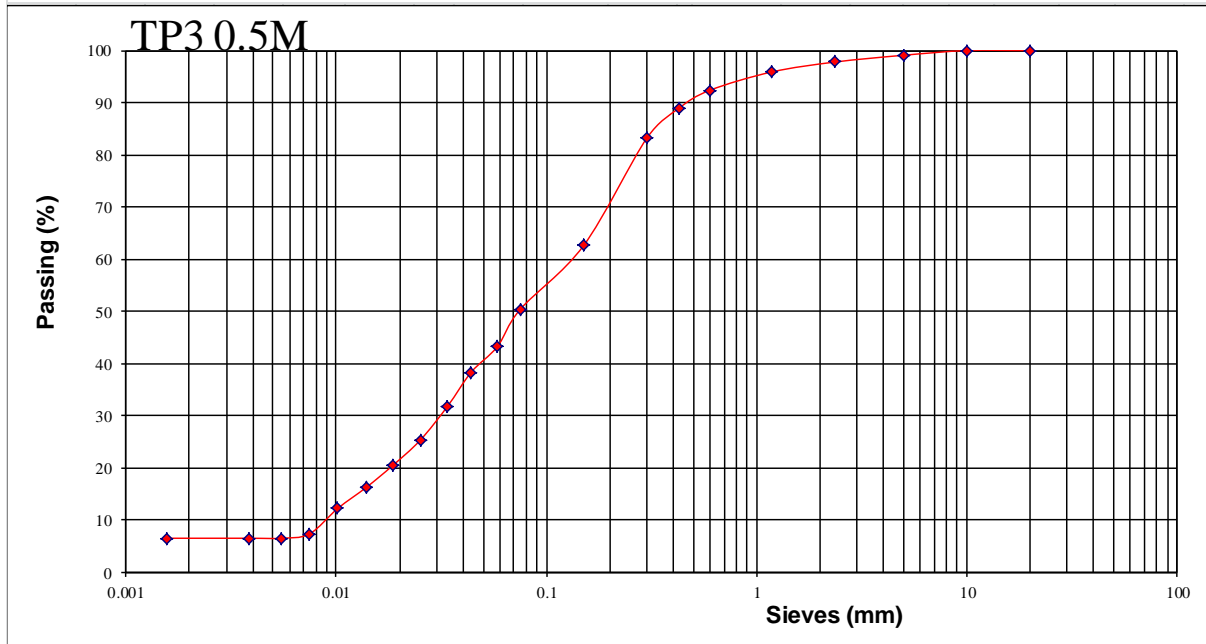
SIEVE ANALYSIS

SITE	Maai Mahiu-Narok road		
Depth (m)	TP3	S/No	0.5M
Test date:	22-Oct-15		
Specification	According to BS 1377:1990		

Pan mass	(gm)	0		
Initial dry sample mass + pan	(gm)			
Initial dry sample mass	(gm)	100	Fine mass	50.4
Washed dry sample mass + pan	(gm)		Fine percent	50.4
Washed dry sample mass	(gm)	49.6	Acceptance Criteria	

Wet & Dry Sieve Analysis to BS 1377				Hydrometer Analysis to BS 1377								
Sieve size (mm)	Retained mass (gm)	% Retained (%)	Cumulative passed percentage (%)	Date	Time In min	Temp ° C	Rh1	Rh	HR	D(mm)	K(%)	K(corrected)
				20	0	0.0	100.0	10AM	0.5	20	27	27.5
10	0	0.0	100.0		1	20	24	24.5	10.5	0.0439	76	38
5	0.9	0.9	99.1		2	20	20	20.5	12.5	0.0339	63	32
2.36	1.3	1.3	97.8		4	20	16	16.5	13.7	0.0251	50	25
1.18	1.9	1.9	95.9		8	20	13	13.5	14.9	0.0185	41	20
0.6	3.5	3.5	92.4		15	20	10.5	11	15.9	0.0139	32	16
0.425	3.5	3.5	88.9		30	20	8	8.5	16.9	0.0102	24	12
0.3	5.7	5.7	83.2		60	20	5	5.5	18.1	0.0074	15	7
0.15	20.6	20.6	62.6		120	20	4.5	5	19.4	0.0054	13	7
0.075	12.2	12.2	50.4		240	20	4.5	5	19.4	0.0038	13	7
<0.075	50.4	50.4			1440	20	4.5	5	19.4	0.0016	13	7
TOTAL	100											

GRADING CURVE - HYDROMETER ANALYSIS



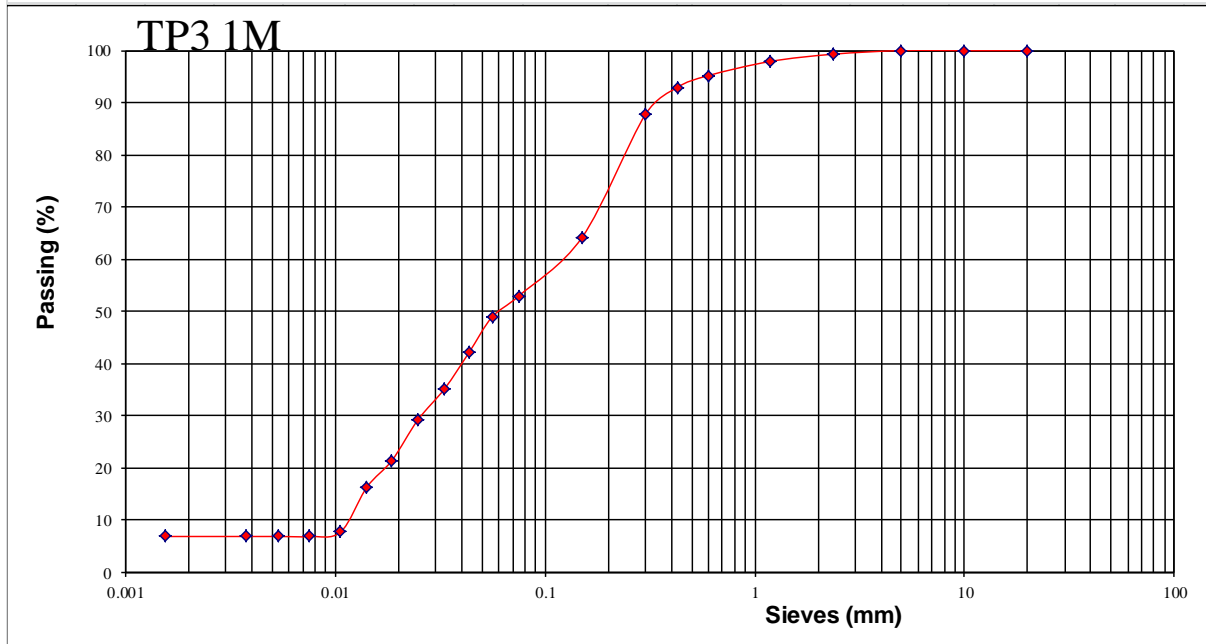
SIEVE ANALYSIS

SITE	Maai Mahiu-Narok road		
Depth (m)	TP3	S/No	1M
Test date:	22-Oct-15		
Specification	According to BS 1377:1990		

Pan mass	(gm)	0		
Initial dry sample mass + pan	(gm)			
Initial dry sample mass	(gm)	100	Fine mass	53
Washed dry sample mass + pan	(gm)		Fine percent	53.0
Washed dry sample mass	(gm)	47	Acceptance Criteria	

Wet & Dry Sieve Analysis to BS 1377				Hydrometer Analysis to BS 1377									
Sieve size (mm)	Retained mass (gm)	% Retained (%)	Cumulative passed percentage (%)	Date	Time In min	Temp ° C	Rh1	Rh	HR	D(mm)	K(%)	K(corrected)	
20	0	0.0	100.0	10AM	0.5	20	29	29.5	8.5	0.0558	92	49	
10	0	0.0	100.0		1	20	25	25.5	10.2	0.0432	79	42	
5	0	0.0	100.0		2	20	21	21.5	12	0.0332	66	35	
2.36	0.7	0.7	99.3		4	20	17.5	18	13.3	0.0247	55	29	
1.18	1.4	1.4	97.9		8	20	13	13.5	15.1	0.0186	41	21	
0.6	2.7	2.7	95.2		15	20	10	10.5	16.3	0.0141	31	16	
0.425	2.3	2.3	92.9		30	20	5	5.5	18.3	0.0106	15	8	
0.3	5.2	5.2	87.7		60	20	4.5	5	18.5	0.0075	13	7	
0.15	23.5	23.5	64.2		120	20	4.5	5	18.5	0.0053	13	7	
0.075	11.2	11.2	53.0		240	20	4.5	5	18.5	0.0038	13	7	
<0.075	53	53.0			1440	20	4.5	5	18.5	0.0015	13	7	
TOTAL	100												

GRADING CURVE - HYDROMETER ANALYSIS



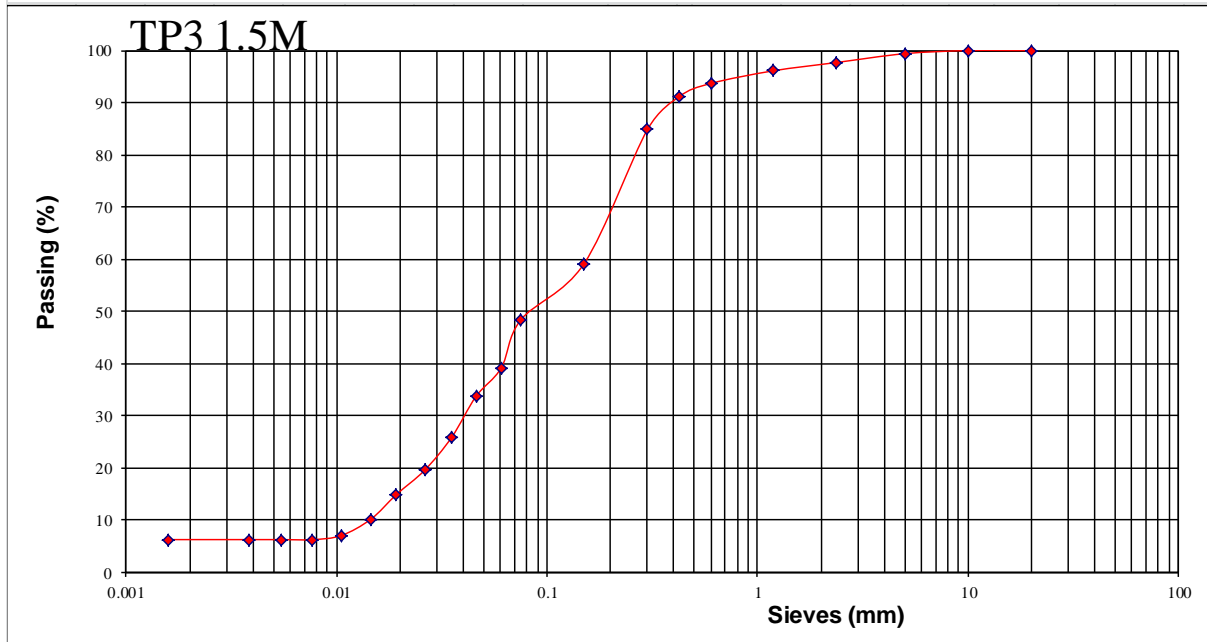
SIEVE ANALYSIS

SITE	Maai Mahiu-Narok road		
Depth (m)	TP1	S/No	0.5M
Test date:	22-Oct-15		
Specification	According to BS 1377:1990		

Pan mass	(gm)	0		
Initial dry sample mass + pan	(gm)			
Initial dry sample mass	(gm)	100	Fine mass	48.4
Washed dry sample mass + pan	(gm)		Fine percent	48.4
Washed dry sample mass	(gm)	51.6	Acceptance Criteria	

Wet & Dry Sieve Analysis to BS 1377				Hydrometer Analysis to BS 1377								
Sieve size (mm)	Retained mass (gm)	% Retained (%)	Cumulative passed percentage (%)	Date	Time In min	Temp ° C	Rh1	Rh	HR	D(mm)	K(%)	K(corrected)
				20	0	0.0	100.0	10AM	0.5	20	25.5	26
10	0	0.0	100.0		1	20	22	22.5	11.5	0.0459	70	34
5	0.6	0.6	99.4		2	20	17	17.5	13.5	0.0352	53	26
2.36	1.7	1.7	97.7		4	20	13	13.5	15	0.0262	41	20
1.18	1.6	1.6	96.1		8	20	10	10.5	16.1	0.0192	31	15
0.6	2.4	2.4	93.7		15	20	7	7.5	17.3	0.0145	21	10
0.425	2.5	2.5	91.2		30	20	5	5.5	18.1	0.0105	15	7
0.3	6.3	6.3	84.9		60	20	4.5	5	19.4	0.0077	13	6
0.15	25.7	25.7	59.2		120	20	4.5	5	19.4	0.0054	13	6
0.075	10.8	10.8	48.4		240	20	4.5	5	19.4	0.0038	13	6
<0.075	48.4	48.4			1440	20	4.5	5	19.4	0.0016	13	6
TOTAL	100											

GRADING CURVE - HYDROMETER ANALYSIS



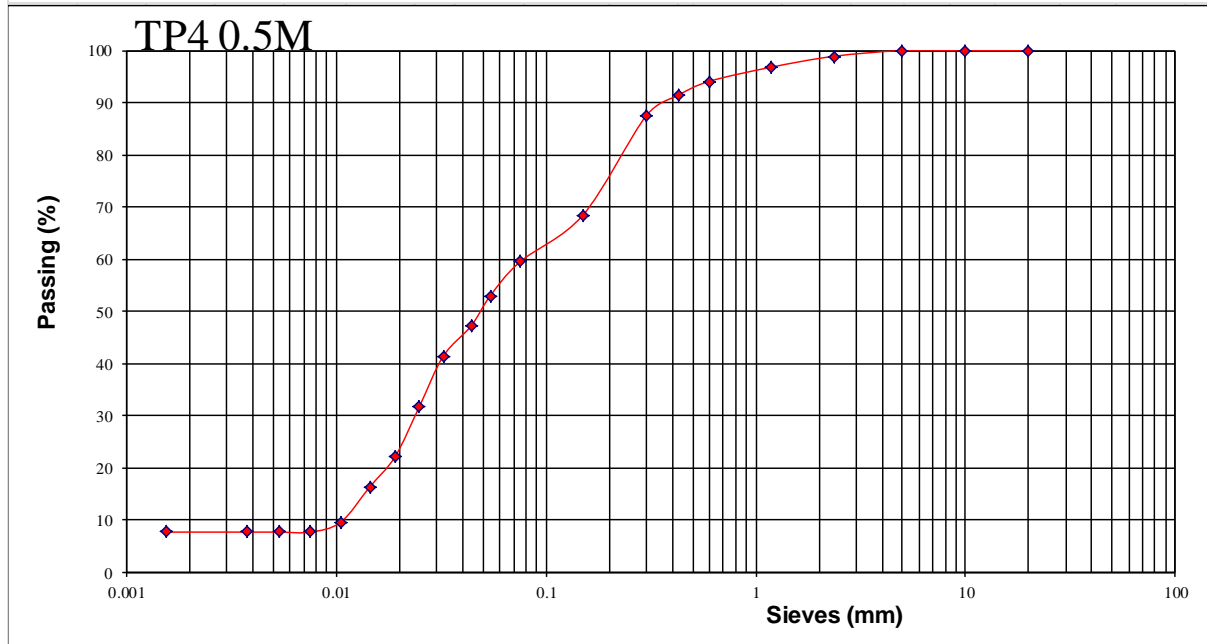
SIEVE ANALYSIS

SITE	Maai Mahiu-Narok road		
Depth (m)	TP4	S/No	0.5M
Test date:	22-Oct-15		
Specification	According to BS 1377:1990		

Pan mass	(gm)	0		
Initial dry sample mass + pan	(gm)			
Initial dry sample mass	(gm)	100	Fine mass	59.5
Washed dry sample mass + pan	(gm)		Fine percent	59.5
Washed dry sample mass	(gm)	40.5	Acceptance Criteria	

Wet & Dry Sieve Analysis to BS 1377				Hydrometer Analysis to BS 1377								
Sieve size (mm)	Retained mass (gm)	% Retained (%)	Cumulative passed percentage (%)	Date	Time In min	Temp ° C	Rh1	Rh	HR	D(mm)	K(%)	K(corrected)
20	0	0.0	100.0	10AM	0.5	20	28	28.5	8	0.0542	89	53
10	0	0.0	100.0		1	20	25	25.5	10.5	0.0439	79	47
5	0	0.0	100.0		2	20	22	22.5	11.4	0.0323	70	41
2.36	1.1	1.1	98.9		4	20	17	17.5	13.5	0.0249	53	32
1.18	2.1	2.1	96.8		8	20	12	12.5	15.8	0.019	37	22
0.6	2.7	2.7	94.1		15	20	9	9.5	17	0.0144	28	16
0.425	2.7	2.7	91.4		30	20	5.5	6	18	0.0105	16	10
0.3	3.9	3.9	87.5		60	20	4.5	5	18.5	0.0075	13	8
0.15	19	19.0	68.5		120	20	4.5	5	18.5	0.0053	13	8
0.075	9	9.0	59.5		240	20	4.5	5	18.5	0.0038	13	8
<0.075	59.5	59.5			1440	20	4.5	5	18.5	0.0015	13	8
TOTAL	100											

GRADING CURVE - HYDROMETER ANALYSIS



SIEVE ANALYSIS

SITE	Maai Mahiu-Narok road		
Depth (m)	TP4	S/No	1M
Test date:	22-Oct-15		
Specification	According to BS 1377:1990		

Pan mass	(gm)	0		
Initial dry sample mass + pan	(gm)			
Initial dry sample mass	(gm)	100	Fine mass	62.8
Washed dry sample mass + pan	(gm)		Fine percent	62.8
Washed dry sample mass	(gm)	37.2	Acceptance Criteria	

Wet & Dry Sieve Analysis to BS 1377				Hydrometer Analysis to BS 1377								
Sieve size (mm)	Retained mass (gm)	% Retained (%)	Cumulative passed percentage (%)	Date	Time In min	Temp ° C	Rh1	Rh	HR	D(mm)	K(%)	K(corrected)
20	0	0.0	100.0	10AM	0.5	20	27	27.5	9.4	0.0587	86	54
10	0	0.0	100.0		1	20	25.5	26	10	0.0428	81	51
5	1.4	1.4	98.6		2	20	22	22.5	11.4	0.0323	70	44
2.36	5.3	5.3	93.3		4	20	17	17.5	13.5	0.0249	53	34
1.18	3.6	3.6	89.7		8	20	12.5	13	15.3	0.0187	39	24
0.6	3.3	3.3	86.4		15	20	9	9.5	16.7	0.0143	28	17
0.425	2.5	2.5	83.9		30	20	6.5	7	17.7	0.0104	19	12
0.3	3.2	3.2	80.7		60	20	4.5	5	18.5	0.0075	13	8
0.15	12.7	12.7	68.0		120	20	4.5	5	18.5	0.0053	13	8
0.075	5.2	5.2	62.8		240	20	4.5	5	18.5	0.0038	13	8
<0.075	62.8	62.8			1440	20	4.5	5	18.5	0.0015	13	8
TOTAL	100											

GRADING CURVE - HYDROMETER ANALYSIS



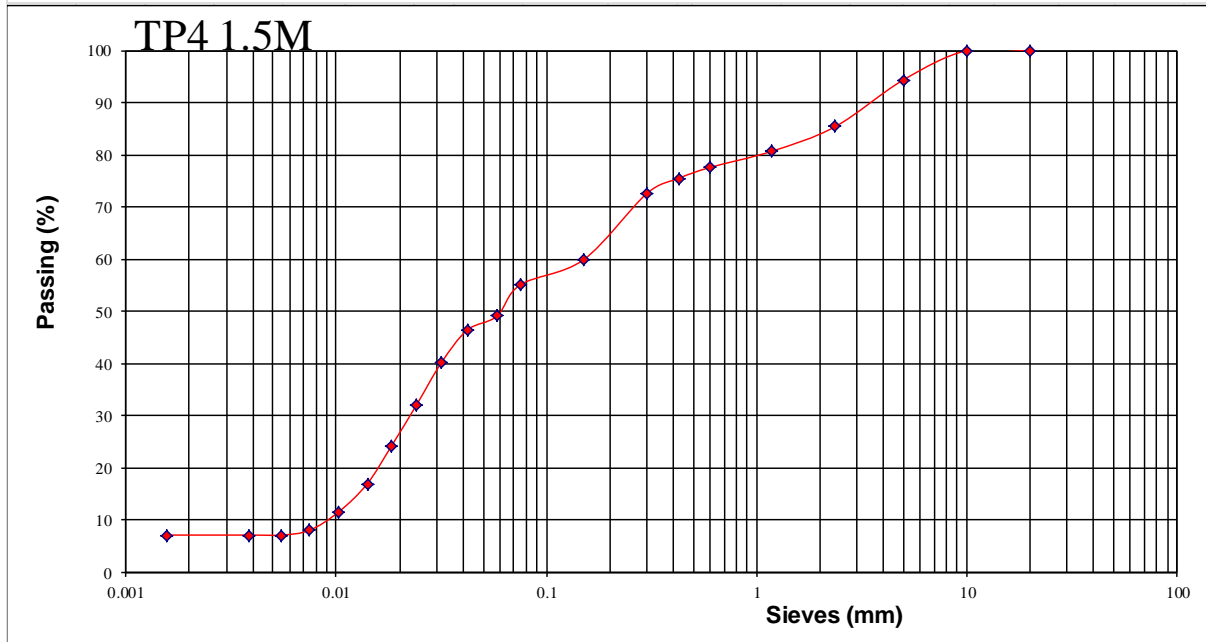
SIEVE ANALYSIS

SITE	Maai Mahiu-Narok road		
Depth (m)	TP4	S/No	1.5M
Test date:	22-Oct-15		
Specification	According to BS 1377:1990		

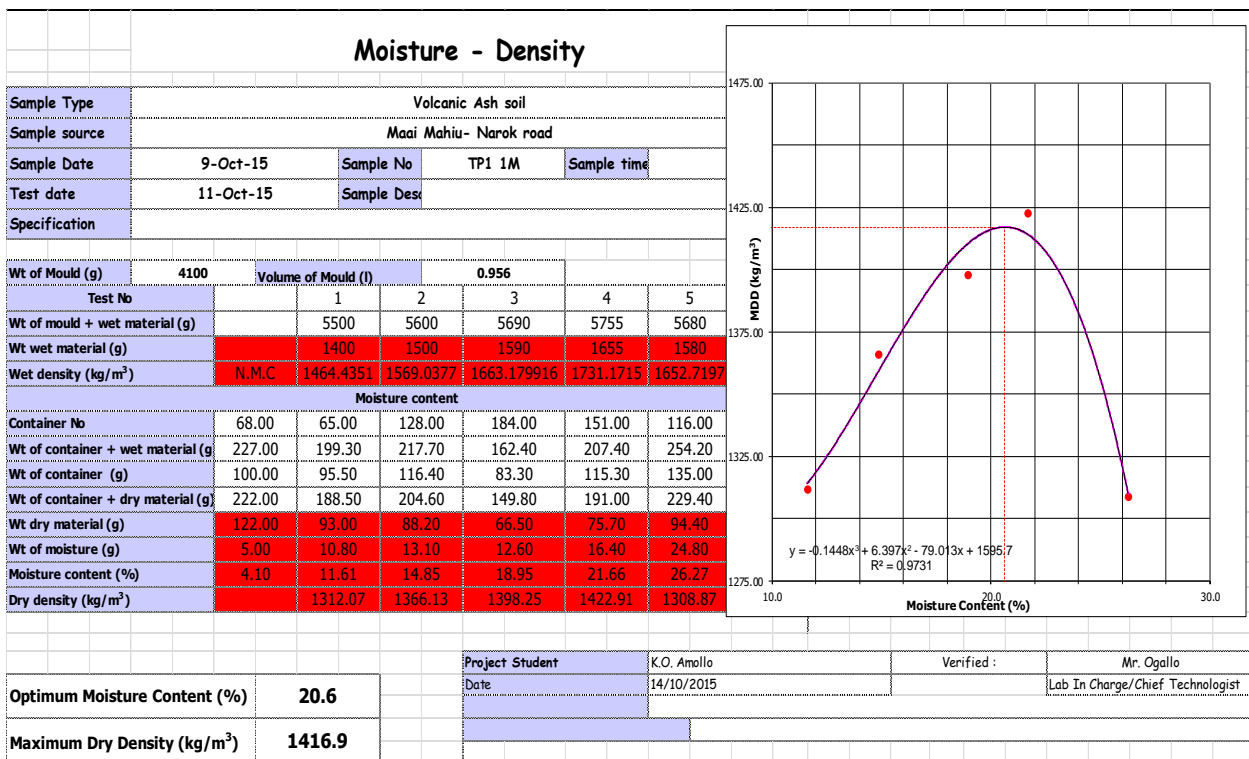
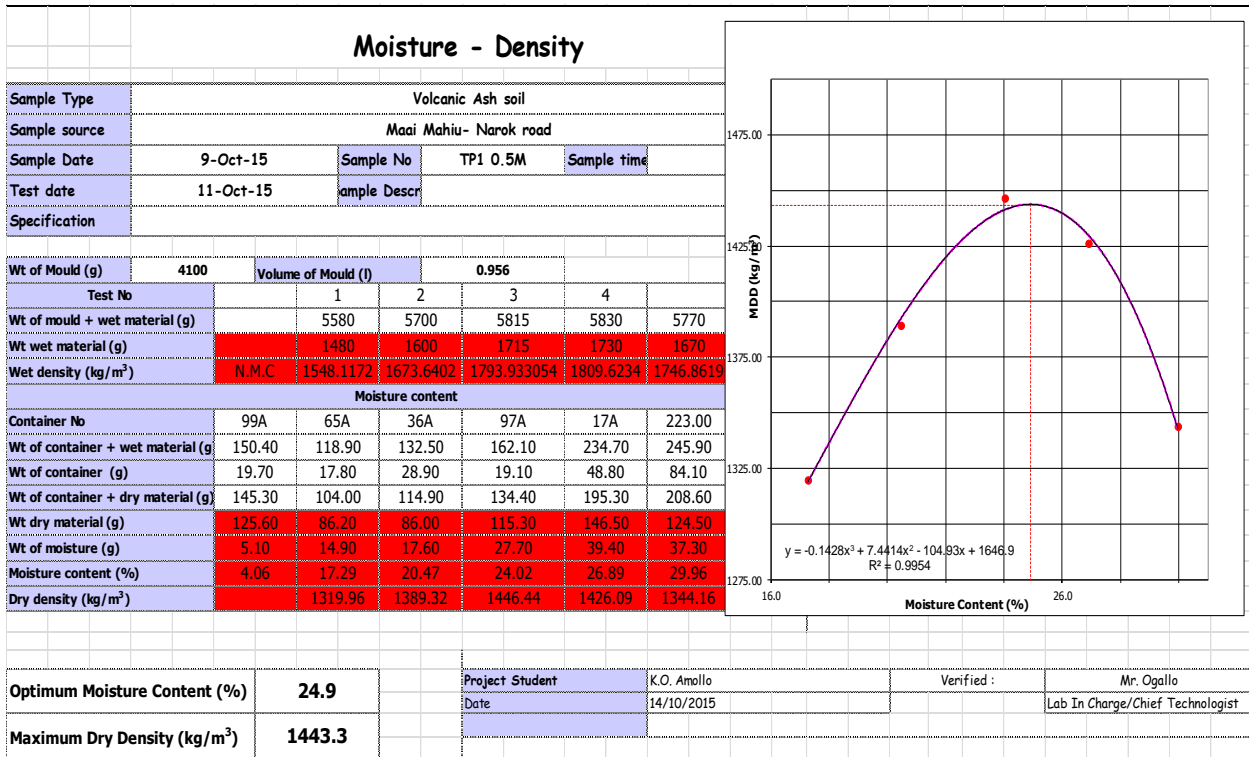
Pan mass	(gm)	0		
Initial dry sample mass + pan	(gm)			
Initial dry sample mass	(gm)	100	Fine mass	55.1
Washed dry sample mass + pan	(gm)		Fine percent	55.1
Washed dry sample mass	(gm)	44.9	Acceptance Criteria	

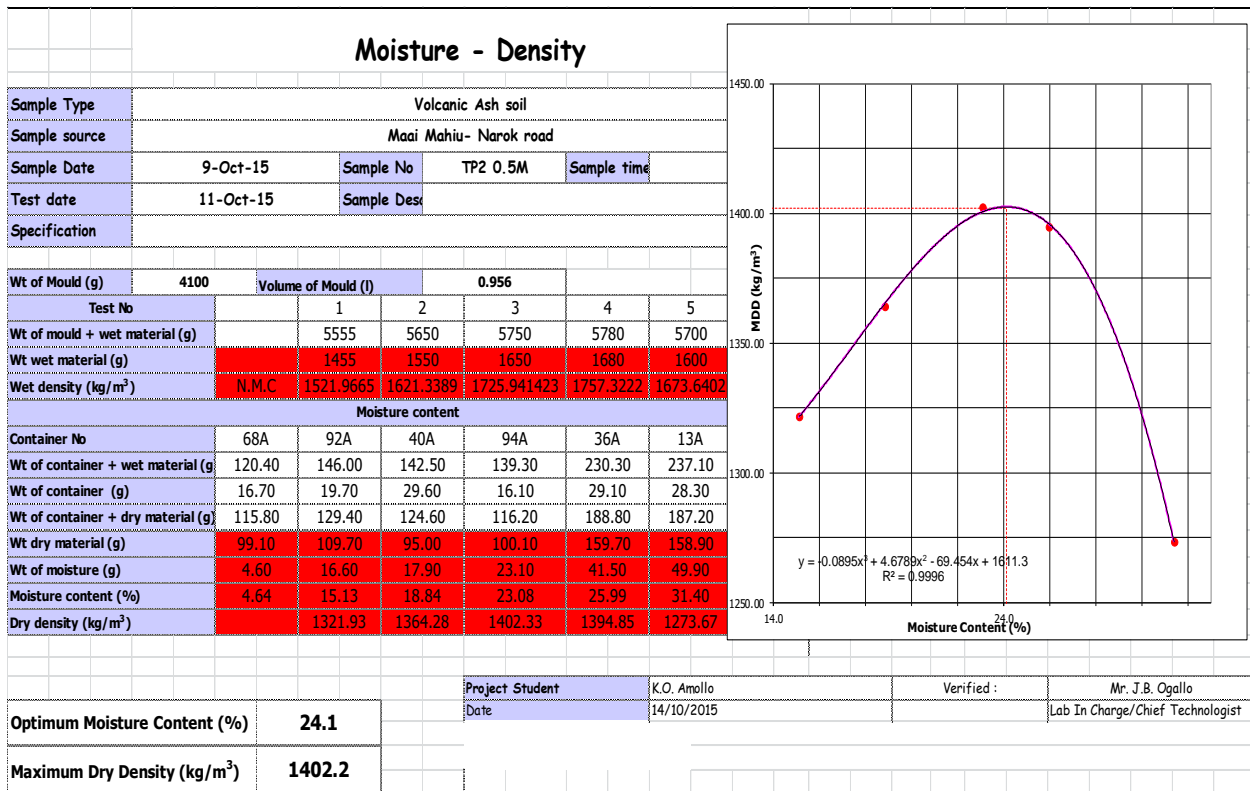
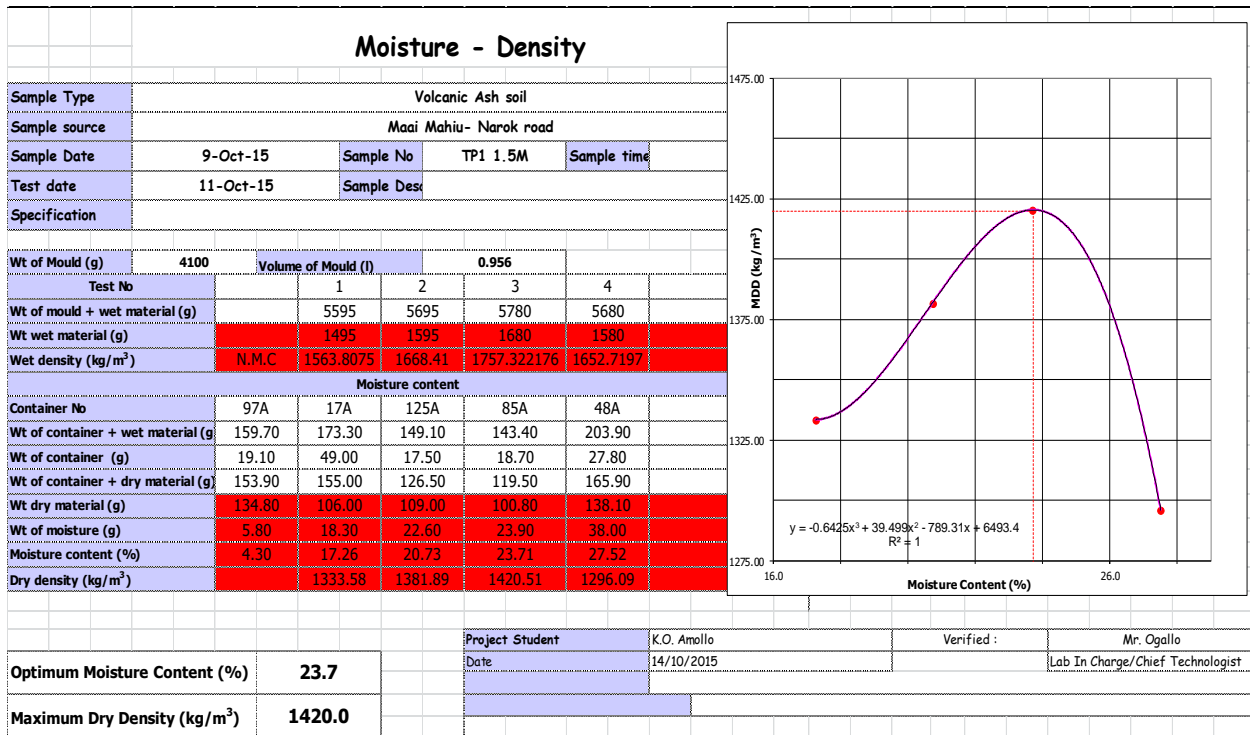
Wet & Dry Sieve Analysis to BS 1377				Hydrometer Analysis to BS 1377								
Sieve size (mm)	Retained mass (gm)	% Retained (%)	Cumulative passed percentage (%)	Date	Time In min	Temp ° C	Rh1	Rh	HR	D(mm)	K(%)	K(corrected)
				20	0	0.0	100.0	10AM	0.5	20	28	28.5
10	0	0.0	100.0		1	20	26.5	27	9.6	0.042	84	46
5	5.6	5.6	94.4		2	20	23	23.5	10.9	0.0316	73	40
2.36	9	9.0	85.4		4	20	18.5	19	12.7	0.0241	58	32
1.18	4.7	4.7	80.7		8	20	14	14.5	14.5	0.0182	44	24
0.6	3.1	3.1	77.6		15	20	10	10.5	16.1	0.014	31	17
0.425	2.1	2.1	75.5		30	20	7	7.5	17.3	0.0103	21	12
0.3	2.9	2.9	72.6		60	20	5	5.5	18.1	0.0074	15	8
0.15	12.7	12.7	59.9		120	20	4.5	5	19.4	0.0054	13	7
0.075	4.8	4.8	55.1		240	20	4.5	5	19.4	0.0038	13	7
<0.075	55.1	55.1			1440	20	4.5	5	19.4	0.0016	13	7
TOTAL	100											

GRADING CURVE - HYDROMETER ANALYSIS



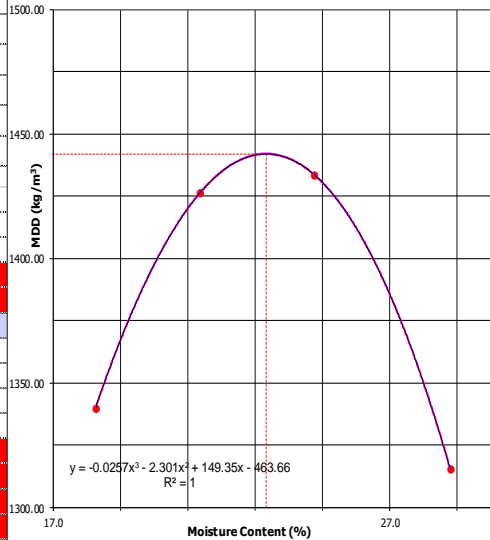
Appendix V: Proctor Compaction





Moisture - Density

Sample Type	Volcanic Ash soil				
Sample source	Maai Mahiu- Narok road				
Sample Date	9-Oct-15	Sample No	TP2 1M	Sample time	
Test date	11-Oct-15	Sample Desc			
Specification					
Wt of Mould (g)	4100	Volume of Mould (l)			0.956
Test No		1	2	3	4
Wt of mould + wet material (g)		5615	5755	5810	5720
Wt wet material (g)		1515	1655	1710	1620
Wet density (kg/m ³)	N.M.C	1584.728	1731.1715	1788.702929	1694.5607
Moisture content					
Container No	65A	62A	99A	108A	55A
Wt of container + wet material (g)	148.30	94.90	103.30	150.60	173.90
Wt of container (g)	17.90	15.90	19.80	17.10	18.70
Wt of container + dry material (g)	142.30	82.70	88.60	124.10	139.20
Wt dry material (g)	124.40	66.80	68.80	107.00	120.50
Wt of moisture (g)	6.00	12.20	14.70	26.50	34.70
Moisture content (%)	4.82	18.26	21.37	24.77	28.80
Dry density (kg/m ³)		1340.00	1426.40	1433.64	1315.69

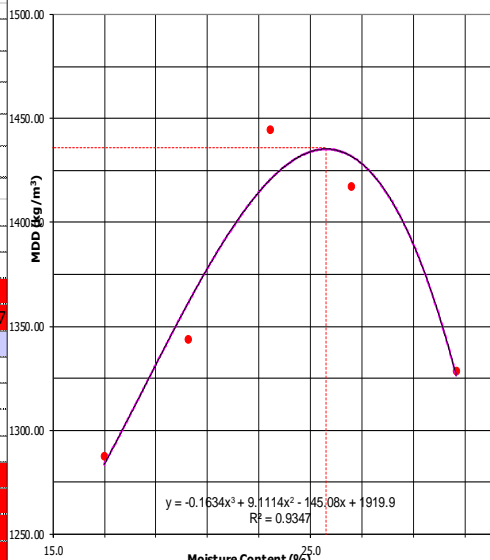


Optimum Moisture Content (%)	23.3
Maximum Dry Density (kg/m ³)	1441.9

Project Student	K.O. Amollo	Verified :	Mr. Ogallo
Date	14/10/2015	Lab In Charge/Chief Technologist	

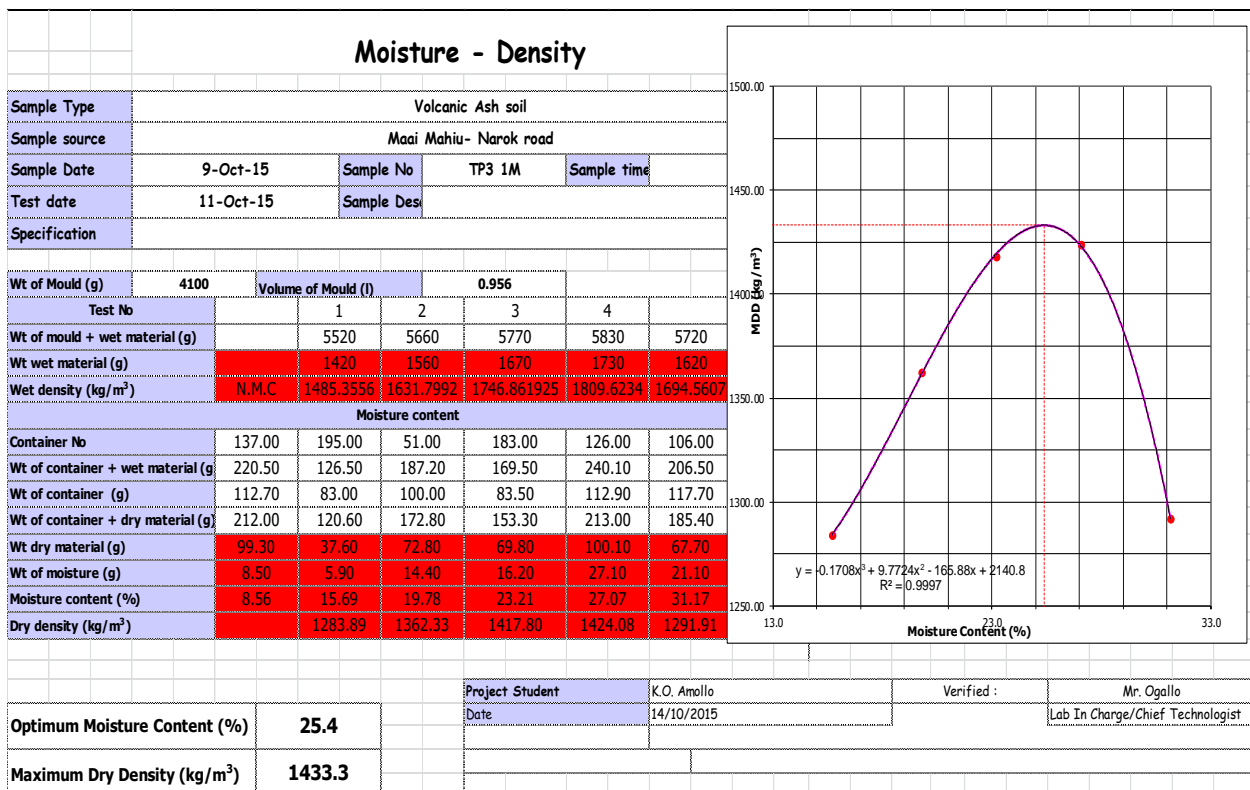
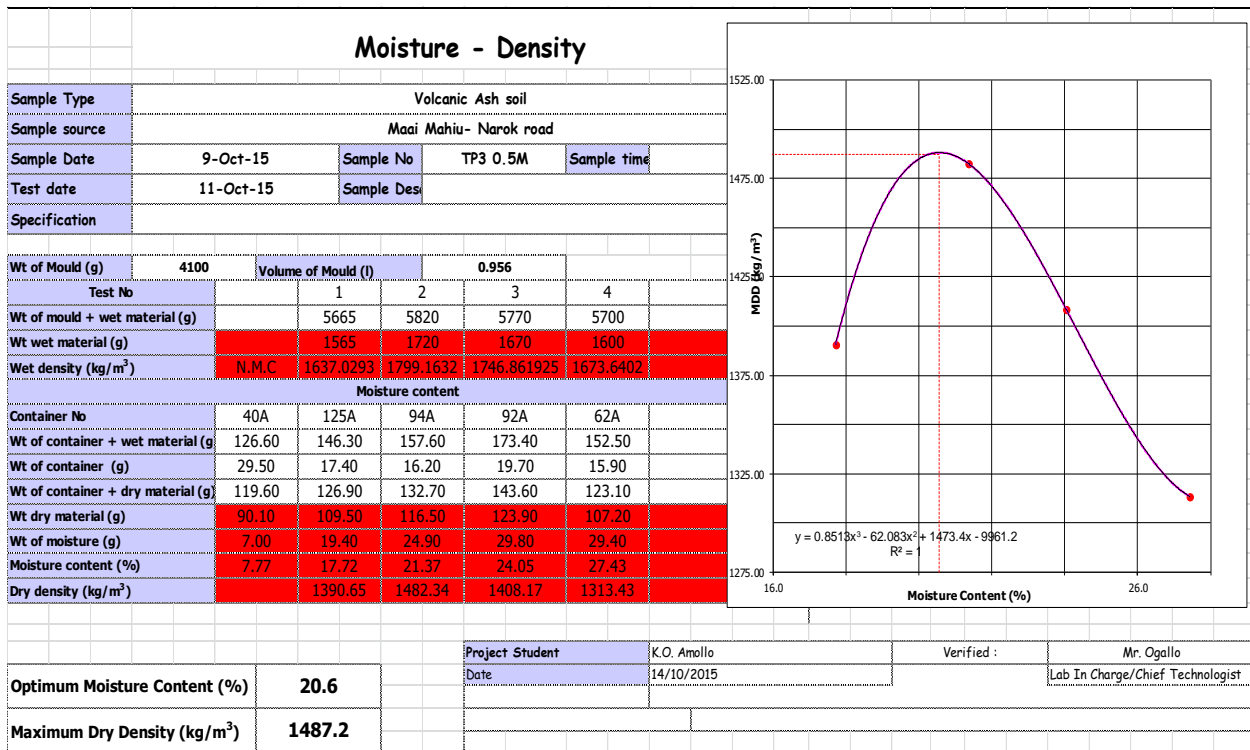
Moisture - Density

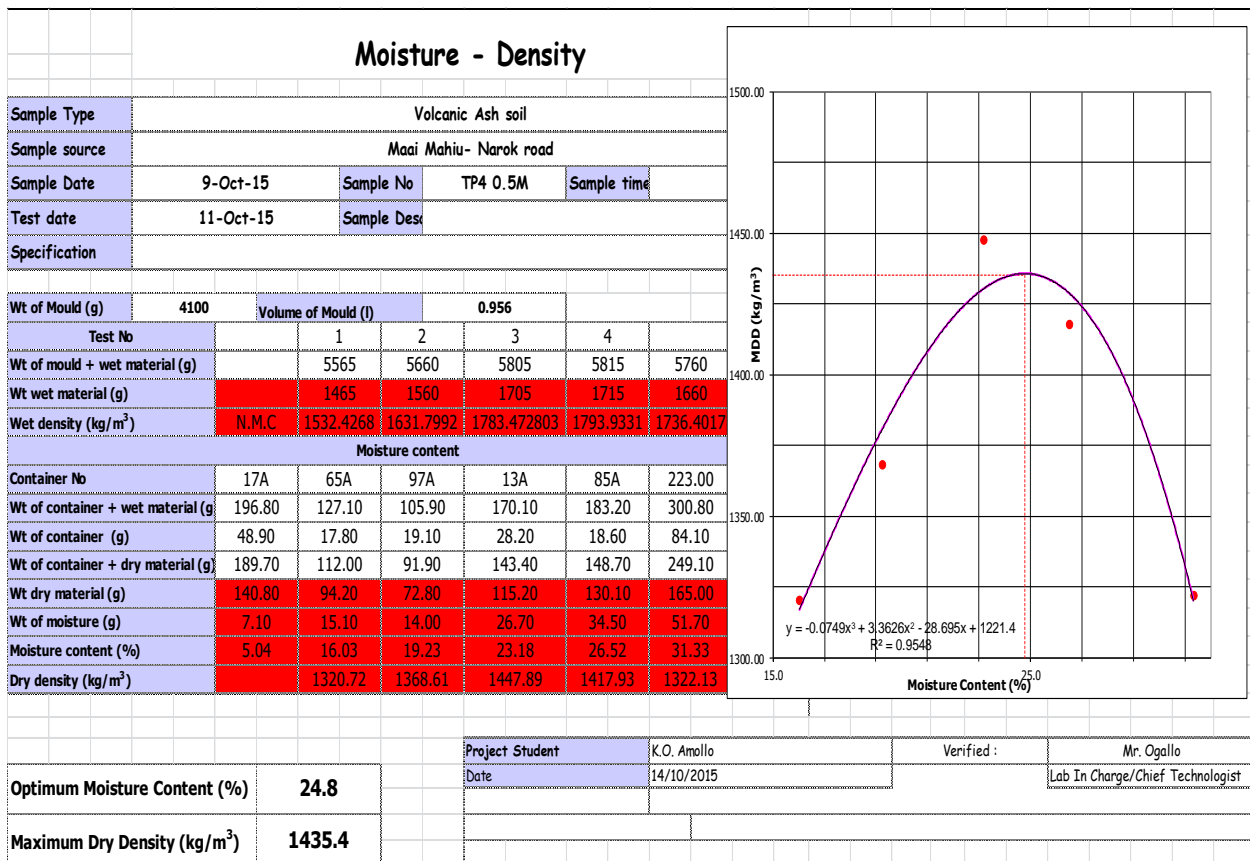
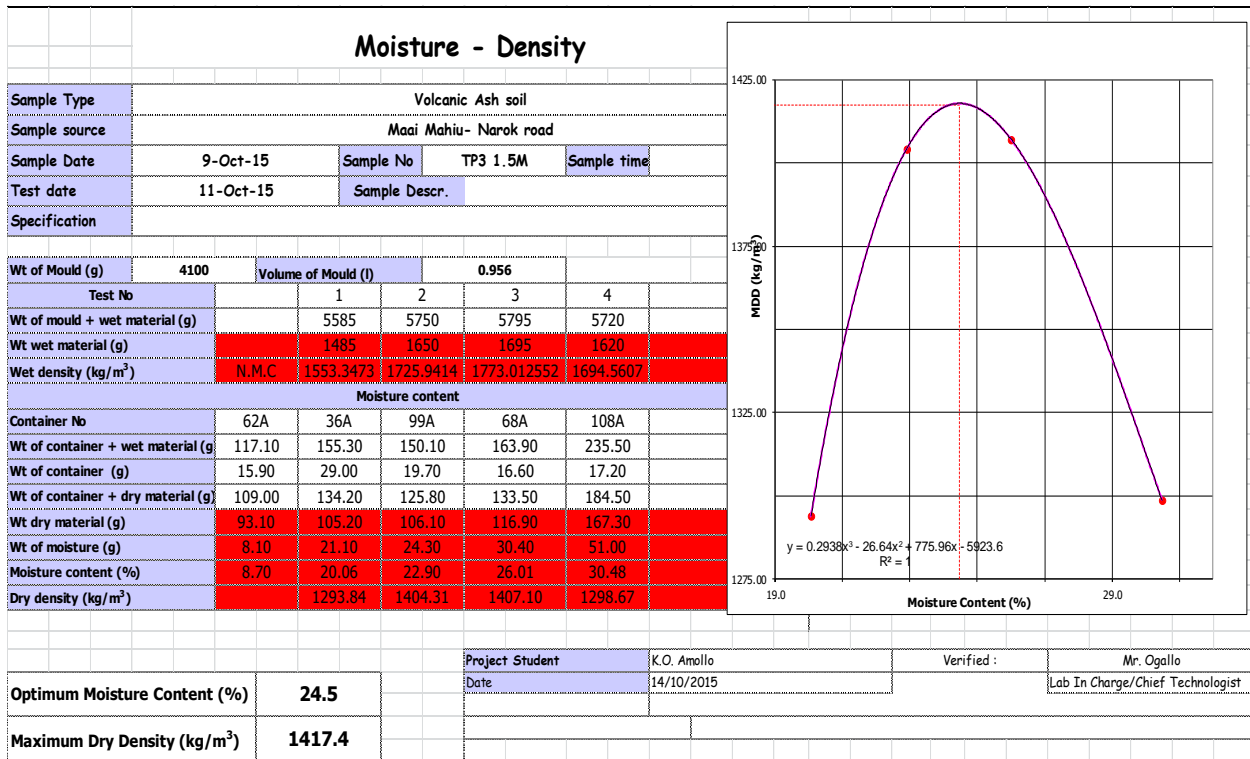
Sample Type	Volcanic Ash soil				
Sample source	Maai Mahiu- Narok road				
Sample Date	9-Oct-15	Sample No	TP2 1.5M	Sample time	
Test date	11-Oct-15	Sample Desc			
Specification					
Wt of Mould (g)	4100	Volume of Mould (l)			0.956
Test No		1	2	3	4
Wt of mould + wet material (g)		5540	5645	5805	5815
Wt wet material (g)		1440	1545	1705	1715
Wet density (kg/m ³)	N.M.C	1506.2762	1616.1088	1783.472803	1793.9331
Moisture content					
Container No	55A	108A	48A	85A	13A
Wt of container + wet material (g)	149.50	121.00	132.10	129.10	195.90
Wt of container (g)	18.70	17.00	27.50	18.50	28.20
Wt of container + dry material (g)	141.60	105.90	114.50	108.10	160.70
Wt dry material (g)	122.90	88.90	87.00	89.60	132.50
Wt of moisture (g)	7.90	15.10	17.60	21.00	35.20
Moisture content (%)	6.43	16.99	20.23	23.44	26.57
Dry density (kg/m ³)		1287.58	1344.18	1444.84	1417.39



Optimum Moisture Content (%)	25.6
Maximum Dry Density (kg/m ³)	1435.7

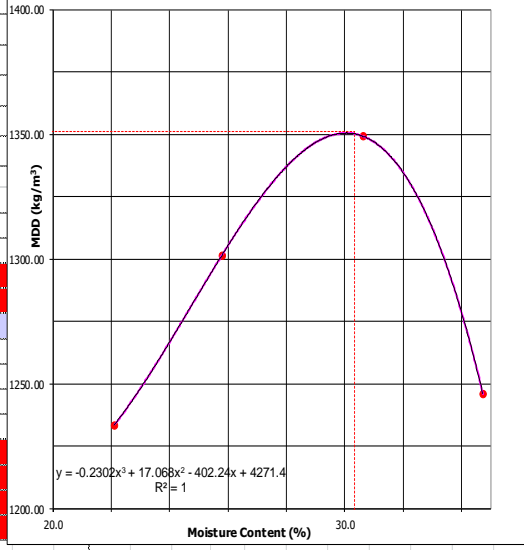
Project Student	K.O. Amollo	Verified :	Mr. Ogallo
Date	14/10/2015	Lab In Charge/Chief Technologist	





Moisture - Density

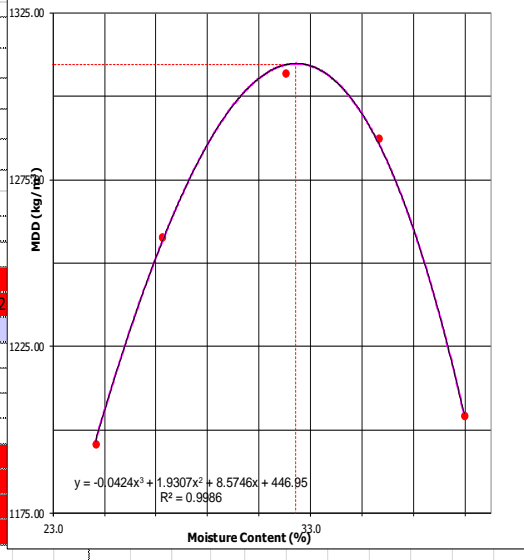
Sample Type	Volcanic Ash soil				
Sample source	Maai Mahiu- Narok road				
Sample Date	9-Oct-15	Sample No	TP4 1M	Sample time	
Test date	11-Oct-15	Sample Des			
Specification					
Wt of Mould (g)	4100		Volume of Mould (l)		0.956
Test No		1	2	3	4
Wt of mould + wet material (g)		5540	5665	5785	5705
Wt wet material (g)		1440	1565	1685	1605
Wet density (kg/m ³)		N.M.C	1506.2762	1637.0293	1762.552301
Moisture content					
Container No	204.00	213.00	164.00	181.00	216.00
Wt of container + wet material (g)	146.10	178.10	202.50	158.10	173.40
Wt of container (g)	84.40	98.00	114.20	84.30	83.80
Wt of container + dry material (g)	137.50	163.60	184.40	140.80	150.30
Wt dry material (g)	53.10	65.60	70.20	56.50	66.50
Wt of moisture (g)	8.60	14.50	18.10	17.30	23.10
Moisture content (%)	16.20	22.10	25.78	30.62	34.74
Dry density (kg/m ³)		1233.60	1301.47	1349.38	1246.04



Optimum Moisture Content (%)	30.3	Project Student	K.O. Amollo	Verified :	Mr. Ogallo
Maximum Dry Density (kg/m ³)	1351.4	Date	14/10/2015		Lab In Charge/Chief Technologist


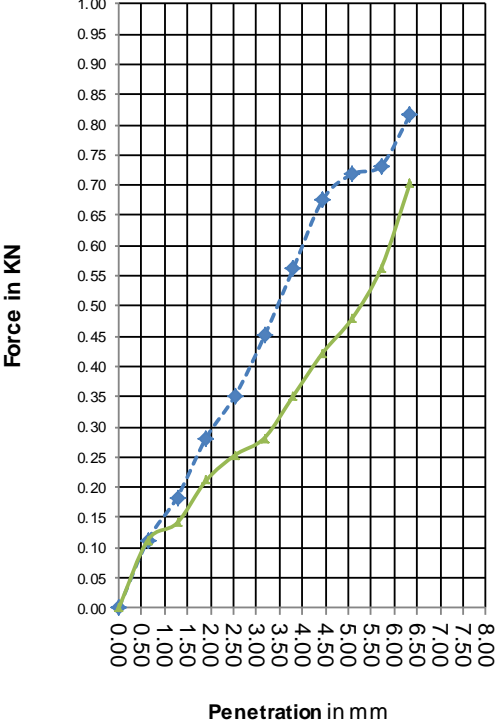
Moisture - Density


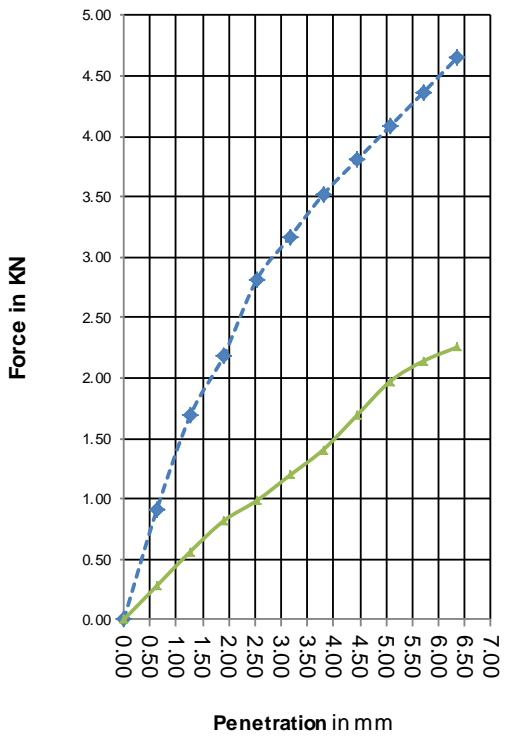
Sample Type	Volcanic Ash soil					
Sample source	Maai Mahiu- Narok road					
Sample Date	9-Oct-15	Sample No	TP4 1.5M	Sample time		
Test date	11-Oct-15	Sample Des				
Specification						
Wt of Mould (g)	4100		Volume of Mould (l)		0.956	
Test No		1	2	3	4	
Wt of mould + wet material (g)		5525	5630	5750	5770	5700
Wt wet material (g)		1425	1530	1650	1670	1600
Wet density (kg/m ³)		N.M.C	1490.5858	1600.4184	1725.941423	1746.8619
Moisture content						
Container No	55A	48A	40A	92A	94A	125A
Wt of container + wet material (g)	144.30	142.90	160.80	156.30	188.80	244.80
Wt of container (g)	18.60	27.60	29.50	19.90	16.10	17.60
Wt of container + dry material (g)	125.70	120.10	132.70	123.20	143.40	181.10
Wt dry material (g)	107.10	92.50	103.20	103.30	127.30	163.50
Wt of moisture (g)	18.60	22.80	28.10	33.10	45.40	63.70
Moisture content (%)	17.37	24.65	27.23	32.04	35.66	38.96
Dry density (kg/m ³)		1195.83	1257.91	1307.11	1287.64	1204.40


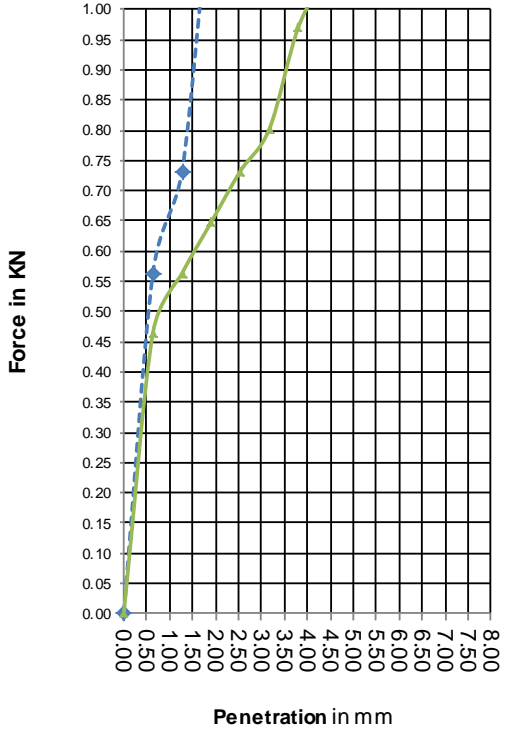



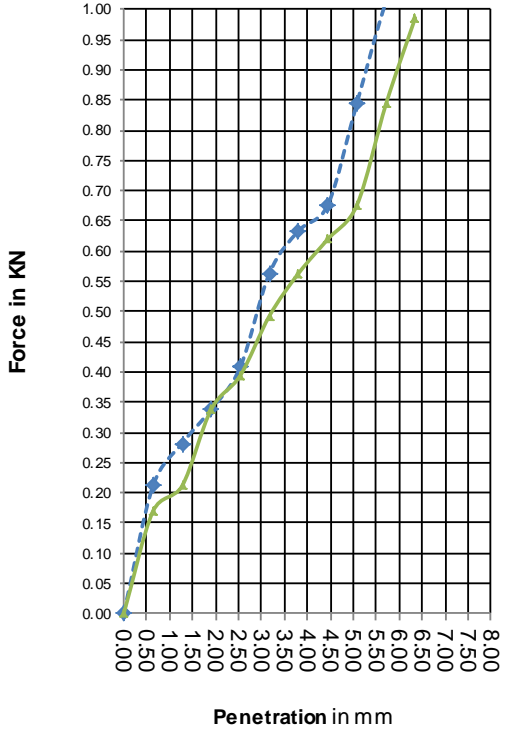
Optimum Moisture Content (%)	32.4	Project Student	K.O. Amollo	Verified :	Mr. Ogallo
Maximum Dry Density (kg/m ³)	1309.4	Date	14/10/2015		Lab In Charge/Chief Technologist

Appendix VI: California Bearing Ratio

UNIVERSITY OF NAIROBI						
(HIGHWAYS LABORATORY)		WORKING SHEET				
		CBR TEST				
		(AASHTO T193:1990)				
TP1 0.5M		Tested: 23/10/2015	Date soaked:	19/10/2015		
SWELL DATA		Mould No.:	Date Moulded:	19/10/2015		
Initial gauge Reading (div)	0	SAMPLE DETAILS		MDD	1420	
Final gauge Reading (div)	0	Type	Stabilized/unstabilized	OMC	23.7	
Difference (div)	0	Stabilizer	Nil	NMC	4.3	
Ring Factor	0.01	%				
		Swell %	0			
Gauge Factor:0.0005 inches/Div		Penetration of the plunger (mm)	Bot (KN)	Top (KN)	Standard Load(KN)	
<div style="text-align: center;"> <p>CBR TEST</p>  </div>					CBR%	
					Bott.	Top
		0.00	0	0		
		0.64	0.1127	0.113		
		1.27	0.1831	0.141		
		1.91	0.2816	0.211		
		2.54	0.3521	0.253	13.2	2.67 1.92
		3.18	0.4506	0.282		
		3.81	0.5633	0.352		
		4.45	0.6759	0.422		
5.08	0.7182	0.479	20.0	3.59 2.394		
5.72	0.7323	0.563				
6.35	0.8168	0.704				
Moulding Data						
Wt.of Mould + Wet soil			g	Will apply for dynamic CBR		
Wt. of Mould			g			
Moisture Content			%			
Wet Density			Kg/m ³			
Dry Density			Kg/m ³			
			% MDD			
MOULDING MOISTURE CONTENT						
Tin No.			94A			
Tin + Wet soil			148.9			
Tin + Dry soil			122.24			
Wt of Tin			26			
Wt of Moisture			26.66			
Wt. of dry soil			96.24			
Moisture content			27.70			
RESULTS						
Penetration(mm)	Standard Force(KN)	Specification	CBR%(top)	CBR%(bott.)		
2.5	13.2		2	3		
5	20		2	4		
CBR = 4 %			Checked:			

UNIVERSITY OF NAIROBI						
(HIGHWAYS LABORATORY)		WORKING SHEET				
		CBR TEST				
		(AASHTO T193:1990)				
TP2 0.5M		Tested: 23/10/2015	Date soaked:	19/10/2015		
SWELL DATA		Mould No.:	Date Moulded:	19/10/2015		
		SAMPLE DETAILS			MDD	1435.7
Initial gauge Reading (div)	0	Type	Stabilized/unstabilized	OMC	25.6	
Final gauge Reading (div)	0	Stabilizer	Nil	NMC	6.43	
Difference (div)	0	%				
Ring Factor	0.01	Swell %	0			
Gauge Factor:0.0005 inches/Div		Penetration of the plunger (mm)	Bot (KN)	Top (KN)	Standard Load(KN)	CBR%
						Bott. Top
		0.00	0	0		
		0.64	0.9153	0.282		
		1.27	1.6898	0.563		
		1.91	2.1827	0.817		
		2.54	2.8164	0.986	13.2	21.3 7.468
		3.18	3.1685	1.197		
		3.81	3.5205	1.408		
		4.45	3.8021	1.69		
		5.08	4.0838	1.971	20.0	20.4 9.857
		5.72	4.3654	2.14		
		6.35	4.6471	2.253		
CBR TEST 		Moulding Data				
		Wt.of Mould + Wet soil	g	Will apply for dynamic CBR		
		Wt. of Mould	g			
		Moisture Content	%			
		Wet Density	Kg/m ³			
		Dry Density	Kg/m ³			
	% MDD					
MOULDING MOISTURE CONTENT						
Tin No.	36A					
Tin +Wet soil	136.5					
Tin + Dry soil	118.69					
Wt of Tin	26					
Wt of Moisture	17.81					
Wt. of dry soil	92.69					
Moisture content	19.21					
RESULTS						
Penetration(mm)	Standard Force(KN)	Specification	CBR%(top)	CBR%(bott.)		
2.5	13.2		7	21		
5	20		10	20		
		CBR = 21 %		Checked:		

UNIVERSITY OF NAIROBI		WORKING SHEET					
(HIGHWAYS LABORATORY)							
		CBR TEST					
		(AASHTO T193:1990)					
TP3 1.5M		Tested: 23/10/2015	Date soaked:	19/10/2015			
SWELL DATA		Mould No.:	Date Moulded:	19/10/2015			
Initial gauge Reading (div)		SAMPLE DETAILS		MDD	1417.4		
Final gauge Reading (div)		Type	Stabilized/unstabilized	OMC	24.5		
Difference (div)		Stabilizer	Nil	NMC	8.7		
Ring Factor		%					
Gauge Factor:0.0005 inches/Div		Swell %	0				
<p style="text-align: center;">CBR TEST</p> 		Penetration of the plunger (mm)	Bot (KN)	Top (KN)	Standard Load(KN)	CBR%	
						Bott.	Top
		0.00	0	0			
		0.64	0.5633	0.465			
		1.27	0.7323	0.563			
		1.91	1.1688	0.648			
		2.54	1.3378	0.732	13.2	10.1	5.547
		3.18	1.6898	0.803			
		3.81	1.9011	0.972			
		4.45	2.0841	1.056			
5.08	2.2531	1.127	20.0	11.3	5.633		
5.72	2.4221	1.296					
6.35	2.6052	1.479					
Moulding Data							
Wt.of Mould + Wet soil			g	Will apply for dynamic CBR			
Wt. of Mould			g				
Moisture Content			%				
Wet Density			Kg/m ³				
Dry Density			Kg/m ³				
			% MDD				
MOULDING MOISTURE CONTENT							
Tin No.			94A				
Tin +Wet soil			148.9				
Tin + Dry soil			122.24				
Wt of Tin			26				
Wt of Moisture			26.66				
Wt. of dry soil			96.24				
Moisture content			27.70				
RESULTS							
Penetration(mm)	Standard Force(KN)	Specification	CBR%(top)	CBR%(bott.)			
2.5	13.2		6	10			
5	20		6	11			
CBR = 11 %			Checked:				

UNIVERSITY OF NAIROBI		WORKING SHEET					
(HIGHWAYS LABORATORY)							
		CBR TEST					
		(AASHTO T193:1990)					
TP4 1.5M		Tested: 23/10/2015	Date soaked:	19/10/2015			
SWELL DATA		Mould No.:	Date Moulded:	19/10/2015			
Initial gauge Reading (div)		SAMPLE DETAILS		MDD	1309.4		
Final gauge Reading (div)		Type	Stabilized/unstabilized	OMC	32.4		
Difference (div)		Stabilizer	Nil	NMC	17.37		
Ring Factor		%					
Gauge Factor:0.0005 inches/Div		Swell %	0				
<p style="text-align: center;">CBR TEST</p> 		Penetration of the plunger (mm)	Bot (KN)	Top (KN)	Standard Load(KN)	CBR%	
						Bott.	Top
		0.00	0	0			
		0.64	0.2112	0.169			
		1.27	0.2816	0.211			
		1.91	0.338	0.338			
		2.54	0.4084	0.394	13.2	3.09	2.987
		3.18	0.5633	0.493			
		3.81	0.6337	0.563			
		4.45	0.6759	0.62			
5.08	0.8449	0.676	20.0	4.22	3.38		
5.72	1.0139	0.845					
6.35	1.1266	0.986					
Moulding Data							
Wt.of Mould + Wet soil				g	Will apply for dynamic CBR		
Wt. of Mould				g			
Moisture Content				%			
Wet Density				Kg/m ³			
Dry Density				Kg/m ³			
				% MDD			
MOULDING MOISTURE CONTENT							
Tin No.				94A			
Tin +Wet soil				148.9			
Tin + Dry soil				122.24			
Wt of Tin				26			
Wt of Moisture				26.66			
Wt. of dry soil				96.24			
Moisture content				27.70			
RESULTS							
Penetration(mm)	Standard Force(KN)	Specification	CBR%(top)	CBR%(bott.)			
2.5	13.2		3	3			
5	20		3	4			
CBR = 4 %			Checked:				

Appendix VII: Consolidation

CONSOLIDATION TEST					
SITE	Maai Mahiu - Narok road				
PROJECT	FINAL YEAR PROJECT				
Depth (m)	1.5M	TEST ID	TP1		
Test date:	29-Oct-15	APPARATUS No.	1		
Specification	According to BS 1377:1990.	Sample and submitted by	K.O. AMOLLO		
DIA OF RING	76	mm	HEIGHT OF RING	19	mm
AREA (A)	45.4 cm ²				
STAGE - AFTER TEST					
MEASURED THICKNESS OF SPECIMEN (H1)				19	mm
WET SPECIMEN				147.5	g
MASS OF RING + WATCH GLASS + DRY SPECIMEN				...	g
MASS OF RING				...	g
MASS OF WATCH GLASS				...	g
MASS OF DRY SPECIMEN (ms)				114.5	g
MASS OF MOISTURE				33	g
MOISTURE CONTENT (m)				28.8	%
BULK DENSITY (ρ)				1.71	g/cm ³
DRY DENSITY (ρ _d)				1.33	g/cm ³
DEGREE OF SATURATION (S _r)	$m / (\rho_w / \rho_d - 1 / G_s)$			91.3	%
DENSITY OF SOIL PARTICLES MEASURED/ASSUMED	G _s ρ _w			2.288	g/cm ³
HEIGHT OF SOIL PARTICLES (H ₀)	$(m_s \times 1000) / (G_s \rho_w \times A)$			11.0	mm
APPLIED PRESSURE	TOTAL DEFLECTION D	THICKNESS OF SPECIMEN, H (H ₁ -D)	PERCENTAGE THICKNESS H/H ₁ X 100	HEIGHT OF VOIDS (H-H ₀)	VOIDS RATIO H-H ₀ /H ₀
KN/M ²	mm	mm		mm	
0	0	19.00	100.00	7.97	0.72
50	0.15	18.85	99.21	7.82	0.71
100	0.1	18.75	98.68	7.72	0.70
FLOODED 100	0.03	18.72	98.53	7.69	0.70
200	0.13	18.59	97.84	7.56	0.69
400	1.10	17.49	92.05	6.46	0.59

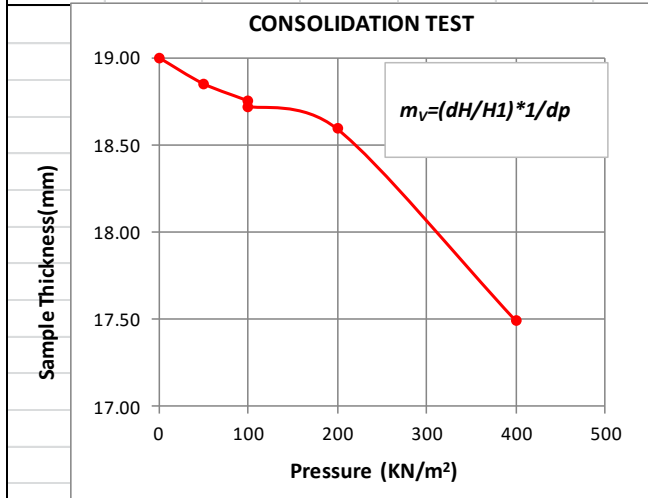
FIFTH YEAR PROJECT

CONSOLIDATION TEST

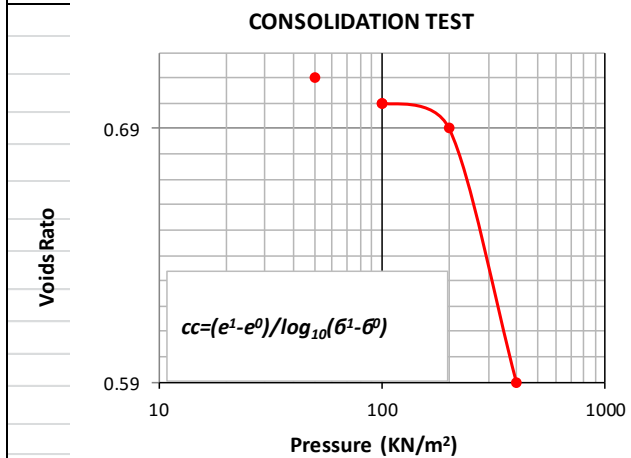
BS 1377: 1990

Site:	Maai Mahiu-Narok road	Pit No.:	TP 1	Date received:	3/10/2005
Sample classification:	Volcanic soil	Lab Ref:	UON	Sample number:	TP1 1.5M
Sampled by:	K.O. AMOLLO	Depth:	1.5 m	Date tested:	29-10-2015

Total Deflection -D (mm)	0.00	0.15	0.10	0.03	0.13	1.10
Pressure (KN/m ²)	0	50	100	100	200	400
% Thickness - H/H ₁	100.00	99.21	98.68	98.53	97.84	92.05
Ht. of Voids (mm)	8.0	7.8	7.7	7.7	7.6	6.5
Voids Ratio (H-H ₀)/H ₀	0.72	0.71	0.70	0.70	0.69	0.59
Thickness Specimen - H ₁ -D (mm)	19.00	18.85	18.75	18.72	18.59	17.49



Coefficient of Volume Compressibility (m _v)			
Sample Ht - H ₁	18.72	dH = H ₁ -H ₂	0.13
Sample Ht - H ₂	18.59	dH / H ₁	0.0069
Pressure @ H ₁ =	400	dP = H ₁ -H ₂	200
Pressure @ H ₂ =	200	1/dp	0.0050
$m_v = (dH/H_1) * 1/dp$	0.00003		m ² /KN
Settlement			
Soil Layer	1.5 m		
Settlement = m _v Hdp	5.2083E-05		mm



Compression Index (cc)			
Voids ratio e ₁	0.70	e ₀ -e	0.01
Voids ratio e ₀	0.69		
Pressure 1(σ ¹)	400	σ ¹ -σ ⁰	200
Pressure 1(σ ⁰)	200	log ₁₀ (σ ¹ -σ ⁰)	2.3000
$cc = (e^1 - e^0) / \log_{10}(\sigma^1 - \sigma^0)$	0.00435		mm ² /s
Settlement			
Soil Layer	1.5 m		
Settlement = m _v Hdp	6.52173913		mm

CONSOLIDATION TEST

SITE	Maai Mahiu - Narok road				
PROJECT	FINAL YEAR PROJECT				
Depth (m)	1.5M	TEST ID	TP2		
Test date:	29-Oct-15	APPARATUS No.	2		
Specification	According to BS 1377:1990.	Sample and submitted by	K.O. AMOLLO		
DIA OF RING	50	mm	HEIGHT OF RING	20	mm
AREA (A)	19.6 cm ²				
STAGE - AFTER TEST					
MEASURED THICKNESS OF SPECIMEN (H1)				20	mm
WET SPECIMEN				69.5	g
MASS OF RING + WATCH GLASS + DRY SPECIMEN				...	g
MASS OF RING				...	g
MASS OF WATCH GLASS				...	g
MASS OF DRY SPECIMEN (ms)				51.5	g
MASS OF MOISTURE				18	g
MOISTURE CONTENT (m)				35.0	%
BULK DENSITY (p)				1.77	g/cm ³
DRY DENSITY (pd)				1.31	g/cm ³
DEGREE OF SATURATION (Sr)	$m / (p_w / p_d - 1 / G_s)$			108.1	%
DENSITY OF SOIL PARTICLES MEASURED/ASSUMED	$G_s p_w$			2.277	g/cm ³
HEIGHT OF SOIL PARTICLES (Ho)	$(m_s \times 1000) / (G_s p_w \times A)$			11.5	mm
APPLIED PRESSURE	TOTAL DEFLECTION D	THICKNESS OF SPECIMEN, H (H1-D)	PERCENTAGE THICKNESS H/H1 X 100	HEIGHT OF VOIDS (H-Ho)	VOIDS RATIO H-H0/H0
kN/M ²	mm	mm		mm	
0	0	20.00	100.00	8.48	0.74
50	0.03	19.97	99.85	8.45	0.73
100	0.04	19.93	99.65	8.41	0.73
FLOODED 100	0.02	19.91	99.55	8.39	0.73
200	0.11	19.80	99.00	8.28	0.72
400	0.15	19.65	98.25	8.13	0.71

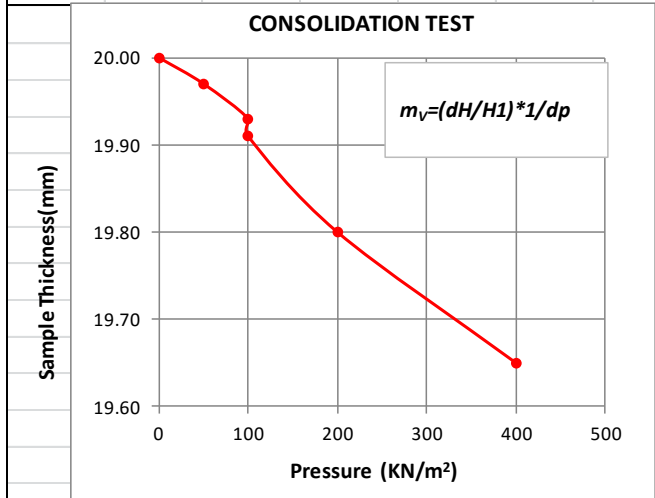
FINAL YEAR PROJECT

CONSOLIDATION TEST

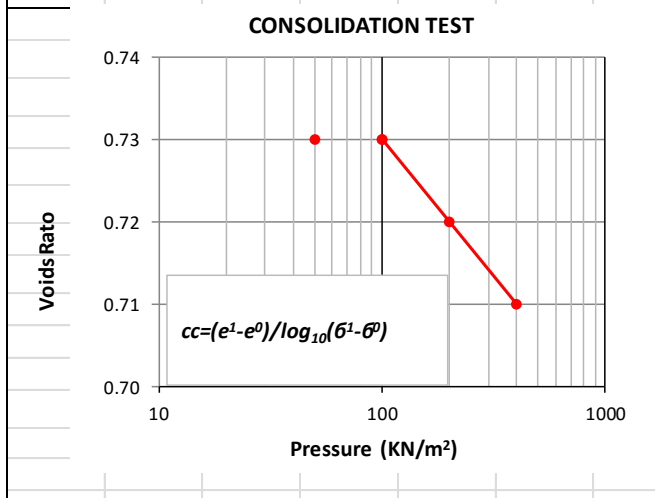
BS 1377: 1990

Site:	Maai Mahiu-Narok road	Pit No.:	TP 2	Date received:	3/10/2005
Sample classification:	Volcanic soil	Lab Ref:	UON	Sample number:	TP2 1.5M
Sampled by:	K.O. AMOLLO	Depth:	1.5 m	Date tested:	29-10-2015

Total Deflection -D (mm)	0.00	0.03	0.04	0.02	0.11	0.15
Pressure (KN/m²)	0	50	100	100	200	400
% Thickness - H/H ₁	100.00	99.85	99.65	99.55	99.00	98.25
Ht. of Voids (mm)	8.5	8.5	8.4	8.4	8.3	8.1
Voids Ratio (H-H ₀)/H ₀	0.74	0.73	0.73	0.73	0.72	0.71
Thickness Specimen - H ₁ -D (mm)	20.00	19.97	19.93	19.91	19.80	19.65



Coefficient of Volume Compressibility (m _v)			
Sample Ht - H ₁	19.91	dH = H ₁ -H ₂	0.11
Sample Ht - H ₂	19.80	dH / H ₁	0.0055
Pressure @ H ₁ =	400	dP = H ₁ -H ₂	200
Pressure @ H ₂ =	200	1/dp	0.0050
$m_v = (dH/H_1) * 1/dp$	0.00003		m ² /KN
Settlement			
Soil Layer	1.5 m		
Settlement = m_v Hdp		4.1436E-05	mm



Compression Index (cc)			
Voids ratio e ₁	0.73	e ₀ -e	0.01
Voids ratio e ₀	0.72		
Pressure 1(σ ¹)	400	σ ¹ -σ ⁰	200
Pressure 1(σ ⁰)	200	log ₁₀ (σ ¹ -σ ⁰)	2.3000
$cc = (e^1 - e^0) / \log_{10}(\sigma^1 - \sigma^0)$	0.00435		
Settlement			
Soil Layer	1.5 m		
Settlement = m_v Hdp		6.52173913	mm

CONSOLIDATION TEST

SITE	Maai Mahiu - Narok road				
PROJECT	FINAL YEAR PROJECT				
Depth (m)	1.5M	TEST ID	TP3		
Test date:	29-Oct-15	APPARATUS No.	3		
Specification	According to BS 1377:1990.	Sample and submitted by	K.O. AMOLLO		
DIA OF RING	76	mm	HEIGHT OF RING	19	mm
AREA (A)	45.4 cm ²				
STAGE - AFTER TEST					
MEASURED THICKNESS OF SPECIMEN (H1)				19	mm
WET SPECIMEN				150.4	g
MASS OF RING + WATCH GLASS + DRY SPECIMEN				...	g
MASS OF RING				...	g
MASS OF WATCH GLASS				...	g
MASS OF DRY SPECIMEN (ms)				114.4	g
MASS OF MOISTURE				36	g
MOISTURE CONTENT (m)				31.5	%
BULK DENSITY (p)				1.74	g/cm ³
DRY DENSITY (pd)				1.33	g/cm ³
DEGREE OF SATURATION (Sr)	$m / (p_w / p_d - 1 / G_s)$			98.3	%
DENSITY OF SOIL PARTICLES MEASURED/ASSUMED	$G_s p_w$			2.308	g/cm ³
HEIGHT OF SOIL PARTICLES (Ho)	$(m_s \times 1000) / (G_s p_w \times A)$			10.9	mm
APPLIED PRESSURE	TOTAL DEFLECTION D	THICKNESS OF SPECIMEN, H (H1-D)	PERCENTAGE THICKNESS H/H1 X 100	HEIGHT OF VOIDS (H-Ho)	VOIDS RATIO H-H0/H0
KN/M ²	mm	mm		mm	
0	0	19.00	100.00	8.08	0.74
50	0.05	18.95	99.74	8.03	0.73
100	0.1	18.85	99.21	7.93	0.73
FLOODED 100	0.16	18.69	98.37	7.77	0.71
200	0.34	18.35	96.58	7.43	0.68
400	0.60	17.75	93.42	6.83	0.62

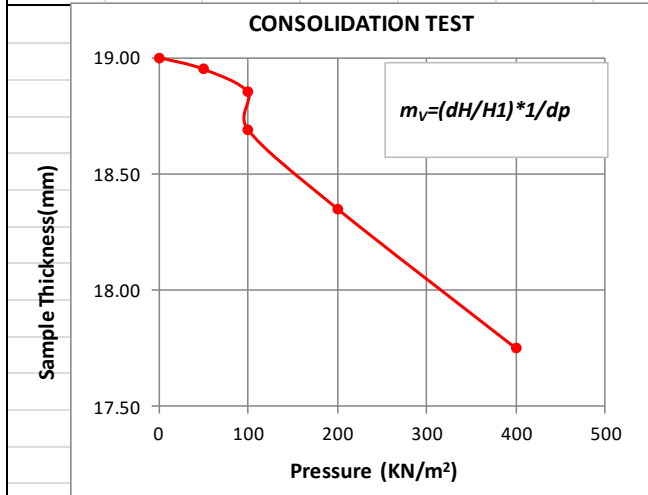
FINAL YEAR PROJECT

CONSOLIDATION TEST

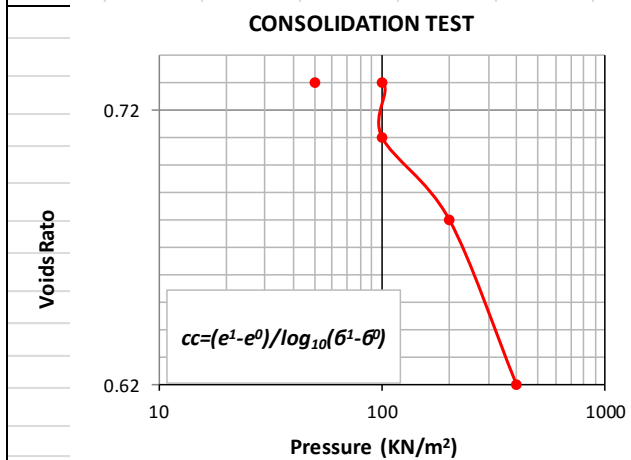
BS 1377: 1990

Site:	Maai Mahiu-Narok road	Pit No.:	TP 3	Date received:	3/10/2005
Sample classification:	Volcanic soil	Lab Ref:	UON	Sample number:	TP3 1.5M
Sampled by:	K.O. AMOLLO	Depth:	1.5 m	Date tested:	29-10-2015

Total Deflection -D (mm)	0.00	0.05	0.10	0.16	0.34	0.60
Pressure (KN/m²)	0	50	100	100	200	400
% Thickness - H/H ₁	100.00	99.74	99.21	98.37	96.58	93.42
Ht. of Voids (mm)	8.1	8.0	7.9	7.8	7.4	6.8
Voids Ratio (H-H ₀)/H ₀	0.74	0.73	0.73	0.71	0.68	0.62
Thickness Specimen - H ₁ -D (mm)	19.00	18.95	18.85	18.69	18.35	17.75



Coefficient of Volume Compressibility (m _v)			
Sample Ht - H ₁	18.69	dH = H ₁ -H ₂	0.34
Sample Ht - H ₂	18.35	dH / H ₁	0.0182
Pressure @ H ₁ =	400	dP = H ₁ -H ₂	200
Pressure @ H ₂ =	200	1/dp	0.0050
$m_v = (dH/H_1) * 1/dp$	0.00009		m ² /KN
Settlement			
Soil Layer	1.5 m		
Settlement = m_v Hdp	0.00013644		mm



Compression Index (cc)			
Voids ratio e ₁	0.71	e ₀ -e	0.03
Voids ratio e ₀	0.68		
Pressure 1(σ ¹)	400	σ ¹ -σ ⁰	200
Pressure 1(σ ⁰)	200	log ₁₀ (σ ¹ -σ ⁰)	2.3000
$cc = (e^1 - e^0) / \log_{10}(\sigma^1 - \sigma^0)$	0.01304		
Settlement			
Soil Layer	1.5 m		
Settlement = m_v Hdp	19.5652174		mm

CONSOLIDATION TEST

SITE	Maai Mahiu - Narok road				
PROJECT	FINAL YEAR PROJECT				
Depth (m)	1.5M	TEST ID	TP4		
Test date:	29-Oct-15	APPARATUS No.	4		
Specification	According to BS 1377:1990.	Sample and submitted by	K.O. AMOLLO		
DIA OF RING	50	mm	HEIGHT OF RING	20	mm
AREA (A)	19.6 cm ²				
STAGE - AFTER TEST					
MEASURED THICKNESS OF SPECIMEN (H1)				20	mm
WET SPECIMEN				67.3	g
MASS OF RING + WATCH GLASS + DRY SPECIMEN				...	g
MASS OF RING				...	g
MASS OF WATCH GLASS				...	g
MASS OF DRY SPECIMEN (ms)				47.3	g
MASS OF MOISTURE				20	g
MOISTURE CONTENT (m)				42.3	%
BULK DENSITY (p)				1.71	g/cm ³
DRY DENSITY (pd)				1.20	g/cm ³
DEGREE OF SATURATION (Sr)	$m / (p_w / p_d - 1 / G_s)$			109.3	%
DENSITY OF SOIL PARTICLES MEASURED/ASSUMED	$G_s p_w$			2.254	g/cm ³
HEIGHT OF SOIL PARTICLES (Ho)	$(m_s \times 1000) / (G_s p_w \times A)$			10.7	mm
APPLIED PRESSURE	TOTAL DEFLECTION D	THICKNESS OF SPECIMEN, H (H1-D)	PERCENTAGE THICKNESS H/H1 X 100	HEIGHT OF VOIDS (H-Ho)	VOIDS RATIO H-H0/H0
KN/M ²	mm	mm		mm	
0	0	20.00	100.00	9.31	0.87
50	0.08	19.92	99.60	9.23	0.86
100	0.2	19.72	98.60	9.03	0.85
FLOODED 100	0.04	19.68	98.40	8.99	0.84
200	0.26	19.42	97.10	8.73	0.82
400	0.64	18.78	93.90	8.09	0.76

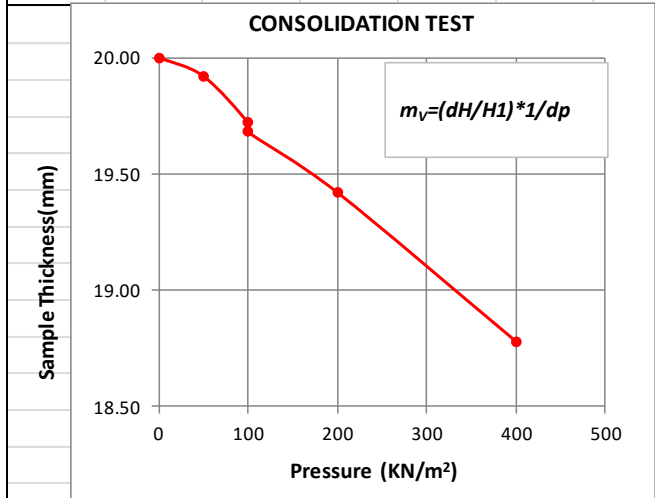
FINAL YEAR PROJECT

CONSOLIDATION TEST

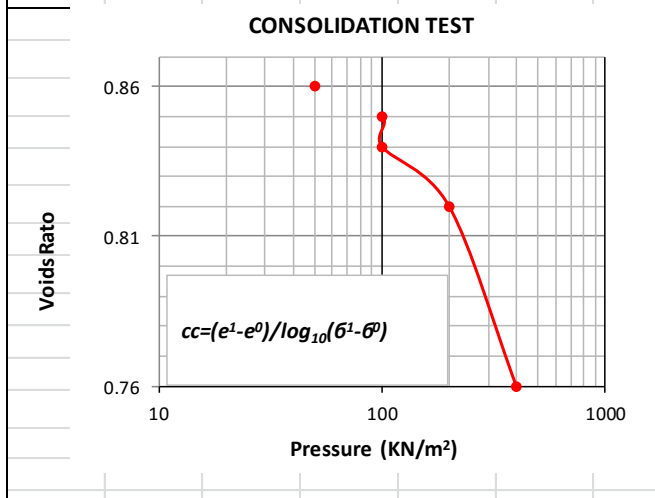
BS 1377: 1990

Site:	Maai Mahiu-Narok road	Pit No.:	TP 4	Date received:	3/10/2005
Sample classification:	Volcanic soil	Lab Ref:	UON	Sample number:	TP4 1.5M
Sampled by:	K.O. AMOLLO	Depth:	1.5 m	Date tested:	29-10-2015

Total Deflection -D (mm)	0.00	0.08	0.20	0.04	0.26	0.64
Pressure (KN/m²)	0	50	100	100	200	400
% Thickness - H/H ₁	100.00	99.60	98.60	98.40	97.10	93.90
Ht. of Voids (mm)	9.3	9.2	9.0	8.1	8.7	8.1
Voids Ratio (H-H ₀)/H ₀	0.87	0.86	0.85	0.84	0.82	0.76
Thickness Specimen - H ₁ -D (mm)	20.00	19.92	19.72	19.68	19.42	18.78



Coefficient of Volume Compressibility (m _v)			
Sample Ht - H ₁	19.68	dH = H ₁ -H ₂	0.26
Sample Ht - H ₂	19.42	dH / H ₁	0.0132
Pressure @ H ₁ =	400	dP = H ₁ -H ₂	200
Pressure @ H ₂ =	200	1/dp	0.0050
$m_v = (dH/H_1) * 1/dp$	0.00007		m ² /KN
Settlement			
Soil Layer	1.5 m		
Settlement = m_v Hdp		9.9085E-05	mm



Compression Index (cc)			
Voids ratio e ₁	0.84	e ₀ -e	0.02
Voids ratio e ₀	0.82		
Pressure 1(σ ¹)	400	σ ¹ -σ ⁰	200
Pressure 1(σ ⁰)	200	log ₁₀ (σ ¹ -σ ⁰)	2.3000
$cc = (e^1 - e^0) / \log_{10}(\sigma^1 - \sigma^0)$	0.00870		
Settlement			
Soil Layer	1.5 m		
Settlement = m_v Hdp		13.0434783	mm

Appendix VIII: Direct Shear Box

K.O. AMOLLO		TEST ID : TP 1	
SITE: Maai Mahiu-Narok Road			
DEPTH : 1.5M		Soil bulk density: 1447kg/m³	
DATE :13/11/2015		Unit weight=14.2N/m³	
SPECIFICATION : According to BS 1377:1990			
<u>DIRECT SHEAR TEST</u>			
LOADS APPLIED		Area of shear box = 36 square cm	
weight of hanger = 4.5 kg			
1st load = 32.2 kg			
Total = 1st load + weight of hanger =		36.7	kg
2nd load =68.9 kg			
Total = 2nd load + weight of hanger =		73.4	kg
3rd load = 105kg			
Total = 3rd load + weight of hanger =		109.5	kg
Normal stress = applied load/area of shear box		shear stress = shear force at failure/ area of shear box	
Normal stress =	1.02	kg per square cm	Shear stress = 0.51 kg per square cm
Normal stress =	2.04	kg per square cm	Shear stress = 1.07 kg per square cm
Normal stress =	3.04	kg per square cm	Shear stress = 1.52 kg per square cm
A graph of shear stress against normal stress			
	C = 0.02kg/cm²	B=1m	Q(soil bearing capacity)=391.365kN/m³
		Nq=14.55	Safe bearing capacity=q/3=130.46kN/m³
		Nc=25.5	
	Ø = 27°	Ny=11.4	

K.O. AMOLLO TEST ID : TP 2

SITE: Maai Mahiu- Narok road

DEPTH : 1.5M Soil bulk density: 934kg/m³

DATE :13/11/2015 Unit weight=9.16N/m³

SPECIFICATION : According to BS 1377:1990

DIRECT SHEAR TEST

LOADS APPLIED

weight of hanger = 4.5 kg Area of shear box = 36 square cm

1st load = 32.2 kg

Total = 1st load + weight of hanger = 36.7 kg

2nd load = 68.9 kg

Total = 2nd load + weight of hanger = 73.4 kg

3rd load = 105kg

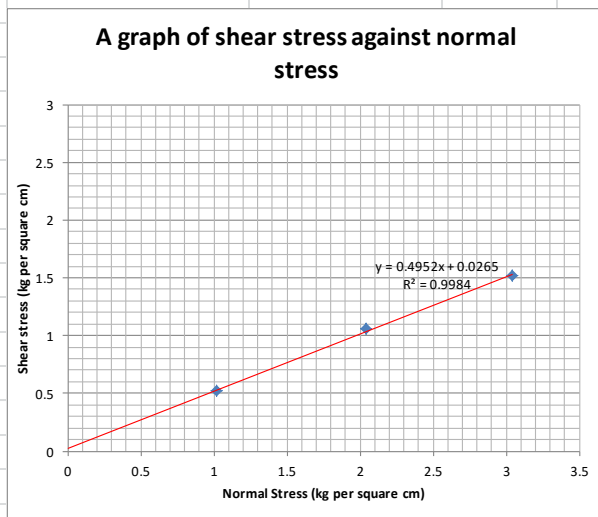
Total = 3rd load + weight of hanger = 109.5 kg

Normal stress = applied load/area of shear box shear stress = shear force at failure/ area of shear box

Normal stress = 1.02 kg per square cm Shear stress = 0.52 kg per square cm

Normal stress = 2.04 kg per square cm Shear stress = 1.06 kg per square cm

Normal stress = 3.04 kg per square cm Shear stress = 1.52 kg per square cm



B=1m Q(soil bearing capacity)=231.31kN/m³

C = 0.03kg/cm² Nq=13.4 Safe bearing capacity=q/3=77.1kN/m³

Nc=24

Ø = 26° Ny=10.2

K.O. AMOLLO

TEST ID : TP 3

SITE: Maai Mahiu-Narok Road

DEPTH : 1.5M

Soil bulk density: 1031kg/m³

DATE :13/11/2015

Unit weight=10.11N/m³

SPECIFICATION : According to BS 1377:1990

DIRECT SHEAR TEST

LOADS APPLIED

weight of hanger = 4.5 kg

Area of shear box = 36 square cm

1st load = 32.2 kg

Total = 1st load + weight of hanger = 36.7 kg

2nd load = 68.9 kg

Total = 2nd load + weight of hanger = 73.4 kg

3rd load = 105kg

Total = 3rd load + weight of hanger = 109.5 kg

Normal stress = applied load/area of shear box

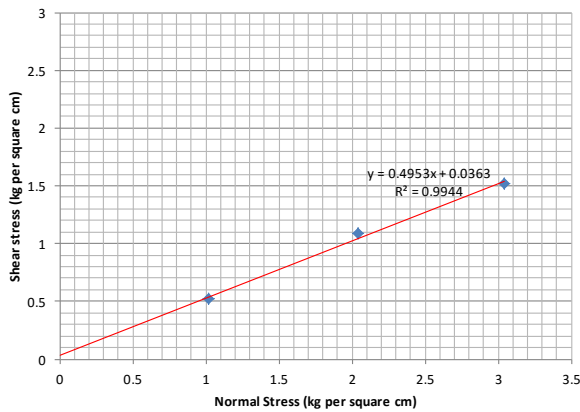
shear stress = shear force at failure/ area of shear box

Normal stress = 1.02 kg per square cm Shear stress = 0.52 kg per square cm

Normal stress = 2.04 kg per square cm Shear stress = 1.09 kg per square cm

Normal stress = 3.04 kg per square cm Shear stress = 1.52 kg per square cm

A graph of shear stress against normal stress



C = 0.04kg/cm²

B=1m

Q(soil bearing capacity)=255.25kN/m³

Nq=13.4

Safe bearing capacity=q/3=85.08kN/m³

Nc=24

Ø = 26°

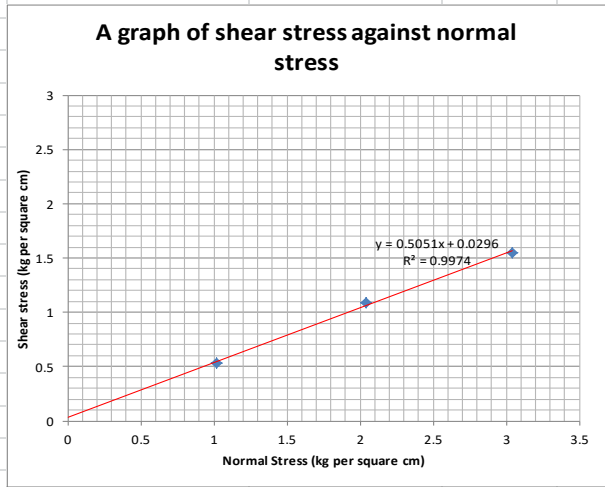
Ny=10.2

K.O. AMOLLO		TEST ID : TP 4	
SITE: Maai Mahiu-Narok road			
DEPTH : 1.5M	Soil bulk density: 992kg/m ³		
DATE :13/11/2015	Unit weight=9.73N/m ³		
SPECIFICATION : According to BS 1377:1990			

DIRECT SHEAR TEST

LOADS APPLIED		Area of shear box = 36 square cm	
weight of hanger = 4.5 kg			
1st load = 32.2 kg			
Total = 1st load + weight of hanger =	36.7	kg	
2nd load = 68.9 kg			
Total = 2nd load + weight of hanger =	73.4	kg	
3rd load = 105kg			
Total = 3rd load + weight of hanger =	109.5	kg	

Normal stress = applied load/area of shear box		shear stress = shear force at failure/ area of shear box	
Normal stress =	1.02	kg per square cm	Shear stress = 0.53 kg per square cm
Normal stress =	2.04	kg per square cm	Shear stress = 1.09 kg per square cm
Normal stress =	3.04	kg per square cm	Shear stress = 1.55 kg per square cm



C = 0.03kg/cm ²	B=1m	Q(soil bearing capacity)=268.33kN/m ³
	Nq=14.55	Safe bearing capacity=q/3=89.44kN/m ³
	Nc=25.5	
Ø = 27°	Nγ=11.4	

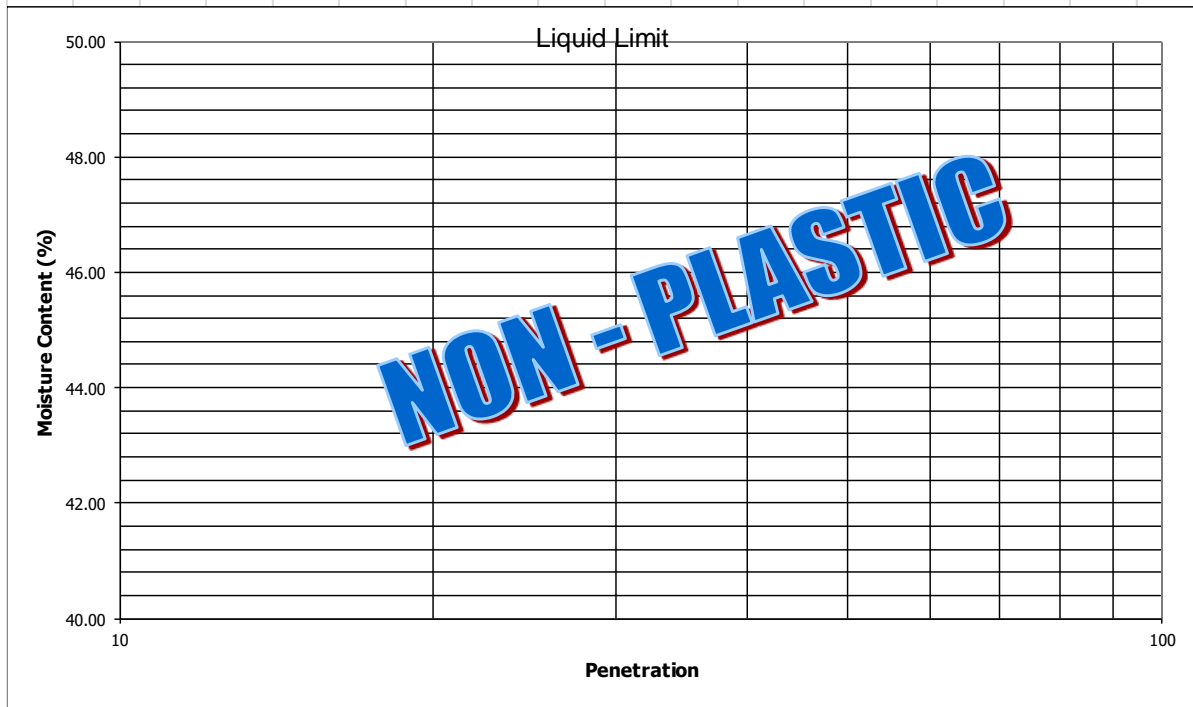
Appendix IX: Atterberg Limits

Plasticity Indices					
SITE	Maai mahiu-Narok road				
DEPTH	0.5M, 1M, 1.5M	Sample No	TP1	Sample type	Volcanic ash soil
Test date	10-Nov-15	Lab Ref No			
Specification					

	Liquid Limit	Plastic Limit
Container No		
Penetration (mm)		
Wt of Container + Wet Soil (g)		
Wt of Container + Dry Soil (g)		
Wt of Container (g)		
Wt of Moistuer (g)		
Wt of Dry Soil (g)		
Moisture Content (%)		

NON - PLASTIC

Linear Shrinkage	Initial Length (mm)	No1		No 2	
		140	140	Final Length (mm)	No 1
				No 2	140



NON - PLASTIC

Liquid Limit	Non Plastic
Plastic Limit	Non Plastic
Plasticity Index	Non Plastic
Linear Shrinkage (%)	0.0

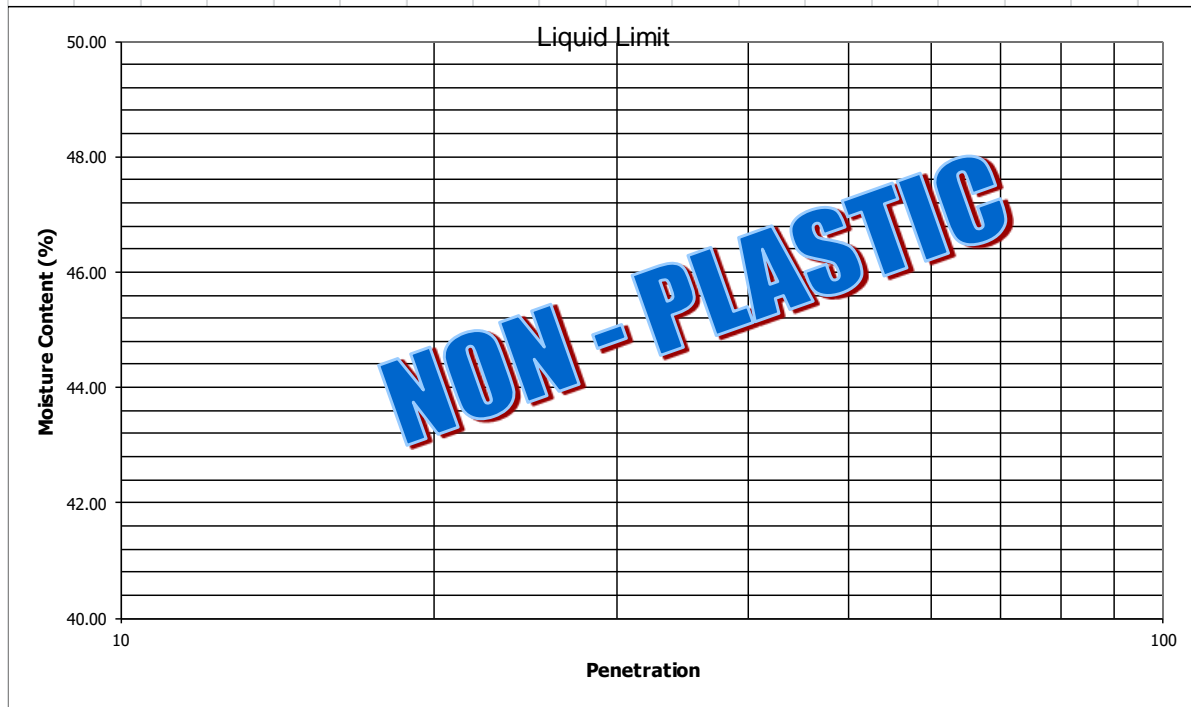
Plasticity Indices

SITE	Maai mahiu-Narok road		
DEPTH	0.5M, 1M, 1.5M	Sample No	TP2
Test date	10-Nov-15	Sample type	Volcanic ash soil
Specification	Lab Ref No		

	Liquid Limit	Plastic Limit
Container No		
Penetration (mm)		
Wt of Container + Wet Soil (g)		
Wt of Container + Dry Soil (g)		
Wt of Container (g)		
Wt of Moistuer (g)		
Wt of Dry Soil (g)		
Moisture Content (%)		

NON-PLASTIC

Linear Shrinkage	Initial Length (mm)	No1	140	Final Length (mm)	No 1	140
		No 2	140		No 2	140



NON-PLASTIC

Liquid Limit	
Plastic Limit	Non Plastic
Plasticity Index	Non Plastic
Linear Shrinkage (%)	0.0

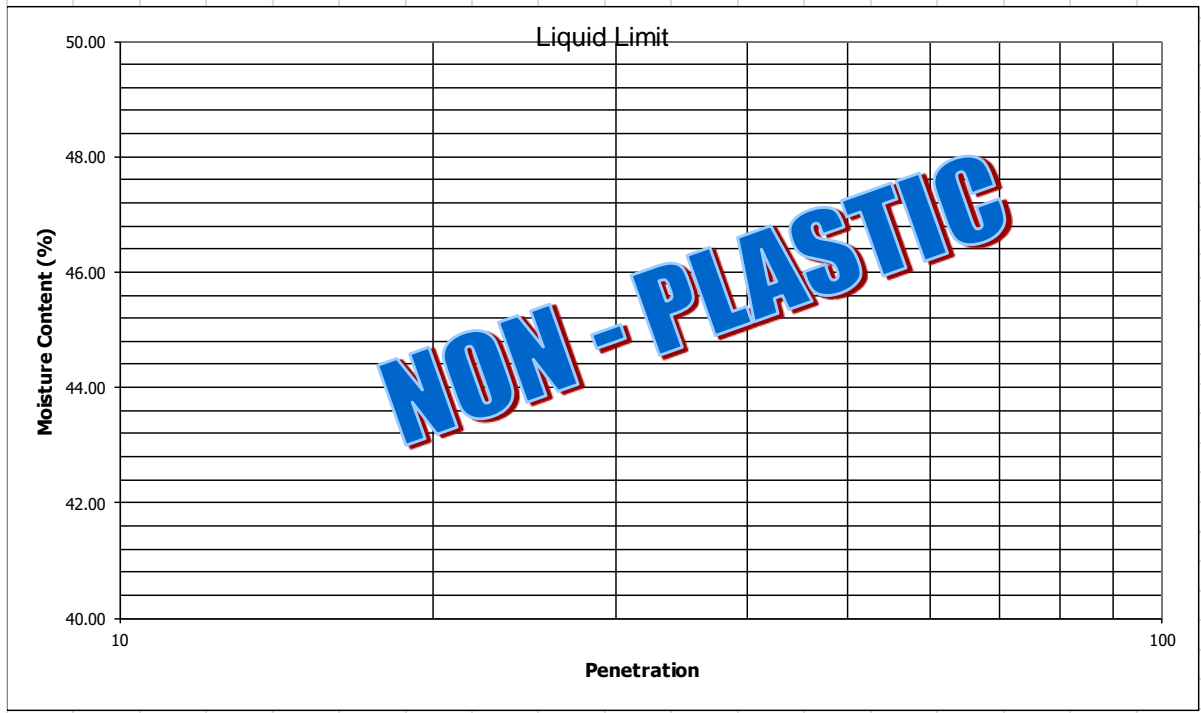
Plasticity Indices

SITE	Maai mahiu-Narok road		
DEPTH	0.5M, 1M, 1.5M	Sample No	TP3
Test date	10-Nov-15	Sample type	Volcanic ash soil
Specification	Lab Ref No		

	Liquid Limit	Plastic Limit
Container No		
Penetration (mm)		
Wt of Container + Wet Soil (g)		
Wt of Container + Dry Soil (g)		
Wt of Container (g)		
Wt of Moistuer (g)		
Wt of Dry Soil (g)		
Moisture Content (%)		

NON-PLASTIC

Linear Shrinkage	Initial Length (mm)	No1	140	Final Length (mm)	No 1	140
		No 2	140		No 2	140



NON-PLASTIC

Liquid Limit	
Plastic Limit	Non Plastic
Plasticity Index	Non Plastic
Linear Shrinkage (%)	0.0

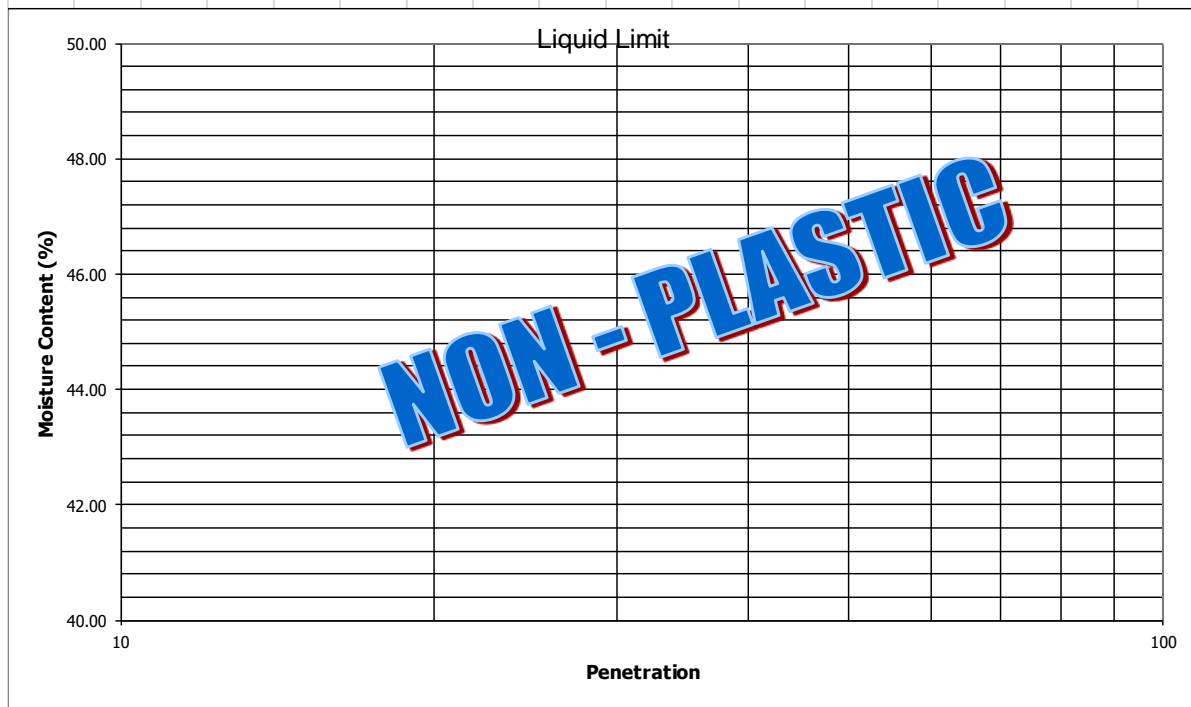
Plasticity Indices

SITE	Maai mahiu-Narok road		
DEPTH	0.5M, 1M, 1.5M	Sample No	TP4
Test date	10-Nov-15	Sample type	Volcanic ash soil
Specification	Lab Ref No		

	Liquid Limit	Plastic Limit
Container No		
Penetration (mm)		
Wt of Container + Wet Soil (g)		
Wt of Container + Dry Soil (g)		
Wt of Container (g)		
Wt of Moistuer (g)		
Wt of Dry Soil (g)		
Moisture Content (%)		

NON-PLASTIC

Linear Shrinkage	Initial Length (mm)	No1	140	Final Length (mm)	No 1	140
		No 2	140		No 2	140

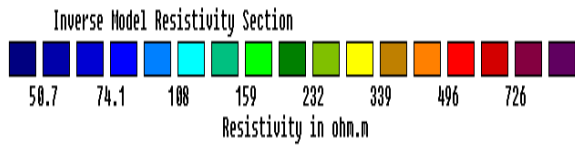
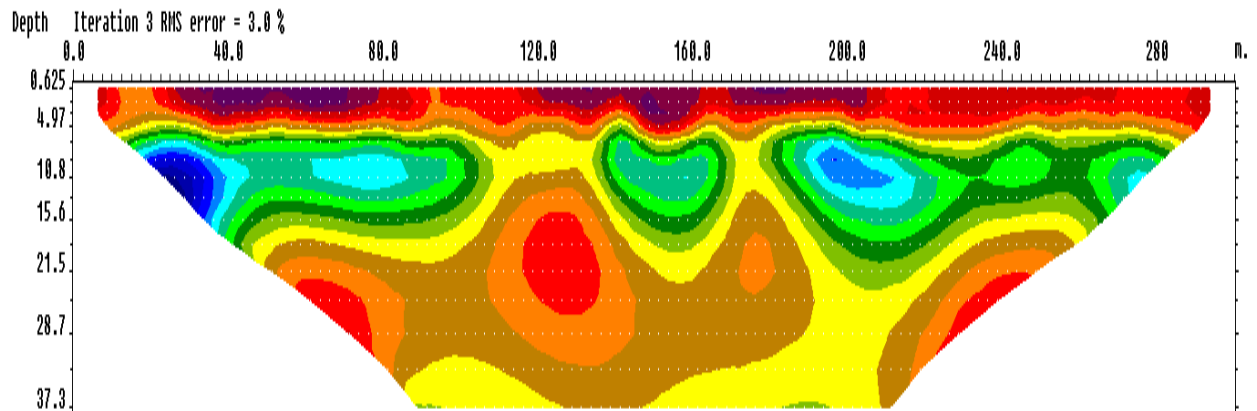
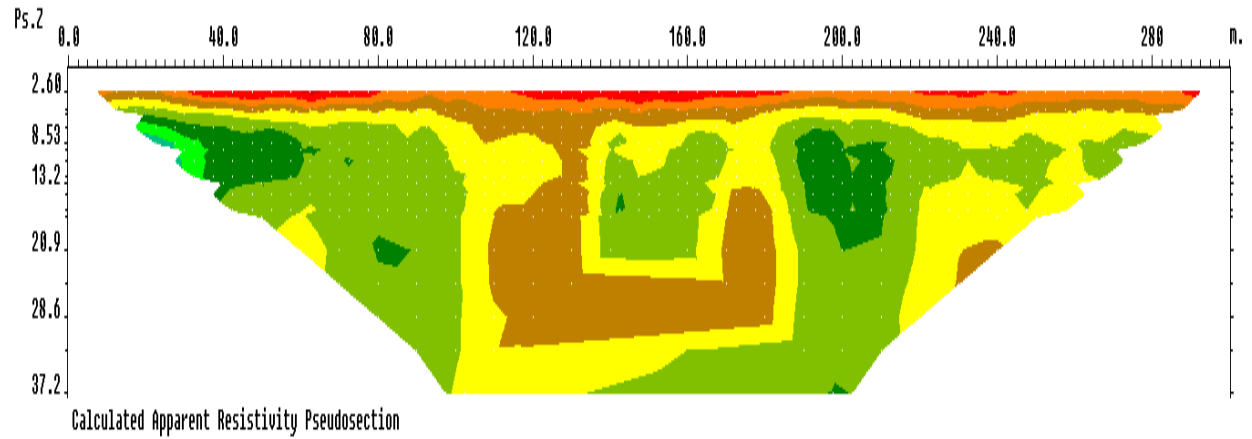
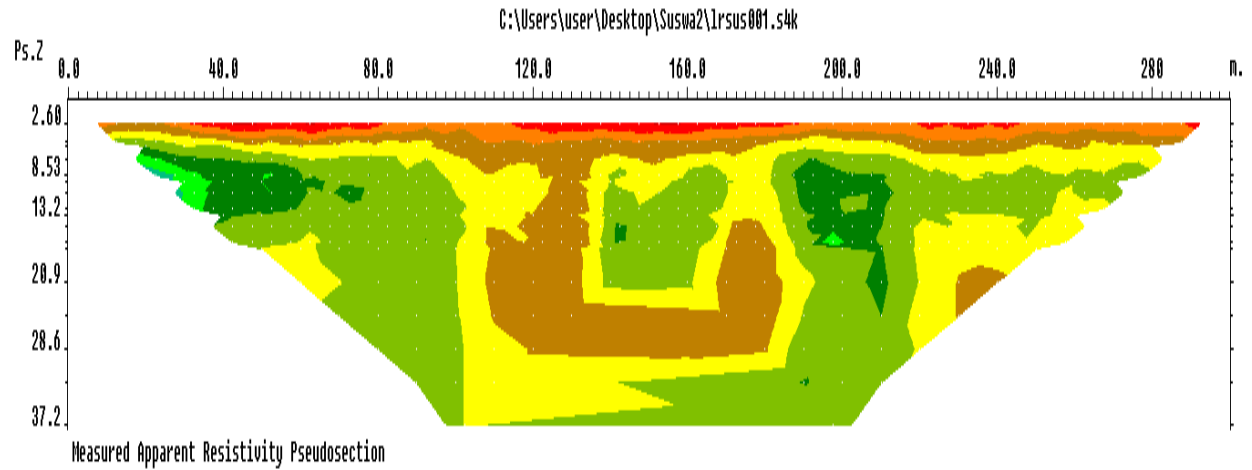


NON-PLASTIC

Liquid Limit	
Plastic Limit	Non Plastic
Plasticity Index	Non Plastic
Linear Shrinkage (%)	0.0

Appendix X: Electrical Resistivity Tomography

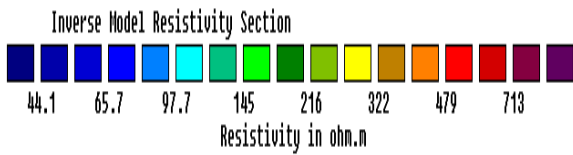
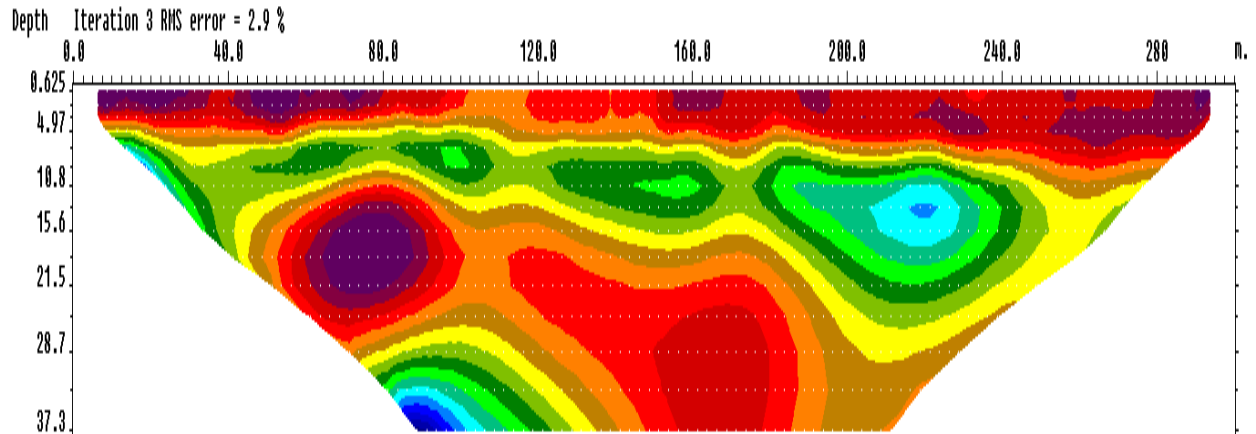
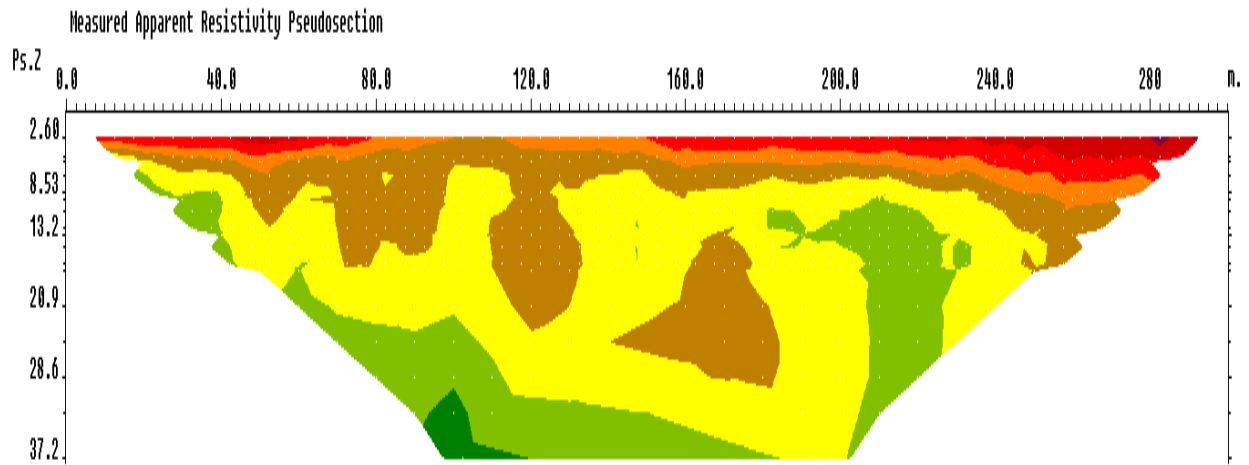
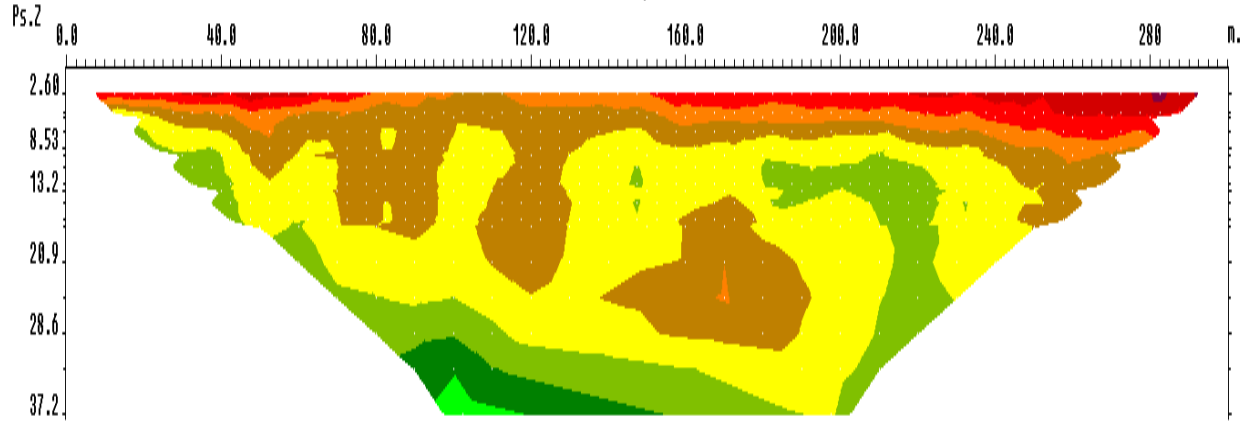
ELECTRICAL RESISTIVITY TOMOGRAPHY PROFILE 1



Unit electrode spacing 2.50 m.

ELECTRICAL RESISTIVITY TOMOGRAPHY PROFILE 2

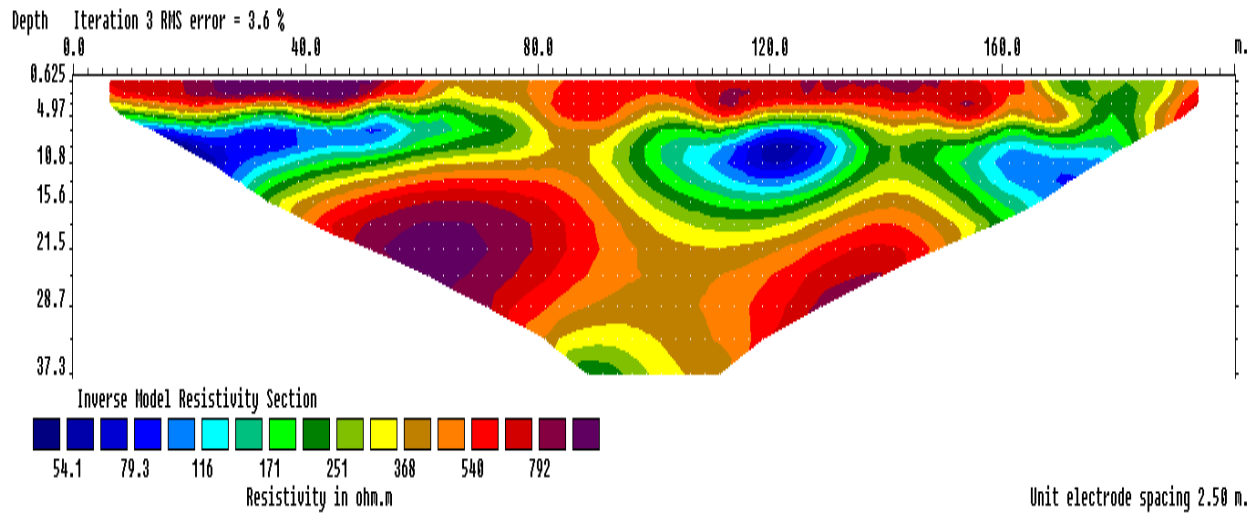
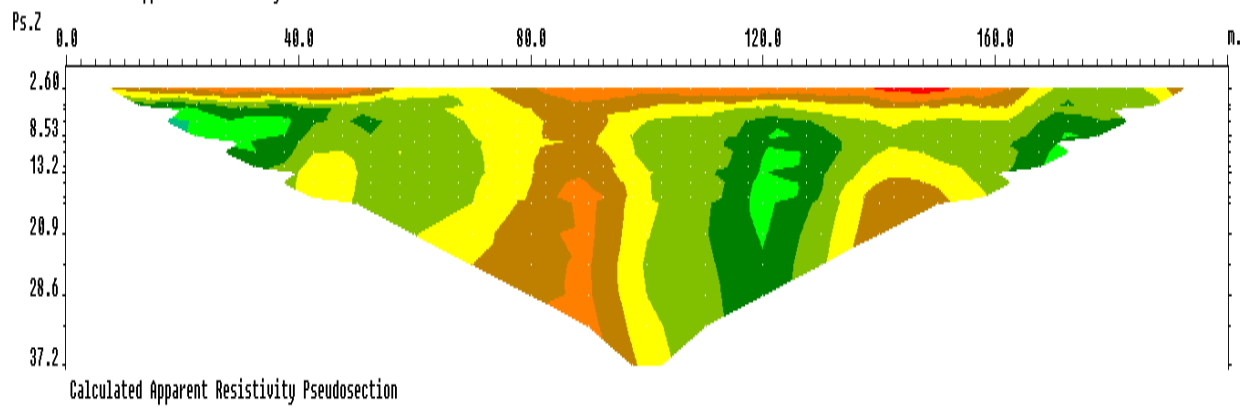
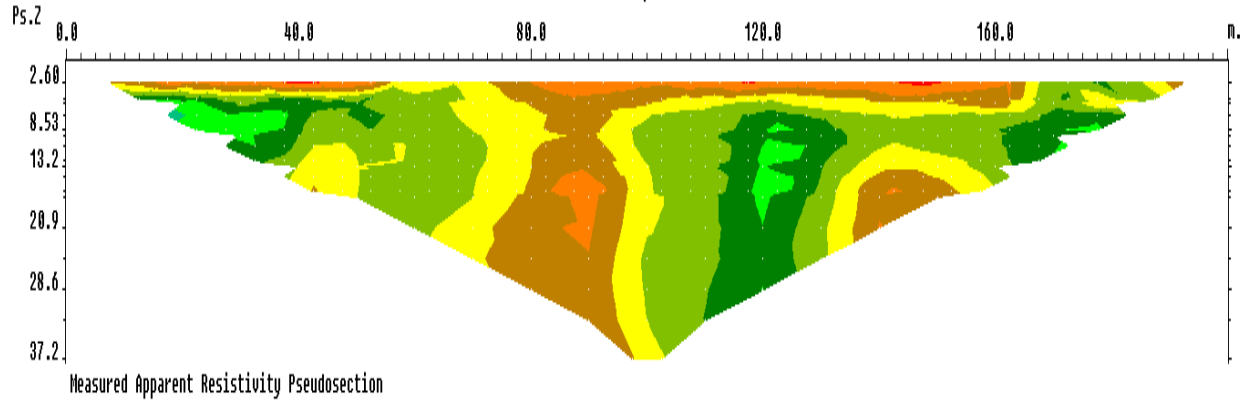
C:\Users\user\Desktop\Suswa2\Irsus002.s4k



Unit electrode spacing 2.50 m.

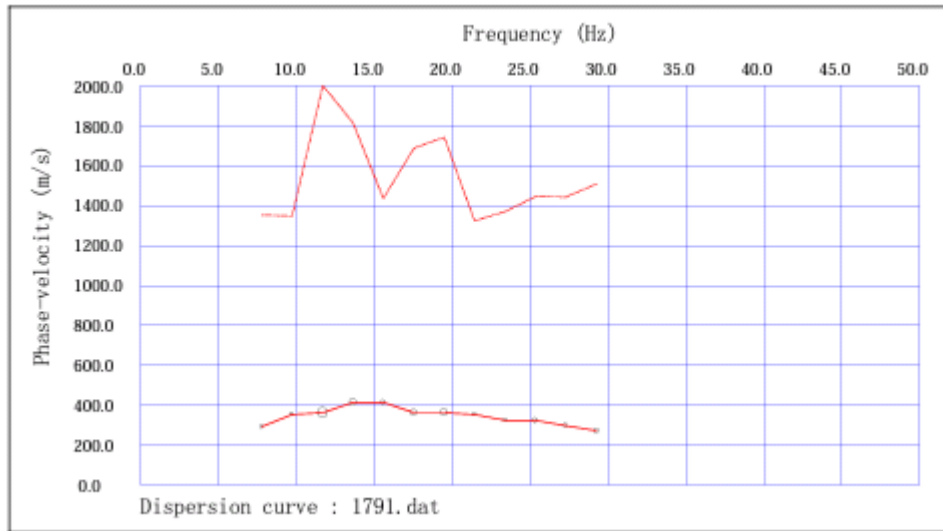
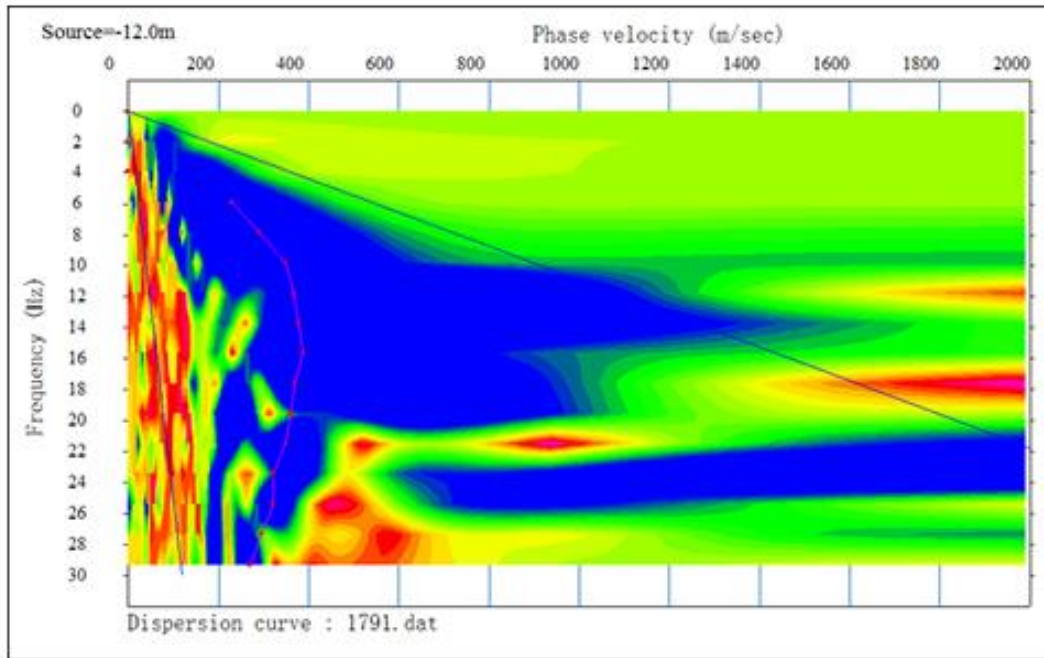
ELECTRICAL RESISTIVITY TOMOGRAPHY PROFILE 2

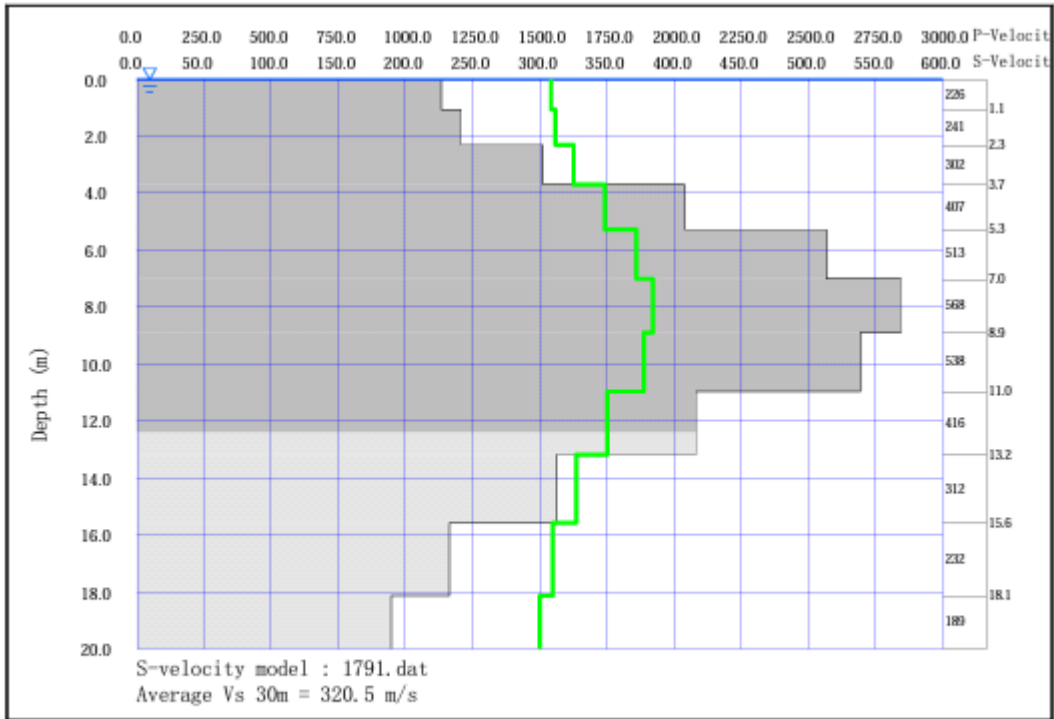
C:\Users\user\Desktop\Suswa2\Irsus003.s4k



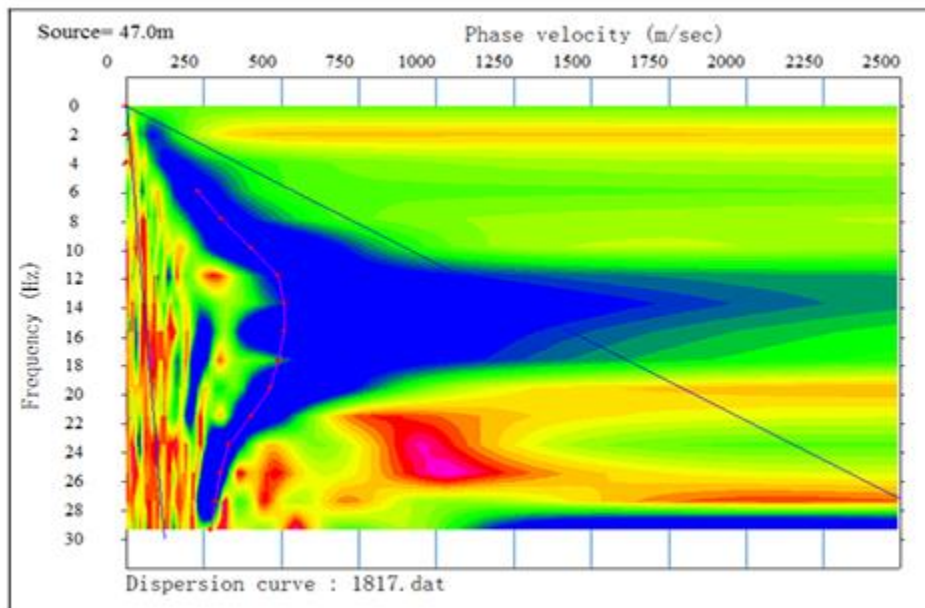
Appendix XI: MASW Dispersion curves

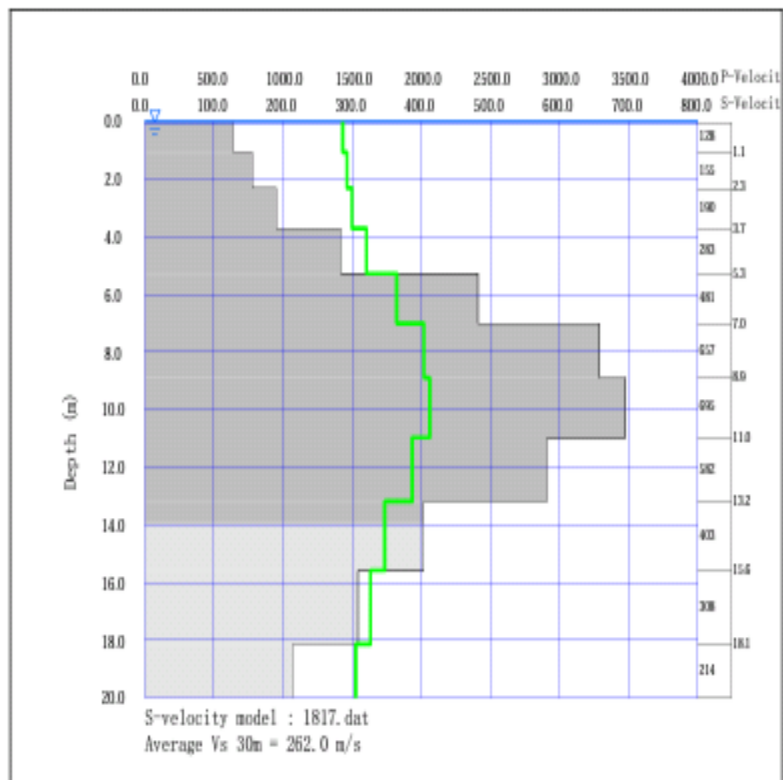
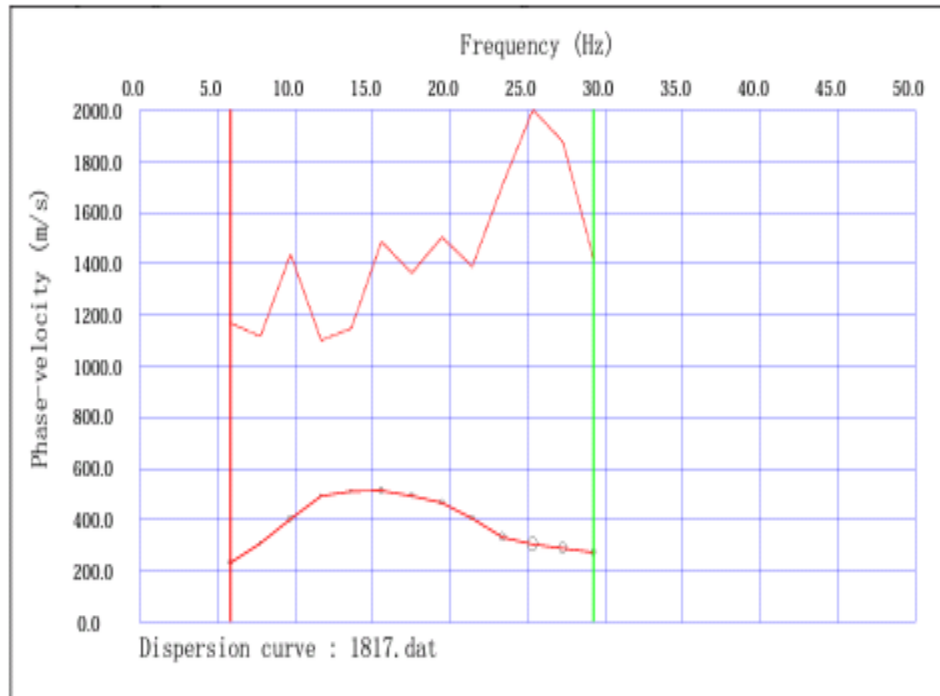
QMRP01S3



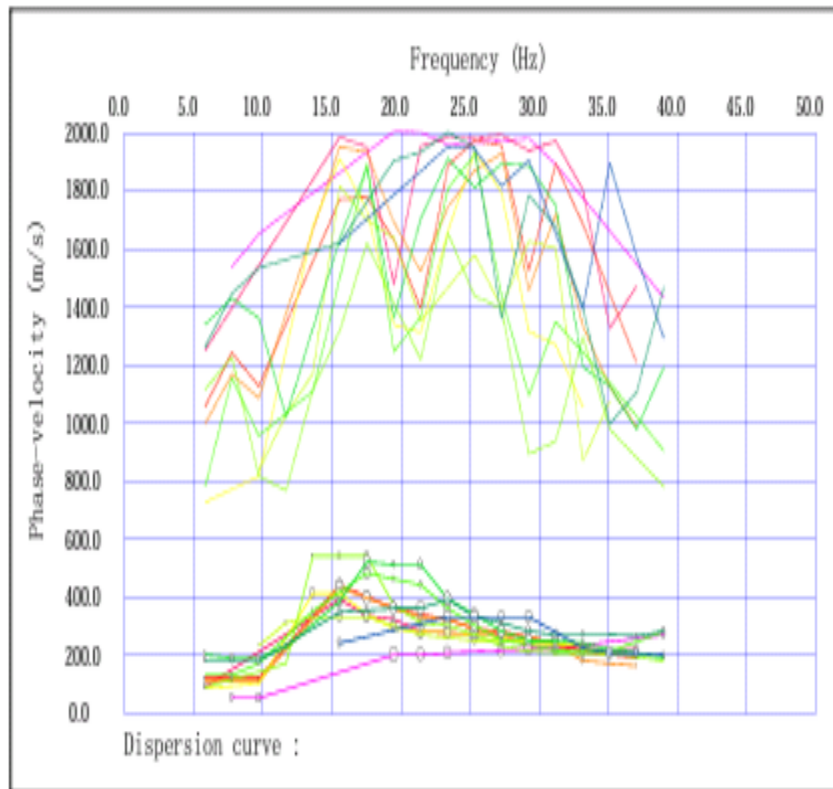
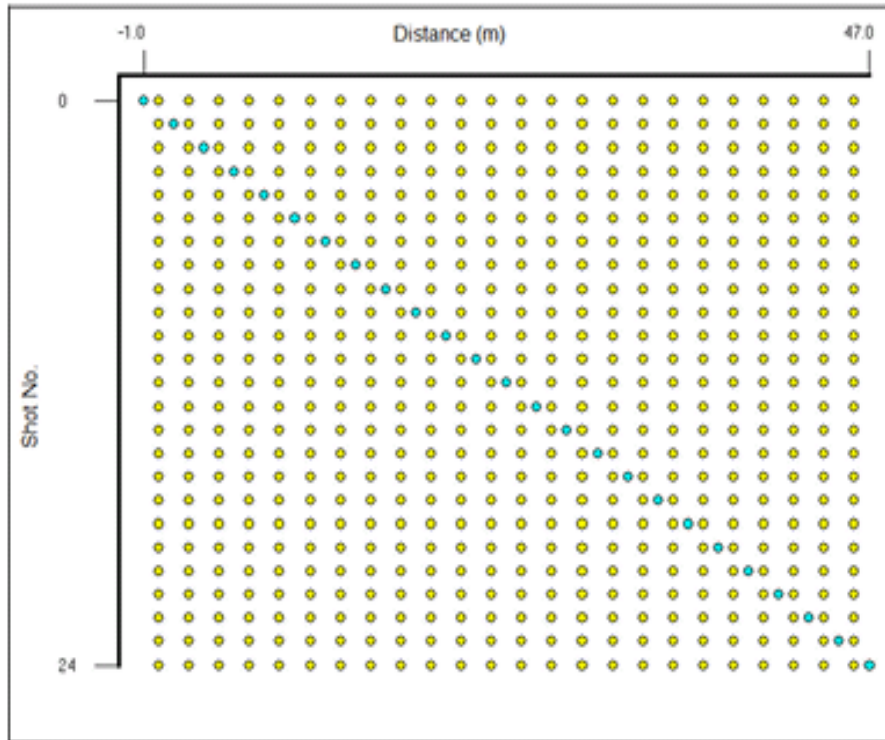


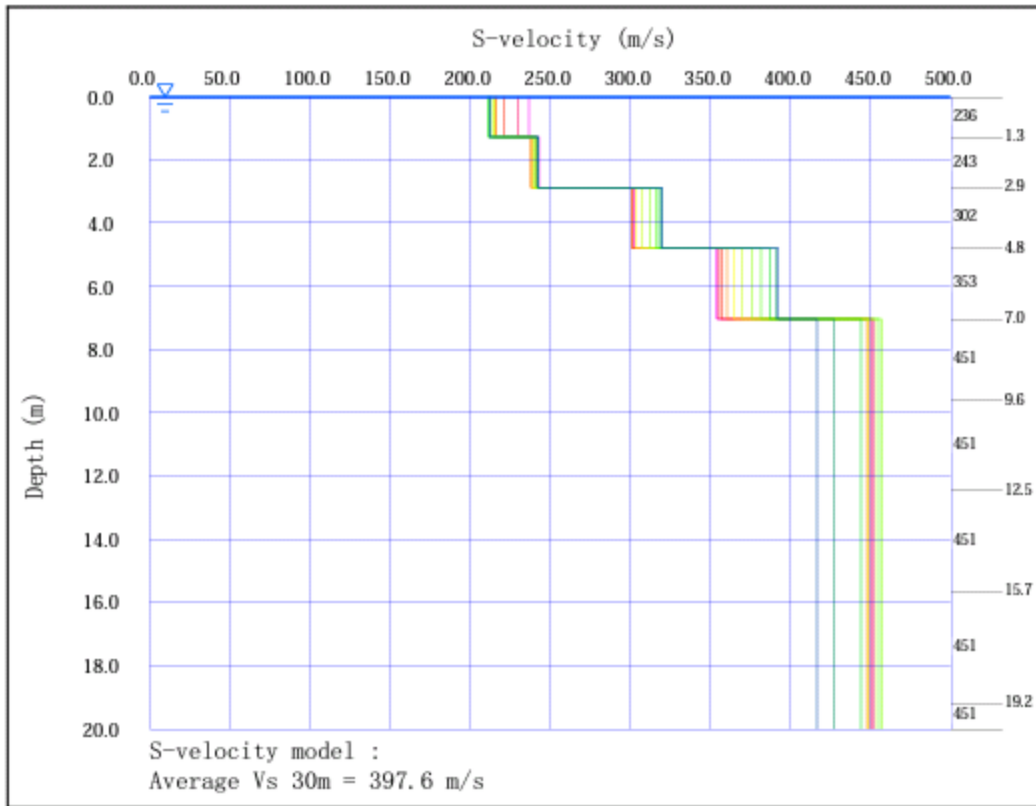
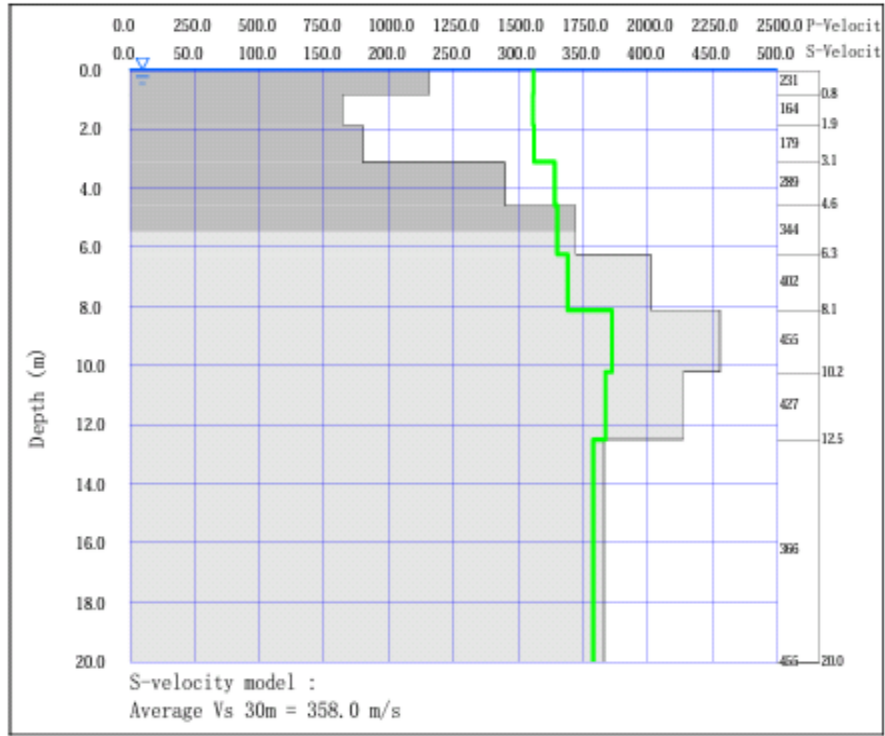
QMRP01S26

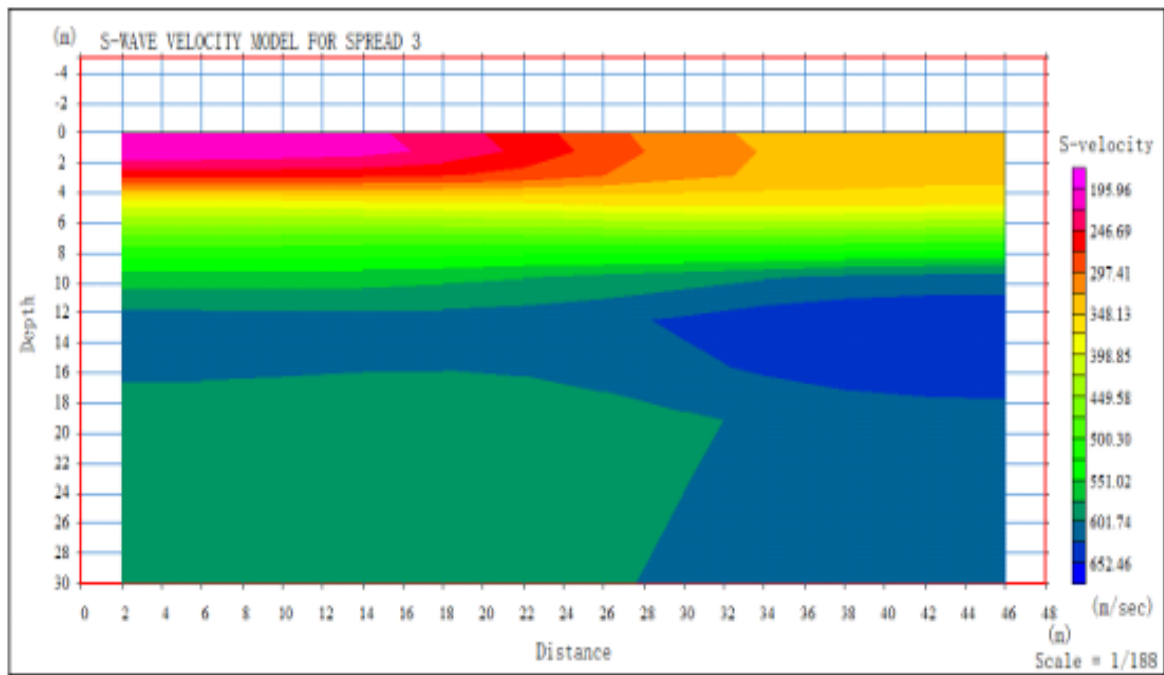
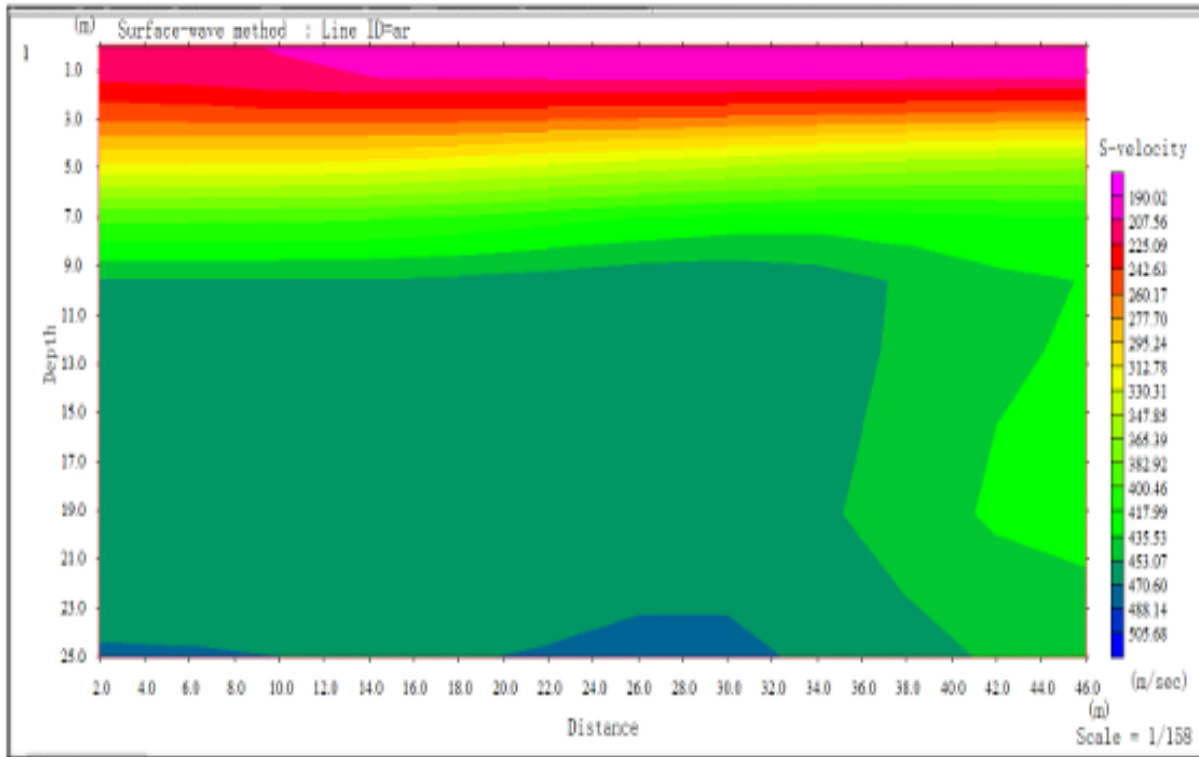


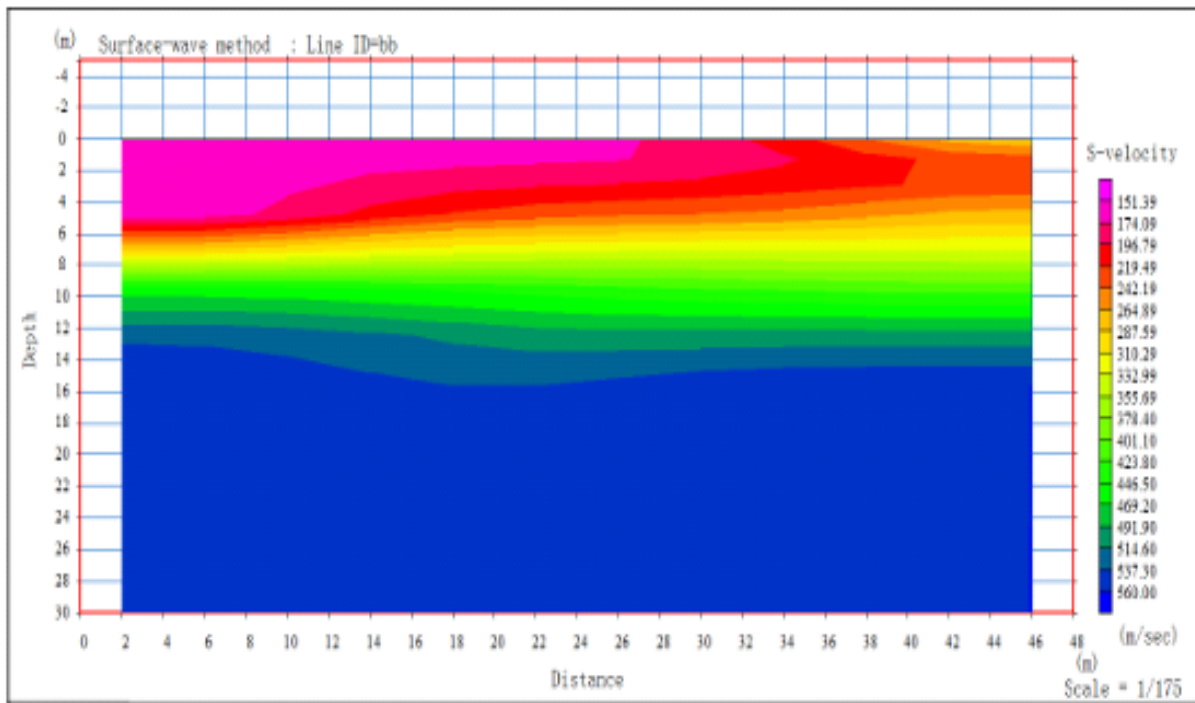
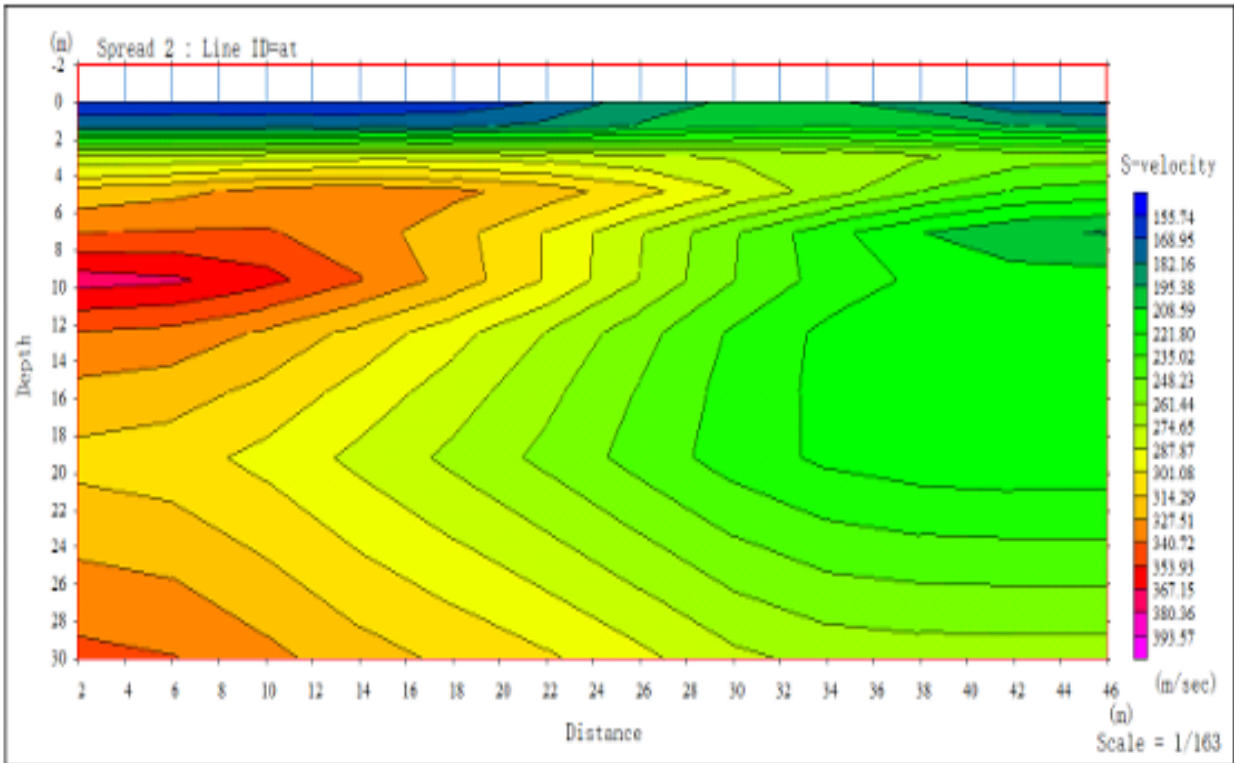


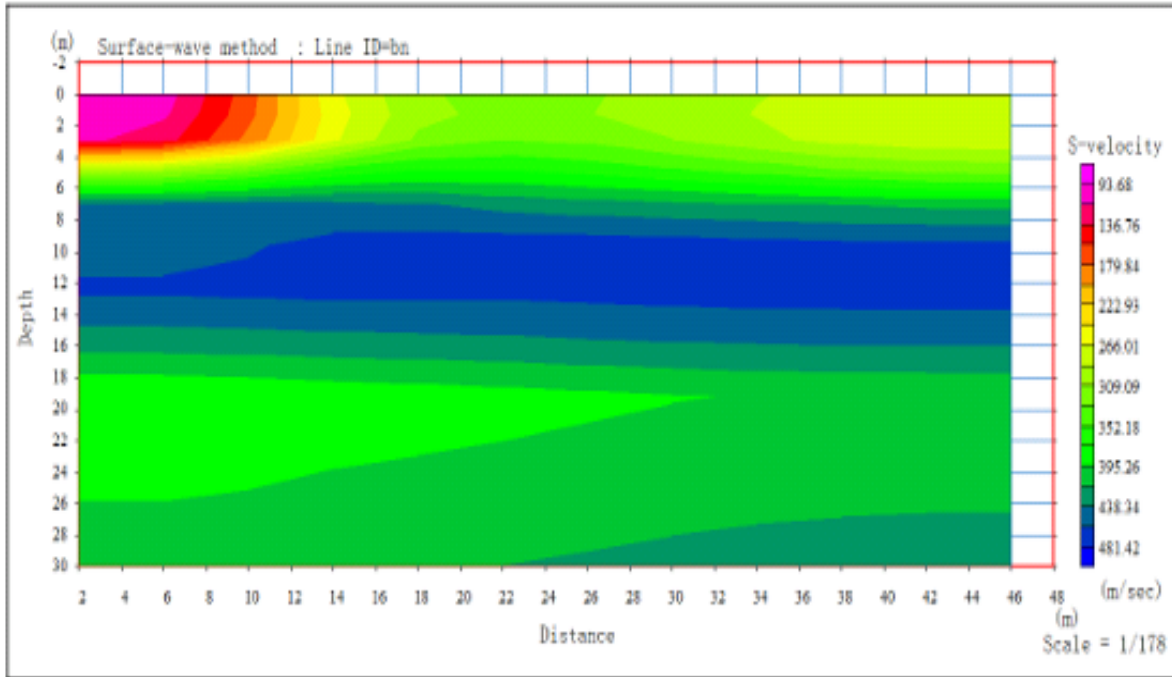
2D shot location geometry











Appendix XII: Geophone coordinates

PROFILE P1 SRT (S-N)									
Waypoint	Eastings	Northings	Elevation	Shot	Waypoint	Eastings	Northings	Elevation	Shot
Spread 1					Spread 3				
513	172311	9978186	2015	1	558	172333	9978324	2007	1
514	172316	9978219	2025	2	574	172338	9978356	2001	2
515	172317	9978220	2025		575	172338	9978358	2001	
516	172317	9978223	2024		576	172339	9978361	2001	
517	172318	9978226	2023		577	172339	9978363	2001	
518	172317	9978230	2024		578	172340	9978367	2001	
519	172319	9978233	2023		579	172340	9978370	2001	
520	172319	9978235	2022		580	172341	9978373	2002	
521	172320	9978237	2022	3	581	172341	9978374	2002	3
522	172318	9978237	2023		582	172341	9978375	2002	
523	172319	9978241	2022		583	172341	9978378	2000	
524	172320	9978244	2022		584	172344	9978382	2001	
525	172321	9978246	2022		585	172342	9978385	2000	
526	172321	9978250	2022		586	172342	9978387	2000	
527	172322	9978253	2019		587	172343	9978390	1999	
528	172322	9978255	2021	4	588	172342	9978392	2001	4
529	172322	9978256	2021		589	172343	9978393	2001	
530	172322	9978259	2021		590	172343	9978396	2000	
531	172323	9978263	2020		591	172344	9978400	2000	
532	172322	9978266	2019		592	172345	9978401	2001	
533	172322	9978269	2020		593	172345	9978405	1999	
534	172324	9978271	2020		594	172346	9978407	2000	
535	172324	9978272	2019	5	595	172345	9978408	1999	5
536	172324	9978274	2020		596	172347	9978410	2000	
537	172326	9978277	2019		597	172347	9978414	1999	
538	172326	9978280	2019		598	172348	9978416	1999	
539	172326	9978283	2020		599	172346	9978420	1999	
540	172327	9978286	2019		600	172347	9978423	1998	
541	172328	9978288	2020		601	172349	9978426	1998	
542	172327	9978290	2019	6	602	172349	9978427	1999	6
543	172333	9978323	2018	7	603	172357	9978458	1996	7
Waypoint	Eastings	Northings	Elevation	Shot	Waypoint	Eastings	Northings	Elevation	Shot
Spread 2									
528	172322	9978255	2021	1	559	172336	9978327	2007	
545	172327	9978292	2007	2	560	172334	9978330	2007	

541	172328	9978288	2020		561	172335	9978333	2007	
546	172329	9978294	2008		562	172335	9978337	2007	
547	172329	9978298	2007		563	172337	9978339	2007	
548	172329	9978300	2009		564	172334	9978340	2007	
549	172329	9978303	2008		565	172337	9978341	2007	5
550	172331	9978304	2007		566	172337	9978345	2007	
551	172330	9978306	2007	3	567	172336	9978348	2006	
552	172331	9978309	2007		568	172337	9978351	2007	
553	172332	9978312	2008		569	172337	9978354	2006	
554	172331	9978315	2008		570	172338	9978357	2005	
555	172332	9978318	2008		571	172337	9978358	2005	
556	172334	9978321	2007		572	172342	9978392	2003	6
557	172334	9978323	2008		573	172338	9978356	2001	7
558	172333	9978324	2007	4	Note: Shaded cells are shot coordinates				

PROFILE PROFILE 2 SRT (NW-SE)									
Waypoint	Eastings	Northings	Elevation (M)		Waypoint	Eastings	Northings	Elevation (M)	
Spread 1					Spread 2				
Waypoint	Eastings	Northings	Elevation (M)	Shot	Waypoint	Eastings	Northings	Elevation (M)	Shot
604	172273	9978443	1997	1	619	172307	9978383	2001	1
605	172291	9978414	1999	2	635	172322	9978354	2004	2
606	172290	9978412	1999		636	172323	9978352	2004	
607	172292	9978410	2000		637	172324	9978350	2005	
608	172292	9978408	2000		638	172326	9978347	2005	
609	172295	9978404	2002		639	172328	9978344	2005	
610	172295	9978402	2002		640	172329	9978341	2005	
611	172297	9978399	2002		641	172331	9978339	2005	
612	172298	9978398	2001	3	642	172331	9978338	2005	3
613	172298	9978398	2002		643	172332	9978336	2006	
614	172300	9978395	2003		644	172333	9978334	2005	
615	172302	9978392	2002		645	172335	9978331	2005	
616	172303	9978389	2002		646	172336	9978328	2005	
617	172305	9978387	2002		647	172337	9978326	2005	
618	172306	9978384	2001		648	172338	9978324	2005	
619	172307	9978383	2001	4	649	172340	9978323	2005	4
620	172307	9978381	2001		650	172341	9978321	2005	
621	172309	9978378	2002		651	172342	9978318	2005	
622	172311	9978376	2002		652	172342	9978315	2005	
623	172313	9978374	2002		653	172345	9978313	2006	
624	172314	9978370	2000		654	172346	9978310	2007	
625	172315	9978369	2002		655	172348	9978308	2006	

626	172317	9978368	2002	5	656	172348	9978306	2006	5
627	172317	9978366	2003		657	172349	9978305	2007	
628	172318	9978364	2003		658	172351	9978302	2007	
629	172320	9978361	2003		659	172352	9978300	2006	
630	172321	9978358	2003		660	172353	9978297	2006	
631	172321	9978355	2003		661	172354	9978295	2007	
632	172324	9978353	2003		662	172356	9978291	2008	
633	172325	9978352	2003	6	663	172358	9978291	2008	6
634	172340	9978322	2006	7	664	172372	9978262	2007	7

PROFILE 1 MASW (NW-SE)							
Spread 1				Spread 3			
Waypoint	Eastings	Northings	Elevation (M)	Waypoint	Eastings	Northings	Elevation (M)
757	172272	9978381	2000	860	172322	9978305	2008
758	172276	9978371	2002	861	172328	9978296	2009
759	172278	9978371	2002	862	172329	9978295	2009
760	172280	9978370	2002	863	172329	9978295	2008
761	172280	9978369	2001	864	172329	9978293	2008
762	172280	9978369	2001	865	172330	9978293	2009
763	172280	9978368	2001	866	172331	9978292	2009
764	172282	9978367	2001	867	172331	9978291	2009
765	172281	9978366	2001	868	172331	9978290	2010
766	172282	9978365	2001	869	172332	9978289	2010
767	172282	9978365	2001	870	172332	9978288	2010
768	172283	9978364	2000	871	172333	9978287	2010
769	172283	9978362	2000	872	172334	9978287	2009
770	172284	9978362	2000	873	172334	9978285	2009
771	172285	9978361	2000	874	172334	9978285	2009
772	172286	9978361	2001	875	172336	9978284	2010
773	172286	9978359	2001	876	172336	9978283	2009
774	172286	9978358	2001	877	172337	9978282	2009
775	172287	9978358	2001	878	172337	9978281	2009
776	172288	9978357	2002	879	172338	9978281	2010
777	172288	9978356	2002	880	172338	9978280	2009
778	172288	9978356	2002	881	172338	9978279	2009
779	172290	9978354	2002	882	172339	9978278	2010
780	172288	9978353	2003	883	172340	9978278	2010
781	172289	9978352	2002	884	172341	9978277	2010
782	172290	9978352	2002	885	172341	9978276	2010
783	172291	9978350	2002	886	172342	9978275	2010

784	172293	9978350	2003	887	172343	9978274	2010
785	172292	9978349	2003	888	172343	9978273	2010
786	172292	9978349	2003	889	172344	9978272	2009
787	172293	9978347	2003	890	172345	9978272	2009
788	172294	9978346	2003	891	172345	9978271	2009
789	172295	9978345	2003	892	172345	9978270	2009
790	172295	9978344	2003	893	172346	9978268	2009
791	172295	9978344	2003	894	172346	9978268	2010
792	172296	9978344	2003	895	172347	9978267	2010
793	172297	9978342	2003	896	172348	9978267	2009
794	172297	9978341	2003	897	172348	9978266	2011
795	172298	9978340	2003	898	172347	9978265	2010
796	172299	9978340	2003	899	172349	9978265	2011
797	172298	9978340	2003	900	172350	9978263	2011
798	172300	9978339	2002	901	172350	9978262	2010
799	172300	9978338	2002	902	172351	9978261	2010
800	172301	9978338	2002	903	172352	9978262	2010
801	172301	9978336	2002	904	172352	9978261	2011
802	172302	9978335	2002	905	172352	9978259	2010
803	172303	9978334	2002	906	172354	9978258	2010
804	172303	9978334	2002	907	172354	9978257	2010
805	172302	9978333	2002	908	172354	9978257	2010
806	172303	9978331	2002	909	172354	9978256	2010
807	172308	9978323	2003	910	172359	9978246	2010

Spread 2

Waypoint	Eastings	Northings	Elevation (M)				
808	172296	9978343	2003	834	172315	9978314	2006
809	172301	9978334	2004	835	172314	9978313	2006
810	172301	9978333	2004	836	172317	9978312	2006
811	172303	9978331	2004	837	172317	9978311	2006
812	172303	9978331	2005	838	172318	9978311	2007
813	172304	9978331	2005	839	172318	9978310	2007
814	172304	9978330	2005	840	172318	9978308	2007
815	172305	9978329	2006	841	172319	9978308	2007
816	172306	9978328	2006	842	172320	9978307	2007
817	172306	9978327	2005	843	172321	9978307	2007
818	172307	9978327	2005	844	172321	9978305	2007
819	172307	9978326	2005	845	172321	9978304	2007
820	172307	9978325	2005	846	172321	9978303	2006
821	172308	9978324	2005	847	172322	9978303	2006
822	172309	9978323	2005	848	172324	9978302	2006

823	172310	9978323	2006	849	172324	9978301	2007
824	172309	9978322	2005	850	172324	9978301	2007
825	172310	9978321	2005	851	172325	9978299	2007
826	172311	9978320	2007	852	172325	9978299	2008
827	172311	9978319	2007	853	172326	9978298	2008
828	172312	9978318	2007	854	172327	9978298	2008
829	172313	9978317	2005	855	172327	9978297	2007
830	172313	9978317	2006	856	172327	9978295	2007
831	172313	9978316	2006	857	172329	9978295	2007
832	172314	9978315	2006	858	172334	9978286	2007
833	172314	9978314	2006	Note: The shaded cells are shot coordinates			

PROFILE 2 MASW (W-E)							
Spread 1				Spread 3			
Waypoint	Eastings	Northings	Elevation (M)	Waypoint	Eastings	Northings	Elevation (M)
911	172270	9978281	2006	1016	172359	9978289	2002
912	172280	9978282	2005	1017	172372	9978291	2003
913	172282	9978282	2005	1018	172373	9978291	2003
914	172283	9978283	2005	1019	172374	9978291	2004
915	172283	9978282	2005	1020	172374	9978291	2004
916	172283	9978282	2005	1021	172376	9978291	2005
917	172285	9978283	2005	1022	172376	9978291	2005
918	172285	9978283	2005	1023	172378	9978291	2005
919	172287	9978282	2005	1024	172379	9978292	2005
920	172288	9978283	2005	1025	172380	9978291	2005
921	172288	9978284	2005	1026	172380	9978291	2004
922	172290	9978284	2004	1027	172381	9978291	2004
923	172290	9978283	2004	1028	172383	9978292	2004
924	172292	9978284	2004	1029	172384	9978292	2004
925	172293	9978284	2005	1030	172385	9978291	2004
926	172294	9978282	2004	1031	172386	9978292	2005
927	172294	9978284	2005	1032	172387	9978292	2005
928	172296	9978283	2005	1033	172388	9978292	2005
929	172296	9978283	2005	1034	172388	9978292	2005
930	172298	9978283	2005	1035	172389	9978292	2005
931	172299	9978284	2004	1036	172390	9978291	2006
932	172299	9978285	2005	1037	172391	9978291	2003
933	172301	9978284	2005	1038	172392	9978291	2003
934	172301	9978285	2006	1039	172393	9978291	2003
935	172303	9978285	2006	1040	172394	9978292	2003
936	172304	9978284	2006	1041	172395	9978292	2004

937	172305	9978285	2006	1042	172396	9978291	2004
938	172306	9978285	2007	1043	172398	9978292	2004
939	172306	9978284	2007	1044	172398	9978292	2004
940	172307	9978284	2006	1045	172400	9978293	2004
941	172308	9978285	2007	1046	172400	9978293	2004
942	172309	9978284	2007	1047	172401	9978292	2004
943	172309	9978284	2008	1048	172402	9978293	2004
944	172312	9978285	2007	1049	172403	9978293	2004
945	172311	9978285	2007	1050	172403	9978293	2004
946	172314	9978285	2008	1051	172405	9978293	2004
947	172314	9978286	2007	1052	172406	9978293	2004
948	172316	9978286	2007	1053	172407	9978294	2004
949	172316	9978286	2007	1054	172409	9978294	2006
950	172318	9978286	2006	1055	172409	9978293	2006
951	172319	9978286	2006	1056	172411	9978293	2006
952	172320	9978286	2007	1057	172411	9978294	2006
953	172321	9978285	2007	1058	172412	9978295	2006
954	172321	9978285	2006	1059	172412	9978294	2005
955	172322	9978287	2007	1060	172414	9978294	2005
956	172323	9978286	2006	1061	172415	9978294	2005
957	172324	9978286	2007	1062	172415	9978295	2005
958	172325	9978286	2006	1063	172417	9978294	2006
959	172326	9978287	2005	1064	172418	9978294	2006
960	172329	9978286	2006	1065	172419	9978295	2006
961	172328	9978287	2006	1066	172430	9978295	2007

Spread 2

Waypoint	Eastings	Northings	Elevation (M)	Waypoint	Eastings	Northings	Elevation (M)
964	172316	9978285	2009	991	172352	9978289	2005
965	172327	9978286	2009	992	172353	9978290	2005
966	172328	9978286	2010	993	172353	9978289	2005
967	172328	9978287	2009	994	172354	9978290	2005
968	172329	9978287	2009	995	172355	9978291	2005
969	172331	9978287	2008	996	172358	9978290	2005
971	172331	9978287	2008	997	172358	9978291	2006
972	172332	9978287	2007	998	172359	9978291	2006
973	172334	9978288	2009	999	172360	9978290	2006
974	172334	9978288	2008	1000	172361	9978290	2004
975	172336	9978287	2008	1001	172361	9978290	2004
976	172337	9978288	2007	1002	172363	9978291	2005
977	172338	9978288	2006	1003	172364	9978291	2005
978	172338	9978288	2006	1004	172365	9978291	2005

979	172339	9978288	2006	1005	172366	9978291	2005
980	172340	9978289	2006	1006	172367	9978291	2005
981	172342	9978289	2006	1007	172368	9978291	2005
982	172343	9978288	2006	1008	172370	9978291	2005
983	172344	9978288	2005	1009	172370	9978292	2004
984	172346	9978288	2007	1010	172371	9978292	2004
985	172345	9978288	2005	1011	172372	9978291	2004
986	172346	9978289	2005	1012	172373	9978292	2005
987	172348	9978289	2005	1013	172374	9978292	2005
988	172349	9978289	2005	1014	172375	9978293	2004
989	172350	9978289	2005	1015	172387	9978293	2005
990	172351	9978289	2005	Note: Shaded cells are shot coordinates			

Appendix XIII: *Field photos*







